From the Department of Infectious Diseases and Microbiology

of the University of Lübeck

Director: Prof. Dr. med. Jan Rupp

Immunometabolic networks in the regulation of visceral leishmaniasis

Dissertation

for Fulfillment of

Requirements

for the Doctoral Degree

of the University of Lübeck

from the Department of Computer Sciences and Technical Engineering or

from the Department of Natural Sciences

Submitted by

Mareike Ohms

from Tegernsee

Lübeck, 2020

First referee: Prof. Dr. rer. nat. Tamás Laskay

Second referee: Dr. rer. nat. Kathrin Kalies

Date of oral examination: 11th of December 2020

Approved for printing. Lübeck, 15th of December 2020

Abbreviations

$^1O_2$	Singlet oxygen
2-DG	2-Desoxy-D-glucose
2-NBDG	2-(N-(7-Nitrobenz-2-oxa-1,3-diazol-4-yl)Amino)-2-Desoxyglucose
ADCC	Antibody-dependent cell-mediated cytotoxicity
AIDS	Acquired immune deficiency syndrome
AMP	Adenosine monophosphate
AMPK	AMP-activated protein kinase
ANOVA	Analysis of variance
APC	Antigen presenting cell
ARG1	Arginase 1
ATP	Adenosine triphosphate
AUC	Area under the curve
BAFF	B-cell activating factor
BHI	Brain heart infusion
BPI	Bacterial/permeability increasing protein
BSA	Bovine serum albumin
C	Complement factor
CCL	C-C motif ligand
CCR	C-C motif receptor
CD	Cluster of differentiation
CG	Cathepsin G
CL	Cutaneous leishmaniasis
CO_2	Carbon dioxide
CP	Cystein protease
CPAF	Chlamydial protease-like activating factor
CR	Complement receptor
CXCL	C-X-C motif ligand
CXCR	C-X-C motif receptor
DC	Dendritic cell
DHR123	Dihydrorhodamine 123
(D)PBS	(Dulbecco´s) Phosphate-buffered saline
DN	Double negative
DNA	Desoxyribonucleic acid
DTT	Dithiothreitol
ECAR	Extracellular acidification rate
ECM	Extracellular matrix
EGFR	Epidermal growth factor receptor
eIF4F	Eukaryotic initiation factor 4F
ELISA	Enzyme-linked immunosorbent assay
ER	Endoplasmatic reticulum
ERK	Extracellular signal-regulated kinases
ETC	Electron transport chain
FACS	Fluorescence-activated cell sorting
$FADH_2$	Flavin adenine dinucleotide

FAO	Fatty acid oxidation
FAS	Fatty acid synthase
FasL	Fas ligand
FasR	Fas receptor
FCCP	Carbonyl cyanide-4 (trifluoromethoxy)phenylhydrazone
FcR	Fc receptor
FML	Fructose-mannose ligand
fMLP	N-Formylmethionyl-leucyl-phenylalanine
G3P	Glycerol-3-phosphate
G6P	Glucose-6-phosphate
G-CSF	Granulocyte-colony stimulating factor
GLUT	Glucose transporter
G-MDSC	Granulocyte-like myeloid derived suppressor cell
GMP	Granulocyte-monocyte progenitor
Gp63	Glycoprotein of 63 kDa
GPI	Glycogen phosphorylase inhibitor
H^+	Proton
H_2O	Water
H_2O_2	Hydrogen peroxide
HASB1	Hydrophilic acylated surface protein B1
HB-EGF	Heparin-binding EGF-like growth factor
HBSS	Hank´s balanced salt solution
hCAP-18	Human cathelicidin antimicrobial protein 18
HDG	High-density granulocyte
HDT	Host-directed therapy
HEPES	4-(2-hydroxyethyl)-1-piperazineethanesulfonic acid
HIF-1α	Hypoxia-inducible factor 1 alpha
HIV	Human immunodeficiency virus
HMG-CoA	3-hydroxyl-3-methylglutaryl-CoA
HOCl	Hyperchlorous acid
hpi	Hours post infection
HSC	Hematopoietic stem cell
IC	Immune complex
ICAM	Intercellular adhesion molecule
IFN	Interferon
Ig	Immunoglobulin
IKK	IκB kinase
IL	Interleukin
iNOS	Inducible nitric oxide synthase
IP-10	Interferon-gamma induced protein 10 kDa
IRS-1	Insulin receptor substrate 1
ITK	IL-2 inducible protein kinase
JNK	c-Jun N-terminal kinase
KMP-11	Kinetoplastid membrane protein-11
LB	Lysogeny broth

LCF	*Leishmania* chemotactic factor
LDG	Low-density granulocyte
LDH	Lactate dehydrogenase
LDL	Low-density lipoprotein
LeIF	*Leishmania* elongation and initiation factor
LFR1	*Leishmania* ferric iron reductase 1
LHR1	*Leishmania* heme response 1
LIT1	*Leishmania* iron transporter 1
LKB1	Liver kinase B1
LMPP	Lymphoid-primed multipotent progenitor
LmSTI1	*Leishmania major* stress-inducible protein 1
LOX-1	Oxidized low-density lipoprotein receptor 1
LPG	Lipophosphoglycan
LPS	Lipopolysaccharide
LR	Leishmaniasis recidivans
LTB4	Leukotrine B
MAC	Membrane attack complex
Mac-1	Macrophage-1 antigen
MAPK	Mitogen-activated protein kinase
MCL	Mucocutaneous leishmaniasis
MCP-1	Monocyte chemotactic protein 1
M-CSF	Macrophage colony-stimulating factor
MEK	Mitogen-activated protein kinase kinase
MHC	Major histocomparability complex
M-MDSC	Monocyte-like myeloid derived suppressor cell
MMP	Matrix metalloproteinase
MPO	Myeloperoxidase
MRSA	Methicillin-resistant *S. aureus*
mTOR	Mammalian target of rapamycin
NAD	Nicotinamide adenine dinucleotide
NADPH	Nicotinamide adenine dinucleotide phosphate
NAMPT	Nicotinamide phospho-ribosyltransferase
NE	Neutrophil elastase
NET	Neutrophil extracellular trap
NFκB	Nuclear factor-kappa-light-chain-enhancer of activated B cells
NGAL	Neutrophil gelatinase-associated lipocalin
NK	Natural killer
NLR	Neutrophil lymphocyte ratio
NNN	Novy MacNeal-Nicolle
NO·	Nitric oxide
NOS	Nitric oxide synthase
ns	Not significant
O_2	Oxygen
$O_2^{-}\cdot$	Superoxide
OCR	Oxygen consumption rate

OH·	Hydroxyl radical
OLFM-4	Olfactomedin 4
OONO-	Peroxynitrite anion
OxPHOS	Oxidative phosphorylation
PAD4	Peptidyl arginase deaminase
PAMP	Pathogen associated molecular pattern
PARP	Poly(ADP-ribose) polymerase
PAS	Periodic acid-Schiff
PBMC	Peripheral blood mononuclear cell
PD-L1	Programmed death-ligand 1
PFA	Paraformaldehyde
PFK-2	6-phosphofructo-2-kinase
PGE2	Prostaglandine E2
PI	Propidiumiodid
PI3K	Phosphoinositide 3-kinase
PKC	Protein kinase C
PKDL	Post-kala-azar dermal leishmaniasis
PLC	Phospholipase C
PLP	Pyridoxal phosphate
PMA	Phorbol 12-myristate 13-acetate
PMN	Polymorphnuclear
PPG	Proteophosphoglycan
PPP	Pentose phosphate pathway
PR3	Proteinase 3
PS	Phosphatidylserine
PV	Parasitophorous vacuole
Rac	Rho-related C3 botulinum toxin substrate
RIN	RNA integrity number
RNA	Ribonucleic acid
RNP	Ribonucleoprotein complex
RNS	Reactive nitrogen species
ROS	Reactive oxygen species
RPMI	Roswell Park Memorial Institute
RT	Room temperature
SCFA	Short chain fatty acid
SD	Standard deviation
SDF-1α	Stromal cell-derived factor 1 alpha
SDH	Succinate dehydrogenase
SIRT1	Sirtuin 1
SLC	Solute carrier type transporters
SLE	Systemic lupus erythematosus
SNAT	Sodium-coupled neutral amino acid transporter
SOD	Superoxide dismutase
TAM	Tumor-associated macrophage
TAN	Tumor-associated neutrophil
TCA	Tricarboxylic acid

TCR	T cell receptor
TGFβ	Transforming growth factor beta
TIMP	Tissue inhibitor of metalloproteinases
TNF	Tumor necrosis factor
TRAIL	TNF-related apoptosis-inducing ligand
Treg	Regulatory T cell
TRPM2	Transient receptor potential cation channel, subfamily M, member 2
Tsp1	Thrombospondin
VEGF	Vascular endothelial growth factor
VL	Visceral leishmaniasis
WHO	World Health Organization
ZVL	Zoonotic visceral leishmaniasis
$\Delta\psi_m$	Membrane potential

Table of contents

Abbreviations 3

Introduction 13

Neutrophils – Key players of innate immunity 13

- Granulopoiesis 13
- Neutrophil exit from the bone marrow and recruitment to the tissue 14
- Antimicrobial effector mechanisms of neutrophils 15
- Neutrophils as host cells for pathogens 18
- Immunoregulatory role of neutrophils 18

Leishmania 19

- Leishmaniasis – Clinical features 19
- Biology of the *Leishmania* parasite 21
- *Leishmania* life cycle 23
- Neutrophils as host cells of *Leishmania* 25
- *Leishmania* – Immune response 25
- Modulation of host cell metabolism by *Leishmania* 28
  - L-arginine metabolism 28
  - AMPK and mTOR 28
  - Heme and iron metabolism 29
  - Cholesterol homeostasis 29
- Leishmaniasis treatment – Current objectives 29
- Status of vaccine research for leishmaniasis 30
- Host-directed therapies (HDTs) in leishmaniasis 31

Neutrophil heterogeneity in health and disease 32

- Neutrophil subpopulations in cancer 33
  - TANs 33
  - G-MDSCs 33
  - LDNs 34
- Neutrophil recruitment into the tumor 34
- Neutrophil polarization in the tumor microenvironment 35
- Pro-tumor role of neutrophils 37
  - ROS 37
  - Proteases 37
  - Cytokine and growth factors 38

NETs 38
Anti-tumor role of neutrophils 39
ROS 39
Apoptosis of tumor cells 39
MMP-8 39
ADCC 39
T cell activation 40
Neutrophil metabolism 41
Major metabolic pathways in neutrophils 41
Metabolic regulation of neutrophil development, functions and apoptosis 42
Granulopoiesis and steady state 42
Phagocytosis 43
ROS production 43
NETs 43
Chemotaxis 44
Apoptosis 44
Metabolic changes in neutrophils during infection 45
Metabolic changes in neutrophil subpopulations 46
Key objectives of this project 47
Materials 49
Solutions, buffers and media 49
Laboratory supply/Consumables 49
Instruments and laboratory equipment 51
Chemicals and laboratory reagents 52
Cytokines 55
Antibodies 55
Kits 56
Software 56
Methods 57
Leishmania donovani culture 57
Bacterial culture 57
Isolation of primary human peripheral blood neutrophil granulocytes 57
In vitro polarization of neutrophils 57
Flow cytometry analysis of cell surface molecules 58

Determination of cytokines in culture supernatants ... 58
Detection of intra- and extracellular ROS ... 58
In vitro infection of neutrophils with *L. donovani* promastigotes ... 58
Quantification of *L. donovani* survival in neutrophils ... 58
Assessment of neutrophil apoptosis and viability ... 59
SYTOXGreen kinetic assay ... 59
Visualization of NETs by fluorescence microscopy ... 59
Seahorse XF Glycolysis stress test and Seahorse XF Mito stress test ... 59
Bacterial killing assay ... 61
Glucose uptake assay ... 61
DHR assay ... 62
RNA isolation, quality control and RNA sequencing ... 62
ATP assay ... 62
Lactate assay ... 63
Pyruvate assay ... 63
PAS staining ... 63
MitoSOX™ Red mitochondrial superoxide indicator staining ... 63
NAD/NADH-Glo™ assay ... 63
Fatty acid uptake assay ... 63
Arginase activity assay ... 63
Statistical analysis ... 64
Results ... 65
Part I: Polarization of primary human neutrophils toward N1 and N2 phenotypes *in vitro* ... 65
QVD-OPh suppresses apoptosis and cell death of *in vitro* polarized neutrophils up to 48 h ... 65
QVD-OPh treatment neither induces CD62L shedding nor MPO-derived ROS production ... 67
N1-like neutrophils show higher degranulation than N2-like neutrophils ... 69
N1-like neutrophils show increased CD62L shedding compared to N2-like neutrophils ... 71
In vitro polarized neutrophils express typical surface markers of N1 and N2 TANs ... 73
In vitro polarized neutrophils show typical N1 and N2 protein secretion ... 75
N1-like neutrophils show the tendency to produce more MPO-derived ROS than N2-like neutrophils ... 76
PMA-induced superoxide formation of N2-like neutrophils is increased compared to N1-like neutrophils after 48 h ... 78
N1-like neutrophils produce more intracellular ROS than N2-like neutrophils ... 79
N1-like neutrophils show the tendency to kill less bacteria than N2-like neutrophils ... 81

N2-like neutrophils exert decreased capacity to kill *L. donovani* promastigotes 82
N2-like neutrophils tend to have higher arginase 1 activity than N1-like neutrophils 83
N1-like neutrophils form more NETs than N2-like neutrophils 84
N1-like neutrophils show higher expression of CD64 and CD89 but lower expression of CD16 and CD32 than N2-like neutrophils 86
Part II: Metabolic phenotyping of *L. donovani*-infected neutrophils 88
Oxidative metabolism of *L. donovani*-infected neutrophils 89
Contact with *L. donovani* promastigotes upregulates ROS production of neutrophils 89
MPO-derived ROS production of *L. donovani*-infected neutrophils is upregulated after PMA stimulation 91
Superoxide production of *L. donovani*-infected neutrophils is increased after PMA stimulation 92
L. donovani-infected neutrophils produce more intracellular ROS after stimulation with PMA or fMLP 94
L. donovani-infected neutrophils show increased mitochondrial ROS production 96
L. donovani-infected neutrophils secrete high levels of IL-8 and TNF but release no IP-10 upon IFNγ/LPS stimulation 98
L. donovani-infected neutrophils have an increased glycolytic metabolism 98
L. donovani-infected neutrophils show increased respiratory parameters 100
L. donovani-infected neutrophils exhibit increased levels of lactate and pyruvate 101
L. donovani infection upregulates the glucose uptake of neutrophils 101
The ATP content of *L. donovani*-infected neutrophils decreases upon glycolysis and oxidative phosphorylation inhibition 103
L. donovani-infected neutrophils show an increased NAD^+/NADH ratio after 24 hpi 104
L. donovani infection upregulates the fatty acid uptake of neutrophils after 24 hpi 106
Survival of *L. donovani* promastigotes in 2-DG treated neutrophils is decreased 108
2-DG treatment reduces ROS production of *L. donovani*-infected neutrophils after 24 hpi 108
2-DG treatment reduces the survival of *L. donovani* promastigotes in culture 109
Survival of *L. donovani* promastigotes in 3PO-treated neutrophils is reduced 110
3PO treatment reduces ROS production of *L. donovani*-infected neutrophils 111
3PO treatment seems to reduce the survival of *L. donovani* promastigotes in culture 112
Glucose replacement by galactose does neither affect anti-leishmanial capacity nor ROS production of neutrophils 113
Glutaminolysis inhibition neither affects the anti-leishmanial capacity nor the ROS production of neutrophils 114
L. donovani-infected neutrophils use glycogen storages upon glucose deprivation 114
Part III: Transcriptomic profiling of *L. donovani*-infected neutrophils 116
Discussion 118

Part I: Polarization of primary human neutrophils toward N1 and N2 phenotypes *in vitro*.....118
Part II: Metabolic characterization of *L. donovani*-infected neutrophils.....122
Part III: Transcriptomic profiling of *L. donovani*-infected neutrophils.....127
Summary.....128
Zusammenfassung.....130
References.....132
Acknowledgements.....163
Supplementary Material.....164
Curriculum vitae.....180

Introduction

Neutrophils – Key players of innate immunity

Neutrophils, also known as polymorphonuclear (PMN) leukocytes, are the most common leukocytes and make up 70 % of all blood cells. They are regarded as the first line of defense against invading pathogens and form a key component of the innate immune system. First described at the end of the 19th century by Paul Ehrlich, this cell type was named as "neutrophil" due to its tendency to retain neutral dyes (Ehrlich, 1880; Steven, 1892). The morphology of neutrophils is further characterized by their lobulated nucleus and their high granule content. Under homeostasis neutrophils are produced at a rate of ~10^{11} cells per day (Rosales, 2018).

Granulopoiesis

The formation of neutrophils from hematopoietic stem cells occurs in the bone marrow during a process called granulopoiesis (**Figure 1**) (Görgens et al., 2013). Self-renewing hematopoietic stem cells (HSCs) differentiate into multipotent progenitor cells, which give rise to lymphoid-primed multipotent progenitors (LMPPs). From these LMPPs emerge granulocyte-monocyte progenitors (GMPs), which turn under the influence of granulocyte-colony stimulating factor (G-CSF) into the first recognizable granulocytic precursor, the myeloblast. It follows a maturation process involving the different stages of promyelocyte, myelocyte, metamyelocyte, band cell and finally the mature neutrophil (von Vietinghoff and Ley, 2008).

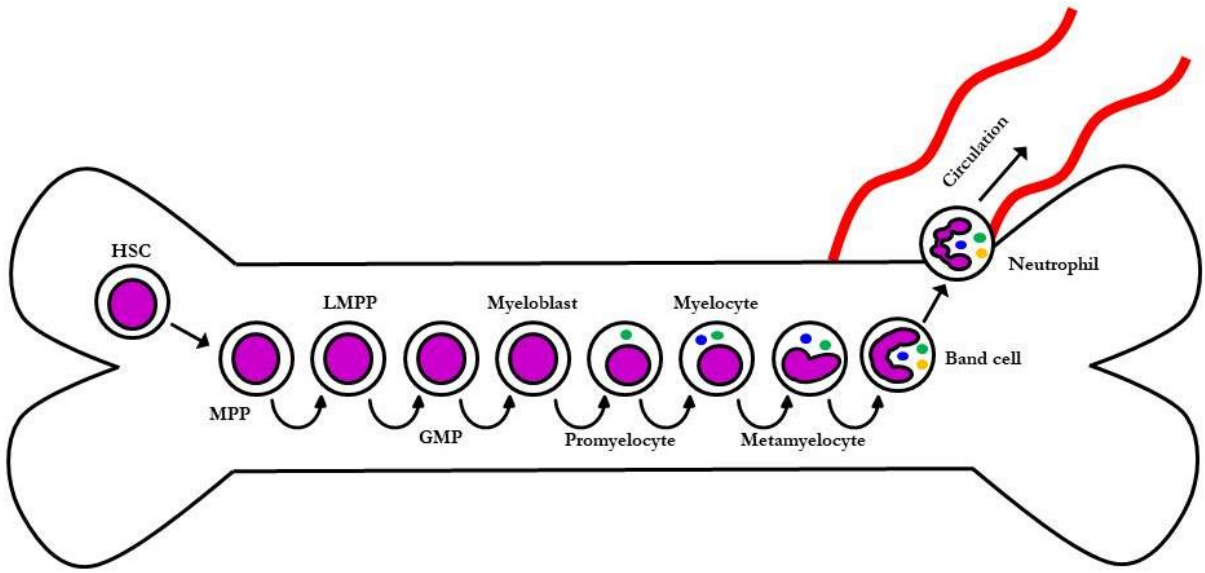

Figure 1. Granulopoiesis. In the bone marrow a self-renewing hematopoietic stem cell (HSC) gives rise to a multipotent progenitor cell (MPP). MPPs develop into lymphoid-primed multipotent progenitors (LMPPs) which differentiate into granulocyte-monocyte progenitors (GMPs). Under the control of the granulocyte colony-stimulating factor (G-CSF), GMPs turn into myeloblasts which then follow a maturation process that induces the stages of promyelocyte, myelocyte, metamyelocyte, band cell and finally the mature neutrophil which enters the circulation.

Retention of neutrophils in the bone marrow is mediated by the interaction of stromal cell-derived factor 1α (SDF-1α) secreted by osteoblasts and other bone marrow stromal cells and the chemokine (C-X-C motif) receptor 4 (CXCR4) on the neutrophil surface (Summers et al., 2010). During neutrophil differentiation G-CSF weakens the SDF-1α/CXCR4 axis by inhibition of SDF-1α secretion by bone marrow stromal cells (Petit et al., 2002) and CXCR4 expression on neutrophils (Kim et al., 2006) (**Figure 2**). Additionally, CXCR2 upregulation

supports neutrophil exit from the bone marrow. If neutrophils have to be mobilized outside the bone marrow, ligands for CXCR2 like CXCL1, 2, 5 and 8 are expressed by endothelial cells (Eash et al., 2010; Köhler et al., 2011). In order to maintain homeostasis the large-scale production of neutrophils is balanced by an equivalent removal and the characteristic short lifespan of neutrophils. Traditionally, it is estimated that circulating neutrophils undergo constitutive apoptosis after 8-12 h (Mayadas and Cullere, 2005). The survival of neutrophils invaded into tissues is prolonged up to 1-2 days with their turnover delayed due to inflammatory processes (Dancey et al., 1976). Apoptotic neutrophils express "eat-me" signals on their surface and are mainly cleared by marcophages during efferocytosis which promotes anti-inflammatory signaling and prevents secondary necrosis (Bratton and Henson, 2011). Engulfment of apoptotic neutrophils decreases the secretion of IL-23 by macrophages and dendritic cells (Stark et al., 2005), which in turn lowers the IL-17 expression by T lymphocytes (Gaffen et al., 2014). As IL-17 promotes granulopoiesis through upregulation of G-CSF (von Vietinghoff and Ley, 2008), the lowered levels of IL-17 aid to keep a steady-state release of neutrophils.

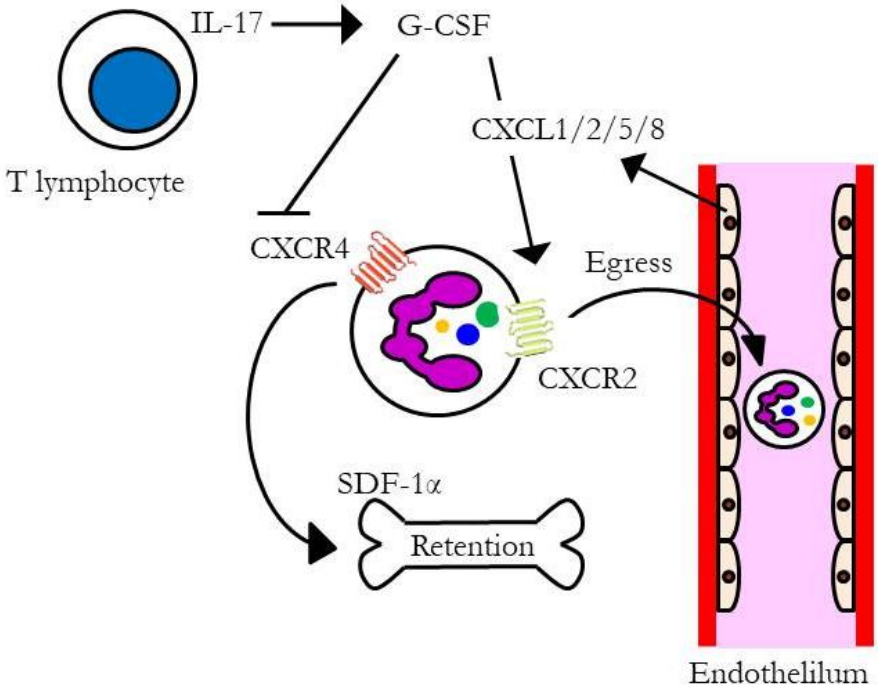

Figure 2. Regulation of the neutrophil egress from the bone marrow by the CXCR2/CXCR4 axis. The CXCR4 ligand SDF-1α which is largely expressed by osteoblasts retains neutrophils in the bone marrow. CXCR2 ligands like CXCL1, 2, 5 and 8 are expressed mainly by endothelial cells and promote neutrophil egress. The granulocyte colony-stimulating factor (G-CSF) reduces the expression of SDF-1α and CXCR4 and simultaneously upregulates the expression of CXCL2 ligands. Interleukin 17 (IL-17) produced by T lymphocytes enhances neutrophil egress from the bone marrow by increasing G-CSF release.

Neutrophil exit from the bone marrow and recruitment to the tissue

The early entry of neutrophils into a site of infection or inflammation often decides disease outcome. Within minutes after pathogen invasion, neutrophils respond to soluble factors including chemokines and cytokines and are recruited from the circulation to the site of infection. This rapid mobilization is possible through a process known as the leukocyte adhesion cascade (Ley et al., 2007). Initially, endothelial cells of blood vessels get activated and express P-, E- and L-selectin whose transient low-affinity interaction with fucosylated glycoproteins on neutrophils decelerates the flow of neutrophils and allows neutrophils to roll on the endothelium (Mayadas et al., 2014). Next, a secondary signal from immobilized chemokines on the endothelium activates the neutrophils

and induces conformational changes in β1 and β2 integrins on the neutrophil surface which allows them to bind their ligands like the intercellular adhesion molecule-1 (ICAM-1) or ICAM-2 which are expressed on inflamed endothelium (Rosales, 2018). Lastly, the neutrophils transmigrate into the peripheral tissue (Hajishengallis and Chavakis, 2013), where they follow the gradient of chemoattractants to their final site of destination (Kolaczkowska and Kubes, 2013).

Antimicrobial effector mechanisms of neutrophils

After arrival at the site of infection neutrophils have a broad antimicrobial repertoire including phagocytosis, production of reactive oxygen species (ROS), degranulation and the release of neutrophil extracellular traps (NETs) to fight invading pathogens. Interaction with microbes can be either direct, through opsonization, or through recognition of pathogen associated molecular patterns by pattern recognition receptors like toll-like receptors (TLR) (Hayashi et al., 2003), NOD-like receptors (Ekman and Cardell, 2010) and c-type lectin receptors (Kennedy et al., 2007). The receptor-mediated phagocytosis of opsonized microbes includes two prototypes, the Fcγ-mediated pseudopod extension which engulfs IgG-opsonized targets, and the complement receptor-mediated phagocytosis, during which the target appears to be sinking into the neutrophil (Allen and Aderem, 1996) and which is independent of membrane extensions or pseudopods (Underhill and Ozinsky, 2002). In neutrophils the maturation of the phagosome occurs via the rapid fusion of preformed granules to the phagosome in a calcium-dependent manner, whereby delivering antimicrobial molecules into the phagosomal lumen (Lee et al., 2003). Simultaneously, the NADPH oxidase is recruited to the phagosomal membrane and allows ROS production for efficient killing of pathogens (Karlsson and Dahlgren, 2002). In contrast to macrophages, the phagosomal pH in neutrophils does not decrease during phagosome maturation, but remains at a pH of 7 (Jankowski et al., 2002). Granules either fuse with the phagosome and contribute to the antimicrobial activities of this compartment or fuse with the plasma membrane in process of regulated exocytosis called degranulation to release their potent antimicrobial content into the tissue. Granules are specific storage organelles, which are distinguished based on their varying protein composition (**Figure 3**). The difference in protein content among neutrophil granules is not driven by protein sorting, instead the different granule proteins are synthesized during the different differentiation stages of neutrophils (Gullberg et al., 2009; Le Cabec et al., 1996). Neutrophils contain at least four different types of granules: (1) primary granules, also known as azurophilic granules named after their ability to take up the basic dye azure A; (2) secondary granules, also known as specific granules; (3) tertiary or gelatinase granules; and (4) secretory vesicles. Primary granules are developed during the differentiation from the myeloblast to the promyelocyte differentiation. With a diameter of 0.3 μM primary granules are the largest among all neutrophilic granules and contain the most important antimicrobial compounds like myeloperoxidase (MPO) (Lacy, 2005; Nüsse and Lindau, 1988), defensins, lysozyme, bactericidal/permeability increasing protein (BPI), the serine proteases neutrophil elastase (NE) and proteinase 3 (PR3) as well as cathepsin G (CG) (Faurschou and Borregaard, 2003). Secondary granules develop during the differentiation from the myelocyte to the metamyelocyte stage and have a diameter of 0.1 μM. Further, they are MPO-negative but characterized by the presence of the iron-binding protein lactoferrin and the antimicrobial compounds NGAL, hCAP-18 and lysozyme (Faurschou and Borregaard, 2003; Lacy, 2005). Tertiary granules are developed during the band stage of neutrophils. Compared to the other granule classes they are much smaller in diameter. Additionally, they are also MPO-negative and store metalloproteases like gelatinase and leukolysin (Amulic et al., 2012). Structures called secretory vesicles are also considered to be part of the granule family. In contrast to the other granule classes secretory vesicles are mainly formed during endocytosis and only a small amount forms during budding from the Golgi apparatus (Sheshachalam et al., 2014). Secretory vesicles can only be detected in mature neutrophils (Borregaard et al., 2007). Moreover, they contain plasma-derived proteins such as albumin, cytokines and their membrane serves as reservoir for membrane-bound molecules involved in neutrophil migration (Amulic et al., 2012). Upon activation of neutrophils, granules are mobilized in reverse order

to their formation during granulopoiesis, starting with secretory vesicles, followed by tertiary granules, secondary granules and finally primary granules (Rørvig et al., 2009). Especially, the fusion of secondary granules with the plasma or phagosomal membrane is of great importance for the ROS production, as flavocytochrome b558, a component of the NADPH oxidase machinery, resides in the secondary granule membrane (Jesaitis et al., 1990).

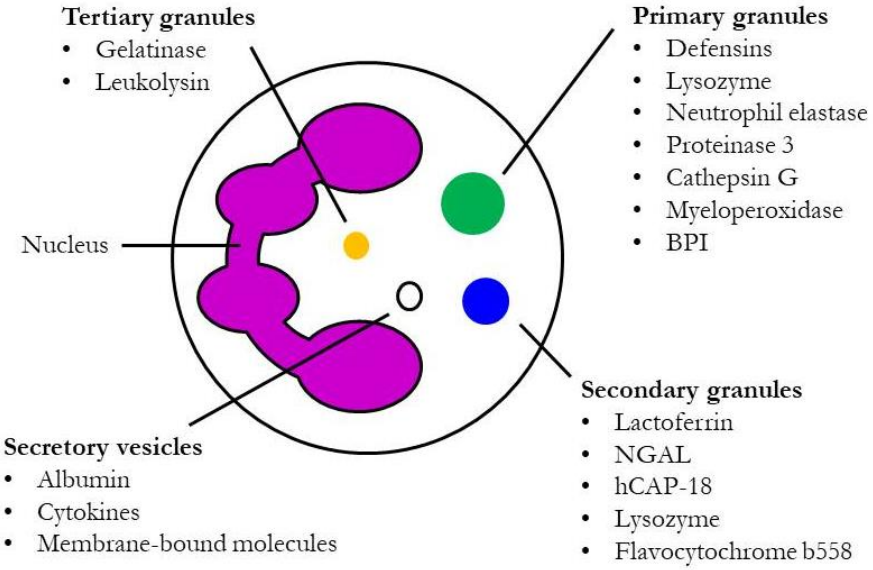

Figure 3. Neutrophil granules. Neutrophils contain primary, secondary and tertiary granules as well as secretory vesides. Each of the four granule types has specific contents, of which some are listed here, that are produced at different stages of granulopoiesis.

ROS production, i.e. oxidative burst by neutrophils greatly contributes to antimicrobial host defense. ROS can be either released extracellularly into the extracellular space at the site of infection or intracellular into the phagosome (Robinson, 2008). Initiation of the oxidative burst begins with the assembly of the multi-protein membrane-bound NADPH (Nicotinamide adenine dinucleotide phosphate oxidase/Nox2) oxidase complex at the phagosomal and plasma membrane (Lambeth, 2004), which transfers electrons from NADPH on the cytoplasmic side of the membrane to oxygen in the extracellular fluid or intraphagosomal space (**Figure 4**). The reduction of molecular oxygen leads to superoxide ($O_2^{-\cdot}$) formation (Cross and Segal, 2004). The enzyme superoxide dismutase rapidly converts superoxide to hydrogen peroxide (H_2O_2) (Nguyen et al., 2017). The superoxide dismutase and the glutathione peroxidase can convert reactive species into water to protect the host from damage of an overshooting oxidative burst (Imlay, 2008). Further, superoxide can also react with nitric oxide ($NO\cdot$) to form the highly toxic peroxynitrite anion ($OONO^-$) (Brunelli et al., 1995). Upon degranulation in the phagosome, MPO uses hydrogen peroxide to produce an array of reactive species including hypochlorous acid (HOCl) (Bokoch and Zhao, 2006). MPO can also directly convert superoxide into singlet oxygen ($^1O_2$) (Nguyen et al., 2017). Moreover, ferric iron is capable of converting superoxide and hydrogen peroxide into a hydroxyl radical ($OH\cdot$) (Nguyen et al., 2017). The direct antimicrobial action of ROS might be surpassed by downstream effects of ROS production inducing degranulation, pro-inflammatory cytokine release and generation of neutrophil extracellular trap formation (Miralda et al., 2017).

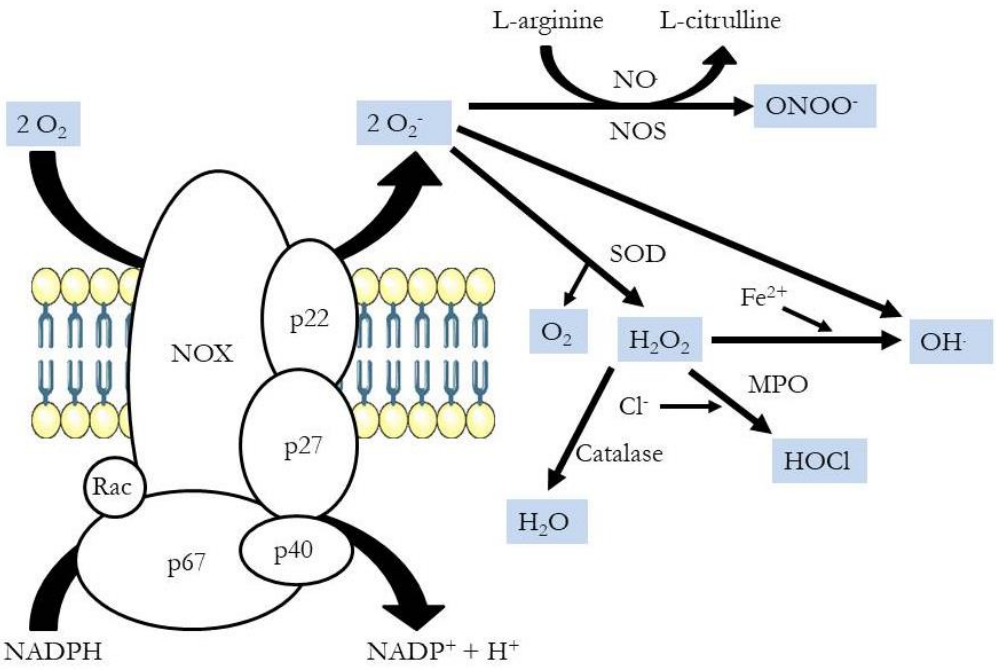

Figure 4. Radical oxygen species (ROS) production during the oxidative burst. Activation of the NADPH oxidase multiprotein complex on the outer side of the plasma membrane induces the generation of superoxide ($O_2^{-}\cdot$) from oxygen (O_2). The inducible nitric oxide synthase (NOS) generates nitric oxide ($NO\cdot$) which reacts with superoxide to form peroxynitrite anion ($OONO^-$). Superoxide can be catalyzed to hydrogen peroxide (H_2O_2) by the superoxide dismutase (SOD). Hydrogen peroxide can further react to a hydroxyl radical ($OH\cdot$) during the Fenton reaction. The myeloperoxidase (MPO) uses hydrogen peroxide as substrate for the formation of hypochlorous acid (HOCl). Enzymes like the catalase or glutathione peroxidase neutralize hydrogen peroxide by converting it to water (H_2O_2).

NETs are the manifestation of an active and neutrophil-specific cell death called NETosis (Fuchs et al., 2007). NETs are composed of a meshwork of chromatin fibers with a diameter of 15-17 mm that is decorated with granule-derived antimicrobial peptides and enzymes like NE, CG and MPO (Brinkmann, 2004). The primary functions of NETs are the trapping of pathogens including the formation of a physical barrier to limit infectious spreading as wells as killing pathogens by the increase of antimicrobial compounds in the extracellular compartment (Kruger et al., 2015). Formation of NETs is triggered by various stimuli, including microbial structures, pro-inflammatory cytokines, platelets, high-glucose medium, complement-derived peptides, activated endothelial cells, nitric oxid, cigarette smoke, monosodium urate crystals and diverse autoantibodies (Brinkmann, 2018; Hoppenbrouwers et al., 2017; Mitroulis et al., 2011; Qiu et al., 2017). Experimental induction of NETs is mainly conducted by the application of phorbol 12-myristate 13-acetate (PMA), bacterial lipopolysaccharide (LPS) and immune complexes (ICs) (Brinkmann, 2018; Takei et al., 1996). Many NET inducers lead to the activation of the protein kinase C (PKC) through ER calcium store release and opening of membrane channels that lead to cytoplasmic calcium increase. PKC, as key modulator of NETosis, is directly responsible for the NADPH activation and the oxidative burst in neutrophils (Yipp and Kubes, 2013). ROS generation further increases cytoplasmic calcium levels, which serve as cofactor for the peptidyl arginase deaminase 4 (PAD4) (Estúa-Acosta et al., 2019). Histone deamination by PAD4 is a posttranslational modification that promotes chromatin decondensation (Delgado-Rizo et al., 2017). Simultaneously, NE and MPO translocate from the cytoplasm to the nucleus, where MPO binds to chromatin and interacts with NE decondensing chromatin. In this context, ROS play a crucial role as second messenger that favor nuclear membrane disintegration as NE binds to F-actin filaments in the cytoplasm and must degrade them to enter the nucleus (Metzler et al., 2014).

Consequently, NETosis includes the breakdown of nuclear and granule membranes and the mixing of nuclear, granular and cytoplasmic contents, finally reaching its climax with a rupture in the plasma membrane and the release of NETs (Kaplan and Radic, 2012) (**Figure 5**).

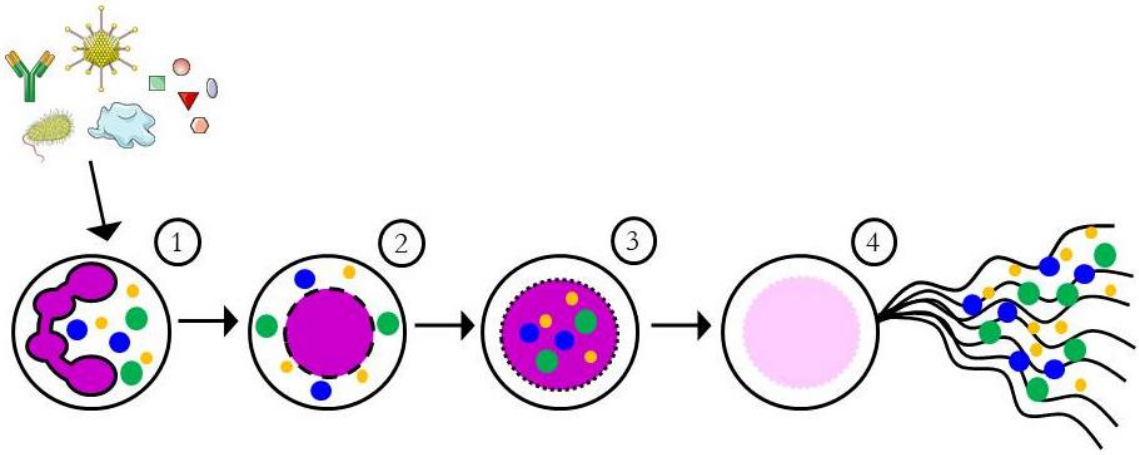

Figure 5. Formation of neutrophil extracellular traps (NETs). (1) Various stimuli, e.g. bacteria, viruses, autoantibodies, platelets, pro-inflammatory cytokines etc., activate neutrophils and induce NETosis. (2) After initiation of NETosis, the nuclear enzyme PAD4 citrullinates histones in activated neutrophils leading to chromatin condensation. Decondensed DNA with citrullinated histones and granule proteins converge in the cytosol. (3) After breakdown of the nuclear and granule membrane, the neutrophil elastase (NE) and the myeloperoxidase (MPO) translocate into the nucleus to further promote chromatin unfolding by processing histones. (4) Finally, chromatin decorated with granule proteins is expelled via vesicles from the neutrophil resulting in NET formation.

Neutrophils as host cells for pathogens

During the mutual coevolution of invading pathogens and the human immune system, several strategies have evolved that overcome neutrophil mediated host defense. Especially, *S. aureus* is capable of producing a large variation of secreted and surface-bound molecules altering and interfering with the antimicrobial functions in neutrophils (McGuinness et al., 2016). As also intracellular pathogens use neutrophils as host cells, they can manipulate signaling pathways and subvert host defense mechanisms. For example, *Chlamydia trachomatis* paralyzes neutrophils by secretion of chlamydial protease-like activating factor (CPAF) which suppresses oxidative burst and prevents neutrophil activation. Furthermore *C. trachomatis*-infected neutrophils fail to produce neutrophil extracellular traps and the bacteria are able to survive in them for an extended period of time (Rajeeve et al., 2018). The causative agent of the disease human granulocytic anaplasmosis (HGA), *Anaplasma phagocytophilum*, is one of the very few bacteria known to survive and to replicate within neutrophils (Choi et al., 2005). *A. phagocytophilum* activates expression of adhesion molecules and chemokine secretion in infected neutrophils (Akkoyunlu et al., 2001; Choi et al., 2003). At the same time oxidative burst, endothelial cell adhesion, and transmigration are inhibited by the bacterium (Banerjee et al., 2000; Choi et al., 2003, 2005). *Streptococcus pyogenes,* one of the most common human pathogens causing pharyngitis, impetigo, scarlet fever and also severe systemic disease, survives in neutrophils by preventing degranulation and fusion of primary granules with the phagosomal membrane. Furthermore, the bacterium forms large capsules after phagocytosis which enables it to survive in the hostile environment of the phagosome (Urban et al., 2006).

Immunoregulatory role of neutrophils

In addition to their antimicrobial function, recent findings have highlighted neutrophils as import source of cytokines. So far human neutrophils have been shown to express and produce upon appropriate stimulation,

many pro- and anti-inflammatory cytokines (including TNF, IL-1β, IL-1ra, IL-6), chemokines (including CXCL1, CXCL8, CXCL10, CCL2, CCL3, CCL4, CCL23), colony-stimulating and angiogenic factors (including G-CSF and VEGF), TNF family members (including TRAIL, FasL and BAFF) and growth factors (HB-EGF) (Arruda-Silva et al., 2017; Cassatella, 1999; Tamassia et al., 2014). The synthesis of cytokines by activated neutrophils can be either modulated negatively by IL-10 (Rossato et al., 2007) or positively by IFNγ (Meda et al., 1994). Due to their low amount of total RNA, neutrophils express generally lower levels of cytokines compared to other immune cells. Nonetheless, it has to be considered that this deficit is easily overcome by the high number of neutrophils (Tamassia et al., 2018). By the production and release of chemokines, neutrophils can modulate the recruitment and activation of different leucocyte populations as well as themselves. For example neutrophils have been shown to release CXCL1 and CXCL8, two chemokines that act in a feedback mechanism to recruit further neutrophils (Riedel and Kaufmann, 1997). Furthermore, neutrophils as first cells at the side of inflammation or infection can mobilize macrophages by the release of chemoattractants like CCL2 and CCL3. Neutrophils are even capable of directly modulating adaptive immunity by antigen presentation. Traditionally, only dendritic cells (DCs), B cells and monocytes/macrophages are regarded as antigen-presenting cells. As resting neutrophils show no or very little expression of MHCII and are unable to prime naïve T cell responses, they do not fulfill the classical definition of APCs (Vono et al., 2017). Nonetheless, recent findings in a mouse model have shown that CCR7 expressing neutrophils could carry an injected antigen to draining lymph nodes, a phenomenon that could not be observed in CCR7-deficient mice (Beauvillain et al., 2011). Additionally, neutrophils can capture bacteria in peripheral tissue and transport them to the lymphoid system through afferent lymphatics in pathogen induced inflammation (Abadie et al., 2005). Moreover, it has been shown that human neutrophils can present antigens to memory CD4+ T cells through HLA-DR (Li et al., 2019). Despite the low level of MHCII during their resting state, neutrophils can gain antigen presenting capacities through the stimulation with specific cytokines, like IFNγ (Müller et al., 2009). Neutrophils contain CD80, CD86 and MHCII mainly preformed in their cytoplasm. Upon stimulation the MHCII and co-stimulatory molecules are translocated to the neutrophil surface (Sandilands et al., 2005). Also the co-culture of murine neutrophils from the peritoneal cavity with CD4+ T cells induces the expression of MHCII and CD86 (Abi Abdallah et al., 2011).

Leishmania

Leishmaniasis – Clinical features

Protozoan parasites of the genus *Leishmania* (*L.*) are the causative agents of leishmaniasis, a tropical neglected disease with diverse clinical manifestations. The WHO states that leishmaniasis is endemic in 98 countries on five continents and recent estimates suggest that 12 million people are affected and 350 million people are at risk (Alvar et al., 2012). Leishmaniasis is a vector-borne disease, in which the parasite can be transmitted by approximately 30 species of Phlebotomine sandflies, including the two different genera, *Lutzomyia* (*Lu.*) and *Phlebotomus* (*P.*) (Kobets et al., 2012). Female sandflies, which suck blood for nutritional support of egg laying, transmit the parasite between various hosts. Over 20 *Leishmania* species are known to be infectious to humans. They are classified into four complexes. The two New World *Leishmania* species complexes are constituted by *L. mexicana* complex and *L. braziliensis* complex, whereas the two Old World *Leishmania* complexes are the *L. major* complex and *L. donovani* complex (Kobets et al., 2012). Depending on the infecting parasite species, leishmaniasis can manifest as: (1) cutaneous leishmaniasis (CL); (2) mucocutaneous leishmaniasis (MCL); or (3) visceral leishmaniasis (VL) (**Figure 6**) (Pearson and Sousa, 1996). CL is the most common form of leishmaniasis and is displayed as localized ulcerating skin lesion at the site of the sandfly bite that is normally self-healing. In immunosuppressed patients a diffuse or disseminated form of CL can develop with multiple nodular, ulcerative and crusted lesions covering face, trunk and extremities, leaving life-long scars, serious disability or stigma. CL is

caused by the *L. major* complex in Middle East and central Asia, the *L. braziliensis* complex and *L. mexicana* complex in America, and *L. aethiopica* in Africa (Ghorbani and Farhoudi, 2017a). An unusual variant of CL due to *L. tropica* infection is the occurrence of leishmaniasis recidivans (LR). LR recurs within the sites of previous healed CL lesions and often within the edge of the scar (Marovich et al., 2001). The onset of LR happens often two years after CL and commonly children are affected by these recurrent lesions. This specific manifestation of CL is often referred to as "chronic cutaneous leishmaniasis" (Oliveira-Neto et al., 1998). MCL manifests from days to years after CL with a dissemination of parasites from the skin to the naso-oropharyngeal mucosa leading to partial or total tissue destruction (Aliaga et al., 2003). Parasites of the *L. braziliensis* complex are responsible for the highest number of MCL cases, which is also referred to as American tegumentary leishmaniasis due to its high endemic occurrence in Latin America (Couto et al., 2014; Lessa et al., 2007). VL is the most fatal form of leishmaniasis with mortality up to 90 % if untreated. Characteristic symptoms are a persistent fever, substantial weight loss, pancytopenia and organomegaly. VL is caused by a systemic dissemination of parasites and parasite-infected macrophages from the initial site of infection to liver, spleen and bone marrow, where the parasite proliferates (Mahdy et al., 2016). The species *L. infantum* has as zoonotic reservoir dogs and causes canine and zoonotic visceral leishmaniasis (ZVL) which impedes disease control (Quinnell and Courtenay, 2009). A well-recognized complication of VL is post-kala-azar dermal leishmaniasis (PKDL) that is often observed in recovered patients infected with *L. donovani* in Sudan and India where it follows treated VL in 50 % and 5-10 % of cases (Zijlstra et al., 2003). Former VL patients remain asymptomatic for months to years until they develop progressive replication of parasites within the skin leading to the development of a skin rash consisting of macules, papules or nodules in an otherwise healthy individual. It is proclaimed that the pathogenesis of PKDL is related to an aggressive interferon γ (IFNγ) driven host response (McGwire and Satoskar, 2014). During the severe course of VL production of IFNγ by peripheral blood mononuclear cells (PBMCs) is decreased. After the treatment of VL, the production of IFNγ is resumed and IFNγ-producing cells inflict an inflammation as response against persisting parasites in the skin (Zijlstra, 2016).

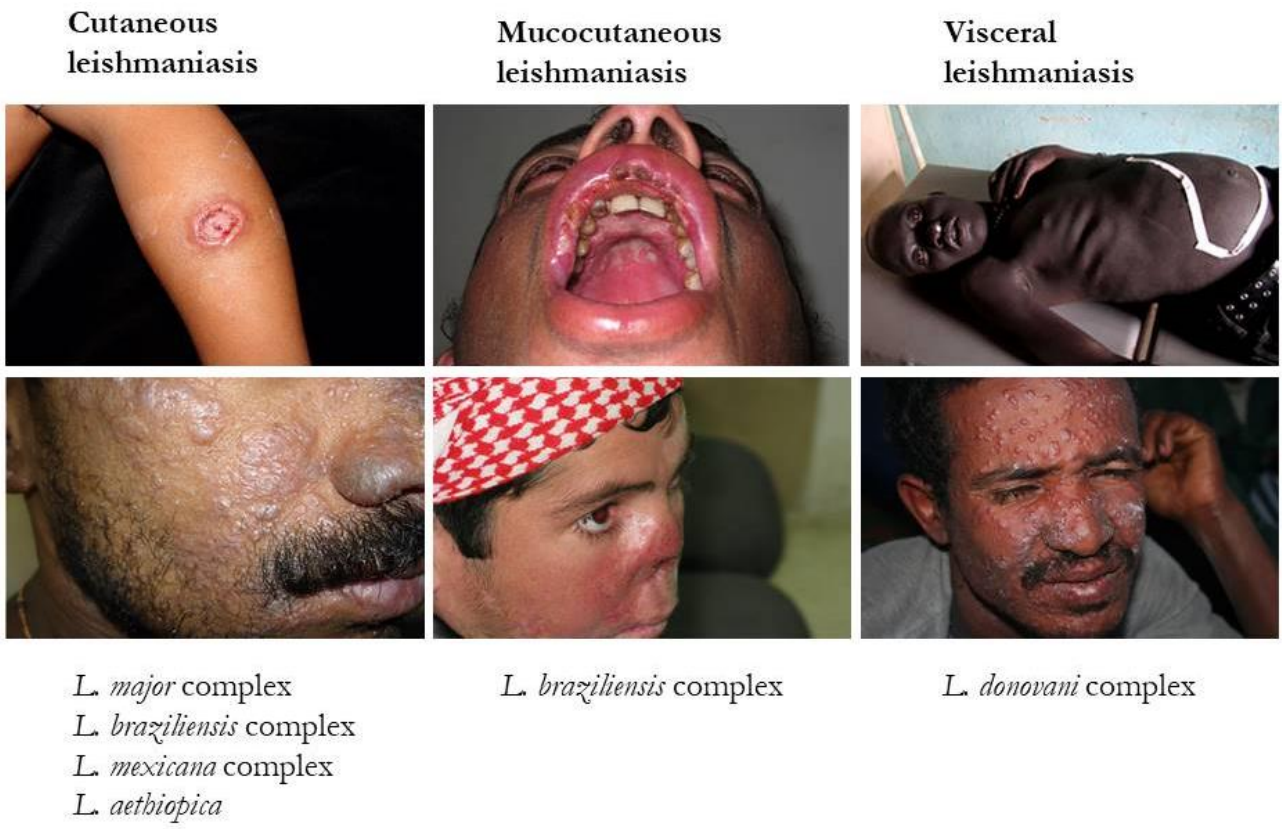

Figure 6. Clinical manifestations of leishmaniasis. The neglected tropical disease leishmaniasis manifests as cutaneous, mucocutaneous and visceral form. Cutaneous leishmaniasis (CL) is the most common form of this disease and causes localized skin lesions. Under certain immunological conditions cutaneous leishmaniasis can become diffuse or disseminated and ulcers develop all over the body. Causative agents of CL are parasites of the *L. major* complex, the *L. braziliensis* complex and the *L. mexicana* complex. In mucocutaneous leishmaniasis (MCL), lesions lead to partial or total destruction of the mucosal membranes of nose, mouth, throat cavities and surrounding tissues. MCL is caused by the *L. braziliensis* complex. Visceral leishmaniasis is characterized by irregular bouts of fever, cachexia, hepatosplenomegaly and pancytopenia. If untreated, severe cases of VL are fatal. Some patients develop post kala-azar dermal leishmaniasis (PKDL), a syndrome there skin lesions develop at variable intervals after completed VL therapy. VL is caused by parasites of the *L. donovani* complex. (Image sources https://www.who.int/leishmaniasis/en/, https://www.researchgate.net)

Biology of the *Leishmania* parasite

The taxonomy of the *Leishmania* parasites can be summarized as kingdom Protista, class Kinetoplastea, subclass Metakinetoplastina, order Trypanosomatida, family Trypanosomatidae, subfamily Leishmaniinae and genus *Leishmania* (Akhoundi et al., 2016). As member of the Trypanosomatidae family, *Leishmania* belong to the class of Kinetoplastea, whose species are characterized by containing a kinetoplast situated at the base of the flagellum. The kinetoplast is an organelle which yields a concatenated network of circular DNA, i.e. the mitochondrial DNA or mitochondrion, which is composed of minicircles and maxicircles (Ceccarelli et al., 2014). *Leishmania* have a digenic life cycle shuttling between the flagellated promastigote form that resides in the intestinal tract of sandflies and the amastigote form that lives in phagocytes of the reticulo-endothelial system of mammals. Despite their two different cell morphologies, the basic cellular organization of *Leishmania* is conserved in both forms and defined by the same basic cell layout with the kinetoplast anterior to the nucleus and a flagellum extending from the basal body (**Figure 7**) (Aleman, 1969). Cell division occurs via insertion and elongation of microtubules in a pre-existing arrangement of cross-linked sub-pellicular corset microtubules (Sunter and Gull, 2017). In addition

to the kinetoplast, the cytoplasm of *Leishmania* contains the nucleus and single-copy organelles like the Golgi apparatus (Sunter and Gull, 2017). At the base of the flagellum is the flagellar pocket, an invagination of the plasma membrane, which is the only site of endocytosis and exocytosis in the parasite (Wheeler et al., 2016). The promastigote morphology is characterized by an elongated cell body with a long flagellum emerging from the flagellar pocket providing high motility. The amastigote morphology is defined by a smaller more spherical shape fulfilling rather sensory functions as the flagellum is short, immotile and barely extending the flagellar pocket. The transition from promastigote to amastigote, and *vice versa*, is solely triggered by the temperature difference in the sandfly (27°C) and mammalian host (37°C) (Sunter and Gull, 2017), and involves substantial changes in cellular shape and surface to volume ratio. One of the most astonishing changes between promastigote and amastigote form is the transformation of a motile flagellum with a 9+2 axoneme to a short immotile flagellum with a 9+0 (9v) structure. In the process of axoneme differentiation the long flagellum is disassembled and the central pair is removed resulting in a short new flagellum with a 9v axoneme. The backward transformation is driven by the pro-basal body which assembles a 9+2 motile axoneme in the amastigote mother cells, leading to promastigote daughter cells with a motile flagellum after the first cell division (Wheeler et al., 2015). The changes in the flagellum structure are accompanied by restructuring of the flagellar pocket and its neck region as well as changes in the localization of the flagellum attachment zone proteins. The promastigote to amastigote transition induces a closing of the flagellar pocket neck minimizing the gap between the flagellum and the flagellar pocket neck membrane. This process is reversed during differentiation into a promastigote form, resulting in an opening of the neck region of the flagellar pocket, enabling the uptake of large macromolecules and increasing motility of the parasite (Wheeler et al., 2016). In addition to the clearly distinguishable promastigote and amastigote from, variations of the promastigote cell type have been described in the sandfly. Currently, four different cells types as developmental form have been recognized which have been categorized based on length/width of cell body and flagellum, namely (1) procyclic; (2) nectomonad; (3) leptomonad; and (4) metacyclic promastigotes (Rogers et al., 2002).

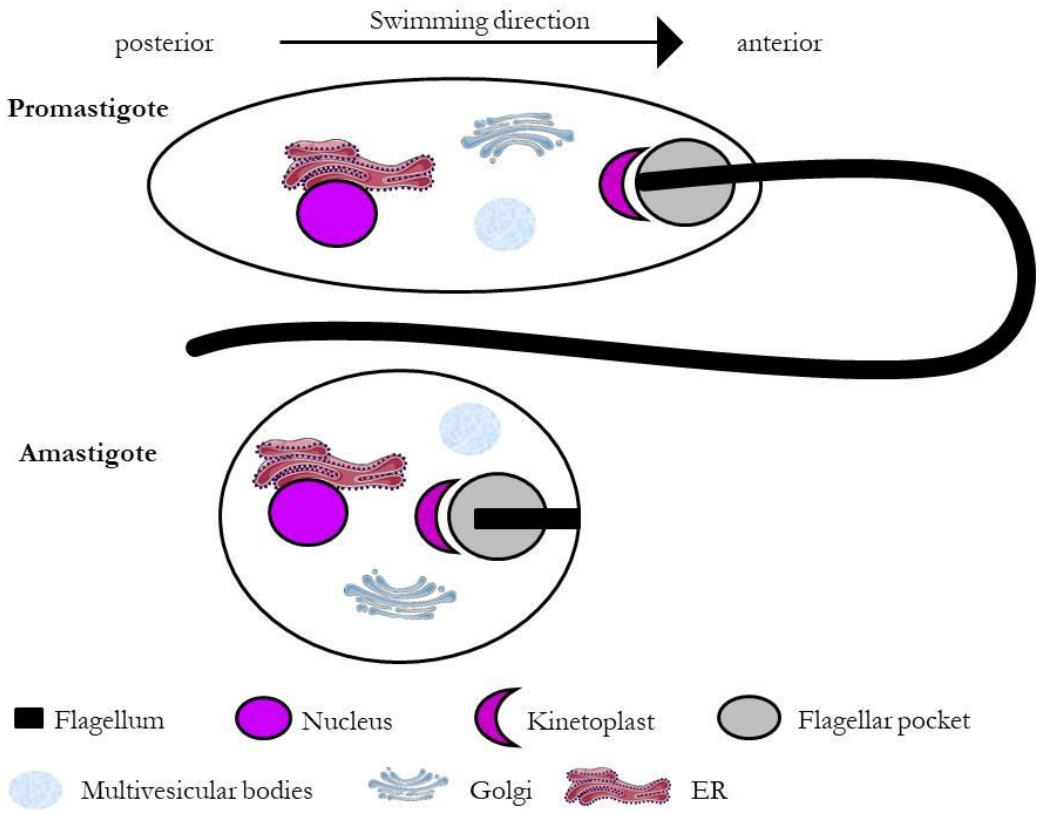

Figure 7. Schematic of promastigote and amastigote morphologies. Promastigote and amastigote morphologies aligned along the posterior anterior axis with key structures in the cells highlighted.

Leishmania life cycle

The life cycle of *Leishmania* involves a mammalian host and a sandfly as vector (**Figure 8**). During the blood meal from an infected mammal the female sandfly takes up *Leishmania* amastigotes. The transition of amastigotes to promastigotes occurs within the midgut of the sandfly, where they reproduce in high numbers in 4 to 14 days (Esch and Petersen, 2013). The presence of the invading parasite, the vascular damage and factors in the sandfly saliva act as chemoattractants and rapidly recruit neutrophils to the site of infection. Promastigotes are phagocytosed by neutrophils, in which they persist transiently (Kamhawi, 2006). Free parasites or infected neutrophils are engulfed by resident professional phagocytes, dendritic cells (DCs) and macrophages, which migrate away from the site of sandfly inoculation (Perkins and Sacks, 1985). Although Leishmania parasites live and replicate inside phagocytic cells, also other non-phagocytic cell types have been reported to be infected by *Leishmania*. Several studies show that both *Leishmania* promastigotes and amastigotes can infect murine skin or lymph node fibroblasts. Especially during the latent phase of infection, fibroblasts present a less hostile environment for the parasite than macrophages (Bogdan et al., 2000; Minero et al., 2014; Pearson and Schwartzman, 1985). Internalization into the phagolysosome of their definite host cell, the macrophage, initiates the transformation from promastigotes to amastigotes. The parasite survives the hostile environment in the parasitophorous vacuole (PV) and replicates many times by simple binary fission, which eventually ruptures the infected macrophage (Walker et al., 2014). Extracellular amastigotes are engulfed by local phagocytes leading to subsequent cycles of infection and parasitemia. Days to weeks after the initial infection a second wave of neutrophils is recruited to the site of infection, which induces a chronic inflammation (Hurrell et al., 2016). The life cycle is completed once infected phagocytes or extracellular parasites are taken up by feeding sandflies.

The axenic culture of Leishmania parasites *in vitro* has many advantages to insect and mammalian host models as it is cost-effective and allows the growth of large quantities of uncontaminated parasites under controlled conditions. For the axenic culture of *Leishmania* promastigotes a variety of media has been reported, including M199 medium (Morgan et al., 1950), Schneider´s Drosophila medium (Schneider, 1972) and Novy MacNeal-Nicolle (NNN) medium (Nayak et al., 2018). In contrast, the development of a defined medium for axenic amastigotes is challenging due to the many factors present in animal sera which are relevant for parasite persistence in the vertebrate host. Good results for the cultivation of axenic amastigotes were obtained with BHI medium and Grace´s insect medium (Siripattanapipong et al., 2019). The most crucial step for the differentiation of promastigotes towards axenic amastigotes is a temperature shift from 27°C for promastigotes to 37°C for amastigotes.

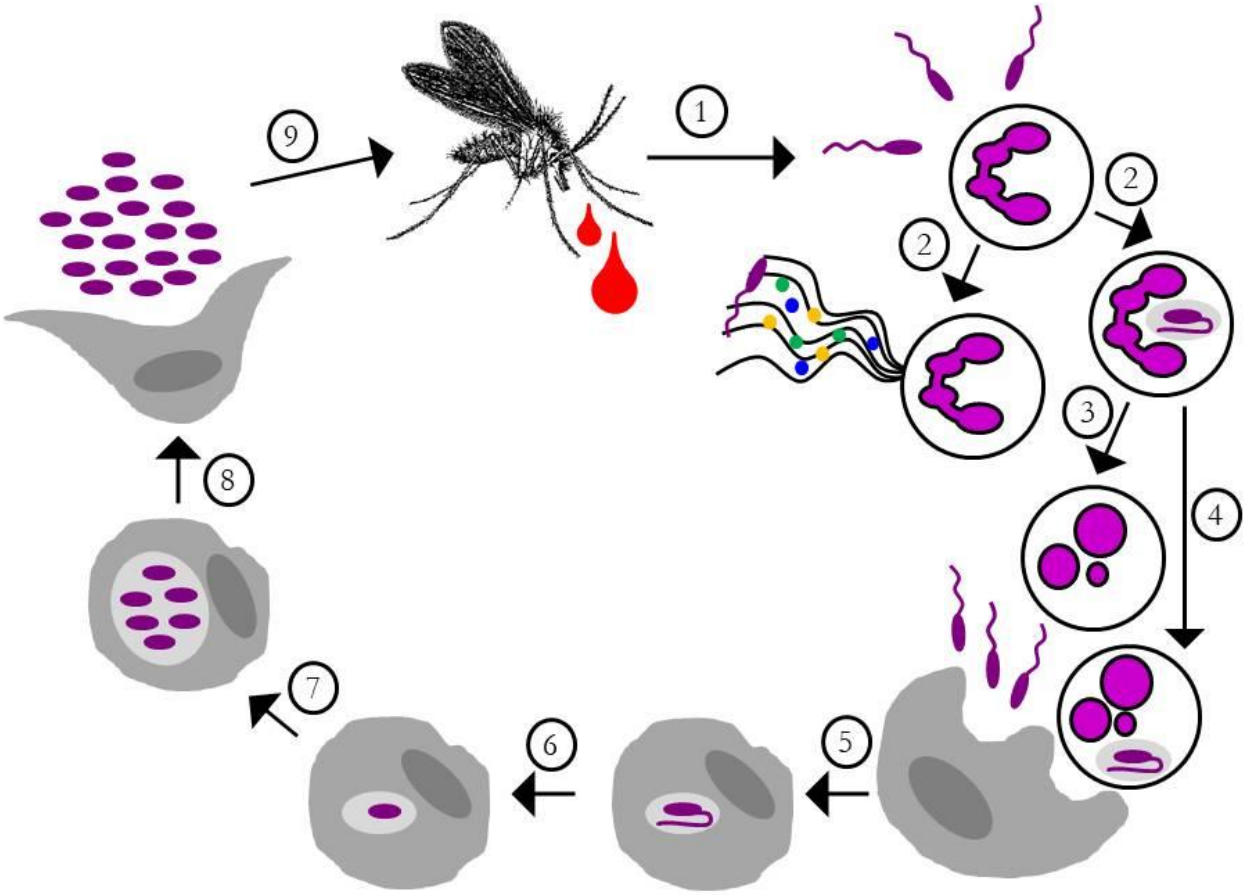

Figure 8. Life cycle of *Leishmania* parasites. (1) During its blood meal a female sandfly transmits *Leishmania* promastigotes. Chemoattractants released through vascular damage, sandfly saliva or the parasite itself rapidly recruit neutrophils to the site of infection. There, (2) *Leishmania* are either phagocytosed or killed by the induction of NETosis. *Leishmania* can use neutrophils as "Trojan Rabbit" (3) or "Trojan Horse" (4) to enter their definite host cells, macrophages, silently but can also be directly phagocytosed by macrophages (5). Within macrophages, promastigotes transform into amastigotes (6) and divide by binary fission (7). Amastigotes are released by rupturing macrophages (8) and will be ingested by a sandfly during its blood meal (9). Inside the sandfly, the amastigotes transform into promastigotes completing the *Leishmania* life cyde.

Neutrophils as host cells of *Leishmania*

Most of our current understanding of the role of neutrophils in *Leishmania* infection has been obtained by work in experimental mouse models, thus differences between human and murine neutrophils must be considered. Rapid and massive recruitment of neutrophils follows sterile needle injection of a high dose of *Leishmania* inoculum (Beil et al., 1992) and is even more pronounced during natural infection via sandfly bite (Peters et al., 2009). Several studies, including murine infection models and human *ex vivo* models, proved that neutrophils are the first cells infiltrating the site of infection. In a study with primary human neutrophils, 50 % of the neutrophils phagocytosed the co-cultured *L. major* promastigotes within 10 min (Laufs et al., 2002). Flow cytometry analysis of *L. major*-infected BALB/c mice revealed that neutrophils were already 10 h after infection present at the site of infection (Müller et al., 2001). Only after 3 days mononuclear phagocytes became the dominant cell population in cutaneous lesions of *L. major*-infected BALB/c mice (Beil et al., 1992). Recruitment of neutrophils is favored by the secretion of *Leishmania* chemotactic factor (LCF) by the parasite which induces IL-8 secretion by human neutrophils which in turn amplifies neutrophil recruitment (van Zandbergen et al., 2002). The early influx of neutrophils at the site of infection seems to be transient as neutrophil numbers return to steady state levels 3 days after *Leishmania* inoculation (Thalhofer et al., 2011). At least in CL, a second wave of neutrophils is recruited after one week in *L. major*-infected mice, an observation which is associated with lesion necrosis, ulceration and maximal parasite burden (Peniche et al., 2017). The fate of ingested *Leishmania* is still under debate. Early *in vitro* investigations on *L. donovani* infection of human neutrophils implicate parasite killing mediated by oxidative burst (Chang, 1981; Pearson and Steigbigel, 1981). An increasing number of studies describes *Leishmania* killing induced by NET formation. Although various *Leishmania* species trigger NET formation, the outcome of parasite survival upon NETosis differs between *Leishmania* species. NET formation and killing of *L. amazonensis* is mediated through the promastigote surface molecule lipophosphoglycan (LPG) (Guimarães-Costa et al., 2009), whereas *L. donovani* promastigotes survive despite NET formation and LPG was associated in this context with parasite resistance (Gabriel et al., 2010). Also the parasite-specific nuclease 3' nucleotidase/nuclease of *L. donovani* promastigotes and the endonuclease Lundep in the saliva of *Lu. longipalpis* were able to free parasites from NETs (Hurrell et al., 2015). The impact of *Leishmania* infection on neutrophil apoptosis is controversial and varies with the origin of the neutrophils (Aga et al., 2002; Laskay et al., 2008). Infection of peritoneal cavity derived human and murine neutrophils delayed neutrophil apoptosis, while *L. major* infection of neutrophils from the dermal site accelerated apoptosis (Ribeiro-Gomes et al., 2007). If the parasite survives the antimicrobial arsenal of neutrophils, it resides a transient time period within the neutrophil until it is transmitted to macrophages. Two potential transmission strategies from neutrophils to macrophages are discussed. The "Trojan Horse" model is based on silent transmission of the parasite through phagocytosis of *Leishmania*-containing apoptotic neutrophils by macrophages (Laskay et al., 2008). In contrast, the "Trojan Rabbit" model based on observations of Peters et al. describes the escape of parasites from dying neutrophils, which infect recruited macrophages (Peters et al., 2009; Ritter et al., 2009).

Leishmania – Immune response

The immune response in leishmaniasis is characterized by two general mechanisms, an innate immune response which kicks in during the early stage of infection and the adaptive immune response that serves as second line response. In addition to the early recruitment of phagocytes, also humoral factors of the complement system are affecting the outcome of the primary infection phase. Upon their entry into the mammalian dermis, *Leishmania* promastigotes activate the complement system. Complement mediated lysis by the membrane attack complex (MAC) efficiently eliminates the parasite, as the spreading of *L. amazonensis* in cutaneous lesions of BALB/c mice is inhibited by the complement system (Laurenti et al., 2004) and *L. tropica* amastigotes are susceptible to complement lysis *in vitro* (Hoover et al., 1984). By manipulation of the complement cascade, the parasite avoids lysis and promotes complement-mediated opsonization that triggers parasite uptake by phagocytes. The

Leishmania surface glycoprotein of 63 kDa (gp63) binds C3b and converts it to its inactive form (Lopes et al., 2014), C3bi, which prevents the assembly of the lytic MAC on the parasite surface. Additionally, C3bi opsonization of the parasite surface is recognized by complement receptor 3 (CR3) and favors parasite engulfment by phagocytes (Russell, 1987). The long-lasting *Leishmania* infection is established in macrophages and either mediated by infected neutrophils or phagocytosis of free parasites. In order to use macrophages for replication, the parasite has to inhibit or circumvent the antimicrobial effector mechanisms of host macrophages. *Leishmania* parasites can induce the polarization of macrophages to M1 and M2 macrophages. Differentiation towards M1 macrophages is stimulated by the pro-inflammatory cytokines IFNγ and TNF, which induce the expression of the inducible nitric oxide synthase (iNOS). This enzyme degrades arginine into OH-arginine, citrulline and NO, which makes up the major anti-leishmanial activity of macrophages (Martinez et al., 2009). In contrast, M2 macrophages are induced through the presence of different immunomodulators, like macrophage colony-stimulating factor (M-CSF), IL-4 and IL-2. M2 macrophages express arginase 1 (ARG1), which hydrolyzes arginine into urea and ornithine, the latter being further metabolized towards polyamines which support parasite growth and survival (Rath et al., 2014). Natural killer (NK) cells are a source of IFNγ and TNF, hence they favor differentiation towards M1 macrophages and CD4+ Th1 cells and induce the anti-leishmanial activity of macrophages (Ambrosio and De Messias-Reason, 2005; Scharton and Scott, 1993). NK cell exhibit a strong activation peak at 12 h to 48 h after infection, but afterwards return to steady-state levels (Bogdan, 2012). Continuous onset of NK cells from the blood stream is probably inhibited through the parasite by decrease of NK cell-attracting chemokine IP-10 production by neutrophils (van Zandbergen et al., 2002). *Leishmania* abrogate the secretion of IL-2 and IL-12 by NK cells through binding of gp63 to the NK cell surface (Lieke et al., 2008). Dendritic cells (DCs) are important APCs and play a dual role in the modulation of the host immune response against leishmaniasis. In *L. amazonensis* infection, dermal DCs, also called Langerhans cells, are associated with a Th2-type immune response, while in *L. braziliensis* infection, DCs are related to the protective Th1 immune response (Silveira et al., 2008). Of all APCs, DCs are the first cells which process and present *Leishmania* antigens to T cells inducing preferential stimulation of IFNγ activation produced by CD4+ T cells (Silveira et al., 2009). On contrary, other studies in *L. major*-infected mice revealed that DCs expand Treg cell subsets (Kautz-Neu et al., 2011). Resolution of *Leishmania* infection is established by activation and differentiation of T lymphocytes that stimulate the production of cytokines which activate infected macrophages and promote parasite killing. The murine model of *L. major* infection was initially used to define the Th1/Th2 paradigm which determines the disease outcome (**Figure 9**). The differentiation of CD4+ T cells towards Th1 cells upon antigen presentation via MHCII is associated with a healing form of leishmaniasis. The secretion of TNF, IL-1β, IL-6, IL-12, IL-18 and IL-23 creates a pro-inflammatory micro milieu which activates macrophages and induces ROS and NO production (Atri et al., 2018). Nonetheless, an overshooting Th1 response is probably associated with the high levels of TNF in the lesions of diffuse CL patients and creates a hyper-inflammatory state (Silveira et al., 2009). The Th2 response leads to a susceptible phenotype and is associated with non-healing forms of leishmaniasis. The production of IL-4, IL-13, IL-10 and TGFβ by Th2 cells enhances arginase 1 activity, polyamine synthesis and leads to IL-21 mediated down regulation of iNOS, TNF and TLR4 expression (Li et al., 2013; Muxel et al., 2018).

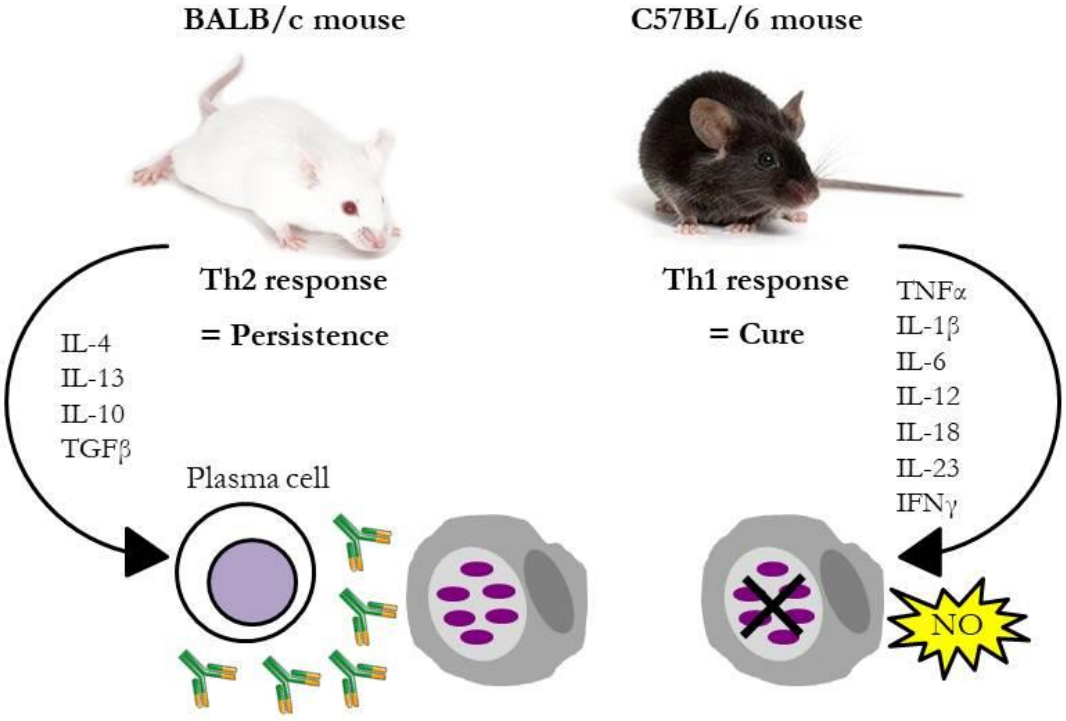

Figure 9. Th1/Th2 paradigm in leishmaniasis. A protective immune response against *Leishmania* in C57BL/6 mice is linked to the development of a Th1 response. Of all released Th1 cytokines especially IFNγ activates macrophages to produce NO, which results in parasite elimination and disease control. BALB/c mice develop a Th2 response and are therefore susceptible to *Leishmania infection*. Th2 cytokines deactivate macrophages and induce antibody formation by plasma cells leading to parasite survival and dissemination.

Recently, the role of other T cell subsets like Tregs, γδ T cells, NK T cells, Th17 cells and cytotoxic CD8+ T cells has become a matter of interest. Th17 cells release IL-17 which recruits neutrophils to the site of infection sustaining an inflammatory environment that is associated with lesion persistence and severity in CL (Gonçalves-de-Albuquerque et al., 2017). Further, Th17 cells have been associated with healing in *L. infantum* and *L. braziliensis* infection and worsened the outcome of *L. major*- and *L. guyanensis* infection (Gabriel et al., 2019) . Moreover, Th17 cells contribute to parasite dissemination and metastatic infectious lesion formation in the absence of IFNγ (Rossi and Fasel, 2018). Tregs help to maintain homeostasis within the immune system and control inflammatory processes involved in leishmaniasis pathology. IL-10-producing Tregs are associated with parasite latency, treatment resistance and disease relapse in *Leishmania* infection (Belkaid et al., 2002). In contrast, Tregs downregulate inflammatory cytokines in *L. panamensis* infection, reduce immune cells recruitment and lesion size (Ehrlich et al., 2014). In *L. braziliensis* patients $CD4^{-}CD8^{-}$ (DN) T lymphocytes were discovered which either expressed αβ T cell receptors (TCRs) or γδ TCRs. The αβ DN T cell subset was associated with a pro-inflammatory response activating macrophages, while γδ DN T cells favor the reduction of inflammatory processes (Antonelli et al., 2006). Additionally, the specialized T cell subpopulation of NK T cells was detected in

L. major-infected mice, where they appear to control the parasite burden in spleen and skin lesions, and in dermal lesions of *L. braziliensis* patients, where they exhibit a cytotoxic ability (Ferraz et al., 2017; Mattner et al., 2006). Also the role of cytotoxic CD8+ T cells ranges from protective to disease exacerbating in leishmaniasis. During *L. major* infection high numbers of CD8+ T cells can be detected during the acute and healing phase, where they control low-dose infections through the production of IFNγ (Nateghi Rostami et al., 2010). Furthermore, they have a beneficial effect during VL as they promote proper granuloma formation (Rossi and Fasel, 2018). Indeed, it has been reported that IL-10-producing CD8+ T cells lead disease dissemination and tissue destruction in MCL patients (Bourreau et al., 2007). Although *Leishmania* infection induces strong humoral responses, antibodies play a negligible role in protection and even exacerbate the disease outcome. However, a few studies describe a positive role of B cells and *Leishmania*-specific antibodies in disease control and parasite killing during *L. major* and *L. amazonensis* infection (Mukbel et al., 2006).

Modulation of host cell metabolism by *Leishmania*

Intracellular pathogens like *Leishmania* are well adapted to their host cells and have developed a broad spectrum of mechanisms to circumvent host immunity and to guarantee pathogen survival. During infection *Leishmania* use host metabolic pathways to scavenge host nutrients, as well as target metabolic pathways to abrogate the host immune response. However, although metabolic processes in both the parasite and the host may be crucial determinants of disease outcome, less is so far known on the mechanisms leading to metabolic reprogramming of the host metabolism in *Leishmania* infection.

L-arginine metabolism

The non-essential amino acid L-arginine plays a crucial role in NO-mediated *Leishmania* killing and polyamine-mediated parasite replication. L-arginine can be catabolized by the inducible nitric oxide synthase (iNOS) to NO that efficiently kills the intracellular parasite. Macrophage exposure to Th1 cytokines upregulates the expression and activity of the iNOS enzyme which increases the NO production (Bhattacharyya et al., 2002; Brandonisio et al., 2002; Green et al., 1990; Liew et al., 1991). In contrast, Th2 cytokines upregulate the expression and activity of the arginase which converts L-arginine to L-ornithine. L-ornithine serves as substrate for the ornithine decarboxylase which converts it to putrescine (Raina and Jänne, 1968). Putrescine, like spermidine and spermine, is a polyamine which is an important nutrient source for *Leishmania* and promotes parasite growth and persistence (Barksdale et al., 2004; Iniesta et al., 2002; Kane and Mosser, 2001a). The two L-arginine pathways are tightly regulated by the availability of L-arginine. Also *Leishmania* have an L-arginine metabolism, including arginase and NOS, and compete with the host cell for L-arginine whereby decreasing its availability (Wanasen and Soong, 2008). Furthermore, L-arginine is not only crucial for macrophage effector mechanisms but also influences the T cell-mediated immune response. It was shown that murine tumor-associated myeloid cells, that expressed high levels of arginase, depleted the local L-arginine pool and suppressed the T cell response by downregulation of the T cell receptor CD3ζ chain expression (Rodriguez et al., 2004; Zabaleta et al., 2004). Additionally, L-arginine depletion arrests T cells in the G_0-G_1 phase of the cell cycle (Rodriguez et al., 2007). Infection with *L. amazonensis* in humans and mice is characterized by defective T cell proliferation and activation. Local arginine depletion by upregulated arginase activity in this context might contribute to T cell hyporesponsiveness (Ji et al., 2003).

AMPK and mTOR

The AMP-activated protein kinase (AMPK) is a central regulator of energy metabolism which activity is often altered during infection. When intracellular ATP levels fall due to restricted nutrient supply, the AMP levels rise at the same time. An increase in the AMP:ATP ratio induces AMPK activity which upregulates glycolytic flux, glucose uptake and fatty acid oxidation (Inoki et al., 2012). Energy consuming processes like protein synthesis are inhibited by AMPK activation. The antagonist of the AMPK is mammalian target of rapamycin (mTOR). The activity of the mTOR kinase is crucial for the formation of the eIF4F complex for translation initiation.

Autophagy and recycling of intracellular metabolites are inversely regulated by AMPK and mTOR. While AMPK promotes the autophagic breakdown of macromolecules, mTOR suppresses autophagy (Brunton et al., 2013). Moreira et al. showed that murine macrophages infected with *L. infantum* switch from an early glycolytic metabolism to oxidative phosphorylation (Moreira et al., 2015). In this process the parasite modulates the SIRT1-LKB1-AMPK axis. An impairment of the metabolic switch by AMPK deficiency reduced parasite load *in vitro* and *in vivo*. Activated AMPK stimulates increased glucose utilization and autophagy, thus supporting parasite persistence by providing anabolic precursors for parasite growth. Consistent with this finding is a transcriptome analysis of murine macrophages infected with *L. major* which showed that glucose transport, glycolysis and starch degradation were increased in infected cells (Rabhi et al., 2012). The replication of *Leishmania* relies on GP63, which clears and inactivates mTOR, whereby reducing the type I interferone production (Jaramillo et al., 2011). The antagonistic relationship between AMPK and mTOR further supports *Leishmania* survival, as AMPK activation leads to mTOR inhibition.

Heme and iron metabolism

Despite the harsh environment within the parasitophorous vacuole (PV) of macrophages *Leishmania* amastigotes have adapted to its special micromilieu and can even acquire nutrients from this compartiment. Iron is present as inorganic iron or in form of iron-containing porphyrin, like heme, in the PV. *Leishmania* take up iron by the ferric iron reductase LFR1, the ferrous iron transporter LIT1 and the heme transporter LHR1 (Flannery et al., 2013). The capture of iron ions serves not only metabolic reactions crucial for *Leishmania* survival and multiplication but is also required for anti-oxidizing functions. The host cell enzyme heme oxygenase 1, the rate-limiting enzyme of heme degradation, is activated by *Leishmania* amastigotes. Increased heme degradation results in incomplete processing of $gp91^{phox}$, a heme containing glycoprotein that recruits components of the NADPH oxidase to the PV membrane, decreasing the superoxide production during infection (Pham et al., 2005).

Cholesterol homeostasis

Cholesterol is the major constituent of plasma membranes and lipid rafts, and plays an important role in cellular membrane organization, dynamics and signaling. Alterations in the host cell cholesterol homeostasis can also be observed during *Leishmania* infection. VL patients infected with *L. donovani* show hypocholesterolemia and reduced low-density lipoprotein (LDL) cholesterol (Lal et al., 2007). Furthermore, it was shown that *L. donovani* extracts membrane cholesterol from murine macrophages and disrupts lipid rafts, leading to the inability to stimulate T cells (Chakraborty et al., 2005; Ghosh et al., 2012). *Leishmania* disrupt the cholesterol metabolism by GP63-mediated cleavage of DICER1 which hinders the miR-122 maturation to miRNP-122, a ribonucleoprotein which regulates many enzymes in the cholesterol metabolism (Ghosh et al., 2012). Genetic and diet-induced hypercholesterolemia of C57BL/6 mice and susceptible BALB/c mice protected the animals against *L. donovani*-infection (Sen et al., 2011). Moreover, decreased cholesterol levels in the plasma membrane of murine *L. major*-infected macrophages lead to the association of CD40 with signalosome complexes which activate the ERK pathway and trigger IL-10 production (Rub et al., 2009).

Leishmaniasis treatment – Current objectives

Considered as one of the main neglected diseases on the planet, leishmaniasis affects primarily the poor population of underdeveloped or developing countries. Therefore, economically interest in the development of new pharmaceutical compounds is low, despite the urgent need for alternative drugs and new treatment strategies. First line drugs and gold standard of anti-leishmanial therapy since the 1920s are pentavalent antimonials. Unfortunately, treatment with pentavalent antimonials has witnessed a drastic increase in clinical resistance during the last decade. For example, over 60 % of VL patients in the Indian state Bihar do not respond to treatment with pentavalent antimonials due to acquired resistance. The precise mechanism of action of pentavalent antimonials is so far unknown, however some studies suggest that their anti-leishmanial activity

involves the inhibition of the parasite adenosine diphosphate phosphorylation of DNA I topoisomerase and trypanothione reductase (Cobo, 2014). Pentavalent antimonials are highly toxic. Cardiotoxicity, nephrotoxicity, hepatotoxicity and the tendency to induce pancreatitis have been proven (de Menezes et al., 2015). Second-line drugs against leishmaniasis are pentamidine and amphotericin B. Utilization of pentamidine is only rare due to emerging resistance and high cytotoxicity including important adverse effects, such as diabetes mellitus, severe hypoglycemia, hypotension, myocarditis and renal toxicity that can ultimately cause death (Singh et al., 2012b). Currently, pentamidine is used in combined therapeutic protocols (Croft and Coombs, 2003) and for prevention of relapse in patients that were successfully cured with another drug but have a high risk of secondary relapse to HIV or another immunodeficiency (Patel and Lockwood, 2009). An abundance of evidence suggests that the site of action for pentamidine is the mitochondria of the parasites. Treatment with pentamidine leads to enormous expansion of mitochondrial morphology, followed by condensation and disruption of kinetoplast DNA (Croft & Brazil, 1982). Amphotericin B has good *in vitro* activity against *Leishmania* parasites but its use in clinical treatment is limited due to adverse effects like fever, chills, nephrotoxicity, hypokalemia, myocarditis and even death, as well as a very low bioavaiability (Ghorbani and Farhoudi, 2017b). Liposomal formulations of amphotericin B were developed to increase tissue penetration and to reduce toxicities (Adler-Moore and Proffitt, 2002). The mechanism of action of amphotericin B and its formulations is drug-binding to parasite ergosterol precursors causing disruption of parasite membrane (Sundar and Jaya, 2010). Another anti-leishmanial compound is paromomycin, an aminoglycoside, with a broad antimicrobial activity spectrum. As paromomycin must be applied by intramuscular injections resulting side effects include ototoxicity, injection site pain and raised liver enzymes (Lockwood and Moore, 2010). Treatment with paromomycin is the cheapest leishmaniasis therapy. The mechanism of action of paromomycin is associated with interference with the protein synthesis through 16S RNA (Maran et al., 2016). Miltefosine, an original anti-cancer agent, was identified as anti-leishmanial drug during the 1990s (Kuhlencord et al., 1992). High oral efficacy and a short treatment period are the main advantages of this drug, whereas its teratogenicity effects and long life span that favors drug resistance, are its major drawbacks (Lockwood and Moore, 2010). An often reported but mild side effect of miltefosine is gastrointestinal discomfort. Miltefosine opens shingosine-activated plasma membrane calcium channels and directly affects acidocalcisomes in the parasite (Pinto-Martinez et al., 2017).

Status of vaccine research for leishmaniasis

To date, several approaches to develop anti-leishmanial vaccines have been tested, however no efficiently protective vaccine for humans is available yet. First generation vaccines were composed of whole killed parasites with variable potency to induce a sufficient immune response leading to inconclusive results (Noazin et al., 2008). Most of the vaccine studies of the second generation are based on recombinant proteins, poly-proteins, DNA vaccines or dendritic cells loaded with peptides from a *Leishmania* antigen. Usage of gp63, the best characterized virulence factor of *Leishmania*, as potential vaccine antigen resulted in negative T cell responses in humans (Russo et al., 1991). Several other antigens from different *Leishmania* species were tested in animal models. These include amastigote cysteine proteases (CP) (Rafati et al., 2005), cysteine proteinase A2 and amastigote membrane proteins P4 and P8 (Soong et al., 1995), kinetoplastid membrane protein-11 (KMP-11) (Basu et al., 2005), amastigote LCR1 (Streit et al., 2000), hydrophilic acylated surface protein B1 (HASPB1) (Stäger et al., 2000), leishmanial antigen ORFF (Tewary et al., 2005), acidic ribosomal protein P0 (Iborra et al., 2003), paraflagellar rod protein 2 (PRP-2) (Saravia et al., 2005), NH36, a main component of the fucose-mannose ligand (Aguilar-Be et al., 2005) and proteophosphoglycan (PPG) (Samant et al., 2009). In addition, molecules such as ATP synthase alpha chain, beta-tubulin and heat shock 70-related protein 1 precursor have been recently identified as novel vaccine candidates (Bhowmick and Ali, 2009). So far, only the second generation approach with Leish-111f managed to enter clinical trials (Coler and Reed, 2005). Leish-111f is a fusion polyprotein formed by combination of the *L. major* homologue of eukaryotic thiol-specific antioxidant (TSA), the *L. major* stress-inducible protein-1 (LmSTI1)

and the *L. braziliensis* elongation and initiation factor (LeIF) (Coler and Reed, 2005). Leish-111f protected mice against *L. major* and *L. amazonensis* infection (Skeiky et al., 2002), but failed to prevent infection and disease development in dogs (Gradoni et al., 2005). Nonetheless, human phase I and II clinical trials have been conducted in Brazil, Peru, Columbia and India. Although human vaccines are not ready for the market yet, the two fractionated first-line vaccines Leishmune® and CaniLeish® protect dogs efficiently against canine leishmaniasis and block the parasite transmission from dog to human (Wylie et al., 2014). Leishmune® is based on the fucose-mannose ligand (FML) which is expressed in all cycles of *Leishmania* spp. The production of CaniLeish® is based on extracted secreted proteins of *L. infantum* (LiESP). Also molecules from the sandfly saliva were tested in vaccine approaches. The compounds maxadilan (Morris et al., 2001) and SP15 (Valenzuela et al., 2001) showed a protective effect against CL. Immunization of hamsters with LJM19 was protective against VL (Gomes et al., 2008). Moreover, a study with non-human primates showed that animals exposed to uninfected sand fly bites or immunized with the salivary protein PdSP15 were protected against cutaneous leishmaniasis induced by infected bites (Oliveira et al., 2015). Additionally, immunization of dogs with vector salivary proteins appeared promising as a significant IFNγ production was induced (Collin et al., 2009). As most vaccine approaches tested so far did not result in long-term immunity, vaccines based on live-attenuated parasites might become an appealing alternative in nearby future (Kedzierski, 2010).

Host-directed therapies (HDTs) in leishmaniasis

An increasing problem is treatment failure of leishmaniasis patients. Drug resistance is a fundamental aspect of treatment failure however the causes for treatment failure are multifactorial. Although long neglected but of crucial importance are host factors and the state of the immune system. Especially, patients with immunodeficiency, like in *Leishmania*-HIV coinfection are particularly vulnerable, as the *Leishmania* infection accelerates HIV replication and the progression to AIDS. Further, many of the anti-leishmanial drugs require an effective immune response. A new strategy to overcome drug resistance and treatment failure are host-directed therapies (HDTs), also known as host-targeted therapies. HDTs aim to interfere with host cell factors that are required for pathogen replication or persistence. Further, they enhance protective immune responses and reduce exacerbated inflammation. HDTs are used to target specific host-derived pathways that promote the disease development or boost an immune response against the pathogen. Also approaches to introduce HDTs as treatment of leishmaniasis are in progress. Repurposing of the anti-cancer agent imatinib, an inhibitor of the Abl/Arg kinase family of tyrosine kinases, which are involved in phagocytosis of *Leishmania* promastigotes, reduced efficiently the uptake of opsonized and non-opsonized parasites and dampened lesion severity in mice (Wetzel et al., 2012). Blocking of phosphoinositide-3 kinase γ, an enzyme mediating cell migration by initiating actin cytoskeletal reorganization in leukocytes, resulted in significant impairment of parasite entry into phagocytes (Cummings et al., 2012). Ibrutinib, a small molecule inhibitor of Bruton´s tyrosine kinase overexpressed in malignant B cells, can bind the IL-2 inducible kinase (ITK) on T lymphocytes and promotes a Th1 polarized immune response (Dubovsky et al., 2013). Berberine chloride, a quaternary isoquinoline, that promotes phosphorylation of p38 in MAPK signaling, upregulates NO and IL-12 production and downregulates IL-10 production during *L. donovani* infection (Saha et al., 2011). Statins are HMG-CoA inhibitors and are commonly used to regulate cholesterol levels. As only the optimal cholesterol levels in the phagocyte allow parasite entry, chronic cholesterol depletion with statin or cholesterol enrichment in the plasma membrane of macrophages reduced parasite invasion (Kumar et al., 2016). The opiod-receptor antagonist Naloxonazine upregulates the vacuolar ATPase proton pump in parasitophorous vacuoles of phagocytes. Although amastigotes are resistant to acidic pH, promastigotes are eliminated before they can transform into amastigotes.(De Muylder et al., 2016). Also natural components like pentalinonsterol, isolated from the roots of a native plant of the Yucatan peninsula or mahanine, carbazole alkaloid isolated from a native plant on the Indian subcontinent, upregulate NO and ROS production in macrophages and drive a Th1 immune response (Oghumu et al., 2017; Roy et al., 2017).

Furthermore, microRNAs (miRNAs) are promising host targets for new therapeutic strategies as they have been implicated to play an important role in VL infection of macrophages and DCs (Geraci et al., 2015).

Neutrophil heterogeneity in health and disease

Traditionally, neutrophils are considered to be a short-lived, terminally differentiated homogenous pool of cells with low transcriptional activity that does not recirculate. Lately, this dogma was replaced by the scientific acceptance that neutrophils have unexpected high phenotype heterogeneity with distinct functions under both steady state and pathologic conditions. Already in the 1980s it was reported that circulating neutrophils can show differences in effector functions like phagocytosis and oxidative burst, but with the state of knowledge and technical possibilities it was impossible at that time to confirm the importance of neutrophil subpopulations (Gallin, 1984). A driving factor of the renaissance of emerging neutrophil subpopulations was the discovery of new and highly specific markers for neutrophils.

In addition to neutrophil subpopulations detected during pathologic conditions, also neutrophil markers have been described that represent distinct neutrophil subsets in homeostasis including CD177 and olfactomedin (OLFM-4) (Silvestre-Roig et al., 2016). The surface glycoprotein CD177 is a 55 kDa glycosyl-phosphatidylinositol-anchored receptor whose abundance on the neutrophil surface varies highly between different individuals (Stroncek et al., 1996). As CD177 serves as a receptor for the proteinase 3 (PR3), all CD177-positive neutrophils also selectively present PR3 on their cell surface (Bauer et al., 2007). The CD177-PR3 interaction is poorly understood, but was recently addressed to modulate neutrophil transmigration as ligation of CD177 promotes immobilization of neutrophils at stimulated endothelial cells via β2-integrin signaling (Bai et al., 2017). OLFM-4 is post-transcriptionally regulated glycoprotein present in the secondary granules of 20-25 % of all circulating neutrophils. Although no clear functional difference between OLFM-4-positive and –negative neutrophils have been described yet, OLFM-4 inhibits the activation of several granular proteases, including CG, NE and PR3 (Clemmensen et al., 2012). Also "senescent" or "aged" neutrophils can be considered as neutrophil subpopulation. Changes in the surface receptor expression have been observed, including increased levels of CD18 and reduced levels of ICAM-3 in human neutrophils (De Martinis et al., 2004; Valente et al., 2009) and reduced CXCR2 signaling in murine neutrophils (Nomellini et al., 2012). Besides aging promotes overactivation of neutrophils as shown through increased CD11b expression and a higher susceptibility for NET formation. Further subpopulations include angiogenic neutrophils which are recruited under ischemia conditions to hypoxic areas where they facilitate restoration of oxygen supply in the affected tissue (Christoffersson et al., 2012), and circulating neutrophils which express a repertoire of TCR variants on their surface (Puellmann et al., 2006).

Numerous changes in neutrophil phenotype have been identified in pathological conditions of infection and inflammation. Two different neutrophil subpopulations, PMN-I and PMN-II, have been identified in an experimental murine model of methicillin-resistant *Staphylococcus aureus* (MRSA) infection. These two subpopulations developed from normal neutrophils (PMN-N). PMN-I were isolated from MRSA-resistant mice and expressed TLR2, 4, 5 and 8, secreted IL-12 and CCL3, and activated M1 macrophages. In contrast, PMN-II expressed TLR2, 4, 7 and 9 and activated M2 macrophages (Tsuda et al., 2004). Neutrophil populations resembling PMN-I and PMN-II were also detected in a mouse model of *Candida albicans* infection. A CD80+ neutrophil subpopulation was also described which expanded upon *C. albicans* hyphae exposure, released IL-10 and inhibited CD4+ T cell proliferation (Mencacci et al., 2002). In a model of *Trypanosoma cruzi* infection neutrophils first displayed an inflammatory response against the parasite, but after migrating into the liver their phenotype changed towards IL-10 producing neutrophils which inhibited IFNγ production and CD4+ T cell proliferation (Tosello Boari et al., 2012). Moreover, a distinct population of neutrophils with a $CD11b^{+}Ly6C^{+}Ly6G^{+}$ phenotype was identified in vaccinia virus-infected tissues where they produce high levels

of type I interferons (Fischer et al., 2011). Analysis of circulating neutrophils in a LPS-stimulated sepsis model revealed the presence of a $CD16^{dim}$ neutrophil subpopulation with reduced capacity to interact with opsonized bacteria and impaired ROS production. At the same time a $CD16^{bright}$ neutrophil population was detected which showed increased antimicrobial functions and enhanced ROS production (Pillay et al., 2010). Based on these findings it was proposed that the $CD16^{dim}$ neutrophils increase susceptibility to infections, while the $CD16^{bright}$ neutrophils contribute to tissue damage. In a subsequent study the existence of an immunosuppressive mature hypersegmented neutrophil population with the surface marker profile $CD16^{bright}CD62L^{dim}CD11b^{bright}CD11c^{bright}$ was reported (Pillay et al., 2012). This neutrophil subpopulation exhibited suppressive effects on T cell proliferation through expression of Mac-1 and local release of ROS into the interspace between neutrophils and T cells. The presence of different neutrophils subpopulations in autoimmune disorders is well studied. A very prominent example is systemic lupus erythematosus (SLE) in which so-called low-density granulocytes (LDGs) were detected. LDGs owe their name their localization in the PBMC fraction during density gradient sedimentation. LDGs in SLE express high levels of type I interferons, TNF and IFNγ (Denny et al., 2010). Furthermore, they show decreased phagocytic capacity and undergo spontaneous NETosis. Generation of autoantibodies to NET-components triggers the inflammation in a positive feedback loop (Villanueva et al., 2011).

Neutrophil subpopulations in cancer

In the recent decade, the traditional belief that neutrophils act as mere bystanders in the tumor microenvironment has been revolutionized and the active contribution of neutrophils in tumor initiation, development and progression has become a matter of increasing interest. Neutrophils accumulate in the peripheral blood of cancer patients and make up a substantial proportion of immune cells infiltrating the solid tumor. Neutrophilia is a common characteristic of cancer-associated chronic inflammation and is often accompanied by relative lymphocytopenia, reflecting a drastic decline in cell-mediated adaptive immune response. In cancer patients a high neutrophil-to-lymphocyte (NLR) ratio is associated with poor survival outcome (Howard et al., 2019). Although the existence of different neutrophil subpopulations in cancer is highly accepted, the characterization and differentiation of diverse subpopulations is challenging due to the lack of clear membrane-bound markers.

TANs

Fridlender et al. reported the influx of neutrophils in tumors in a murine cancer model (Fridlender et al., 2009). This phenotypically distinct neutrophil population termed tumor-associated neutrophils (TANs) exhibits high plasticity and manifests as two antagonistic phenotypes, the anti-tumorigenic N1 phenotype and the pro-tumorigenic N2 phenotype. This nomenclature is conform with the well-established tumor-associated macrophage (TAM) subsets, the anti-tumorigenic M1 phenotype and the pro-tumorigenic M2 phenotype (Beyrau et al., 2012).

G-MDSCs

Another cell population detected in tumor-bearing mice and cancer patients are myeloid-derived suppressor cells (MDSCs) (Gabrilovich et al., 2012), which exhibit a granulocytic (G-MDSC) or monocytic (M-MDSC) phenotype and are characterized by their ability to suppress T cell proliferation (Ostrand-Rosenberg and Fenselau, 2018). G-MDSCs share many morphological and functional features with neutrophils and are polymorphonuclear (Christoffersson and Phillipson, 2018). G-MDSCs promote tumor progression, inhibit antitumor immunity, and are a hindrance to many cancer immunotherapies. Presently it is unclear whether N2 TANs are G-MDSCs and if they share a common origin. Transcriptome analysis of G-MDSCs compared with TANs and naïve neutrophils in mice with AB12 mesothelioma tumors revealed three distinct populations (Fridlender et al., 2012). Although naïve neutrophils lack the immune suppressive activity of N2 TANs and G-MDSCs, their mRNA repertoire is

more related to G-MDSCs, while the transcriptome of TANs and G-MDSCs show less similarities. Major differences could be observed for cytokine and MHC antigen presentation.

LDNs

Information regarding cancer-related neutrophils is mainly acquired from isolation of circulating blood neutrophils by using a density gradient. During cancer the distribution of neutrophils in the fraction of the density gradient is different than under healthy conditions. Normally, the major population of neutrophils is found in the high-density granulocytic fraction, whereas a small population of neutrophils is found in the low-density mononuclear fraction, where PBMCs accumulate (Böyum, 1968). In contrast to high-density granulocytes (HDGs) that are mature, tumor-associated mouse and human low-density granulocytes (LDGs) consist of mature and immature neutrophils (Sagiv et al., 2015). The mature LDGs have a segmented nucleus and are derived from HDGs in a TGFβ-dependent shift (Liu et al., 2017). The immature LDGs have banded or ring-shaped nuclei. As origin of immature LDGs the bone marrow and spleen are discussed, where these cells fail to undergo terminal differentiation. LDGs rapidly accumulate in the circulation, whereas HDGs appear after approximately 48 h in the circulation. As newly formed neutrophils enrich first in the LDG fraction, it is suggested that these cells rapidly left the bone marrow. LDGs are negligible in healthy individuals, but their numbers expand rapidly during tumor development and all LDGs are pro-tumorigenic, displaying immunosuppressive properties (Silvestre-Roig et al., 2016).

Currently it is unclear, whether there is any overlap between LDGs, N2 TANs and G-MDSCs with regard to their similar pro-tumorigenic phenotype. Rather than focusing on the extreme ends of the spectrum, it is discussed to define neutrophil subpopulations in cancer as a continuum of behavior reflecting their properties to aid or abate the process of tumor development (Eruslanov et al., 2017; Grecian et al., 2018). Most data of neutrophils in cancer is derived from murine models with transplantable tumors, whose development is very different compared to the gradual evolution of a natural tumor. So far N1 and N2 TANs have only been detected in mice and the concepts of human TANs has not been verified yet. Additionally, there is a lack of human data as human tissue from later stages of cancer are rarely obtained. Peripheral blood is much easier available than solid tumors, but the behavior of blood neutrophils might differ from that of TANs. Even if tumor samples are acquired, neutrophil behavior might change due to disaggregation and extraction methods.

Neutrophil recruitment into the tumor

As solid tumor are composed of various cell types including tumor cells, infiltrating immune cells and stromal cells like fibroblast and endothelial cells, all these cells shape the tumor microenvironment and influence neutrophil recruitment and polarization. The mobilization of neutrophils to the tumor site follows the expansion and maturation of neutrophils in the bone marrow, their intravasation into circulation and their attraction to the tumor following a gradient of released chemoattractants (**Figure 10**). Responsible for neutrophil recruitment to the tumor site is mainly the CXCR1/CXCR2 axis. Multiple cells in human tumors produce CXCR2 chemokines as CXCL1-3, CXCL5-8 and migration inhibitory factor (MIF) (Uribe-Querol and Rosales, 2015). Many chemoattractants like CXCL8 and CXCL2 act in an autocrine manner as infiltrated neutrophils release them and attract even more neutrophils to the tumor. Another crucial regulator of neutrophil recruitment is IL-17 which is also positively linked with neutrophil numbers in the tumor microenvironment (Akbay et al., 2017). IL-17 was found to upregulate the expression of G-CSF in human renal proximal tubular epithelial cells (Hirai et al., 2012), Il-6 and CCL2 in human colonic myofibroblasts (Hata et al., 2002), and the CXCR2 ligands CXCL1 and CXCL5 in human gastric cancer (Li et al., 2017). Main source of IL-17 in mice bearing mammary tumors were δγ T cells which upon IL-1β stimulation secreted high levels of IL-17 (Coffelt et al., 2015). Similarly to G-CSF, some human cancers show increased GM-CSF expression levels elevating the number of circulating neutrophils (Urdinguio et al., 2013). One study using the murine colon adenocarcinoma C-26 cell line suggests that CD8+ T

cells promote neutrophil recruitment to the tumor site through IFNγ secretion (Stoppacciaro et al., 1993). Moreover, CXCL12 and VEGF are discussed to act as chemoattractants for human neutrophils (Grunewald et al., 2006; Lyden et al., 2001) as both are upregulated in a wide variety of tumors, especially under hypoxic conditions (Santiago et al., 2011). Additionally, neutrophil recruitment into tumors is regulated by IFNβ. Although IFNβ does not directly regulate CXCR2, it controls the release of CXCL1, 2 and 5 in tumor-bearing mice (Masucci et al., 2019).

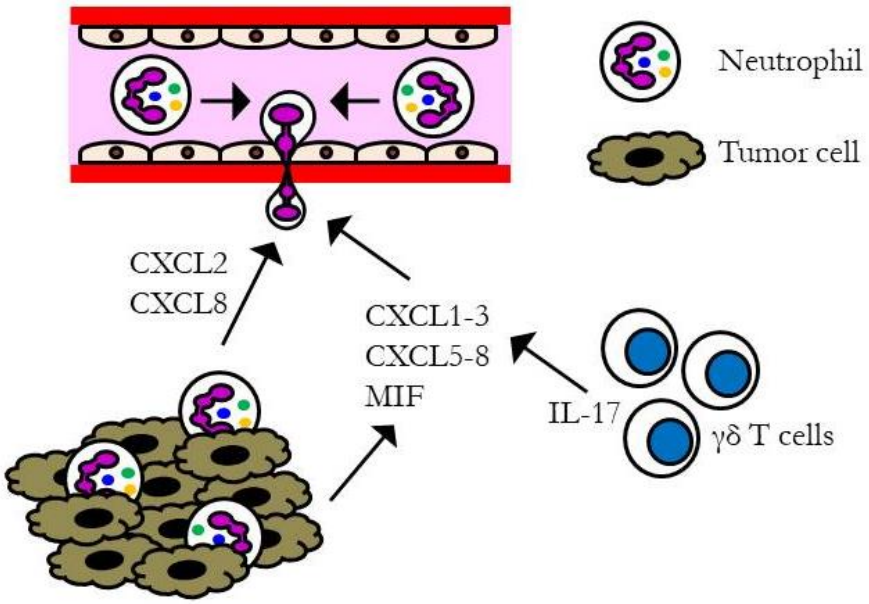

Figure 10. Mechanism of neutrophil recruitment into the tumor. Tumor cells produce chemoattractants like CXCL1-3, CXCL5-8 and MIF to recruit neutrophils from the circulation. Tumor-associated neutrophils (TANs) can also produce CXCL2 and CXCL8, the most potent chemoattractant for neutrophils, creating a positive loop for more neutrophil infiltration into the growing tumor. IL-17 released by γδ T cells upregulates the expression of CXCR2 ligands and is positively linked with high neutrophil numbers in the tumor microenvironment.

Neutrophil polarization in the tumor microenvironment

Factors in the tumor microenvironment modify the phenotype and function of neutrophils and induce the polarization into distinct subpopulations. One of the main modulators of neutrophil polarization in murine tumor models is TGFβ as it promotes the N2 phenotype (Fridlender et al., 2009). Upon inhibition of TGFβ, murine N2 TANs acquire the cytotoxic phenotype of N1 TANs suggesting that neutrophil plasticity allows the transition between both phenotypes depending on the presence of certain factors in the microenvironment (**Figure 11**). Besides TGFβ, neutrophil polarization is primarily controlled by IFNβ that stimulates N1 while inhibits N2 polarization in mice and humans (Andzinski et al., 2016). Another immunosuppressive modulator that might be linked to N2 polarization is prostaglandin E2 (PGE2), which was proven to switch the phenotype of M1 macrophages to M2 macrophages in a human mesenchymal stromal cell 3D spheroid model (Ylöstalo et al., 2012). Studies in murine lung carcinoma and mesothelioma models indicate that the anti-tumorigenic N1 phenotype is present at the early stage tumor, whereas it is converted towards the pro-tumorigenic N2 phenotype during tumor progression (Mishalian et al., 2013). N1 polarized neutrophils have a short life-span and display a mature phenotype with a segmented nucleus. In contrast, N2 polarized neutrophils are long-lived cells and

display an immature phenotype with a circular nucleus (Zhang et al., 2016). The potent anti-tumor activity of murine N1 TANs is mainly mediated through the release of pro-inflammatory cytokines like IL-12, TNF, GM-CSF, VEGF, CCL3, CXCL9 and CXCL10 which recruit and activate CD8+ T cells (Scapini et al., 2000). Further murine N1 TANs are characterized by a TNF^{high}, $CCL3^{high}$, ICAM-1^{high} and $arginase^{low}$ profile, while murine N2 TANs are characterized by upregulation of the chemokines CCL2, 3, 4, 8, 12, and 17 and CXCL1, 2 and 8 (Fridlender and Albelda, 2012). As compared to murine N2 TANs, murine N1 TANs produce more superoxide and hydrogen peroxide and higher levels of Fas, TNF, CCL3, and ICAM-1, but lower levels of CCL2, CCL5, VEGF, CXCR4, MMP-9 and arginase (Fridlender and Albelda, 2012). The strong immunosuppressive activity and the potential to promote tumor angiogenesis, invasion and metastasis in cancer patients is further promoted by the release of various factors like hepatocyte growth factor (Wislez et al., 2003), oncostatin M (Brandau et al., 2013), ROS (Powell and Huttenlocher, 2016), RNS (Powell and Huttenlocher, 2016), MMPs and NE (Dumitru et al., 2013). In addition to the tumor cells, also other cells present in the tumor microenvironment have the potential to polarize neutrophils. For example, human neutrophils co-cultured with TNF-primed mesenchymal stromal cells acquired an immunosuppressive phenotype (Zhu et al., 2014) and IL-6 production by human gastric cancer mesenchymal stem cells directed N2 polarization (Hu et al., 2014). Also the metabolism of cancer cells that is reprogrammed from that of normal cells forms the surrounding micromilieu. Cancer cells preferentially utilize glycolysis, instead of oxidative phosphorylation, for energy metabolism even in the presence of oxygen. This phenomenon is known as the "Warburg effect" (Warburg, 1956; Warburg et al., 1927). Glycolytic metabolism of glucose results in lactic acid, which can acidify the tumor microenvironment after being released by cancer cells (Cairns et al., 2006; Gatenby and Gillies, 2004; Justus et al., 2013). Furthermore, tumor-induced hypoxia can further increase cellular glycolysis as well as lactic acid production and accumulation in the tumor microenvironment due to rapid cancer growth and defective blood vessel perfusion. In addition to glucose, cancer cells also utilize lipids, amino acids, and other substrates for metabolism and biosynthesis (Yang, 2017).

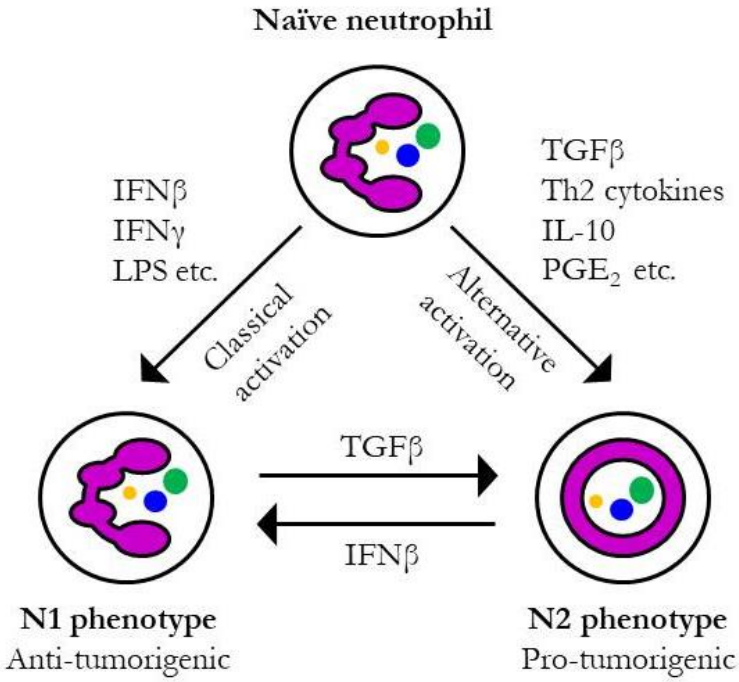

Figure 11. Tumor-associated neutrophil polarization in the tumor microenvironment. Neutrophils develop anti-tumor properties once they are polarized towards a N1 phenotype. These cells get classically activated through microbial components, e.g. LPS, IFNγ and particularly IFNβ. Exposure of naïve neutrophils to immunosuppressive components like

TGFβ, IL-10, PGE_2 or an excessive Th2 response induces the polarization towards the pro-tumorigenic N2 phenotype. TGFβ can drive the transition of N1 to N2, whereas IFNβ is a potent driver of the transition in the opposite direction.

Pro-tumor role of neutrophils

Pro-tumor activities of neutrophils are summarized in **Figure 12**.

ROS

Several studies indicate that neutrophils play an important role in tumor development, progression and metastasis. The release of ROS by neutrophils in the tumor microenvironment can promote tumor growth indirectly. Hypochlorous acid (HOCl) is generated from hydrogen peroxide (H_2O_2) by MPO and activates extracellular matrix (ECM) degrading enzymes, the matrix metalloproteinases (MMP), like MMP-2, -7, -8 and -9 that promote the proliferation of tumor cells and angiogenesis through VEGF which is released by extracellular matrix degradation (De Larco et al., 2004; Shabani et al., 1998). Furthermore, HOCl is inhibiting the tissue inhibitor of metalloproteinases (TIMP-1), thus enhancing the proteolytic activity of MMPs. A more dangerous and direct effect of the oxidative burst and its products, like HOCl, is genotoxicity driving oncogenic transformation (Cadet and Wagner, 2013). ROS-mediated genotoxicity induces oxidative DNA damage and MPO-catalyzed activation of chemical carcinogens (Knaapen et al., 2006). Additionally, ROS are involved in tumor progression as they stabilize HIF-1α which promotes increased production of VEGF and MIF that support tumor development and chemotherapy resistance in an in breast cancer patients (Parekh et al., 2018). ROS can also damage epithelial cells and induce inflammation which promotes tumor development (Coffelt et al, 2016). H_2O_2 serves as messenger in the MAPK, Erk1/2, IKK/NF-κB and PI3/Akt pathway which are upregulated in cancer patients and tumor-bearing mice (Liou and Storz, 2010). Exposure of CD8+ T cells to ROS induces tolerance against tumor-specific antigens in EL-4 tumor-bearing mice (Nagaraj et al., 2007).

Proteases

The proteases CG, NE and MMP-9 are derived from neutrophil granules and act pro-tumorigenic. CG degrades ECM molecules like fibronectin and attenuates the binding between integrin and fibronectin resulting in protease-resistent E-cadherin-mediated homotypic cell-cell adhesions. These tumor cell aggregates allow tumor cells to disseminate to distant sites and to initiate metastasis (Morimoto-Kamata et al., 2012). In the human breast cancer cell line MCF-7, CG facilitated the E-cadherin-dependent formation of spherical cell aggregates and supports tumor migration (Yui et al., 2014). Moreover, CG can enhance TGFβ signaling and promotes angiogenesis through upregulation of VEGF in a murine bone invasion model (Wilson et al., 2010). NE promotes tumor cell growth through interaction with the PI3K and EGFR/MEK/ERK signaling pathway in human tumor cell lines (Yang et al., 2016). Further it increases TGFβ levels in the tumor microenvironment of human gastric carcinoma cells (Wada et al., 2006). NE enters tumor cells via clathrin-coated vesicles and localizes at early endosomes there it acts as on the insulin-receptor substrate (IRS-1). Moreover, NE can promote tumor cell migration as it induces the loss of E-cadherin on the tumor cell surface (Gaida et al., 2012). Both, CG and NE promote metastasis by degradation of the anti-tumor protein Thrombospondin 1 (Tsp1) (El Rayes et al., 2015). Neutrophils are the major source of MMP-9 for tumor cells as this enzyme has not been identified in tumor cells yet. MMP-9 is involved in ECM remodeling during tumor progression and supports angiogenesis, since MMP-9 is responsible for the proteolytic release of VEGF sequestered in the ECM (Ebrahem et al., 2010). As neutrophils lack TIMP, they release proMMP-9 which can be activated easier and has a much longer lasting effect than MMP-9 from other cells types (Ardi et al., 2007, 2009). Another granule-derived enzyme, the arginase 1, exerts an immunosuppressive effect in tumors by inhibiting T cell proliferation as degradation of extracellular arginine results in decreased T cell CD3 ζ chain expression (Sippel et al., 2011).

Cytokine and growth factors

Also the cytokines oncostatin M and hepatocyte growth factor released by neutrophils have pro-tumorigenic potential. Oncostatin M, a member of the IL-6 superfamily, facilitates angiogenesis through induction of VEGF expression in a human breast cancer model (Queen et al., 2005). The hepatocyte growth factor activates the proto-oncogene c-met and promotes tumor cell spreading in a study using human HepG2 hepatocellular carcinoma cells (Imai et al., 2005).

NETs

NETs can play a driving role in tumor progression. Proteases like NE presented on NETs can directly interact with tumor cells and enhance their proliferation (Sangaletti et al., 2014). Furthermore, neutrophils can capture circulating tumor cells and promote tumor cell metastasis (Cools-Lartigue et al., 2013). The level of NETs in the plasma of cancer patients is significantly increased compared to healthy controls (Oklu et al., 2017). Additionally, high levels of NETs lead to early relapse in cancer patients as NETs can awaken dormant cancer cells. Proteases like MMP-9 and NE present on the surface of NETs remodel laminin which in turn activates α3β1 signaling to awaken dormant cancer cells (Albrengues et al., 2018).

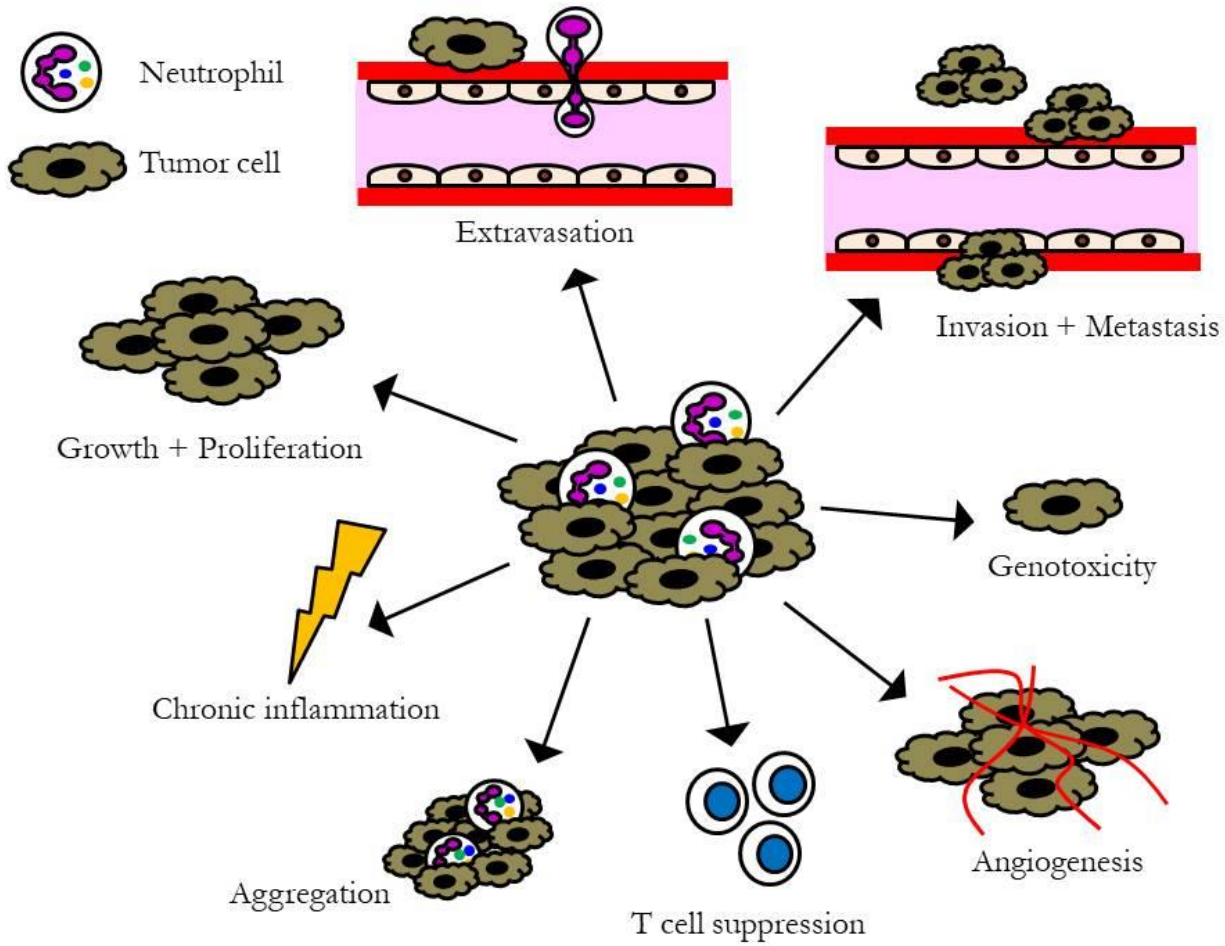

Figure 12. Pro-tumor activities of neutrophils. Tumor-associated neutrophils (TANs) can promote tumor development, progression and metastasis. TANs secrete matrix metalloproteinase 9 (MPP-9) which induces the release of vascular endothelial growth factor (VEGF) through extracellular matrix remodeling that can support angiogenesis. The release of several cytokines like TNF, IL-6, IL-12 or IL-1β induces a chronic state of inflammation in the tumor microenvironment.

Serin proteases like neutrophil elastase (NE) and cathepsin G (CG) released from neutrophil granules directly promote tumor cell growth and proliferation. The production of reactive oxygen species (ROS) has genotoxic effects on tumor cells and increases the accumulation of mutations in tumor cells. Upregulation of arginase 1 expression in neutrophils inhibits T cell proliferation and creates an immunosuppressive state. Moreover, neutrophils can induce leaky vasculature facilitating extravasation, aggregation and invasion of tumor cells thereby initiating metastasis.

Anti-tumor role of neutrophils

Despite the growing evidence that the presence of TANs exacerbates the tumor progression, the cytotoxic behavior of neutrophils against tumor cells was already recognized in the 1970s (Bubeník et al., 1970). Several studies indicate that physical contact between neutrophils and tumor cells is a crucial requirement for neutrophil-mediated tumor cell cytotoxicity (Granot et al., 2011; Lichtenstein and Kahle, 1985). Neutrophils need a specific polarization to exert their ant-tumor activities as N1 phenotype (Sionov et al., 2015). Anti-tumor activities of neutrophils are illustrated in **Figure 13**.

ROS

ROS like H_2O_2 and HOCl are directly involved in the anti-tumor activity of N1 TANs. HOCl delivered directly at the tumor cell membrane induces cell lysis (Dallegri et al., 1991). The production of singlet oxygen can eliminate efficiently tumor cells of rapidly growing tumors at the early phase of tumor development in rats (Zivkovic et al., 2005). Furthermore, H_2O_2 production prevents metastasis formation in a murine breast cancer model (Granot et al., 2011). Murine tumor cell death by H_2O_2 is mediated via Ca^{2+} influx through the TRPM2 Ca^{2+} channel (Gershkovitz et al., 2019). Moreover, the proto-oncogene c-met attracts neutrophils by promoting migration across the endothelium. Interaction between c-met and its ligand, the hepatocyte growth factor, induces the release of nitric oxide (NO) by neutrophils and causes tumor cell killing in mice (Finisguerra et al., 2015).

Apoptosis of tumor cells

Neutrophils can also induce apoptosis of certain tumor cells like A549 cells mediated through the Fas ligand/Fas interaction (Sun et al., 2018). Furthermore, apoptosis of malignant cells can be induced via the tumor necrosis factor-related apoptosis inducing ligand (TRAIL) (Fulda, 2014). TRAIL, as a member of the TNF superfamily, binds two death receptors (TRAIL-R1 and TRAIL-R2) and three decoy receptors (TRAIL-R3, TRAIL-R4 and osteoprotegerin) on its target cell which activates the formation of a death-inducing signaling complex for caspase activation and initiation of apoptosis (Bodmer et al., 2000). An important advantage of the TRAIL-mediated tumor cell apoptosis is its specificity as normal cells and tissue are not harmed (Brincks et al., 2013). Another killing mechanism of neutrophils (Iliopoulos et al., 1989) involving perforin and granzymes as observed for NK cells has been proposed (Bodduluru et al., 2015).

MMP-8

Although the majority of neutrophil-released proteases are pro-tumorigenic, some reports indicate an anti-tumor role for MMP-8. Neutrophil mobilization by MMP-8 is mediated by the generation of a chemotactic Pro-Gly-Pro peptide (Lin et al., 2008). In a murine lung carcinoma model and breast cancer patients MMP-8 prevented metastasis formation by regulating tumor cell adhesion and invasion (Gutiérrez-Fernández et al., 2008; Wu et al., 2019).

ADCC

The most important mechanism by which neutrophils eliminate tumor cells is antibody-dependent cell-mediated cytotoxicity (ADCC), a mechanism that describes the lysis of an antibody-opsonized target cell mediated by an Fc receptor (FcR) bearing effector cell. Matlung et al. demonstrated that human neutrophils exert a trogocytosis-related process, named trogoptosis, which induces necrotic cell death of antibody-opsonized tumor cells (Matlung

et al., 2018). Neutrophil express several subtypes of FcRs capable of inducing ADCC including FcγRI (CD64), FcγRIIa (CD32), FcγRIIIa (CD16a) and FcγRIIIb (CD16b) (Iliopoulos et al., 1989; Kushner and Cheung, 1992; Otten et al., 2007; Valerius et al., 1993). Recently, it was shown that the most potent inducer of ADCC is the high affinity receptor for IgA, FcαRI (CD89) (Brandsma et al., 2019).

T cell activation

N1 neutrophils exert their anti-tumor activity not only by cytotoxic mechanisms but also by eliciting other anti-tumor adaptive immune responses. In a cancer model with rats, N1 TANs were shown to prime anti-tumor CD8+ T cells with tumor-specific antigens (Tanaka and Sendo, 1993). Furthermore, human N1 TANs secrete potent T cell chemoattractants and can increase T cell proliferation and cytokine production via TNF, CG and NE (Tillack et al., 2012). The cooperation between tumor-infiltrating neutrophils and CD8+ T cells is necessary to generate a tumor-specific primary and memory CD8+ T cell response after phototherapy (Kousis et al., 2007).

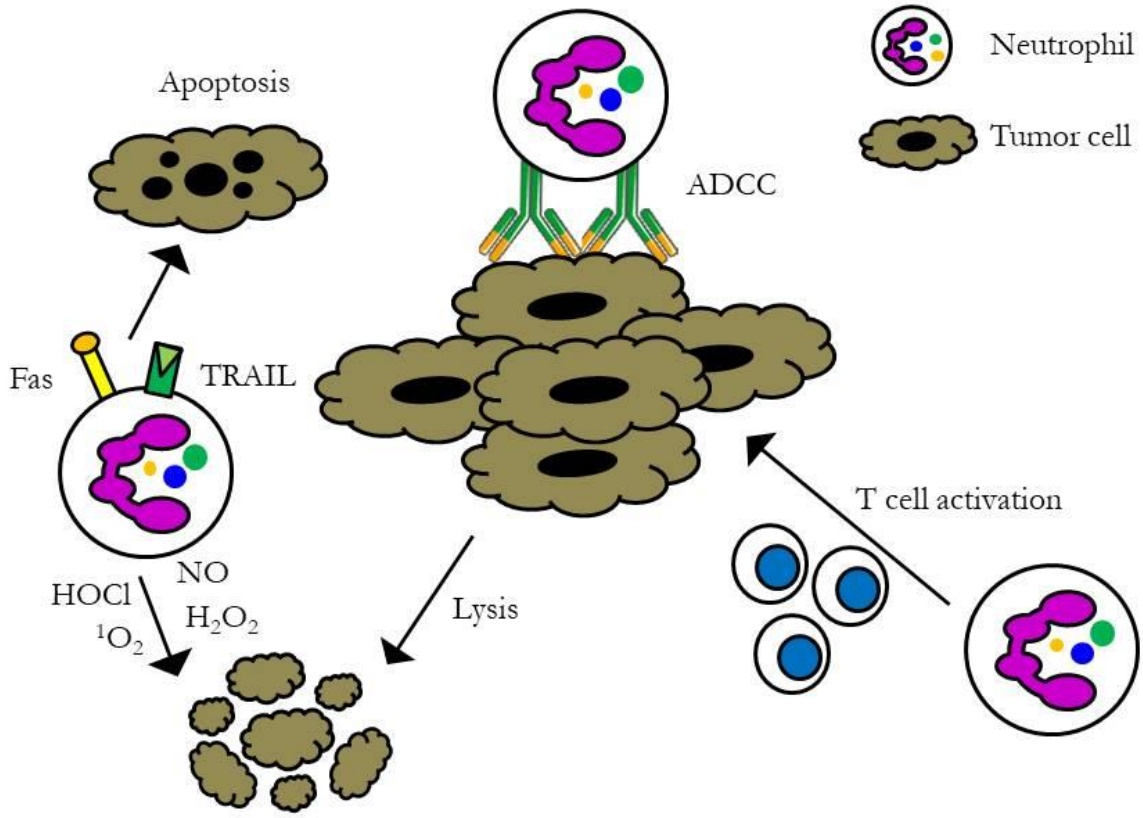

Figure 13. Anti-tumor activities of neutrophils. Production of reactive oxygen species (ROS) like hypochlorous acid (HOCl), hydrogen peroxide (H_2O_2), singlet oxygen ($^1O_2$) and nitric oxide can directly damage tumor cells. The most effective anti-tumor mechanism is antibody-dependent cell-mediated cytotoxicity (ADCC). Antibodies bind to tumor cell antigens and are recognized by Fc receptors on neutrophils. This binding induces a cytotoxic response against the tumor cell. Pro-inflammatory neutrophils can also mediate T cell activation against tumor cells. Furthermore, neutrophils can either by release of tumor necrosis factor-related apoptosis inducing ligand TRAIL or by binding via Fas induce apoptosis of tumor cells.

Neutrophil metabolism

Major metabolic pathways in neutrophils

An overview of the key metabolic pathways in neutrophils is presented in **Figure 14**. Glycolysis is the major metabolic pathway in circulating neutrophils. Extracellular glucose is taken up primarily by glucose transporter 1 (GLUT1) embedded in the neutrophil plasma membrane, although also GLUT3 and GLUT4 are expressed (Maratou et al., 2007). In the neutrophil cytosol glucose is transformed into glucose-6-phosphate (G6P) by the hexokinase. The consumption of one molecule G6P leads to the production of two molecules ATP, NADH and pyruvate. In the absence of oxygen, pyruvate is reduced through the activity of the lactate dehydrogenase into lactate during anaerobic glycolysis. Meanwhile lactate is released by the neutrophil. During aerobic glycolysis pyruvate enters the tricarboxylic acid (TCA) cycle in the mitochondria by its conversion to acetyl-coenzyme A (acetyl CoA) which provides the reducing cofactors NADH and $FADH_2$ which generate ATP through the electron transport chain (ETC) (O'Neill et al., 2016). Depending on glucose abundance, neutrophils store glucose in form of glycogen bodies that on demand provide glucose-based glycolytic intermediate supply (Robinson et al., 1982; Sadiku et al., 2017).

Another glucose-dependent pathway in neutrophils is the pentose phosphate pathway (PPP) that is also known as the hexose monophosphate shunt, which involves an oxidative and non-oxidative phase. During the oxidative phase G6P is converted into CO_2, ribulose-5-phosphate and NADPH, while during the non-oxidative phase ribulose-5-phosphate is converted into nucleic acids, sugar phosphate and glycolytic precursors (Injarabian et al., 2019).

Neutrophils also have a pronounced glutamine metabolism, especially under glucose-limiting conditions (Curi et al., 1997). Glutamine enters the cells via several solute carrier type transporters (SLCs) like the sodium-coupled neutral amino acid transporter (SNAT) family. Once glutamine has reached the neutrophil´s cytosol, it is not completely oxidized and enters as glutamate the mitochondria. During glutaminolysis, glutamate is further converted into α-ketoglutarate, which oxygenates NAD^+ to NADH, it can enter the TCA cycle and produces malate. Malate is further metabolized to pyruvate by the malate dehydrogenase which oxygenates $NADP^+$ to NADPH (Newsholme et al., 1999).

Under resting conditions mitochondria do not contribute significantly to neutrophil energy metabolism and participate primarily in the initiation of apoptosis. However, in a study by Fossati et al. the role of mitochondria in oxidative burst, chemotaxis and activation of neutrophils was highlighted (Fossati et al., 2003). Through oxidation of acetyl-CoA the TCA cycle produces several metabolites of oxidative phosphorylation. The generation of ATP occurs in a series of redox reactions creating an electrochemical membrane potential ($\Delta\psi_m$) through coupling of electron transfer and proton pumping via four complexes in the inner mitochondrial membrane. The four complexes are the NADH-ubiquinone oxidoreductase (complex I), the succinate-ubiquinone oxidoreductase (complex II), the ubiquinol-cytochrome c oxidoreductase (complex III) and the cytochrome c oxidase (complex IV). In neutrophils, $\Delta\psi_m$ is maintained through the transfer of electrons from glycolysis to complex III via the glycerol-3-phosphate (G3P) shuttle (van Raam et al., 2008). Although in most cells ATP synthesis is coupled to the mitochondrial membrane potential, this seems to be inconsistent for neutrophils (van Raam et al., 2008). Furthermore, mitochondria are involved in the fatty acid oxidation (FAO) as fatty acids in the cytosol are converted into fatty-acyl CoA esters by acyl-CoA synthases and enter mitochondria for subsequent oxidation. After dehydrogenation, hydration, a further dehydrogenation reaction and finally thiolysis one molecule of acetyl-CoA, NADH, $FADH_2$, fatty acyl-CoA and one proton are formed. After the first reaction, the fatty acyl-CoA ester is shortened by two carbon atoms and re-enters FAO to be re-oxidized until

only two acetyl-CoA molecules remain. Acetyl-CoA enters the TCA cycle and is oxidized to CO_2 and H_2O generating additional protons and molecules of $FADH_2$ and NADH (Injarabian et al., 2019).

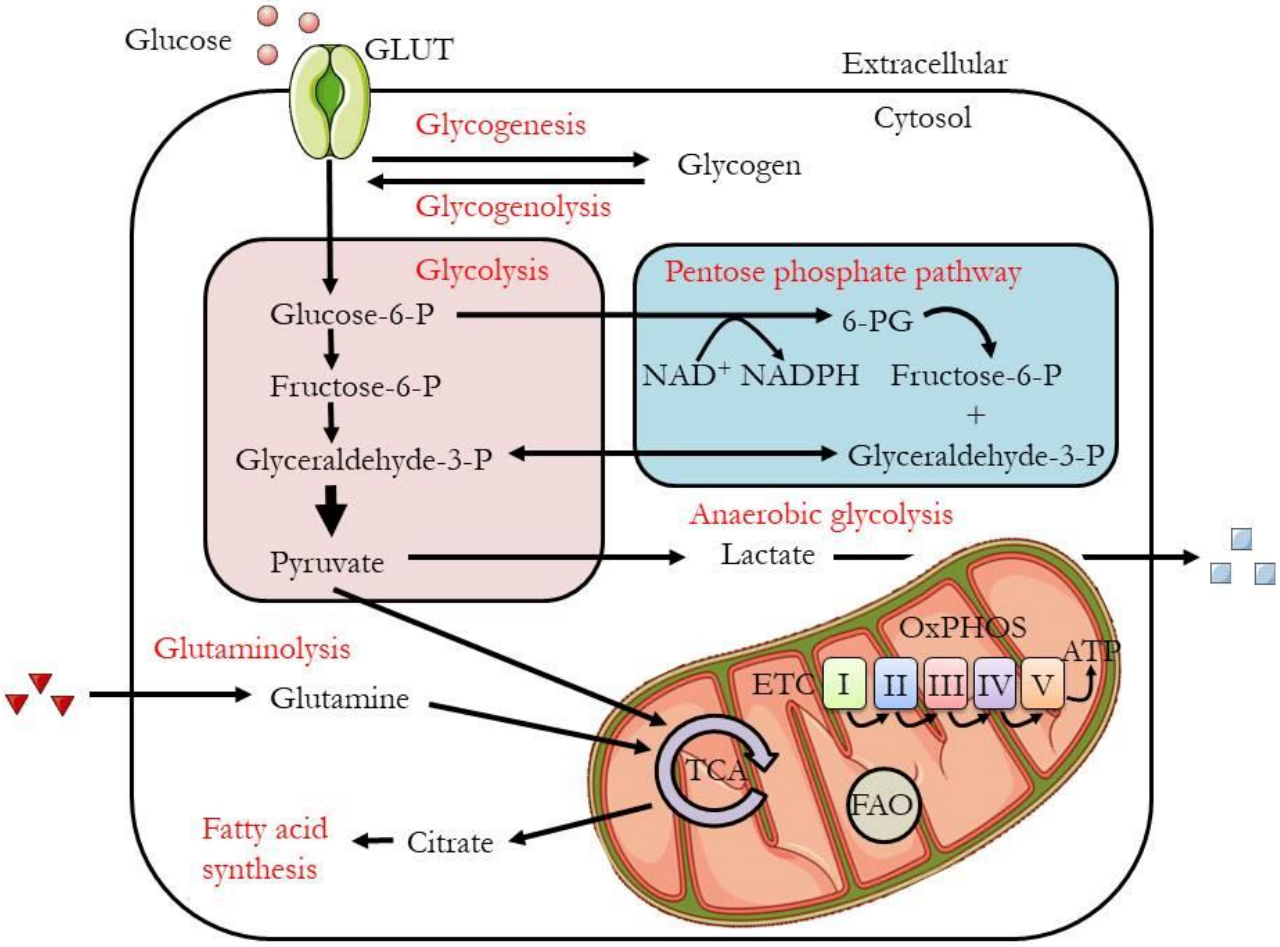

Figure 14. Overview of key metabolic pathways in neutrophils. Glycolysis is the major metabolic pathway in neutrophils which converts glucose after its uptake by glucose transporters (GLUT) through a series of enzymes and reactions into pyruvate. In the presence of oxygen pyruvate participates in the tricarboxylic acid (TCA) cycle, whereas in the absence of oxygen pyruvate is reduced to lactate during anaerobic glycolysis and secreted out of the cell. Neutrophils also use the pentose phosphate pathway (PPP) by using glucose-6-phosphate (glucose-6-P) to produce nucleotides and particularly NADPH which serves as substrate of the NADPH oxidase in neutrophils. Depending on glucose abundance, glycogen stores get enriched or degraded. The TCA cycle intermediate citrate is used during fatty acid synthesis for the generation of free fatty acids (FFA), while FFA and their conversion to acetyl-CoA fuel the TCA cycle to produce high amounts of ATP. During glutaminolysis glutamine is transformed to α-ketoglutarate and enters the TCA cycle.

Metabolic regulation of neutrophil development, functions and apoptosis

An overview of the key metabolic pathways and organelles regulating neutrophil functions is presented in **Figure 15**.

Granulopoiesis and steady state

Neutrophils are produced from HSCs during the highly controlled process of granulopoiesis in the bone marrow. HSCs are highly dependent on glycolysis due to their adaptation to the hypoxic niche in the bone marrow

(Simsek et al., 2010). In comparison to HSCs neutrophil progenitors show a shift towards oxidative phosphorylation (Injarabian et al., 2019). The rate-limiting enzyme of NAD^+ biosynthesis, the nicotinamide phospho-ribosyltransferase (NAMPT), induces FAO and the TCA cycles and upregulates G-CSF production during granulopoiesis (Skokowa et al., 2009). Additionally, vitamin B3, the substrate of NAMPT, promotes neutrophil differentiation indicating a correlation between NAD metabolism and neutrophil development (Skokowa et al., 2009). The metabolic shift during neutrophil differentiation is triggered by the increase in oxygen availability (Spencer et al., 2014) and by autophagy (Riffelmacher et al., 2017). FAO and oxidative phosphorylation enable the breakdown of lipid droplets to provide free fatty acids. The differentiation stages myeloblast and myelocyte show the most autophagy-mediated lipid degradation and have a highly mitochondria-dependent metabolism (Riffelmacher et al., 2017). The precise mechanism how mature neutrophils switch back towards a glycolytic metabolism still has to be elucidated. After their release from the bone marrow into the circulation, HIF-1α facilitates the metabolic adaptation to the low oxygen environment by upregulation of glycolytic enzymes (Walmsley et al., 2005). Moreover, neutrophils in the circulation start to accumulate ascorbate, an antioxidant, which reduces ROS to limit cellular damage during the oxidative burst (Bozonet et al., 2015). However, high levels of ascorbate promote HIF-1α degradation (Vissers et al., 2007). Neutrophil recruitment into tissues is dependent on the maintenance of the mitochondrial membrane potential indicating that mitochondria drive neutrophil migration (Zhou et al., 2018). Early studies reported that during antimicrobial activity neutrophils mainly produce ATP through glycolysis by glucose uptake from the surrounding medium (Borregaard and Herlin, 1982).

Phagocytosis

Phagocytosis, a key antimicrobial function of neutrophils, depends predominantly on glycolysis and is easily disrupted by utilization of glycolysis inhibitors. Also stored glycogen provides glucose through glycogenolysis for phagocytic functions of neutrophils (Sbarra and Karnovsky, 1959). Fossati et al. showed that during phagocytosis no significant change of the ATP generation could be observed, while due to energy consumption a fall in intracellular ATP levels was detected (Fossati et al., 2003). Consequently, mitochondria do not participate in phagocytosis regulation.

ROS production

The production of ROS by the NADPH oxidase complex is mainly dependent on glycolysis. The glycolytic enzyme 6-phosphofructo-2-kinase (PFK-2) localizes with the NADPH oxidase following neutrophil activation and reduction of the glycolysis rate through PFK-2 inhibition reduces ROS production (Baillet et al., 2017). Reciprocally, inhibition of the NADPH oxidase results in reduced PFK-2 catalyzed rate of glycolysis indicating a mutual regulation of oxidative burst and glycolysis. In contrast, inhibition of complex I and III of the respiratory chain led to increased superoxide and hydrogen peroxide production (Zmijewski et al., 2008, 2009). Moreover, addition of the metabolites α-ketoglutarate, pyruvate, asparagine, glutamine, aspartate and glutamate to neutrophil suspension increases superoxide and hydrogen peroxide production *in vitro* (Mühling et al., 2010). Additionally, the key substrate of the NADPH oxidase is NADPH produced during the PPP (Stanton, 2012). Also short chain fatty acids (SCFAs), like acetate, have been suggested to enhance ROS production and phagocytosis (Maslowski et al., 2009).

NETs

NETosis is an energy consuming process which relies on glycolysis. Furthermore, ROS-dependent NET formation is linked to the PPP (Azevedo et al., 2015). Hyperglycemia promotes NET formation, although these NETs are less stable and contain a lower amount of anti-microbial peptides compared to NETs formed under physiological conditions (Wang et al., 2018). Also lactate the end product of glycolysis can induce NETosis

(Rodríguez-Espinosa et al., 2015). However, ROS-independent NET formation appears to be less dependent on the glucose metabolism, instead the pH and oxygen concentration are crucial parameters (Khan et al., 2018).

Chemotaxis

Mitochondria and TCA cycle regulate in neutrophils the chemotaxis, a directed migration towards a concentration gradient of a chemotactic factor. In response to chemotactic factors mitochondria release ATP to stimulate P2Y2 nucleotide receptors and activate mTOR signaling to increase the mitochondrial activity at the leading edge (Bao et al., 2015; Chen et al., 2006). Subsequently, highly active mitochondria show a high calcium uptake and the $\Delta\psi_m$ localizes to the front of the leading edge and delivers ATP to trigger purinergic signaling. Inhibition of mitochondrial ATP production blocks chemotaxis through alternative purinergic signaling. Mutation of the iso-citrate dehydrogenase (IDH), the enzyme which catalizes decarboxylation of iso-citrate to α-ketoglutarate in the TCA cycle, impairs neutrophil chemotaxis (Amankulor et al., 2017). SCFAs like acetate, propionate and butyrate stimulate neutrophil chemotaxis by increase of L-selectin expression (Vinolo et al., 2009). Furthermore, SCFAs are converted to acetyl-CoA that is used to fuel ATP production during the TCA cycle and oxidative phosphorylation.

Apoptosis

Also the clearance of apoptotic neutrophils is an energy consuming process. Mitochondria are necessary to maintain the $\Delta\psi_m$. A loss in $\Delta\psi_m$ in neutrophils induces the exposure of phosphatidylserine and the release of pro-apoptotic factors like cytochrome c into the cytosol initiating the apoptosis cascade (Maianski et al., 2004). Additionally, the succinate dehydrogenase (SDH) which oxidizes succinate to fumarate in the TCA cycle is involved in the apoptosis of neutrophils (Jones et al., 2016). Knock-out of the fatty-acid synthase (FAS), which generates palmitate from malonyl-CoA, impairs *de novo* lipogenesis and enhances apoptosis (Lodhi et al., 2015). The role of fatty acids in neutrophil apoptosis is further pronounced by the induction of the caspase-dependent apoptosis through the presence of the SCFAs propionate and butyrate (Aoyama et al., 2010). Additionally, enhanced neutrophil apoptosis is induced by a decrease in the physiological glutamine concentration (Karinch et al., 2001).

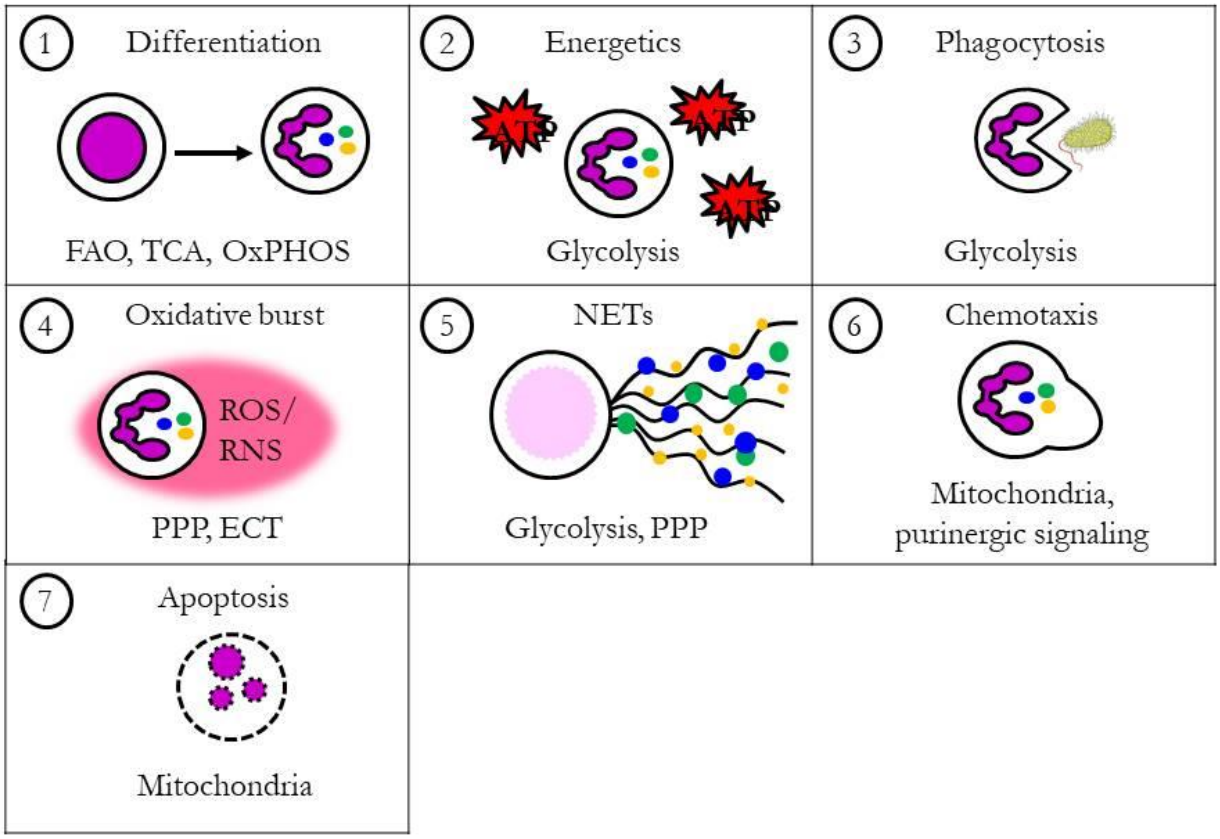

Figure 15. Key metabolic pathways and organelles regulating neutrophil development, functions and apoptosis. (1) During neutrophil differentiation glycolysis and autophagy decrease. The modulation of fatty acid oxidation (FAO), tricarboxylic acid (TCA) cycle and oxidative phosphorylation (OxPHOS) regulate further maturation of neutrophils. (2) Neutrophil ATP levels mainly originate from glycolysis. (3) Phagocytosis highly depends on glycolysis as glycolytic inhibitors abolish neutrophil phagocytosis completely. (4) The pentose phosphate pathway (PPP) potentiates reactive oxygen species (ROS) and reactive nitrogen species (RNS) production by providing NADPH, the substrate of the NADPH oxidase, while inhibition of complex I and III of the respiratory chain cause generation of mitochondrial ROS. (5) Glucose uptake increases during NETosis and a high glucose concentration in the extracellular milieu promotes neutrophil extracellular trap (NET) formation. (6) ATP and purinergic signaling at the leading edge determine neutrophil chemotaxis. Mitochondria with high mitochondrial membrane potential $\Delta\psi_m$ localize at the front of the leading edge and induce purinergic signaling. (7) Defective $\Delta\psi_m$ initiates the release of proapoptotic factors into the cytoplasm and cause apoptosis.

Metabolic changes in neutrophils during infection

Metabolic changes in neutrophils during infection occur as response to changes in the microenvironment, activation of the neutrophil and the presence of the pathogen. Infections with intracellular pathogens lead to a depletion of glucose as many pathogens rely on glycolysis for energy production and oxygen due to bacterial aerobic respiration and the release of ROS and RNS as neutrophil effector mechanisms. The competition between infiltrating immune cells and oxygen-consuming bacteria is often described as "battle for oxygen" in the literature (Arena et al., 2017). Also the transcription factors NFκB and HIF-1α induce changes in the neutrophil metabolism during infection. NFκB signaling is activated through the recognition of PAMPs and upregulates mitochondrial respiration (Mauro et al., 2011). In contrast, HIF-1α allows the adaptation to infection-induced hypoxia by promoting glycolysis which in turn increases the efficacy of neutrophil antimicrobial activity. Several

intracellular pathogens have strategies to change the neutrophil metabolism to evade killing. For example, the causative agent of tularemia, *Francisella tularensis*, secrets acid phosphatases to inhibit neutrophil ROS production (Mohapatra et al., 2013). Also C*oxiella burnetii* produces similar phosphatases which abrogate ROS production by inhibition of the NADPH oxidase (Hill and Samuel, 2011).

Metabolic changes in neutrophil subpopulations

Currently, not much is known about the energy metabolism of neutrophil subpopulations. However, for TANs and its ant-tumorigenic N1 and pro-tumorigenic N2 phenotype some similarities to TAMs can be drawn (Injarabian et al., 2019). M2 TAMs accumulate in hypoxic areas of the tumor microenvironment there they will be exposed to high levels of lactate produced by tumor cells which stabilizes HIF-1α even in the presence of increased oxygen concentration (Mu et al., 2018). As a consequence M2 TAMs will adapt to aerobic glycolysis. Not only tumor cells modulate the metabolism of infiltrating immune cells but also other immune cells as they deplete oxygen inducing hypoxia and secrete TNF supporting in the glycolytic phenotype of tumor cells (Jeong et al., 2019). G-MDSCs have been detected in high numbers in several cancer models. Due to the low glucose availability G-MDSCs shift towards an oxidative lipid metabolism (Hossain et al., 2015). Furthermore, the upregulation of the fatty acid transport protein 2 increases the synthesis of PGE_2 from arachidonic acid (Veglia et al., 2019), thereby contributing to the immunosuppressive phenotype of G-MDSCs. The immature population of LDGs exhibits a mitochondria-dependent ATP production (Rodríguez-Espinosa et al., 2015). In the absence of glucose these cells switch to the utilization of glutamate and proline. Recently, c-Kit+ tumor-elicited neutrophils (TENs) were described, which use the mitochondrial oxidative metabolism under low glucose availability (Rice et al., 2018). Furthermore, TENs are able to use FAO and oxidative phosphorylation to maintain their NADPH supply for ROS production even with limited access to glucose in the tumor microenvironment.

Key objectives of this project

Visceral leishmaniasis (VL), also known as kala-azar, is a neglected tropical disease caused by protozoan parasites of the *Leishmania donovani* complex. With 300.000 estimated cases annually and over 20.000 deaths each year VL is the second most fatal parasitic infection after malaria. The disease is highly endemic in Brazil, India and on the East African continent. The transmission occurs during the blood meal of a female sandfly. Characteristic symptoms of VL are irregular bouts of fever, substantial weight loss, swelling of liver and spleen, and anemia. Currently the treatment of VL relies on a limited number of drugs with severe side effects and complicated administration. For more than 60 years pentavalent antimonials were the gold standard in the treatment of VL, but their first line use in India was mainly abandoned due to the emergence of widespread resistance. Although amphotericin B, paromomycin and the only orally available drug miltefosine expanded the treatment regimen during the last decades treatment failure and drug resistance increased dramatically. Considering this, it exists an urgent need for the development of new therapeutic strategies against VL. A relatively new and promising approach to circumvent the development of resistances is so-called host-directed therapies (HDTs). HDTs no longer target the pathogen itself but aim to interfere with host cell factors and pathways which are required for infection or contribute to the disease.

As intracellular parasites *Leishmania* rely mainly on the nutrient supply by their host cells and even compete with the host cell for the same metabolic resources. Recent evidences have begun to reveal that *Leishmania* hijack metabolic pathways in their host cells to guarantee parasite survival and persistence. For example, Moreira et al. described that during *L. infantum* infection, macrophages switch from an early glycolytic metabolism to an oxidative phosphorylation, and that this metabolic switch requires SIRT1 and LKB1/AMPK (Moreira et al., 2015). Furthermore, the impairment of the SIRT1-AMPK axis reduced the parasitic load *in vitro* and *in vivo*, thus being a potential target for the development of HDTs. Nevertheless, so far *Leishmania*-mediated modulation of host cell metabolism and its impact on their effector functions is poorly understood.

In contrast to their well-described protective roles in many infections, neutrophils may play a detrimental role in leishmaniasis as *Leishmania* use neutrophils transiently as carriers to silently enter their definite host cells, macrophages. With regard to the special role of neutrophils in the onset of leishmaniasis the **1st key objective** of this project was to elucidate the immuno-metabolic network in *L. donovani*-infected neutrophils and to relate metabolic changes to resistance and susceptibility, respectively.

Although macrophages normally rest as naïve cells, their high plasticity allows them to acquire a functionally distinct phenotype depending on the surrounding microenvironment. This concept is well described for tumor-associated macrophages (TAMs) and its manifestation as classically activated M1 phenotype and alternatively activated M2 phenotype. During leishmaniasis, Th1 cytokines trigger the polarization towards the M1 phenotype, whereas Th2 cytokines activate the M2 phenotype. Also neutrophils can acquire a pro-inflammatory N1 phenotype and an anti-inflammatory N2 phenotype as tumor-associated neutrophils (TANs) in the tumor microenvironment. As most studies report that anti-leishmanial effector mechanisms of neutrophils are inefficient to control the establishment of infection and disease development, it is very likely that neutrophils during *Leishmania* infection acquire an immunosuppressive N2 phenotype that allows the parasite to persist. Therefore, the **2nd key objective** was to polarize primary human neutrophils towards a N1 and N2 phenotype *in vitro* and to challenge them with *L. donovani* promastigotes. As most data on neutrophil subpopulations are from tumor models polarization was attempted by mimicking the tumor microenvironment. To evaluate the polarization process neutrophil effector functions like ROS production, degranulation and NETosis, as well as typical N1 and N2 markers, that are described by the current literature, were investigated.

The **3rd key objective** of this project was to generate a comprehensive view on how the metabolic network of neutrophils is differentially modulated during early (3 hpi) and late infection (24 hpi) with *L. donovani* and its causal influence on anti-leishmanial immune response. To assess changes in the energy metabolism of *L. donovani*-infected neutrophils the technique of extracellular flux analysis was used. Metabolome and transcriptome analysis of *L. donovani*-infected neutrophils was utilized to identify central metabolic nodes as potential future targets of HDTs. Targeting of these metabolic nodes was evaluated by monitoring of neutrophil effector functions and parasite multiplication by using the limiting dilution assay.

Materials

Solutions, buffers and media

If not further explained all solutions and buffers were prepared in Aqua dest.

10 x Tris buffered saline (TBS)	200 mM Tris Ultra + 1.4 M NaCl, pH 7.6
Reagent diluent (IL-8 ELISA)	0.1% BSA + 0.05% Tween 20 + TBS
Annexin-V buffer	10 mM HEPES + 140 mM NaCl, pH 7.4
Blocking buffer (ELISA)	1 % BSA in DPBS
Complete medium	Roswell Park Memorial Institute (RPMI) 1640 medium + 2 mM L-glutamine + 10 mM HEPES + 100 U/ml penicillin + 100 µg/ml streptomycin + 10 % FCS
Crystal violet staining solution	0.5 % Crystal violet in 20 % methanol
Deficiency medium	Roswell Park Memorial Institute (RPMI) 1640 medium + 2 mM L-glutamine + 10 mM HEPES
FACS buffer	DPBS + 1 % human serum + 1 % BSA + 0.01 % sodium azide, sterile filtered, pH 7.2
Reagent diluent (ELISA)	1 % BSA in DPBS
Schneider´s *Drosophila* complete medium	Schneider´s Drosophila medium with L-glutamine + 10 mM HEPES + 100 U/ml penicillin + 100 µg/ml streptomycin + 10 % FCS + 2 % human urine
Tween-TBS (T-TBS)	0.1 % Tween 20 + 1 x TBS
Washing buffer (ELISA)	DPBS + 0.05 % Tween 20

Laboratory supply/Consumables

Any kD™ Mini-PROTEAN® TGX™ Precast Protein Gels, 10-well, 50 µl	Bio-Rad, Munich
Any kD™ Mini-PROTEAN® TGX™ Precast Protein Gels, 15-well, 15 µl	Bio-Rad, Munich
Blot Absorbent Filter Paper	Bio-Rad, Munich
Cell culture multiwell plate 12-well, PS, clear, CELLSTAR®, TC, lid with condensation rings, sterile, single packed	Greiner bio-one, Frickenhausen
Cell culture multiwell plate 24-well, PS, clear, CELLSTAR®, TC, lid with condensation rings, sterile, single packed	Greiner bio-one, Frickenhausen
Cell culture multiwell plate 48-well, PS, clear, CELLSTAR®, TC, lid with condensation rings, sterile, single packed	Greiner bio-one, Frickenhausen
Cell culture multiwell plate 6-well, PS, clear, CELLSTAR®, TC, lid with condensation rings, sterile, single packed	Greiner bio-one, Frickenhausen
Cell culture multiwell plate 96-well, PS, clear, CELLSTAR®, TC, lid with condensation rings,	Greiner bio-one, Frickenhausen

sterile, single packed	
Cover glasses, circular	Marienfeld, Lauda-Königshofen
Cuvette, 2x optical, PS	Sarstedt, Nümbrecht
ELISA plate Nunc MaxiSorp™, flat-bottom	Thermo Fisher Scientific, Waltham, Massachusetts, USA
Microplate, 96-well, F-bottom (chimney well), black, FLUOTRAC™, high binding, sterile, 10 pcs./bag	Greiner bio-one, Frickenhausen
Microplate, 96-well, PS, F-bottom (chimney well), white, LUMITRAC™, high binding, sterile, 10 pcs./bag	Greiner bio-one, Frickenhausen
Microtest plate, 96-well, polystyrene, conical bottom (V-bottom)	Sarstedt, Nümbrecht
Nitrocellulose membrane, roll, 0.45 µm, 30 cm x 3.5 m	Bio-Rad, Munich
Pipette , 10 ml, graduated 1/10 ml, sterile, bulk packaging, 25 pcs./bag	Greiner bio-one, Frickenhausen
Pipette , 2 ml, graduated 1/100 ml, sterile, bulk packaging, 25 pcs./bag	Greiner bio-one, Frickenhausen
Pipette , 5 ml, graduated 1/10 ml, sterile, bulk packaging, 25 pcs./bag	Greiner bio-one, Frickenhausen
Pipette Filter Tips, certified Biosphere® plus, 0.5 µl – 10 µl	Sarstedt, Nümbrecht
Pipette Filter Tips, certified Biosphere® plus, 10 µl – 100 µl	Sarstedt, Nümbrecht
Pipette Filter Tips, certified Biosphere® plus, 100 µl – 1000 µl	Sarstedt, Nümbrecht
Pipette, 25 ml, graduated 2/10 ml, sterile, paper-plastic packaging, single packed	Greiner bio-one, Frickenhausen
Plastic test tube 15 ml, 120 x 17 mm, PP	Sarstedt, Nümbrecht
Plastic test tube 50 ml, 114 x 28 mm, PP	Sarstedt, Nümbrecht
Reaction tube, 0.5 ml, PP, with attached lid with retaining cams, with moulded graduation and frosted writing space, Biosphere® plus, 50 pcs./bag	Sarstedt, Nümbrecht
Reaction tubes, 1.5 ml, PP, with attached lid, with moulded graduation and frosted writing space, Biosphere® plus, 500 pcs./bag	Sarstedt, Nümbrecht
Reaction tubes, 2 ml, PP, with attached lid, with moulded graduation and frosted writing space, Biosphere® plus, 500 pcs./bag	Sarstedt, Nümbrecht
Seahorse XF24 Cell Culture Microplates	Agilent, Santa Clara, California, USA
Seahorse XF24 sensor cartridges	Agilent, Santa Clara, California, USA
S-Monovette, 9 ml, Lithium-Heparin	Sarstedt, Nümbrecht
S-Monovetten 9 ml, Serum	Sarstedt, Nümbrecht
Sterican® Gr. 1, G 20 x 1 1/2""/ø 0.90 x 40 mm, yellow	B.Braun, Melsungen

THERMO microscopy slides Superfrost, cut edges, 76 x 26 mm	Thermo Fisher Scientific, Waltham, Massachusetts, USA
Transfer pipette, 3.5 ml	Sarstedt, Nümbrecht
U-tubes, 5 ml, 75 x 12 mm, PS	Sarstedt, Nümbrecht

Instruments and laboratory equipment

Agilent 2100 Bioanalyzer	Agilent, Santa Clara, California, USA
Analytical balance BP61S	Sartorius, Göttingen
Balance	Sartorius, Göttingen
Biological safety cabinet class II, Clean Air EF A6, EN 12469	Telstar Laboratory Equipment, Wörden, The Netherlands
BZ-9000 (BioRevo) Fluorescence Microscope	Keyence, Neu-Isenburg
Centrifuge 5417R	Eppendorf, Hamburg
Centrifuge Biofuge fresco Kendro	Heraeus, Langenselbold
Centrifuge Megafuge 2.0R Kendro	Heraeus, Langenselbold
Centrifuge Multifuge 3 and SR Kendro	Heraeus, Langenselbold
CO_2 incubator, Forma Series II Water Jacket	Thermo Fisher Scientific, Waltham, Massachusetts, USA
Cytocentrifuge Cytospin 3	Shandon, Frankfurt
Deep freezer, – 20°C, – 70°C	Liebherr, Ochsenhausen
Eppendorf Research® pipettes	Eppendorf, Hamburg
Eppendorf® ThermoMixer® comfort, 1.5 ml	Eppendorf, Hamburg
Flow cytometer FACS Canto II	Becton Dickinson, Heidelberg
Gel documentation Quantum ST4	Vilber Lourmat, Marne La Valléé, France
Horizontal shaker	IKA® Labortechnik, Staufen
Hypoxia chamber	Toepffer Lab Systems, Göppingen
Ice machine	Ziegra, Isernhagen
Incubator without CO_2	Thermo Fisher Scientific, Waltham, Massachusetts, USA
Magnetic stirrer Ikamag, Reo	IKA® Labortechnik, Staufen
Magnetic stirrer MR 3003	Heidolph, Schwabach
Microscope Axiostar plus	Carl Zeiss, Jena
Microscope Axiovert 25	Carl Zeiss, Jena
Mini-PROTEAN® Tetra Vertical Electrophoresis Cell	Bio-Rad, Munich
Minishaker MS2	IKA® Labortechnik, Staufen
Multichannel pipette	Eppendorf, Hamburg
NanoPhotometer™	Implen, Munich
Neubauer counting chamber, improved, 0.0025 mm^2, depth 0.02 mm	VWR, Darmstadt
Neubauer counting chamber, improved, 0.0025 mm^2, depth 0.1 mm	Marienfeld, Lauda-Königshofen
pH-meter inolab	WTW GmbH, Weilheim
Photometer Ultrospec 1000	Amersham Biosciences, Freiberg

Plate reader Infinite 200	Tecan, Männedorf, Schweiz
Power supply P25	Biometra, Göttingen
Seahorse XF24 Analyzer	Agilent, Santa Clara, California, USA
Semi-dry protein transfer cell	Bio-Rad, Munich
Shaker vibrofix VF1 Electronic	Janke & Kunkel IKA® Labortechnik, Staufen
Transfer pipette	Brand, Wertheim
Vortex mixer	Heidolph, Schwabach
Water bath	Köttermann, Uetze

Chemicals and laboratory reagents

2-(N-(7-Nitrobenz-2-oxa-1,3-diazol-4-yl)Amino)-2-Deoxyglucose (2-NBDG)	Cayman Chemical, Ann Arbor, Michigan, USA
2-Deoxy-D-glucose	Sigma-Aldrich, Steinheim
2-β-Mercatoethanol	Sigma-Aldrich, Steinheim
3PO	Sigma-Aldrich, Steinheim
Acetone	Merck, Darmstadt
Adenosine	Merck, Darmstadt
Amicon Ultra-0.5 Centrifugal Filter Unit	Merck, Darmstadt
Annexin-V FLUOS	Sigma-Aldrich, Steinheim
Antimycin A	Sigma-Aldrich, Steinheim
BD FACS Clean Solution	Becton Dickinson, Heidelberg
BD FACS Diva™ CS&T Research Beads	Becton Dickinson, Heidelberg
BD FACS Shutdown Solution	Becton Dickinson, Heidelberg
BD FACSFlow Sheath Fluid	Becton Dickinson, Heidelberg
Bovine serum albumin (BSA)	Sigma-Aldrich, Steinheim
BPTES	Sigma-Aldrich, Steinheim
Bromphenol blue dye	SERVA Electrophoresis GmbH, Heidelberg
Calcium chloride	Sigma-Aldrich, Steinheim
Carbonylcyanide-p-trifluoromethoxy-phenylhydrazone (FCCP)	Cayman Chemical, Ann Arbor, Michigan, USA
Cholesterol-Water Soluble	Sigma-Aldrich, Steinheim
Complement C5 deficient serum human	Sigma-Aldrich, Steinheim
Corning® Cell-Tak™ Cell and Tissue Adhesive	Corning Life Sciences, Amsterdam, The Netherlands
Crystal violet	Sigma-Aldrich, Steinheim
D-(+)-Galactose	Sigma-Aldrich, Steinheim
D-(+)-Glucose	Roth, Karlsruhe
Diff-Quick® fixation solution	Medion Diagnostics, Duedingen, Switzerland
Diff-Quick® staining set	Medion Diagnostics, Duedingen, Switzerland
Dimethyl sulfoxide	Sigma-Aldrich, Steinheim
Dithiothreitol (DTT)	Sigma-Aldrich, Steinheim
Ethanol absolute, 99.9 %	J.T. Baker, Deventer, The Netherlands
D-(+) Galactose	Sigma-Aldrich, Steinheim
Gibco™ 1 x DPBS	Thermo Fisher Scientific, Waltham, Massachusetts, USA

Gibco™ 10 x DPBS	Thermo Fisher Scientific, Waltham, Massachusetts, USA
Gibco™ Fetal bovine serum (FBS)	Thermo Fisher Scientific, Waltham, Massachusetts, USA
Gibco™ D-(+) Glucose	Thermo Fisher Scientific, Waltham, Massachusetts, USA
Gibco™ GlutaMAX	Thermo Fisher Scientific, Waltham, Massachusetts, USA
Gibco™ Hank's Balanced Salt Solution (HBSS)	Thermo Fisher Scientific, Waltham, Massachusetts, USA
Gibco™ RPMI 1640 without glucose	Thermo Fisher Scientific, Waltham, Massachusetts, USA
Gibco™ Trypan blue solution 0.4 %	Thermo Fisher Scientific, Waltham, Massachusetts, USA
Glycerol	Sigma-Aldrich, Steinheim
Glycine	SERVA Electrophoresis GmbH, Heidelberg
Glycogen phosphorylase inhibitor	Merck Millipore, Darmstadt
Hematoxylin	Roth, Karlsruhe
HEPES buffer	Thermo Fisher Scientific, Waltham, Massachusetts, USA
Histopaque® 1119	Sigma-Aldrich, Steinheim
ibidy Mounting Medium for fluorescence microsopy	ibidy GmbH, Gräfelfing
Immobilon™ Western chemiluminescence HRP substrate	Millipore, Billerica, Massachusetts, USA
Invitrogen™ BODIPY™ FL C12 (4,4-Difluoro-5,7-Dimethyl-4-Bora-3a,4a-Diaza-s-Indacene-3-Dodecanoic Acid)	Thermo Fisher Scientific, Waltham, Massachusetts, USA
Invitrogen™ BODIPY™ FL C16 (4,4-Difluoro-5,7-Dimethyl-4-Bora-3a,4a-Diaza-s-Indacene-3-Hexadecanoic Acid)	Thermo Fisher Scientific, Waltham, Massachusetts, USA
Invitrogen™ Dihydrorhodamine 123 (DHR123)	Thermo Fisher Scientific, Waltham, Massachusetts, USA
Invitrogen™ Molecular Probes™ *Staphylococcus aureus* BioParticles™, Alexa Fluor™ 488 conjugate	Thermo Fisher Scientific, Waltham, Massachusetts, USA
Invitrogen™ *Staphylococcus aureus* BioParticles™ Opsonizing Reagent	Thermo Fisher Scientific, Waltham, Massachusetts, USA
Invitrogen™ SYTOX Green nucleic acid stain, 5mM solution in DMSO	Thermo Fisher Scientific, Waltham, Massachusetts, USA
Isopropanol	Roth, Karlsruhe
L-(+)-Lactic acid	Sigma-Aldrich, Steinheim
LB agar powder	Becton Dickinson, Heidelberg
LB medium powder	Becton Dickinson, Heidelberg
L-Glutamine	Biochrom, Berlin
Lipopolysaccharide *E. coli* 0111:B4 (LPS)	Sigma-Aldrich, Steinheim
Lucigenin	Enzo Life Science AG, Lausen, Switzerland

Luminol	Sigma-Aldrich, Steinheim
Methanol	J.T. Baker, Deventer, The Netherlands
Molecular Probes ™ MitoSOX™ Red Mitochondrial Superoxide Indicator	Thermo Fisher Scientific, Waltham, Massachusetts, USA
N-Formylmethionyl-leucyl-phenylalanine (fMLP)	Sigma-Aldrich, Steinheim
Oligomycin A	Sigma-Aldrich, Steinheim
Pancoll human for Granulocytes, Density: 1.119 g/ml	PAN Biotech, Aidenbach
Pancoll human, Density: 1.077 g/ml	PAN Biotech, Aidenbach
Paraformaldehyde	Sigma-Aldrich, Steinheim
Penicillin/streptomycin	Biochrom, Berlin
Percoll®	GE Healthcare, Munich
Periodic acid	Roth, Karlsruhe
PFKFB3 Inhibitor, 3PO	Sigma-Aldrich, Steinheim
Phorbol 12-myristate 13-acetate (PMA)	Sigma-Aldrich, Steinheim
Poly-L-Lysine, 0.1% (w/v) in Aqua dest.	Sigma-Aldrich, Steinheim
Propidium iodide solution	Sigma-Aldrich, Steinheim
Prostaglandin E_2	Tocris, Wiesbaden-Nordenstadt
QVP-OPh	R&D, Wiesbaden
RNaseZap™ RNase Decontamination Solution	Thermo Fisher Scientific, Waltham, Massachusetts, USA
Rotenone	Cayman Chemical, Ann Arbor, Michigan, USA
RPMI 1640	Sigma-Aldrich, Steinheim
Saponin	Sigma-Aldrich, Steinheim
Schiff's reagent	Roth, Karlsruhe
Schneider´s Drosophila Medium W/L-Glutamine	Genaxxon, Ulm
Seahorse XF24 FluxPaks	Agilent, Santa Clara, California, USA
Sodium azide	Merck, Darmstadt
Sodium chloride	Merck, Darmstadt
Sodium dodecyl sulfate (SDS)	Roth, Karlsruhe
Sodium iodoacetate (SIA)	Sigma-Aldrich, Steinheim
Sodium pyruvate	PAN-Biotech, Aidenbach
Sulfuric acid	Merck, Darmstadt
Technical buffer solution pH 10.0	WTW GmbH, Weilheim
Technical buffer solution pH 4.01 TPL4	WTW GmbH, Weilheim
Technical buffer solution pH 7.0 TPL7	WTW GmbH, Weilheim
Trichloroacetic acid solution	Sigma-Aldrich, Steinheim
TRIS Ultra	Roth, Karlsruhe
Tween 20 pure	SERVA Electrophoresis GmbH, Heidelberg
XF Assay Medium	Agilent, Santa Clara, California, USA
XF Calibrant Solution	Agilent, Santa Clara, California, USA
Zeiss Immersol 518F	Thermo Fisher Scientific, Waltham, Massachusetts, USA

Cytokines

Recombinant human G-CSF	PeproTech GmbH, Hamburg
Recombinant human IFNβ	R&D, Wiesbaden
Recombinant human IFNγ	R&D, Wiesbaden
Recombinant human IL-10	BioLegend, San Diego, California, USA
Recombinant human IL-8	R&D, Wiesbaden
Recombinant human TGF-β1	PeproTech GmbH, Hamburg
Recombinant human TNF	PeproTech GmbH, Hamburg

Antibodies

APC-conjugated mAb to human CD182 (clone 5E8/CXCr2, IgG1)	BioLegend, San Diego, California, USA
APC-conjugated mAb to human CD54 (clone HA58, IgG1)	BioLegend, San Diego, California, USA
APC-conjugated mAb to human CD62L (clone DREG-56, IgG1)	BioLegend, San Diego, California, USA
APC-conjugated mAb to human LOX-1 (clone 15C4, IgG2a)	BioLegend, San Diego, California, USA
FITC-conjugated mAb to human CD195 (CCR5) (clone J418F1, IgG2b)	BioLegend, San Diego, California, USA
FITC-conjugated mAb to human CD3 (clone HIT3a, IgG2a)	BioLegend, San Diego, California, USA
FITC-conjugated mAb to human CD32 (clone FUN-2, IgG2b)	BioLegend, San Diego, California, USA
FITC-conjugated mAb to human CD66b (clone G10F5, IgM)	Becton Dickinson, Heidelberg
FITC-conjugated mAb to human GLUT-3 (clone G-5, IgG1)	Santa Cruz Biotechnologies, Dallas, Texas, USA
FITC-conjugated mAb to human GLUT-4 (clone I-F8, IgG1)	Santa Cruz Biotechnologies, Dallas, Texas, USA
Pacific Blue™-conjugated mAb to human CD95 (clone DX2, IgG1)	BioLegend, San Diego, California, USA
PE-conjugated mAb to human CD10 (clone HI10a, IgG1)	BioLegend, San Diego, California, USA
PE-conjugated mAb to human CD11b (clone 2LPM19c, IgG1)	Dako, Waldbronn
PE-conjugated mAb to human CD14 (clone TÜK4, IgG2a)	Dako, Waldbronn
PE-conjugated mAb to human CD16 (clone 3G8, IgG1)	BioLegend, San Diego, California, USA
PE-conjugated mAb to human CD178 (Fas-L) (clone NOK-1, IgG1)	BioLegend, San Diego, California, USA
PE-conjugated mAb to human CD64 (clone 10.1, IgG1)	BioLegend, San Diego, California, USA

PE-conjugated mAb to human CD89 (clone A59, IgG1)	BioLegend, San Diego, California, USA
PE-conjugated mAb to human GLUT-1 (clone A-4, IgG1)	Santa Cruz Biotechnologies, Dallas, Texas, USA
PE-conjugated mAb to human GLUT-2 (clone C-10, IgG1)	Santa Cruz Biotechnologies, Dallas, Texas, USA

Kits

Agilent RNA 6000 Pico Kit	Agilent, Santa Clara, California, USA
Arginase activity assay	Sigma-Aldrich, Steinheim
G-CSF DuoSet ELISA	R&D, Wiesbaden
Glutamate/Glutamine-Glo™ assay	Promega, Walldorf
IL-8 DuoSet ELISA	R&D, Wiesbaden
Invitrogen™ Molecular Probes™ ATP Determination Kit	Thermo Fisher Scientific, Waltham, Massachusetts, USA
IP-10 DuoSet ELISA	R&D, Wiesbaden
Lactate assay	Sigma-Aldrich, Steinheim
LDH assay	Promega, Walldorf
MCP-1 DuoSet ELISA	R&D, Wiesbaden
MMP9 DuoSet ELISA	R&D, Wiesbaden
MPO DuoSet ELISA	R&D, Wiesbaden
NAD^+/NADH-Glo™ assay	Promega, Walldorf
Pyruvate assay	Sigma-Aldrich, Steinheim
RNase-free DNase Set	QIAGEN, Hilden
RNeasy Mini Kit	QIAGEN, Hilden
TNF DuoSet ELISA	R&D, Wiesbaden
VEGF DuoSet ELISA	R&D, Wiesbaden

Software

2100 Bioanalyzer Expert Software	Agilent, Santa Clara, California, USA
BD FACSDiva™ software 9	Becton Dickinson, Franklin Lakes, New Jersey, USA
BZ II Analyzer software	Keyence, Neu-Isenburg
FlowJo 10 Software	FlowJo LLC, Ashland, Oregon, USA
GraphPad Prism 6	GraphPad Software, La Jolla, California, USA
ImageJ software	NIH, Bethesda, Maryland, USA
Tecan i-control 1.7 software	Tecan, Männedorf, Schweiz

Methods

Leishmania donovani culture

The virulent strain *Leishmania donovani* MHOM/IN1983/AG83 was used during the whole course of investigation. The strain AG83 was originally obtained from an Indian kala-azar patient (Saha et al., 1995). Promastigotes were cultured under sterile conditions *in vitro* in Schneider´s *Drosophila* complete medium in a humidified atmosphere containing 5 % CO_2. The stationary phase of *L. donovani* promastigotes was determined in preliminary experiments using growth curves. Stationary phase promastigotes were collected after 3 or 4 days in culture, the day of seeding was defined as day 0. Only *L. donovani* promastigotes up to 10 passages were used in the experiments.

Bacterial culture

The bacterial strains *Escherichia coli* DH5 alpha and DSM8695 were kindly provided by the Department of Infectiology and Microbiology at the University Hospital Schleswig-Holstein. Bacteria strains were stored at -80°C in bacterial freezing tubes containing sterile glass beads and glycerol. For bacterial culture on agar plates a single bead from the glycerol stock was transferred on a sterile LB agar plate. The bacteria on the bead were spread by use of the three eyelets smear. The plate was incubated for 24 h at 37°C. For preparation of a liquid culture a single colony from the culture on the LB agar plate was picked with a sterile loop and transferred into 20 ml sterile LB medium in an Erlenmeyer flask. Growth at 37°C with continuous shaking was monitored by measurement of optical density and concentration of bacteria was calculated by using the Lambert-Beer law.

Isolation of primary human peripheral blood neutrophil granulocytes

Blood collection was conducted by trained staff of the Department of Infectiology and Microbiology at the University Hospital Schleswig-Holstein with the written consent from each participant and was approved by the Ethical Committee of the Medical Faculty of the University of Lübeck (18-186). Peripheral blood was collected by venipuncture from healthy adult volunteers using lithium-heparin collection tubes. Blood was layered on a two-layer density gradient consisting of an upper layer of lymphocyte separation medium 1077 or Pancoll human for Granulocytes, density: 1.119 g/ml and a lower layer of Histopaque®1119 or Pancoll human, density: 1.077 g/ml and centrifuged for 5 min at 300 x g followed by 25 min at 800 x g. Cells from the upper layer consisting mainly of lymphocytes and monocytes were discarded. The granulocyte-rich lower layer was collected leaving the erythrocyte pellet at the bottom of the tube. Granulocytes were washed once in 1 x DPBS for 10 min at 800 x g, resuspended in RPMI complete and further fractionated on a discontinuous Percoll® gradient consisting of layers with densities of 1.105 g/ml (85 %), 1.100 g/ml (80 %), 1.087 g/ml (70 %) and 1.081 g/ml (65 %). After centrifugation for 25 min at 800 x g, the interface between the 80 % and 70 % Percoll® layers was collected. The cells were washed once in 1 x DPBS for 10 min at 800 x g and resuspended in RPMI complete to a concentration of $5 \cdot 10^6$ cells/ml. All described procedures were conducted at room temperature and under sterile conditions in a biological safety cabinet (class II). Cell counting was conducted with a hemocytometer and crystal violet staining to distinguish granulocytes and erythrocytes. The preparations contained ≥ 99 % granulocytes, of which > 95 % were neutrophils and 1-4 % were eosinophils, as determined by Giemsa staining of cytocentrifuged samples.

In vitro polarization of neutrophils

Polarization of neutrophils towards a N1-like phenotype was conducted in 6-well plates with 3 ml/well at a cell concentration of $5 \cdot 10^6$/ml in RPMI complete supplemented with a N1 polarization cocktail containing 100 ng/ml LPS, 50 ng/ml IFNγ and 10.000 U/ml IFNβ at 37°C in a humidified air atmosphere containing 5 % CO_2. Polarization of neutrophils towards a N2-like phenotype was conducted in 6-well plates with 3 ml/well in RPMI complete supplemented with a N2 polarization cocktail containing 25 mM L-lactate, 10 µM adenosine, 20 ng/ml TGF-β, 10 ng/ml IL-10, 20 ng/ml PGE2 and 100 ng/ml G-CSF. The pH of the medium containing the N2-

polarization cocktail was adjusted to 6.5. Cultivation of N2-like neutrophils was conducted in a humidified hypoxic chamber with 2 % O_2 and 5 % CO_2 at 37°C. Since neutrophils have a short life span, both in the circulation and in the cell culture they undergo apoptosis within few hours. To investigate longer-term polarization effects as they likely occur in tumor microenvironment, the cultivation of neutrophils in the polarization experiments was carried out in the presence of 3 µM pan caspase inhibitor QVD-OPh. In the polarization experiments the control cells were cultivated in RPMI complete containing 3 µM QVD-OPh. These control cells were named N0. All polarization experiments were conducted at 37°C in a humidified air atmosphere containing 5 % CO_2. Functions and phenotype of the cells were assessed 24 h and 48 h after incubation in the given polarization cocktails (N1 or N2) or without polarizing agents (N0).

Flow cytometry analysis of cell surface molecules

Neutrophils (500 000 cells/sample) were resuspended in 100 µl FACS buffer in a V-bottom 96-well plate. After washing once with 200 µl FACS buffer, the cells were stained with the corresponding antibody for 30 min at 4°C in 100 µl FACS buffer protected from light. After washing twice with FACS buffer, the cells were resuspended in FACS buffer and measured with a BD FACS Canto II (BD) flow cytometer. Data analysis was conducted with FlowJo V10.0.7.

Determination of cytokines in culture supernatants

Cell-free supernatants of neutrophils were collected and stored at -20°C until cytokine determination. The ELISA assays for TNF, VEGF, MCP-1, IP-10, G-CSF, MMP9, MPO and IL-8 were conducted in accordance to the manufacturer´s instructions.

Detection of intra- and extracellular ROS

The sum of intra- and extracellular MPO-derived ROS (Stevens and Hong, 1984) was measured by using a luminol-amplified chemiluminescence assay. Luminol can be oxidized by several ROS, such as H_2O_2, HOCl and HO·. Neutrophils (400 000 cells/sample) were resuspended in deficiency medium (RPMI medium without FCS) and seeded in a flat bottom white 96-well plate. Subsequently, 60 µM luminol was added, and the cells were stimulated by the addition of 20 nM PMA. The chemiluminescence resulting from ROS production was analyzed immediately by an Infinite M200pro-Tecan reader and Tecan i-control 1.7 software. ROS production was monitored every minute for a period of 1 h at 37°C and 5 % CO_2. Extracellular superoxide was detected by using a lucigenin-amplified chemiluminescence assay (Stevens and Hong, 1984). The lucigenin-amplified chemiluminescence assay, is a sensitive technique to quantify extracellular ROS, mainly superoxide anions (O_2-·). This assay was performed the same way as the luminol assay, but with 0.2 mM lucigenin instead of luminol.

In vitro infection of neutrophils with *L. donovani* promastigotes

Neutrophils and *L. donovani* promastigotes were resuspended in RPMI complete and co-incubated at a parasite-neutrophil ratio of 10:1 and a neutrophil density of $5 \cdot 10^6$ cells/ml for 3 h at 37°C in a humidified air atmosphere containing 5 % CO_2. Subsequently, the infection rate was assessed by Giemsa staining stained of cytocentrifuged samples. Only infection rates above 60 % were considered successful. The cells were washed six times in 1x DPBS at 400 x g for 10 min to remove extracellular *Leishmania*. Infected cells were again adjusted to $5 \cdot 10^6$ cells/ml.

Quantification of *L. donovani* survival in neutrophils

A limiting dilution culture assay was used to detect viable *L. donovani* parasites in infected neutrophils as described previously (Laskay et al., 1997). Briefly, serial 1.5-fold dilutions of *L. donovani*-infected neutrophil suspensions ($5 \cdot 10^6$ cells/ml) were plated in 4 replicates in 96-well flat bottom microtiter plates containing Schneider´s Drosophila complete medium. The plates were incubated at 27°C in humidified air atmosphere containing 5 %

CO_2 for 7-10 days. The growth of *L. donovani* promastigotes was detected microscopically. The last dilution resulting in a growth of parasites in ≥ 50 % of the wells is given as a quantitative measure of the parasite load in the neutrophil cell suspension.

Assessment of neutrophil apoptosis and viability

Apoptosis of neutrophils was determined by Annexin-V FLUOS binding as Annexin-V exhibits calcium-dependent binding to phosphatidylserine (PS) expressed in the outer leaflet of the cell membrane of apoptotic neutrophils (Homburg et al., 1995). Assessment of membrane integrity and identification of necrotic cells was performed by counterstaining with propidium iodid (PI). For staining, 500 000 cells/100 µl were transferred to a U-tube and 10 µl Annexin-V buffer, 1 µl 1 M $CaCl_2$, 1 µl PI and 1 µl Annexin-V FLUOS were added. Samples were incubated 10 min at 4°C protected from light. Analysis was carried out by flow cytometry.

SYTOXGreen kinetic assay

The time kinetics of NET release was studied by staining and detection of extracellular DNA with the non-cell-permeable dsDNS dye SYTOXGreen, a well-established and commonly used method to investigate the formation of NETs (Bianchi et al., 2009; Brinkmann, 2004; Kirchner et al., 2012). Per sample 200 µl neutrophils, $1 \cdot 10^6$ cells/ml in deficiency medium, were seeded in a black FLUOTRAC™ high binding 96-well microplates. Afterwards 5 µM SYTOXGreen was added and the cells were treated with either 20 nM PMA alone or the combination of other indicated stimuli. To exclude unspecific effects, like autofluorescence or spontaneous NETosis, cells in medium alone and cells in medium with SYTOXGreen cells served as control. The fluorescence of NET-bound SYTOXGreen (excitation 488 nm, emission 510 nm) was analyzed for a period of 4 h every 5 min at 37°C and 5 % CO_2 by using the Infinite M200pro-Tecan reader and Tecan i-control 1.7 software.

Visualization of NETs by fluorescence microscopy

For each sample one poly-L-lysine coated coverslip was placed into the well of a 24-well plate and 500 µl neutrophils, $1 \cdot 10^6$ cells/ml in deficiency medium, were pipetted on top of the coverslip. Afterwards NET formation was induced by the addition of either 20 nM PMA or the combination of other indicated stimuli. Untreated cells served as control. After 4 h incubation at 37°C and 5 % CO_2, the supernatant was carefully removed without rigorous pipetting. Cells were fixed with 500 µl 4 % paraformaldehyde (PFA) per well for 10 min at room temperature (RT). After the removal of PFA, the cells were washed once with 1 x DPBS. Air-dried coverslips were stained with 500 µl of 100 nM SYTOXGreen in 1 x DPBS for 30 min at RT protected from light. Unstained cells served as control. After washing three times with Aqua dest., the samples were mounted upside down on microscopy slides. Analysis was carried out with the Keyence BZ-9000 fluorescence microscope and the BZ II Analyzer software.

Seahorse XF Glycolysis stress test and Seahorse XF Mito stress test

On the previous day of the experiment 1 ml of XF calibrant solution was added to each well of a Seahorse XF24 sensor cartridge. The filled Seahorse XF24 sensor cartridge was incubated at 37°C without CO_2 overnight. Additionally, a Seahorse XF24 cell culture microplate was coated. For coating 1.4 ml of 0.1 M sodium bicarbonate buffer and 17 µl Corning™ Cell-Tak were mixed and 50 µl were pipetted to the bottom of each well. After incubating the plate 20 min at RT, the wells were washed twice with 500 µl Aqua dest. Before usage the plate was air-dried under the laminar flow workbench. For Seahorse XF glycolysis stress test XF assay medium was preheated at 37°C in a water bath and supplemented with 2 mM L-glutamine. The pH was adjusted to 7.35. For Seahorse XF Mito stress test 37°C-preheated XF assay medium was supplemented with 1 mM sodium pyruvate, 2 mM L-glutamine and 5 mM glucose. The pH was adjusted to 7.4. Neutrophils were adjusted to $25 \cdot 10^6$ cells/ml in the corresponding supplemented XF assay medium and 100 µl of cells were added to each well except

the four blank controls which were filled with XF assay medium. For adherence of cells the plate was centrifuged at 40 x g without brake until the desired speed was reached. Afterwards the plate was turned 180° clockwise and was centrifuged at 80 x g until the desired speed was reached. Finally, 425 µl of the corresponding supplemented XF assay medium were added to each well. The plate was incubated 60 min at 37°C without CO_2 and inserted into the Seahorse XF24 Analyzer.

For Seahorse XF glycolysis stress test the acidification of the medium was measured directly by the Seahorse XF24 Analyzer and reported as the extracellular acidification rate (ECAR). The first three measurements of ECAR prior to glucose injection determined the non-glycolytic acidification. The first injection was 5 mM glucose. Following ECAR measurement represented the rate of glycolysis. The second injection was 1 µM oligomycin, an inhibitor of complex V of the respiratory chain, the ATP synthase. Oligomycin inhibits mitochondrial ATP synthesis and thus shifts the energy production towards glycolysis. The oligomycin injection led to an increase in ECAR and revealed the maximum glycolytic capacity of neutrophils. The last injection was 10 mM 2-deoxy-D-glucose (2-DG), which serves as competitive inhibitor of the first rate-limiting enzyme of glycolysis, the hexokinase, and is shutting down glycolysis. The difference between the glycolytic capacity and glycolysis rate is termed glycolytic reserve. For the Seahorse XF Mito stress test the Seahorse XF24 Analyzer is capable of measuring the oxygen consumption rate (OCR) which can be directly correlated to mitochondrial function. The first three measurements of OCR were referred to as basal respiration. The injection of 1 µM oligomycin inhibited the ATP synthase and led to a decrease in OCR, which was correlating to the mitochondrial respiration associated with cellular ATP production. The injection of FCCP, an uncoupling reagent, induced a collapse in the proton gradient and was disrupting the mitochondrial membrane potential. Consequently, the electron flow through the electron transport chain was unlimited and oxygen consumption became maximal. The final injection was a mix of 1 µM rotenone, inhibitor of complex I of the respiratory chain, and 1 µM antimycin A, an inhibitor of complex III of the respiratory chain. This inhibitor mixture stopped the mitochondrial respiration and enabled the calculation of non-mitochondrial respiration driven by processes outside the mitochondria.

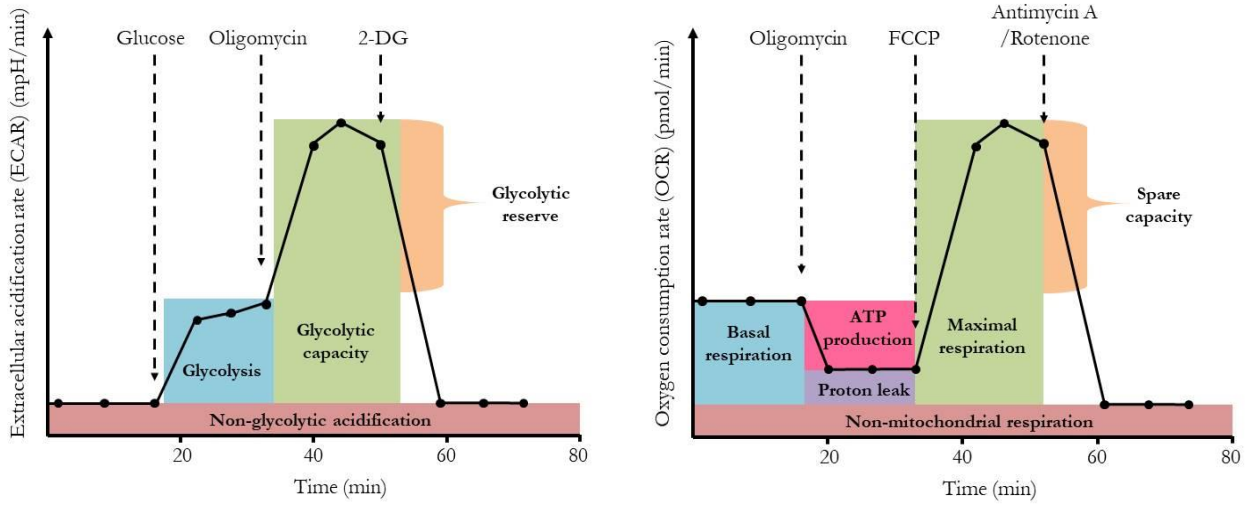

Figure 16. Glycolysis stress test profile and mitochondrial stress test profile. During the glycolysis stress test (A) sequential compound injections of glucose, oligomycin and 2-DG are used to measure glycolysis and glycolytic capacity, and allow the calculation of non-glycolytic acidification and glycolytic reserve. During the mitochondrial stress test (B) sequential compound injections of oligomycin, FCCP and antimycin A and rotenone allow the determination of key oxidative parameters.

Table 1. Calculation of glycolytic and oxidative parameters.

Oxidative parameter	**Equation**
Non-mitochondrial Respiration	Minimum rate measurement after Rotenone/antimycin A injection
Basal Respiration	(Last rate measurement before first injection) – (Non-Mitochondrial Respiration Rate)
Maximal Respiration	(Maximum rate measurement after FCCP injection) – (Non-Mitochondrial Respiration)
H+ (Proton) Leak	(Minimum rate measurement after Oligomycin injection) – (Non-Mitochondrial Respiration
ATP Production	(Last rate measurement before Oligomycin injection) – (Minimum rate measurement after Oligomycin injection)
Spare Respiratory Capacity	(Maximal Respiration) – (Basal Respiration)
Glycolytic parameter	**Equation**
Glycolysis	(Maximum rate measurement before Oligomycin injection) – (Last rate measurement before Glucose injection)
Glycolytic Capacity	(Maximum rate measurement after Oligomycin injection) – (Last rate measurement before Glucose injection)
Glycolytic Reserve	(Glycolytic Capacity) – (Glycolysis)

Bacterial killing assay

A bacterial killing assay with human neutrophils and opsonized bacteria was performed as previously described (Rada et al., 2004). Briefly, neutrophils were adjusted to $10 \cdot 10^6$ cells/ml in 1 x HBSS with 20 mM HEPES. Meanwhile, $90 \cdot 10^6$/90 µl bacteria were opsonized in 1 x HBSS with 20 mM HEPES with 10 µl C5 deficient serum for 10 min at RT. Afterwards $9 \cdot 10^5$ neutrophils and $9 \cdot 10^6$ bacteria were co-incubated at 37°C for 30 min with continuous shaking. As control served a sample with 1 x HBSS with 20 mM HEPES and $9 \cdot 10^6$ bacteria. Following co-incubation, the cells were lysed with 1 mg/ml saponin in 1 x HBSS with 20 mM HEPES for 10 min at RT. Finally, the samples were diluted 1:5 in LB medium and transferred into a 96-well microplate with a final volume of 100 µl per well. A series of 1:2 dilutions over 12 wells in LB medium from the stock bacterial suspension was measured in parallel and used to calculate the percentage of bacterial survival. All samples were measured as duplicates and the mean was used for further calculations. Bacterial growth was measured in an Infinite M200pro-Tecan reader on basis of changes in the optical density at 650 nm every 5 min at 37°C for 15 h with shaking every 3 min.

Glucose uptake assay

Neutrophils were adjusted to $5 \cdot 10^6$ cells/ml in glucose-free XF assay medium. Afterwards 100 µl cell suspension were seeded per well of a 96-well microplate and 100 µg/ml 2(N-(7-nitrobenzen-2oxa-1,3-diazol-4-yl)amino)-2-

deoxyglucose (2-NBDG) was added. The cells were incubated for 10 min at 37°C and 5 % CO_2. Subsequently, the cells were washed twice and resuspended in FACS buffer. Glucose uptake was assessed by flow cytometry.

DHR assay

The intracellular production of ROS was assayed by flow cytometry using the substrate dihydrorhodamine 123 that diffuses into the cells and is oxidized by ROS to the fluorescent rhodamine 123. H_2O_2 rather than $O_2^{-\cdot}$ is required to oxidise the nonfluorescent DHR 123 to the fluorescent rhodamin 123 derivate. This slow reaction is catalysed by enzymes with peroxidase activity such as MPO. Although the DHR oxidation is promoted by H_2O_2, this assay can also be used to detect $O_2^{-\cdot}$, because the dismutation of $O_2^{-\cdot}$ to H_2O_2 and oxygen is rapid even in the absence of the superoxide dismutase. Although the DHR 123-based technique is simple and rapid, this method is not very sensitive. Per sample 100 µl of $5 \cdot 10^6$ cells/ml neutrophils in RPMI complete were added to a U-tube. Subsequently, cells were loaded by addition of 2 µM DHR 123, and the cells were stimulated with either 4 µM PMA or any other indicated stimuli for 5 min at 37°C and 5 % CO_2. The reaction was stopped by 2 min incubation on ice. Afterwards the samples were diluted by adding 100 µl RPMI complete or 1 x DPBS and the fluorescence intensity of the cells was analyzed immediately by flow cytometry.

RNA isolation, quality control and RNA sequencing

RNA isolation from neutrophils was performed as previously described (Tamassia et al., 2014). Shortly, $10 \cdot 10^6$ neutrophils were harvested in 2 ml reaction tubes and centrifuged at 300 x g for 5 min at RT. Further RNA isolation was performed by usage of the RNeasy mini kit in accordance with the manufacturer´s protocol. The washing with 700 µl RW1 buffer as indicated in step 6 of the RNeasy mini kit protocol was not performed, instead an on column DNase digestion as suggested in the optional step 9 was carried out. The RNA was eluted in 30 µl of RNase-free water and stored at -70°C. The concentration of the isolated RNA was measured by a NanoPhotometer™. Further the purity was assessed by measurement of the A260/A280 and the A260/A230 ratio. The A260/A280 ratio represents the amount of remaining phenols and proteins after the nucleic acid isolation and should be for pure RNA around 2.1. The A260/A230 ratio represents the contamination with organic substances. Pure RNA should have a A260/A230 ratio between 2.1 and 2.3. For assessment of RNA integrity the RNA integrity number (RIN) of the isolated RNA was determined. The isolated RNA was diluted to 1 ng/µl in RNase-free water and boiled 2 min at 70°C. The RNA was further prepared as described in the protocol of the Agilent RNA 6000 Pico kit and run on a chip in the Agilent 2100 Bioanalyzer. The Agilent 2100 Bioanalyzer Expert software generates the ratio of the 18S and 28S ribosomal subunits as RIN value, which can range from 10 (highly intact RNA) to 1 (completely degraded RNA). A RIN value $\geq$ 6.5 was defined as acceptable for transcriptome analysis. RNA sequencing was performed by the genome sequencing company Novogene (Hong Kong). The bioinformatics analysis was performed by Prof. Dr. Hauke Busch from the Lübeck Institute of Experimental Dermatology (LIED) at the University of Lübeck. Pre-processed read sequences were aligned to the human genome (Human Genome HRCh38, Ensembl version 97) or the *L. donovani* genome (cDNA sequences corresponding to Ensembl gene predictions, version 44) by using salmon version 14.1. Transcripts were considered significantly differentionally expressed at $p<0.05$. Functional enrichment analysis was done by using Gene Ontology, Hallmark and Reactome gene sets. A Connectivity Map (CMAP) analysis and a protein-protein interaction network were generated for *L. donovani*-infected neutrophils. Visualization of plots was performed by using R.

ATP assay

For quantification of intracellular ATP content, $1 \cdot 10^6$ neutrophils were resuspended in 500 µl Aqua dest. and boiled for 5 min at 100°C. The ATP determination kit was performed with 10 µl lysate according to the manufacturer´s protocol. Luminescence was measured with the Infinite M200pro-Tecan reader and Tecan i-control 1.7 software.

Lactate assay

The metabolite L-(+)-lactate was detected by the lactate assay kit in cell-free culture supernatants. The supernatants of corresponding samples were filtered through an Amicon® 10 kDa molecular weight cutoff ultracentrifuge filter for 15 min at 21 000 x g at RT to remove the lactate dehydrogenase. The lactate assay was performed with 5 µl of the filtrate in accordance to the manufacturer´s instructions. The lactate concentration was calculated by interpolation of a standard curve and after background correction by subtraction of medium only values.

Pyruvate assay

The metabolite pyruvate was detected by the pyruvate assay kit in whole cell lysates. $1 \cdot 10^6$ neutrophils were resuspended in 500 µl Aqua dest. and boiled for 5 min at 100°C. The pyruvate assay was performed with 5 µl of the lysate in accordance to the manufacturer´s instructions. The pyruvate concentration was calculated by interpolation of a standard curve and after background correction by subtraction of medium only values.

PAS staining

For staining 100 000 neutrophils were cytocentrifuged on a microscopy slide and fixed 2 min at RT with Diff-Quick® fixation solution. The microscopy slide was rinsed 1 min with Aqua dest. and immersed in 0.5 % periodic acid solution for 5 min at RT. Afterwards the microscopy slide was washed in several changes of Aqua dest. and immersed in Schiff´s reagent for 15 min at RT. The microscopy slide was rinsed 5 min with Aqua dest.

MitoSOX™ Red mitochondrial superoxide indicator staining

Neutrophils were adjusted to $2 \cdot 10^6$ cell/ml in 1 x HBSS with 20 mM HEPES and loaded with 5 µM MitoSOX™ Red mitochondrial superoxide indicator for 10 min at 37°C. The cells were washed once with 1 x HBSS with 20 mM HEPES and 200 µl (400 000 cells) were transferred to a U-tube. Cells were either stimulated with 20 nM PMA or other indicated stimuli for 30 min at 37°C and 5 % CO_2. Afterwards the samples were further diluted by addition of 100 µl 1 x HBSS with 20 mM HEPES and the fluorescence intensity was analyzed by flow cytometry.

NAD/NADH-Glo™ assay

For detection of total as well as separate amounts of oxidized and reduced nicotinamide adenine dinucleotides (NAD^+ and NADH, respectively) and determination of their ratio the bioluminescent NAD/NADH-Glo™ assay was performed with 200 000 neutrophils per sample in accordance to the manufacturer´s instructions. The luminescence kinetic was measured 1 h with the Infinite M200pro-Tecan reader and Tecan i-control 1.7 software.

Fatty acid uptake assay

For the measurement of fatty acid uptake by neutrophils the green fluorescent fatty acid analogs BODIPY® FL C_{16} and C_{12} were used. Neutrophils were adjusted to $5 \cdot 10^6$ cells/ml in 1 x DPBS and either 10 nM BODIPY® FL C_{16} or C_{12} were added. After 30 min incubation at 37°C and 5 % CO_2, protected from light, the cells were washed twice with 1 x DPBS. Subsequently, 100 µl cell suspension were transferred to a U-tube and fatty acid uptake was assessed by flow cytometry.

Arginase activity assay

The activity of arginase 1 in neutrophils was determined with the arginase activity assay kit. For cell lysate preparation $1 \cdot 10^6$ neutrophils were harvested and washed once with 1 x DPBS at 1000 x g for 10 min at 4°C. The following preparation and lysis of samples was performed in accordance to the manufacturer´s protocol. Finally, the absorption was measured at 430 nm (A430) with the Infinite M200pro-Tecan reader and Tecan i-control 1.7 software. The arginase activity was calculated as:

$$\text{Activity} = \frac{(A430)\text{sample} - (A430)\text{blank}}{(A430)\text{standard} - (A430)\text{water}} \times \frac{(1\ \text{mM} \times 50 \times 1000)}{(\text{sample volume} \times \text{reaction time})}$$

Statistical analysis

If not stated differently, the presented data were generated from a minimum of three independent experiments with neutrophils isolated from different blood donors. Statistical analysis was performed with the GraphPad Prism software 6 using the one-way ANOVA followed by Sidak´s t-test for multiple comparisons or unpaired t-test followed by Welch´s correction. A p-value ≤ 0.05 was considered statistically significant.

Results

Part I: Polarization of primary human neutrophils toward N1 and N2 phenotypes *in vitro*

QVD-OPh suppresses apoptosis and cell death of *in vitro* polarized neutrophils up to 48 h

Increasing evidence over the last decade has demonstrated the existence of several subpopulations of neutrophils with different actions during homeostasis, infection, inflammation and especially cancer. It has been assumed that the tumor microenvironment controls polarization and neutrophil recruitment to the tumor, and that TANs can regulate tumor progression as anti-tumor entity, N1 neutrophils, or as pro-tumor entity, N2 neutrophils. However, a full understanding of neutrophil heterogeneity and plasticity is currently lacking as most data refer to murine cancer models. This highlights the need for phenotypic and functional profiling of human neutrophil subsets. One aim of this study was to polarize primary human neutrophils toward the N1 and N2 phenotype *in vitro*. To achieve polarization toward the N1 phenotype, neutrophils were cultivated in complete medium supplemented with a N1 polarization cocktail containing the activating stimuli LPS, IFNγ and IFNβ. In order to obtain a polarization toward the N2 phenotype neutrophils were cultured under conditions mimicking the tumor microenvironment by adding a N2 polarization cocktail to complete medium containing L-lactate, adenosine, TGFβ, IL-10, PGE_2 and G-CSF. Additionally, the pH was adjusted to 6.5 and the cells were cultured under hypoxic conditions with 2 % O_2.

Neutrophils in the circulation are terminally differentiated cells with a limited lifespan of few hours until they undergo apoptosis. As polarization effects were investigated for 24 h and 48 h, the lifespan of neutrophils had to be prolonged. For this purpose the Pan-caspase inhibitor QVD-OPh was added in the presence of the N1 or N2 polarization cocktail to the neutrophils. For simplification, neutrophils treated with the N1 polarization cocktail in the presence of QVD-OPh will be called in the following N1-like, whereas neutrophils treated with the N2 polarization cocktail in the presence of QVD-OPh will be termed N2-like. Neutrophils treated only with QVD-OPh in complete medium served in all experiments as control and will be referred to as N0. To test the effects to QVD-OPh on the viability and apoptosis of N0, N1-like and N2-like neutrophils an Annexin-V and PI staining was performed and analyzed by flow cytometry. Representative dot plots (**Figure 17**, **A**-**I**) revealed that N0, N1-like and N2-like neutrophils did not show apoptosis (lower right quadrant), late apoptosis (upper right quadrant) or necrosis (upper left quadrant). Untreated neutrophils showed signs of apoptosis and late apoptosis after 24 h and 48 h. N0, N1-like and N2-like neutrophils showed significantly higher viability compared to untreated neutrophils after 24 h (**Figure 17**, **J**) and 48 h (**Figure 17**, **K**). These data showed that a QVD-OPh treatment efficiently suppresses apoptosis of primary human neutrophils *in vitro*.

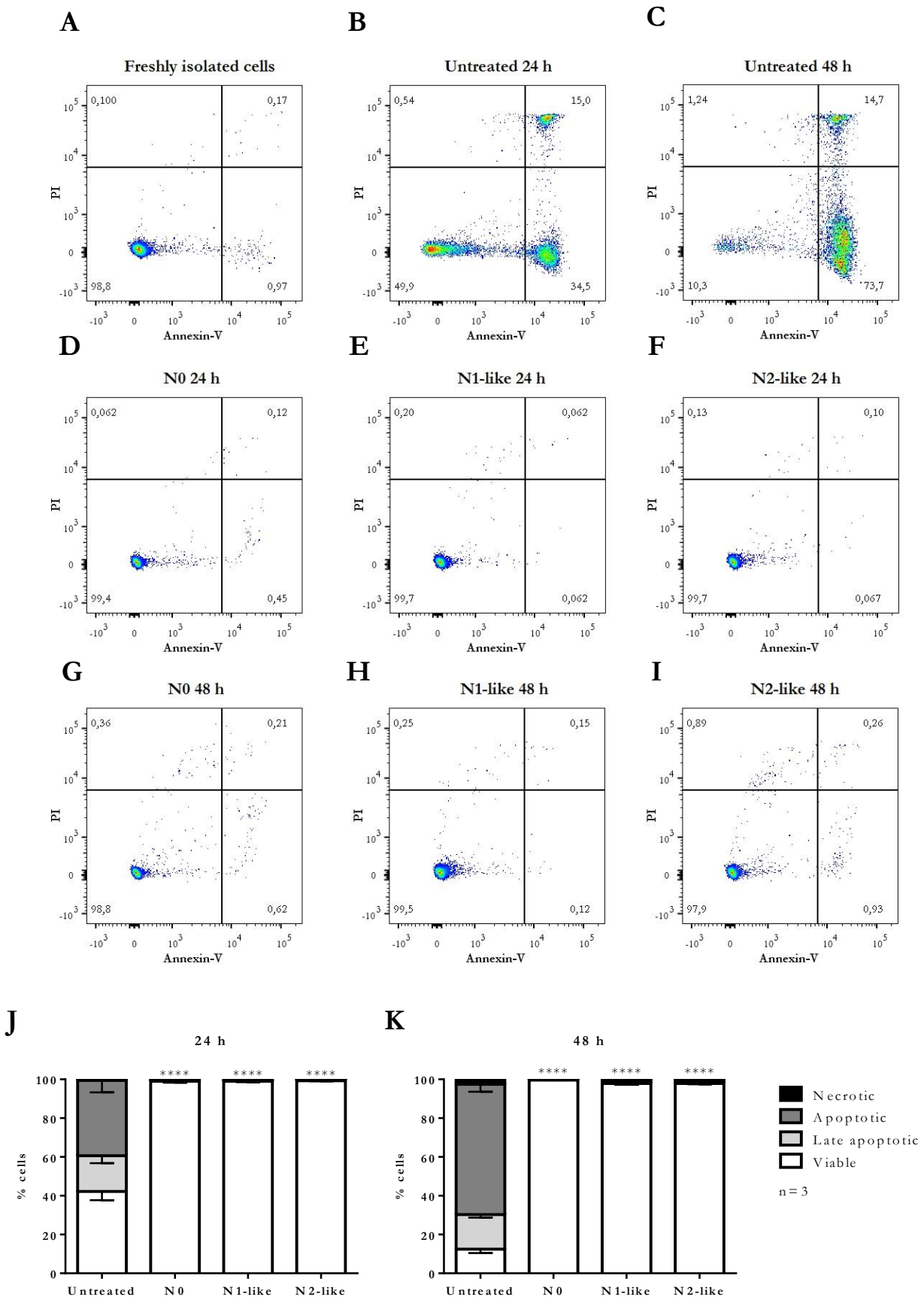
A
Freshly isolated cells
0,100
0,17
98,8
0,97
B
Untreated 24 h
0,54
15,0
49,9
34,5
C
Untreated 48 h
1,24
14,7
10,3
73,7
D
N0 24 h
0,062
0,12
99,4
0,45
E
N1-like 24 h
0,20
0,062
99,7
0,062
F
N2-like 24 h
0,13
0,10
99,7
0,067
G
N0 48 h
0,36
0,21
98,8
0,62
H
N1-like 48 h
0,25
0,15
99,5
0,12
I
N2-like 48 h
0,89
0,26
97,9
0,93
PI
Annexin-V
J
24 h
K
48 h
% cells
Untreated
N0
N1-like
N2-like
****
Necrotic
Apoptotic
Late apoptotic
Viable
n = 3

Figure 17. Apoptosis and viability of *in vitro* polarized neutrophils. Primary human neutrophils were incubated in the presence of a N1 or N2 polarization cocktail (N1-like and N2-like, respectively) including the Pan-caspase inhibitor QVD-OPh for 24 h and 48 h. Neutrophils which were only treated with QVD-OPh (N0) served as control. Untreated cells were cultured in the absence of QVD-OPh. Apoptosis and cell viability was assessed by annexin-V and PI staining and analyzed by flow cytometry. Annexin-V- and PI-negative cells (lower left quadrant) were regarded as viable, whereas annexin-V only positive cells (lower right quadrant) were considered as apoptotic, annexin-V- and PI-positive cells were defined as late apoptotic (upper right quadrant) and PI only positive cells were regarded necrotic (upper left quadrant). Representative dot plots are shown in the panels **A**-**I**. Bar diagrams (**J**, **K**) show mean ± SD of viable, late apoptotic, apoptotic and necrotic cells (n=3), ****p≤0.0001. The ratio (%) of viable cells was used for statistical analysis compared to untreated cells by one-way ANOVA.

To complement the data from the annexin-V and PI staining, cell death of N0, N1-like and N2-like neutrophils was assessed by measuring the release of the cytosolic enzyme lactate dehydrogenase (LDH) in the culture supernatant. LDH serves as conventional marker for cell viability, loss of membrane integrity and necrosis. In contrast to untreated neutrophils, N0, N1-like and N2-like neutrophils released significantly lower amounts of LDH after 24 h and 48 h in culture (**Figure 18**). Consequently, differences between N0, N1-like and N2-like neutrophils that might be caused by apoptosis or cell death can be excluded from the following experiments.

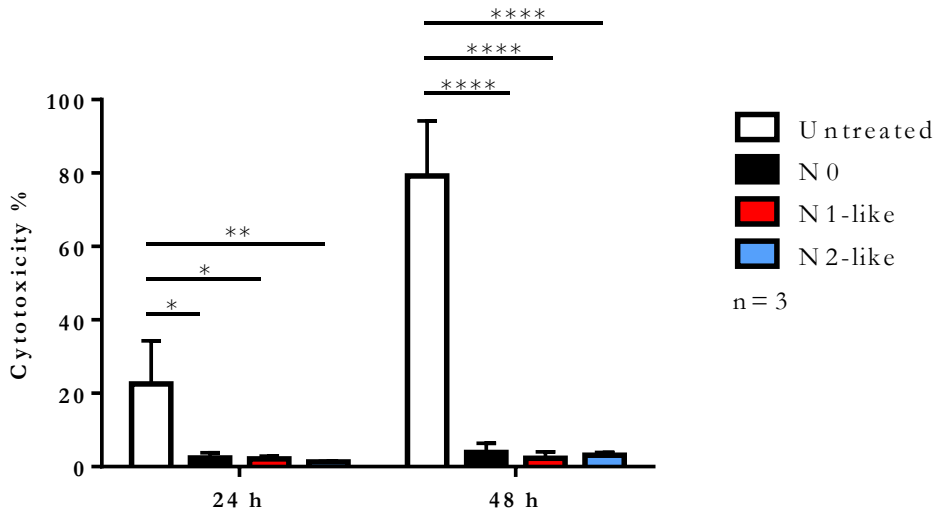

Figure 18. Lactate dehydrogenase (LDH) release of *in vitro* polarized neutrophils. Primary human neutrophils were incubated for 24 h and 48 h in the presence of a N1 or N2 polarization cocktail (N1-like and N2-like, respectively) including the Pan-caspase inhibitor QVD-OPh. Neutrophils which were only treated with QVD-OPh (N0) served as control. Untreated cells were cultured in the absence of QVD-OPh. Released LDH was measured in cell-free supernatants after 24 h and 48 h by using the CytoTox 96® Non-Radioactive Cytotoxicity Assay in accordance with the manufacturer´s instructions. The bar diagram shows mean cytotoxicity (% of total lysis) ± SD (n=3), *p≤0.05, **p≤0.01, ****p≤0.0001.

QVD-OPh treatment neither induces CD62L shedding nor MPO-derived ROS production

In order to test whether QVD-OPh treatment induces neutrophil activation, which might affect further experiments and data on N0, N1-like and N2-like neutrophils, the analysis of L-selectin (CD62L) shedding as widely used method to investigate neutrophil activation was carried out (Neufert et al., 2001). Freshly isolated neutrophils were incubated for 60 min in the presence of QVD-OPh, fMLP, PMA or LPS and IFNγ and CD62L expression was monitored by flow cytometry. Untreated neutrophil expressed CD62L at high levels on their cell

surface and showed therefore only a few events in the CD62L negative region (**Figure 19**, **A**). The activating stimuli fMLP, PMA or LPS and IFNγ led to a shift towards the CD62L negative region (**Figure 19**, **C**-**E**). In contrast, QVD-OPh treatment did not induce a shift towards the CD62L negative region (**Figure 19**, **B**). These data showed that QVD-OPh treatment did not lead to shedding of CD62L (**Figure 19 B**, **F**) and therefore did not lead to the activation of neutrophils.

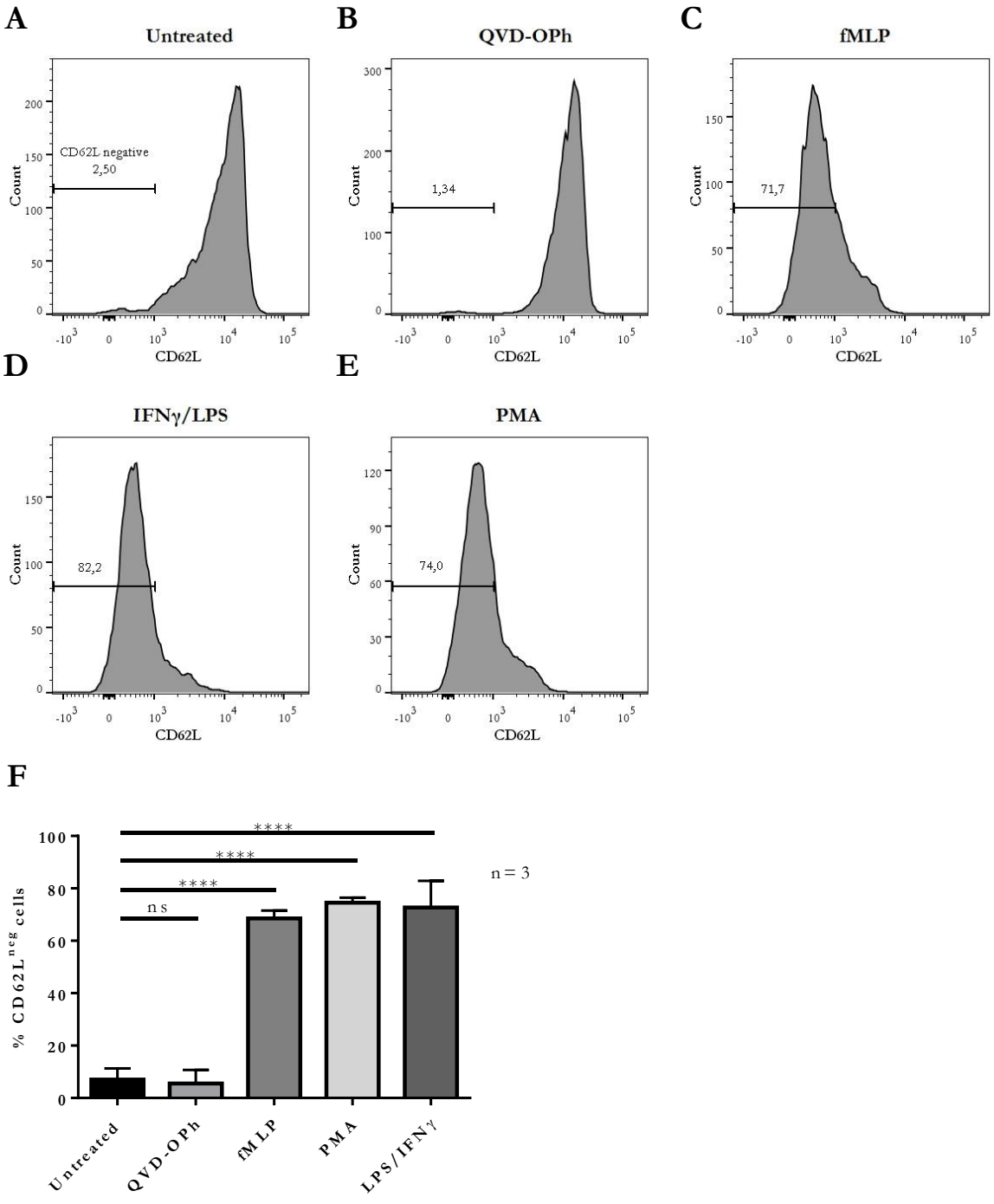

Figure 19. Expression of CD62L on the cell surface of QVD-OP-treated cells. Primary human neutrophils were incubated for 60 min in the presence of QVD-OPh. As positive controls for the induction of CD62L shedding neutrophils

were treated with 1 µM fMLP, 20 nM PMA or 100 ng/mL LPS and 200 U/mL IFNγ. The cell surface expression of CD62L was assessed by flow cytometry. Representative histograms show untreated neutrophils and the definition of $CD62L^{neg}$ cells (**A**), neutrophils treated with QVD-OPh (**B**), fMLP (**C**), PMA (**D**) or LPS and IFNγ (**E**). The numbers indicate the percentage of $CD62L^{neg}$ cells. The bar diagram (**F**) shows the mean ratio (%) of $CD62L^{neg}$ cells ± SD (n=3), ****p≤0.0001, ns = not significant.

The ability to induce ROS production was tested for QVD-OPh treatment by using the luminol-based chemiluminescence assay (Stevens and Hong, 1984). For this purpose freshly isolated neutrophils were treated with either QVD-OPh, medium as negative control or PMA as positive control. QVD-OPh treatment did not increase the MPO-derived ROS (**Figure 20**). Together, these results indicated that QVD-OPh treatment does not activate primary human neutrophils. Consequently, the phenotype and the properties of N1-like and N2-like neutrophils observed in the following experiments were a result of the utilized polarization cocktail.

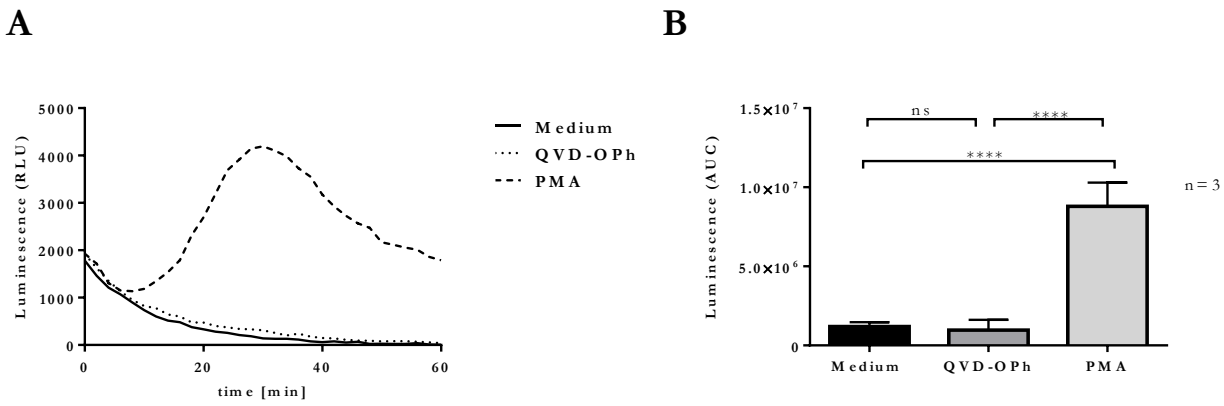

Figure 20. MPO-derived ROS production of QVD-OPh-treated neutrophils. Primary human neutrophils were treated with either QVD-OPh, medium as negative control or 20 nM PMA as positive control. ROS production was measured for 60 min at 37°C and 5 % CO_2 by using the luminol-based chemiluminescence assay. Representative time kinetics curve of the of luminol chemiluminescence are shown (**A**). The bar diagram (**B**) shows the mean of the area under the curve (AUC) values ± SD (n=3), ****p<0.0001, ns = not significant.

N1-like neutrophils show higher degranulation than N2-like neutrophils

In order to evaluate whether the neutrophil phenotypes generated *in vitro* shared typical characteristics of *in vivo* polarized neutrophils, phenotypic markers and features described for N1 and N2 TANs were assessed. First, the activation status of N0, N1-like and N2-like neutrophils was determined by measuring the expression of the degranulation markers CEACAM8 (CD66b) and integrin alpha M (CD11b) via flow cytometry. Since upon activation, the granule membranes fuse with the neutrophil cell membrane, the enhanced cell surface expression of CD66b and CD11b is a reliable indirect marker of neutrophil degranulation. A representative dot plot shows the definition of $CD66b^{high}$ (quadrant Q2 + Q3) and $CD11b^{high}$ (quadrant Q1 + Q2) regions on the basis of CD66b and CD11b cell surface expression of freshly isolated neutrophils (**Figure 21, A**). The ratios of $CD66b^{high}$ and $CD11b^{high}$ cells were significantly increased for N1-like neutrophils as compared to N0 and N2-like neutrophils after 24 h and 48 h *in vitro* polarization (**Figure 21, B-I**). The observed ratio of $CD11b^{high}$ cells of N2-like neutrophils was significantly increased compared to N0 after 48 h (**Figure 21, I**).

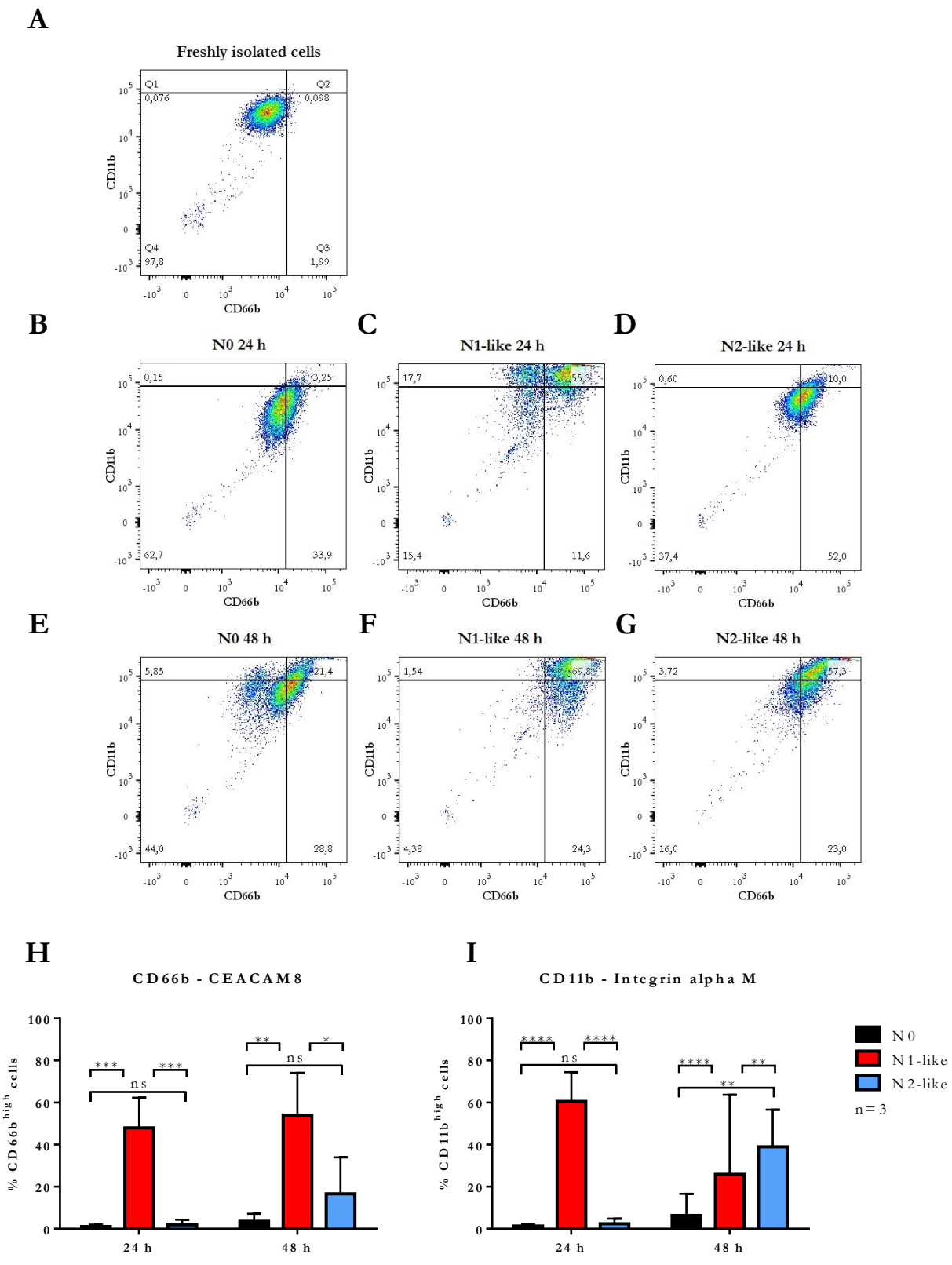

Figure 21. Cell surface expression of the degranulation markers CEACAM8 (CD66b) and integrin alpha M (CD11b) on *in vitro* polarized neutrophils. Primary human neutrophils were incubated in the presence of N1 or N2 polarization cocktail (N1- and N2-like, respectively) containing the Pan-caspase inhibitor QVD-OPh for 24 h and 48 h.

Neutrophils which were only treated with QVD-OPh (N0) served as control. The cell surface expression of CD66b and CD11b was assessed by flow cytometry. A representative dot plot (**A**) shows the definition of CD66b^{high} cells (quadrant Q2 + Q3) and CD11b^{high} cells (quadrant Q1 + Q2) based on the analysis of freshly isolated cells. The representative dot plots in **B**, **C** and **D** show the expression of CD66b and CD11b on N0, N1-like and N2-like neutrophils, respectively, after 24 h of culture. The representative dot plots in **E**, **F** and **G** show the expression of CD66b and CD11b on N0, N1-like and N2-like neutrophils, respectively, after 48 h of culture. The numbers indicate the ratio (%) of cells in the given quadrant. Bar diagrams show the ratio (%) of CD66b^{high} (**H**) and CD11b^{high} (**I**) ± SD (n=3),*p≤0.05, **p≤0.01, ***p≤0.001, ****p≤0.0001, ns = not significant.

In addition to assessment of the indirect degranulation markers CD11b and CD66b, degranulation was investigated by measurement of secreted MPO in the supernatant of N0, N1-like and N2-like neutrophils after 24 h and 48 h in culture. In agreement with the expression of CD66b and CD11b, also MPO secretion by N1-like neutrophils was significantly increased as compared to N0 and N2-like neutrophils (**Figure 22**). N2-like neutrophils showed also significantly higher levels of MPO secretion compared to N0 after 48 h (**Figure 22**). These data demonstrated that incubation of neutrophils with the N1 polarization cocktail induced strong degranulation and associated activation of neutrophils.

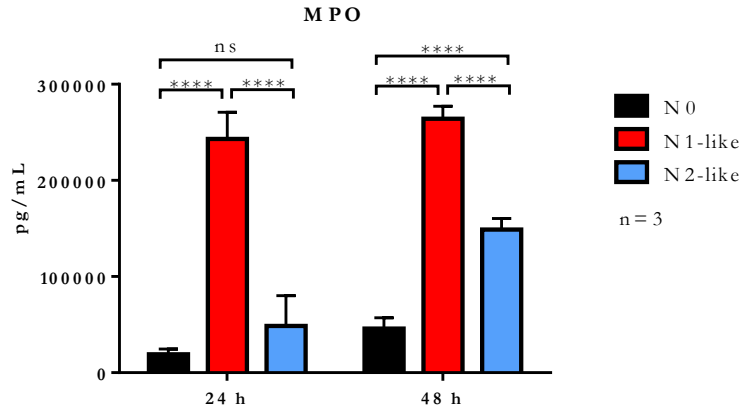

Figure 22. Myeloperoxidase (MPO) secretion of *in vitro* polarized neutrophils. Primary human neutrophils were incubated in the presence of N1 and N2 polarization cocktail (N1- and N2-like, respectively) containing the Pan-caspase inhibitor QVD-OPh for 24 h and 48 h. Neutrophils which were only treated with QVD-OPh (N0) served as control. Cell-free supernatants were collected after 24 h and 48 h. The concentration of secreted MPO was measured by ELISA. The bar diagram shows the mean ± SD (n=3), **** p≤0.0001, ns = not significant.

N1-like neutrophils show increased CD62L shedding compared to N2-like neutrophils

L-selectin (CD62L) contributes to neutrophil rolling and transmigration and is rapidly shed upon activation. To complement the data on the activation status of *in vitro* polarized neutrophils also the cell surface expression of CD62L was investigated. Based on a representative histogram of freshly isolated neutrophils a CD62L negative region was defined (**Figure 23**, **A**). As compared to N0 and N1-polarized cells, a significantly reduced shedding of CD62L was observed on N2-like polarized neutrophils after 24 h and 48 h (**Figure 23**, **H**). Significant differences in CD62L shedding between N0 and N1-like neutrophils were not observed. These results indicated that N2-like neutrophils were less activated than N1-like neutrophils.

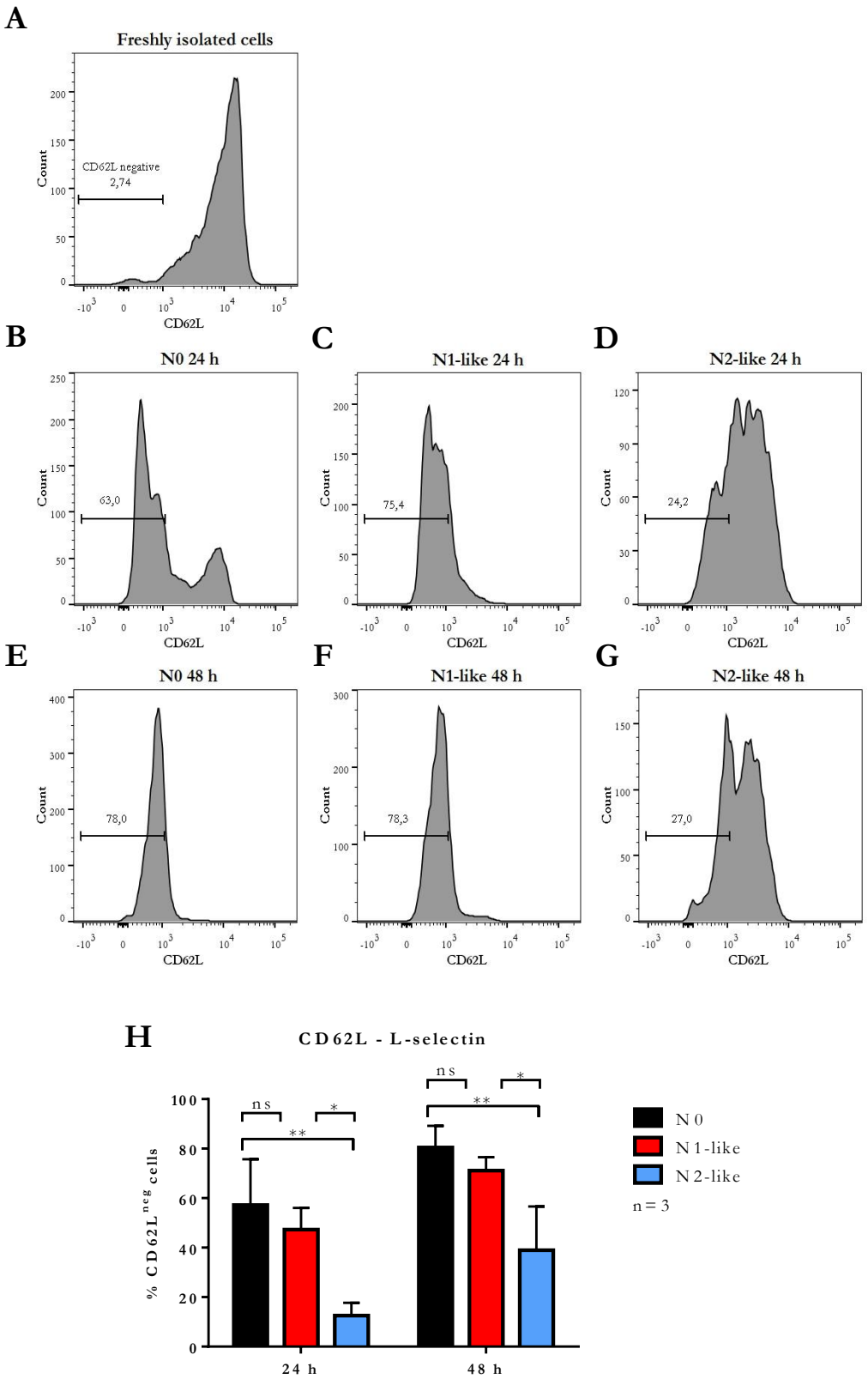

Figure 23. Cell surface expression of the activation marker L-selectin (CD62L) on *in vitro* polarized neutrophils. Primary human neutrophils were incubated in the presence of N1 and N2 polarization cocktail (N1- and N2-like, respectively) containing the Pan-caspase inhibitor QVD-OPh for 24 h and 48 h. Neutrophils which were only treated with

QVD-OPh (N0) served as control. The cell surface expression of CD62L was assessed by flow cytometry. A representative histogram (**A**) shows the region which was set to define $CD62L^{neg}$ cells. The representative histograms in **B**, **C** and **D** show the expression of CD62L on N0, N1-like and N2-like neutrophils, respectively, after 24 h of culture. The representative histograms in **E**, **F** and **G** show the expression of CD62L on N0, N1-like and N2-like neutrophils, respectively, after 48 h of culture. The numbers indicate the ratio (%) of cells in the given quadrant. The bar diagram (H) shows the ratio (%) of $CD62L^{neg}$ cells ± SD (n=3),*p≤0.05, **p≤0.01, ns = not significant.

In vitro polarized neutrophils express typical surface markers of N1 and N2 TANs

To test whether the *in vitro* polarized neutrophils correspond to the N1 and N2 phenotypes observed *in vivo*, several typical N1 and N2 surface markers were investigated by flow cytometry. The typical N1 markers included FasR (CD95) (Fridlender and Albelda, 2012), ICAM-1 (CD54) (Fridlender and Albelda, 2012) and neprilysin (CD10) (Marini et al., 2017). For N2 polarization the cell surface expression of CXCR2 (CD182) (Chao et al., 2016; Nywening et al., 2018) and the typical granulocytic-myeloid-derived suppressor cell (G-MDSC) marker lectin-type oxidized LDL receptor 1 (LOX-1) (Yan et al., 2011) were tested. The typical N1 markers CD95 and CD54 were both significantly increased on N1-like neutrophils compared to N0 and N2-like neutrophils after 24 h and 48 h (**Figure 24**, **A**, **B**, **E**, **F**, **K**, **L**). The expression of the typical N1 marker CD10 showed the tendency to be increased on N1-like neutrophils after 24 h and was significantly increased on N1-like neutrophils compared to N0 and N2-like neutrophils after 48 h (**Figure 24**, **G**, **H**, **N**). The cell surface expression of the typical N2 marker CD182 was significantly higher on N2-like neutrophils compared to N1-like neutrophils after 24 h but showed no difference to N0 (**Figure 24**, **C**, **M**). The same tendency could be observed for 48 h (**Figure 24**, **D**, **M**). The cell surface expression of the typical G-MDSC marker LOX-1 tended to be higher expressed on N1-like neutrophils after 24 h (**Figure 24**, **I**, **O**) and was significantly higher expressed on N1-like neutrophils compared to N0 and N2-like neutrophils after 48 h (**Figure 24**, **J**, **O**). However, N2-like neutrophils showed a higher cell surface expression of LOX-1 than N0 after 48 h (**Figure 24**, **J**, **O**). Despite the deviation of the LOX-1 expression form the expected result, the data demonstrated that *in vitro* polarized neutrophils acquired typical N1 and N2 surface markers according to the utilized polarization cocktail.

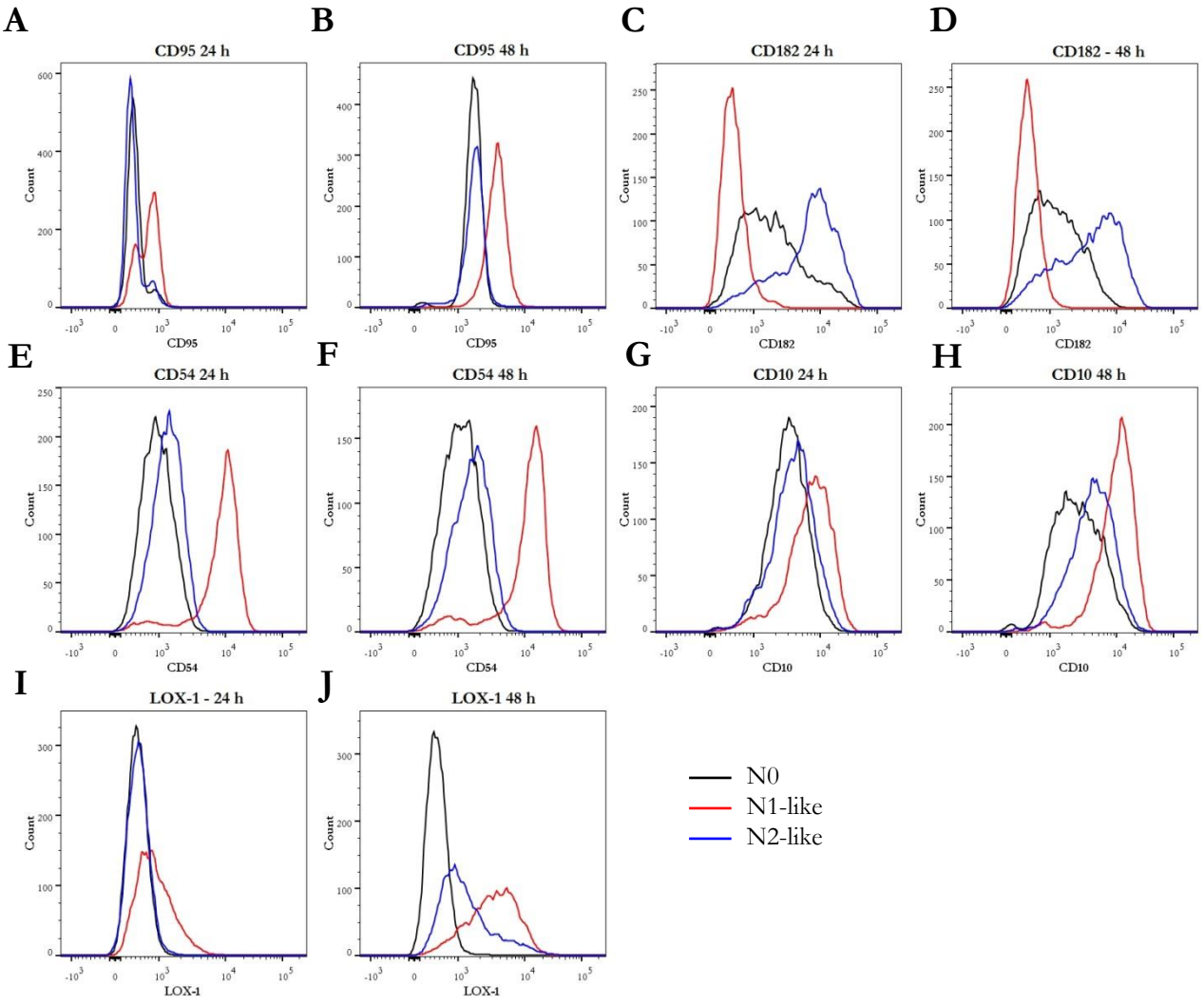
A
CD95 24 h
B
CD95 48 h
C
CD182 24 h
D
CD182 - 48 h
E
CD54 24 h
F
CD54 48 h
G
CD10 24 h
H
CD10 48 h
I
LOX-1 - 24 h
J
LOX-1 48 h
Count
CD95
CD182
CD54
CD10
LOX-1
N0
N1-like
N2-like

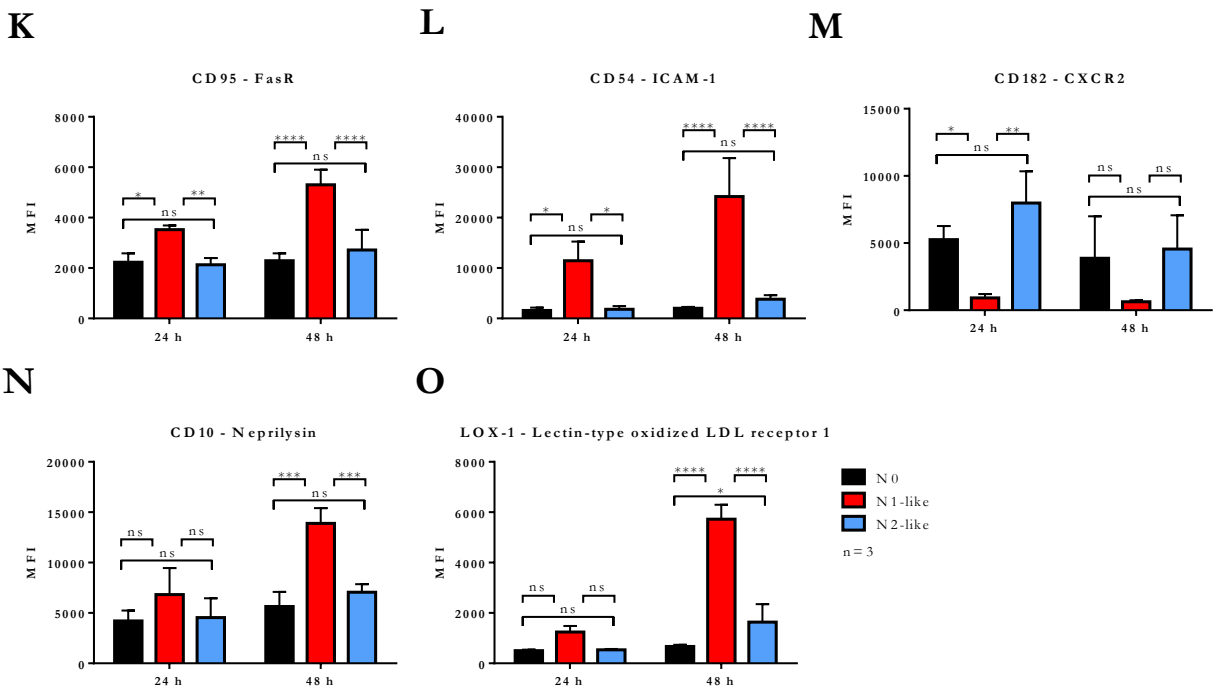

Figure 24. Cell surface expression of typical N1 and N2 markers on *in vitro* polarized neutrophils. Primary human neutrophils were incubated in the presence of N1 and N2 polarization cocktail (N1-like and N2-like, respectively) containing the Pan-caspase inhibitor QVD-OPh for 24 h and 48 h. Neutrophils which were only treated with QVD-OPh (N0) served as control. The cell surface expression of the typical N1 markers FasR (CD95), ICAM-1 (CD54) and neprilysin (CD10) as well as the typical N2 markers CXCR2 (CD182) and LOX-1 was assessed by flow cytometry. Representative histograms show the expression of the mentioned markers on N0, N1-like and N2-like neutrophils stained after 24 h (**A**, **C**, **E**, **G**, **I**) and 48 h (**B**, **D**, **F**, **H**, **J**) in culture. The bar diagrams (**K**-**O**) show the mean fluorescence intensity (MFI) ± SD (n=3),*p≤0.05,**p≤0.01, ***p≤0.001, ****p≤0.0001, ns = not significant.

In vitro polarized neutrophils show typical N1 and N2 protein secretion

Next, the secretion of soluble mediators typical for N1 and N2 TANs was assessed for *in vitro* polarized neutrophils. Data from *in vivo* studies indicate an increased release of the pro-inflammatory cytokines TNF and IP-10 by N1 TANs (Fridlender et al., 2009). On the contrary, it was reported that N2 TANs secrete high amounts of IL-8 to recruit additional neutrophils into the tumor (Fridlender and Albelda, 2012). Moreover, the secretion of the ECM degrading enzyme MMP-9 (Ardi et al., 2007) and the release of VEGF (Christoffersson et al., 2012) by N2 TANs promote tumor angiogenesis and growth. N2 TANs are further characterized by the upregulation of the chemokine MCP-1 (Fridlender and Albelda, 2012). Cell-free supernatants of *in vitro* polarized neutrophils were investigated for the listed soluble mediators after 24 h and 48 h. N1-like neutrophils produced significantly more TNF and IP-10 than N0 and N1-like neutrophils after 24 h and 48 h (**Figure 25**, **A**, **D**). Additionally, it should be noted that N2-like neutrophils did not secrete TNF and IP-10 at any time point and that N0 secreted no TNF after 48 h and no IP-10 at any time point (**Figure 25**, **A**, **D**). The secretion of the typically by N2 TANs released growth factor VEGF was significantly higher by N1-like neutrophils than N0 and N2-like neutrophils after 24 h and significantly higher than the amount of VEGF secreted by N2-like neutrophils after 48 h (**Figure 25**, **B**). The secretion of MCP-1 by N1-like neutrophils showed the tendency to be higher than N0 and N2-like neutrophils after 24 h and was significantly higher than the MCP-1 release by N0 and N2-like neutrophils after 48 h (**Figure 25**, **C**). The release of MMP-9 by N1-like neutrophils was significantly higher than N0 and N2-like neutrophils at both time points (**Figure 25**, **F**). N2-like neutrophils secreted significantly higher levels of IL-8 than N0 and N1-like neutrophils after 24 h and 48 h (**Figure 25**, **E**). However, N1-like neutrophils

also showed a significantly higher release of IL-8 than N0 after 48 h (**Figure 25**, **E**). The high secretion of VEG and MMP-9 by N1-like neutrophils was rather unexpected but is explainable with the pro-inflammatory phenotype induced by the N1 polarization cocktail. Nevertheless, the data indicated a strong resemblance of *in vitro* polarized neutrophils with N1 and N2 TANs.

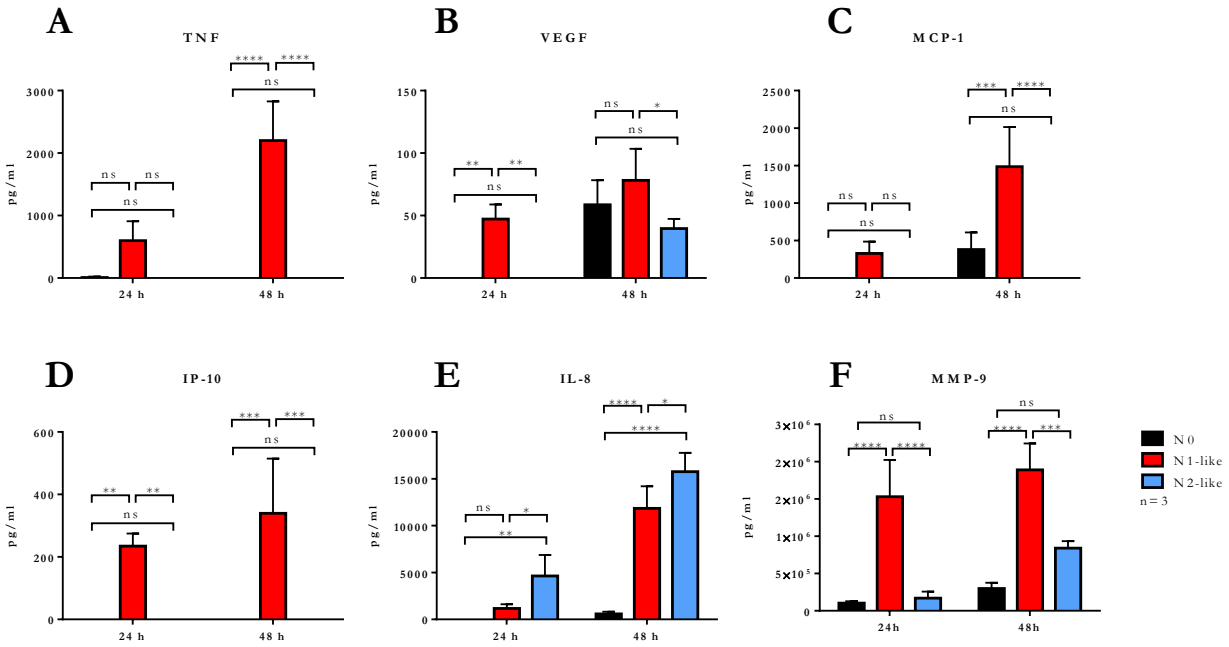

Figure 25. Secretion of typical N1 and N2 proteins by *in vitro* polarized neutrophils. Primary human neutrophils were incubated in the presence of N1 and N2 polarization cocktail (N1- and N2-like, respectively) containing the Pan-caspase inhibitor QVD-OPh for 24 h and 48 h. Neutrophils which were only treated with QVD-OPh (N0) served as control. Cell-free supernatants were collected after 24 h and 48 h. The concentrations of TNF (**A**), VEGF (**B**), MCP-1 (**C**), IP-10 (**D**), IL-8 (**E**) and MMP-9 (**F**) were measured by ELISA. The bar diagrams show mean ± SD (n=3), *p≤0.05, **p≤0.01, ***p≤0.001, ****p≤0.0001, ns = not significant.

N1-like neutrophils show the tendency to produce more MPO-derived ROS than N2-like neutrophils

The role of ROS in the context of TANs is controversially discussed. On the one hand the production of ROS promotes tumor growth indirectly e.g. through MMP activation and triggers genotoxicity, on the other hand some studies imply tumor cell lysis mediated by oxidative burst. Three widely used ROS detection methods were tested in this project to characterize the properties of *in vitro* polarized neutrophils. Firstly, the luminol-amplified chemiluminescence assay used to detect both intra- and extracellular ROS. In contrast to lucigenin, which is mainly oxidized by $O_2^{-\cdot}$, luminol can be oxidized by several ROS, such as H_2O_2, HOCl and $HO\cdot$. The second approach, the lucigenin-amplified chemiluminescence assay, is a sensitive technique to quantify extracellular ROS, mainly superoxide anions ($O_2^{-\cdot}$). Thirdly, the intracellular ROS production in neutrophils loaded with DHR 123 was measured by using flow cytometry. H_2O_2 rather than $O_2^{-\cdot}$ is required to oxidise the nonfluorescent DHR 123 to the fluorescent rhodamin 123 derivate. This slow reaction is catalysed by enzymes with peroxidase activity such as MPO. Although the DHR oxidation is promoted by H_2O_2, this assay can also be used to detect $O_2^{-\cdot}$, because the dismutation of $O_2^{-\cdot}$ to H_2O_2 and oxygen is rapid even in the absence of SOD. Although the DHR 123-based technique is simple and rapid, this method is not very sensitive. For assessment of unstimulated and PMA-induced MPO-derived ROS production the luminol-based chemiluminescence assay was used. N1-like neutrophils showed a significantly increased unstimulated and PMA-induced MPO-derived ROS production

compared to N0 after 48 h (**Figure 26**, **C**, **D**, **E**, **F**). For both time points both unstimulated and PMA-induced N1-like neutrophils showed the tendency of higher MPO-derived ROS production than N2-like neutrophils (**Figure 26**, **A**-**D**, **E**, **F**). Further, this tendency can also be observed after 24 h under unstimulated and PMA-induced conditions in comparison to N0 (**Figure 26**, **A**, **B**, **E**). However, also N2-like neutrophils showed the tendency of higher MPO-derived ROS production under unstimulated and PMA-induced conditions compared to N0 after 24 h (**Figure 26**, **A**, **B, E**). After 48 h the PMA-induced MPO-derived ROS production of N2-like neutrophils was even significantly higher than those of N0 (**Figure 26**, **D**, **F**). These data indicated that N1-like neutrophils tended to produce more MPO-derived ROS than N2-like neutrophils.

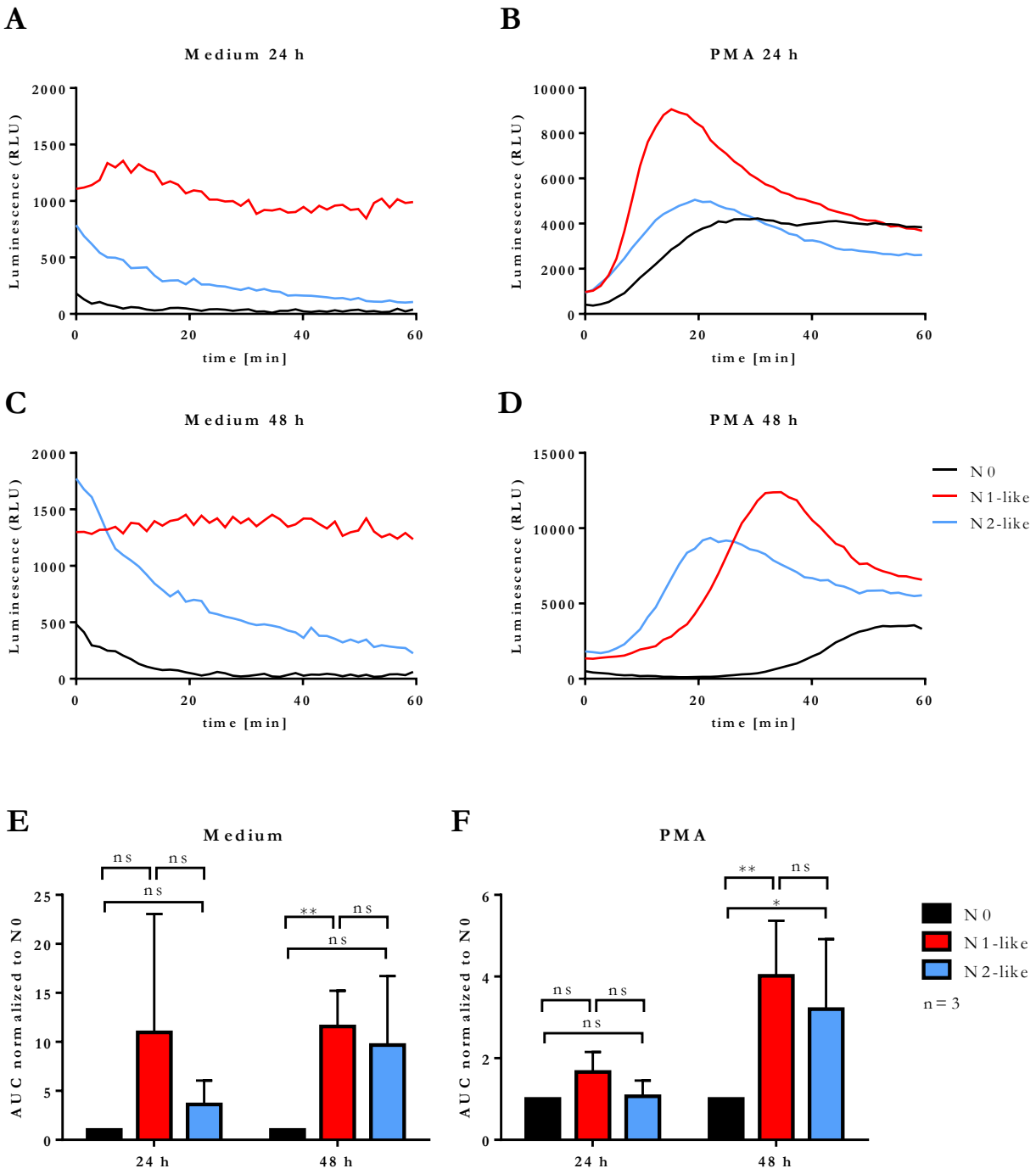

Figure 26. MPO-derived ROS production by *in vitro* polarized neutrophils. Primary human neutrophils were incubated in the presence of a N1 or N2 polarization cocktail (N1- and N2-like, respectively) including the Pan-caspase inhibitor QVD-OPh. Neutrophils which were only treated with QVD-OPh (N0) served as control. After 24 h and 48 h the MPO-derived ROS production was measured for 1 h at 37°C and 5 % CO_2 in medium alone or in the presence or absence of 20 nM PMA by using the luminol-based chemiluminescence assay. Representative curves of luminol chemiluminescence are shown in panels **A**-**D**. The bar diagrams (**E, F**) show the mean area under the curve (AUC) values ± SD normalized to N0 (n=3), *p≤0.05, **p≤0.01, ns = not significant.

PMA-induced superoxide formation of N2-like neutrophils is increased compared to N1-like neutrophils after 48 h

Next, the unstimulated and PMA-induced superoxide formation of *in vitro* polarized neutrophils was assessed by the lucigenin-based chemiluminescence assay. N1-like neutrophils showed increased unstimulated superoxide formation compared to N0 and N2-like neutrophils after 24 h (**Figure 27**, **A**, **E**). After 48 h the unstimulated superoxide formation of N1-like neutrophils showed the tendency to be higher than N0 but no difference to N2-like neutrophils could be observed (**Figure 27**, **C**, **E**). Whereas PMA-induced superoxide formation after 24 h showed no differences between N0, N1-like and N2-like neutrophils, the latter showed significantly increased PMA-induced ROS production compared to N0 and N1-like neutrophils after 48 h (**Figure 27**, **B**, **D**, **F**). These data highlighted again the rather controversial character of ROS in the context of TANs, as the results of the luminol and lucigenin-based chemiluminescence assay were not the same and indicate that the origin of ROS for N1-like and N2-like neutrophils differs.

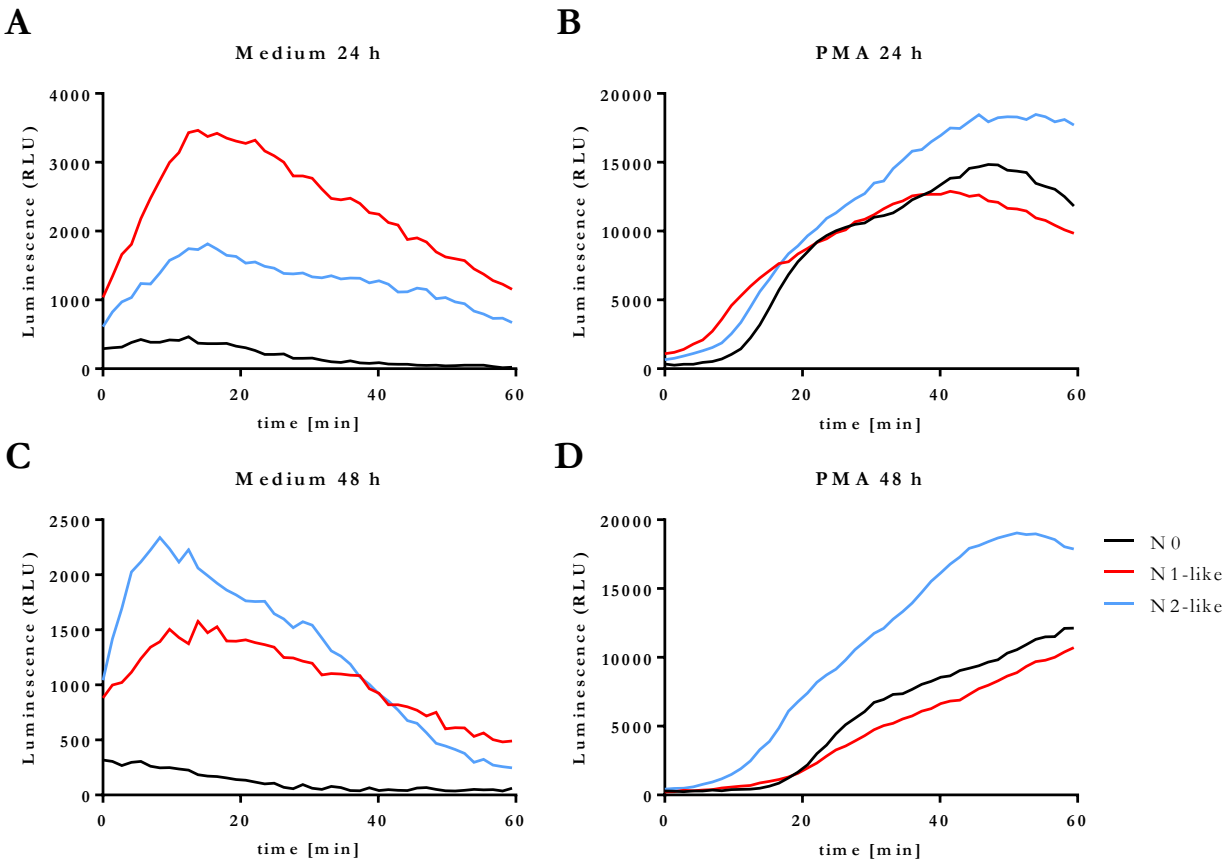

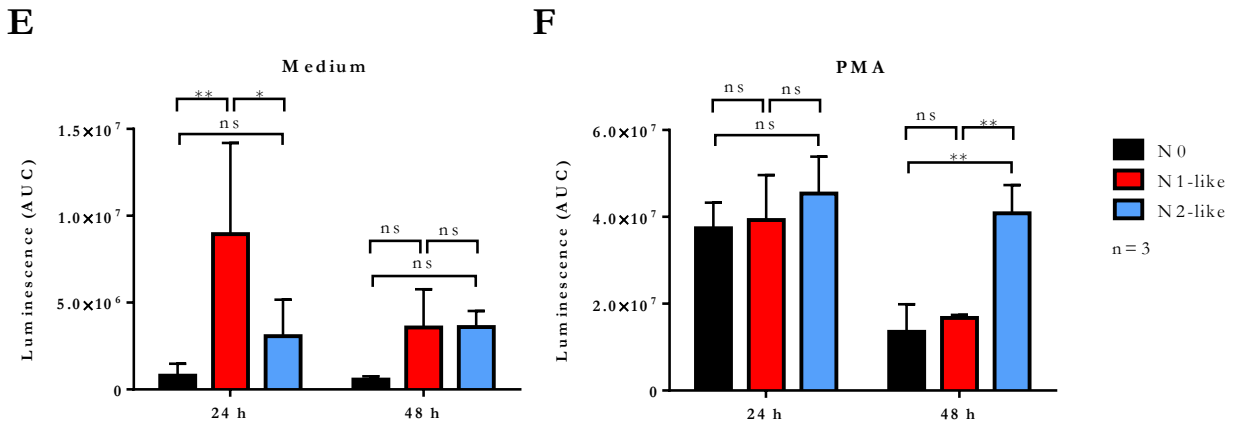

Figure 27. Superoxide production of *in vitro* polarized neutrophils. Primary human neutrophils were incubated in the presence of a N1 or N2 polarization cocktail (N1- and N2-like, respectively) including the Pan-caspase inhibitor QVD-OPh. Neutrophils which were only treated with QVD-OPh (N0) served as control. After 24 h and 48 h the MPO-derived ROS production was measured for 1 h at 37°C and 5 % CO_2 in medium alone or in the presence or absence of 20 nM PMA by using the lucigenin-based chemiluminescence assay. Representative curves of lucigenin chemiluminescence are shown in panels **A**-**D**. The bar diagrams (**E**, **F**) show the mean area under the curve (AUC) values ± SD (n=3), *p≤0.05, **p≤0.01, ns = not significant.

N1-like neutrophils produce more intracellular ROS than N2-like neutrophils

Additionally, also the unstimulated and PMA-induced intracellular ROS production of *in vitro* polarized neutrophils was assessed by using the DHR assay. N1-like neutrophils showed significantly increased unstimulated and PMA-induced intracellular ROS production compared to N0 and N2-like neutrophils after both 24 h and 48 h (**Figure 28**, **A**, **B**, **E**). Significant differences in unstimulated ROS production between N0 and N2-like neutrophils could not be observed (**Figure 28**, **A**, **B**, **E**). Assessment of PMA-induced intracellular ROS production resulted also in no significant differences between N0, N1-like and N2-like neutrophils after 24 h, although N2-like neutrophils showed the tendency to produce less intracellular ROS than N0 and N1-like neutrophils (**Figure 28**, **C**, **F**). After 48 h the intracellular ROS production of N1-like neutrophils was significantly increased compared to N0 and N2-like neutrophils (**Figure 28**, **D**, **F**). These data supported the results obtained by the luminol-based chemiluminescence assay as they implicate a higher ROS production by N1-like neutrophils.

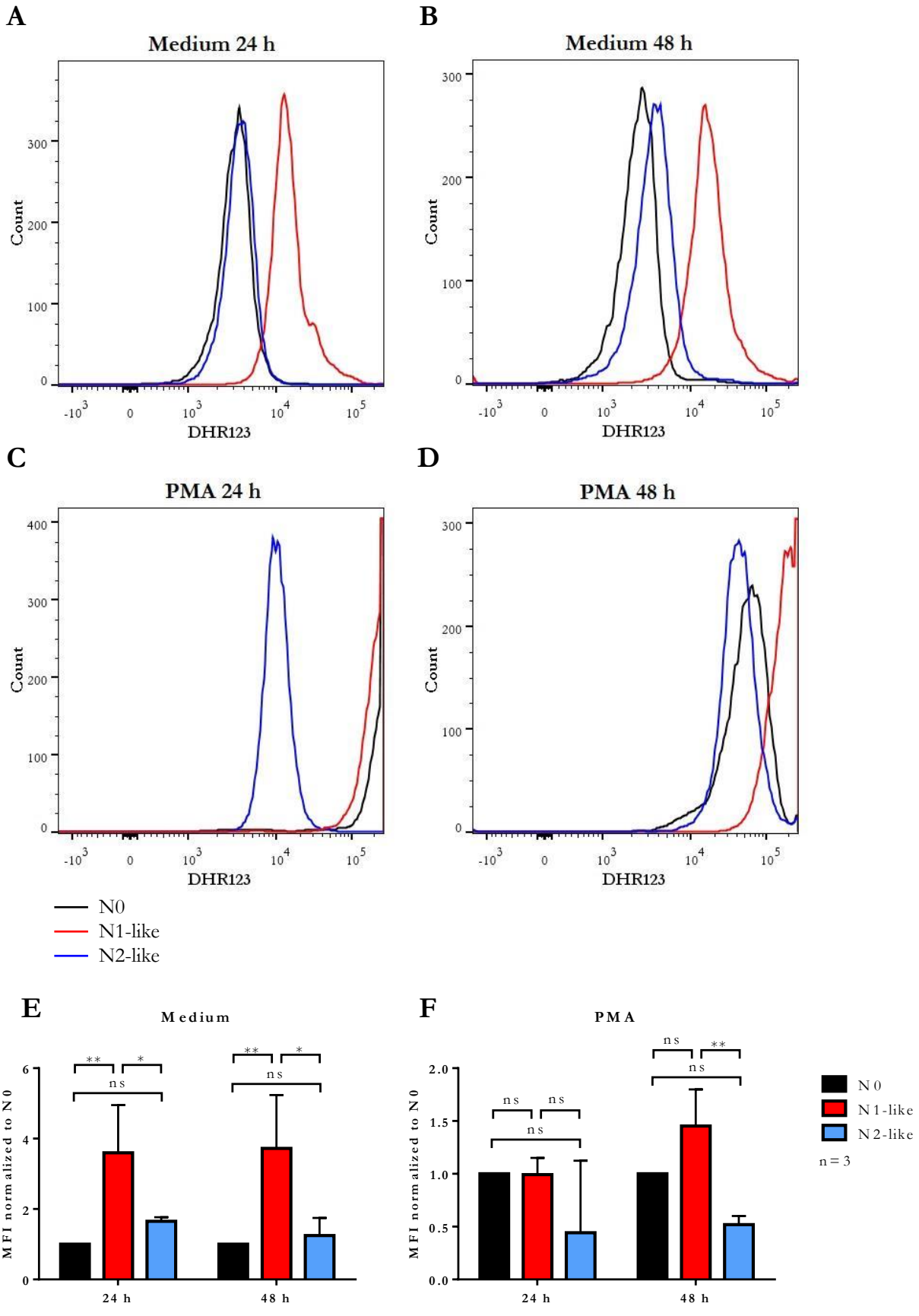
A
Medium 24 h
B
Medium 48 h
C
PMA 24 h
D
PMA 48 h
Count
DHR123
N0
N1-like
N2-like
E
Medium
F
PMA
MFI normalized to N0
24 h
48 h
ns
n = 3

Figure 28. Intracellular ROS production by *in vitro* polarized neutrophils. Primary human neutrophils were incubated in the presence of a N1 or N2 polarization cocktail (N1- and N2-like, respectively) including the Pan-caspase inhibitor QVD-OPh. Neutrophils which were only treated with QVD-OPh (N0) served as control. After 24 h and 48 h the intracellular ROS production was assessed with flow cytometry by using DHR123. Cells were stimulated with 4 µM PMA or medium as control for 30 min at 37°C and 5 % CO_2 in the presence of DHR123. Representative histograms of DHR123 fluorescence of N0, N1-like and N2-like cells are shown in panels **A**-**D**. The bar diagrams (**E**, **F**) show the mean fluorescence intensity (MFI) ± SD normalized to N0 (n=3),*p≤0.05, **p≤0.01, ns = not significant.

N1-like neutrophils show the tendency to kill less bacteria than N2-like neutrophils

Although bacterial killing of N1 and N2 TANs has not been investigated yet, similar neutrophil subpopulations with immunostimulating or immunosuppressive properties, respectively, have been observed in different infection models, including *S.aureus* and *T. cruzi*. It is therefore of interest how the *in vitro* polarized neutrophils react on bacteria as the elimination of invading pathogens in one of the major functions neutrophils fulfill *in vivo*. To investigate the anti-bacterial capacities of *in vitro* polarized neutrophils a bacterial killing assay with the gram negative bacterium *E. coli* and the gram positive bacterium *S. aureus* was performed after 24 h and 48 h of polarization. For this assay growth curves of bacteria were monitored, whereby the turbidity correlated with the bacterial concentration. The more living bacteria were present in the starting material, the faster the growth curve reached its plateau. Despite missing significance, N1-like neutrophils noticeably showed a clear tendency of reduced bacterial killing of *E. coli* and *S. aureus* compared to N0 and N2-like neutrophils after 24 h and 48 h (**Figure 29**). This result was unexpected, as the previous data indicated that N1-like neutrophils are highly activated and showed higher ROS production and degranulation, both effector mechanisms involved in killing bacteria. However, as no data on the killing of bacteria of N1 and N2 TANs are available and the data obtained in this study were not significant, the relevance of bacterial killing might be of minor importance for the evaluation of the *in vitro* polarization of neutrophils.

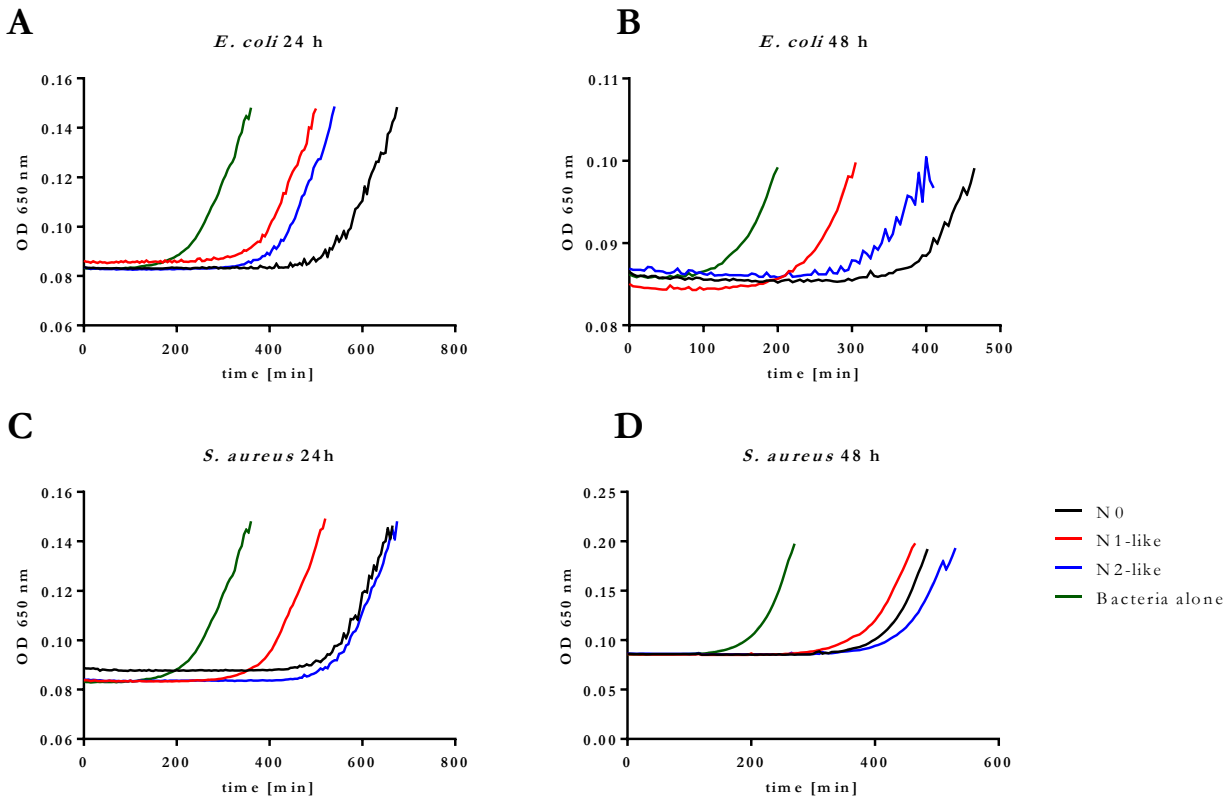

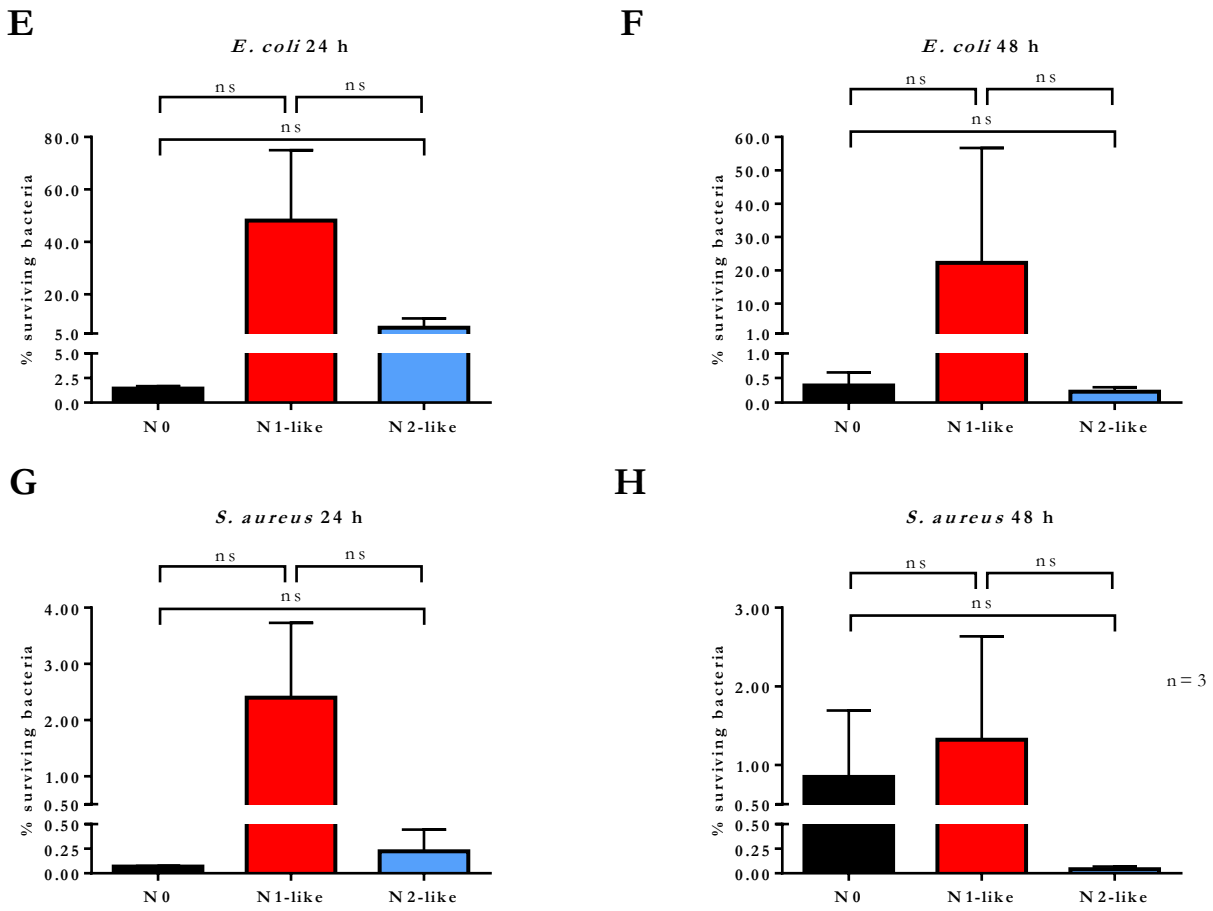

Figure 29. Bacterial killing assay of *in vitro* polarized neutrophils. Primary human neutrophils were incubated in the presence of a N1 or N2 polarization cocktail (N1- and N2-like, respectively) including the Pan-caspase inhibitor QVD-OPh. Neutrophils which were only treated with QVD-OPh (N0) served as control. After 24 h and 48 h polarized neutrophils were adjusted to $10 \cdot 10^6$ cells/ml in 1 x HBSS with 20 mM HEPES. Afterwards, $90 \cdot 10^6$/90 µl *E. coli* or *S. aureus* were opsonized in 1 x HBSS with 20 mM HEPES with 10 µl C5 deficient serum for 10 min at RT. Afterwards $9 \cdot 10^5$ polarized neutrophils and $9 \cdot 10^6$ *E. coli* or *S. aureus* were co-incubated at 37°C for 30 min with continuous shaking. As control served a sample with 1 x HBSS with 20 mM HEPES and $9 \cdot 10^6$ *E. coli* or *S. aureus*. Following co-incubation, the polarized neutrophils were lysed with 1 mg/ml saponin in 1 x HBSS with 20 mM HEPES for 10 min at RT. Finally, the samples were diluted 1:5 in LB medium and transferred into a 96-well microplate with a final volume of 100 µl per well. A series of 1:2 dilutions over 12 wells in LB medium from the stock bacterial suspension was measured in parallel and used to calculate the percentage of bacterial survival. All samples were measured as duplicates and the mean was used for further calculations. Bacterial growth was measured in an Infinite M200pro-Tecan reader on basis of changes in the optical density at 650 nm every 5 min at 37°C for 15 h with shaking every 3 min shown in the representative curves in panels **A**-**D**. The bar diagrams (**G**, **H**) show the mean ratio (%) of surviving bacteria ± SD (n=3), ns = not significant.

N2-like neutrophils exert decreased capacity to kill *L. donovani* promastigotes

To address one of the key objectives of this thesis, that N2-like neutrophils are permissive for *L. donovani*, the anti-leishmanial capacity of *in vitro* polarized neutrophils was assessed by using the limiting dilution assay. Contrary to the standard protocol in which neutrophils were first polarized for either 24 h or 48 h before investigating their properties, for this objective the experimental procedure was changed. As already polarized neutrophils suffered severe damage during washing to remove free, non-ingested parasites, the neutrophils in this

experiment were first infected with *L. donovani* promastigotes (**Figure 30**, **A**) before they were incubated for either 24 h or 48 h in the presence of the N1 or N2 polarization cocktail and the parasite load was determined by using the limiting dilutions assay. As shown in **Figure 30 B**, N2-like neutrophils harbored significant more viable parasite than N1-like neutrophils, indicating a decreased killing ability of *L. donovani* promastigotes in the presence of the N2 polarization cocktail.

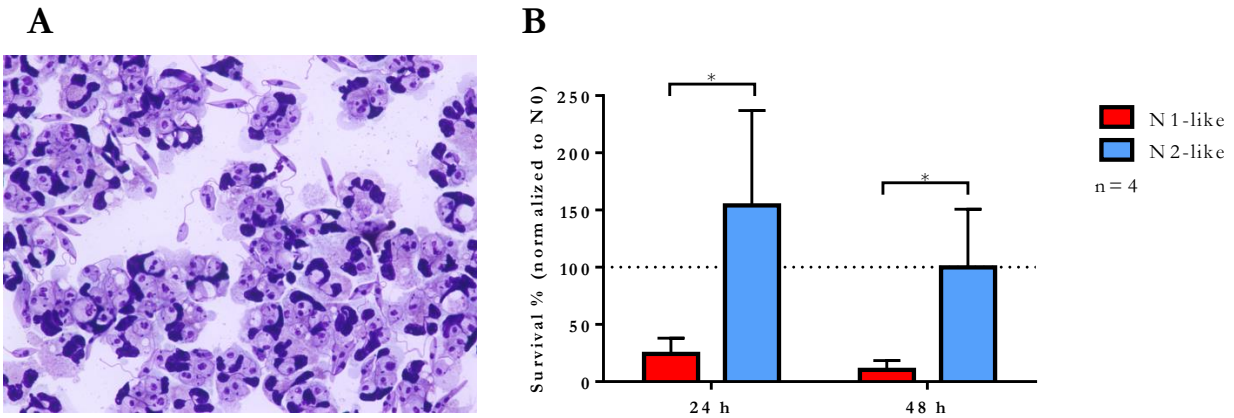

Figure 30. Survival of *L. donovani* promastigotes in *in vitro* polarized neutrophils. Primary human neutrophils were infected with *L. donovani* promastigotes (ratio 1:10) for 3 h at 37°C, 5 % CO_2. The infection rate was determined by Giemsa staining of cytocentrifuged samples, representative microscopy shown in **A**. After removing the free, non-ingested parasites the infected cells were incubated in the presence of a N1 or N2 polarization cocktail at 37°C, 5 % CO_2. Survival of parasites was assessed after 24 h and 48 h by using the limiting dilution assay. The bar diagram (**B**) shows the mean normalized to N0 ± SD (n=4), *p≤0.05.

N2-like neutrophils tend to have higher arginase 1 activity than N1-like neutrophils

One of the major characteristics to distinguish N1 and N2 TANs is the elevated expression of arginase 1 in N2 TANs that suppresses T cell immunity. To assess the arginase 1 activity in *in vitro* polarized neutrophils the Arginase Activity Assay Kit was used after 24 h and 48 h of polarization. As depicted in **Figure 31**, N2-like neutrophils showed the tendency to have higher arginase 1 activity than N1-like neutrophils for both time points. This result demonstrated that the incubation with the N2 polarization cocktail tends to upregulate the activity of the important N2 marker enzyme arginase 1.

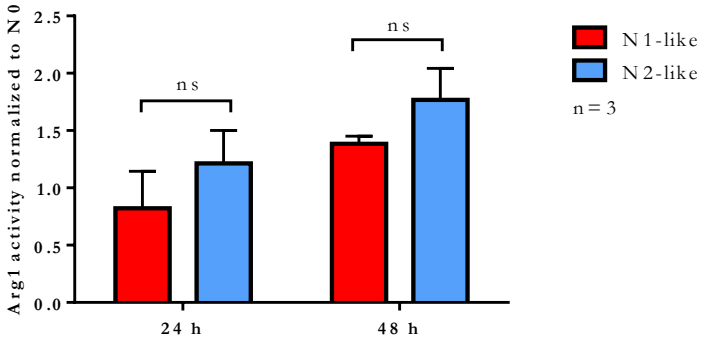

Figure 31. Arginase 1 activity in *in vitro* polarized neutrophils. Primary human neutrophils were incubated in the presence of a N1 or N2 polarization cocktail (N1- and N2-like, respectively) including the Pan-caspase inhibitor QVD-OPh. Neutrophils which were only treated with QVD-OPh (N0) served as control. The arginase 1 (Arg1) activity of polarized

neutrophils was assessed by using the Arginase Activity Assay Kit after 24 h and 48 h in accordance with the manufacturer´s instructions. The bar diagram shows the mean Arg1 activity ± SD normalized to N0 (n=3), ns = not significant.

N1-like neutrophils form more NETs than N2-like neutrophils

Although the role of NETs in cancer has not been completely elucidated, several studies report that NETs promote metastatic progression by trapping circulating tumor cell and thereby allow their proliferation in secondary site. In order to address the NET formation of *in vitro* polarized neutrophils two different technical approaches were applied. First, NET formation upon stimulation with medium or PMA after 24 h and 48 h was assessed by SYTOXGreen staining with fluorescence microscopy (**Figure 32**, **A**-**L**), indicating that N0, N1-like and N2-like neutrophils are capable of forming NETs after PMA stimulation. Subsequently, real-time kinetics of DNA release of medium- and PMA-stimulated polarized neutrophils after 24 h and 48 h were detected by SYTOXGreen staining. As previous studies showed that extracellular DNA stained by SYTOXGreen co-localizes with MPO, the DNA release can be used to quantify NET formation. Stimulation with PMA resulted in no significant differences in NET formation between N0, N1-like and N2-like neutrophils after 24 h and 48 h (**Figure 33**, **A**-**F**, **H**). In contrast, medium-stimulated N1-like neutrophils showed a higher tendency to form NETs than N0 and N2-like neutrophils after 24 and 48 h (**Figure 33**, **A**-**F**, **G**). Although these data were not in line with the elevated NET formation observed for N2 TANs *in vivo*, the upregulated NET formation of N1-like neutrophils matches their pro-inflammatory phenotype.

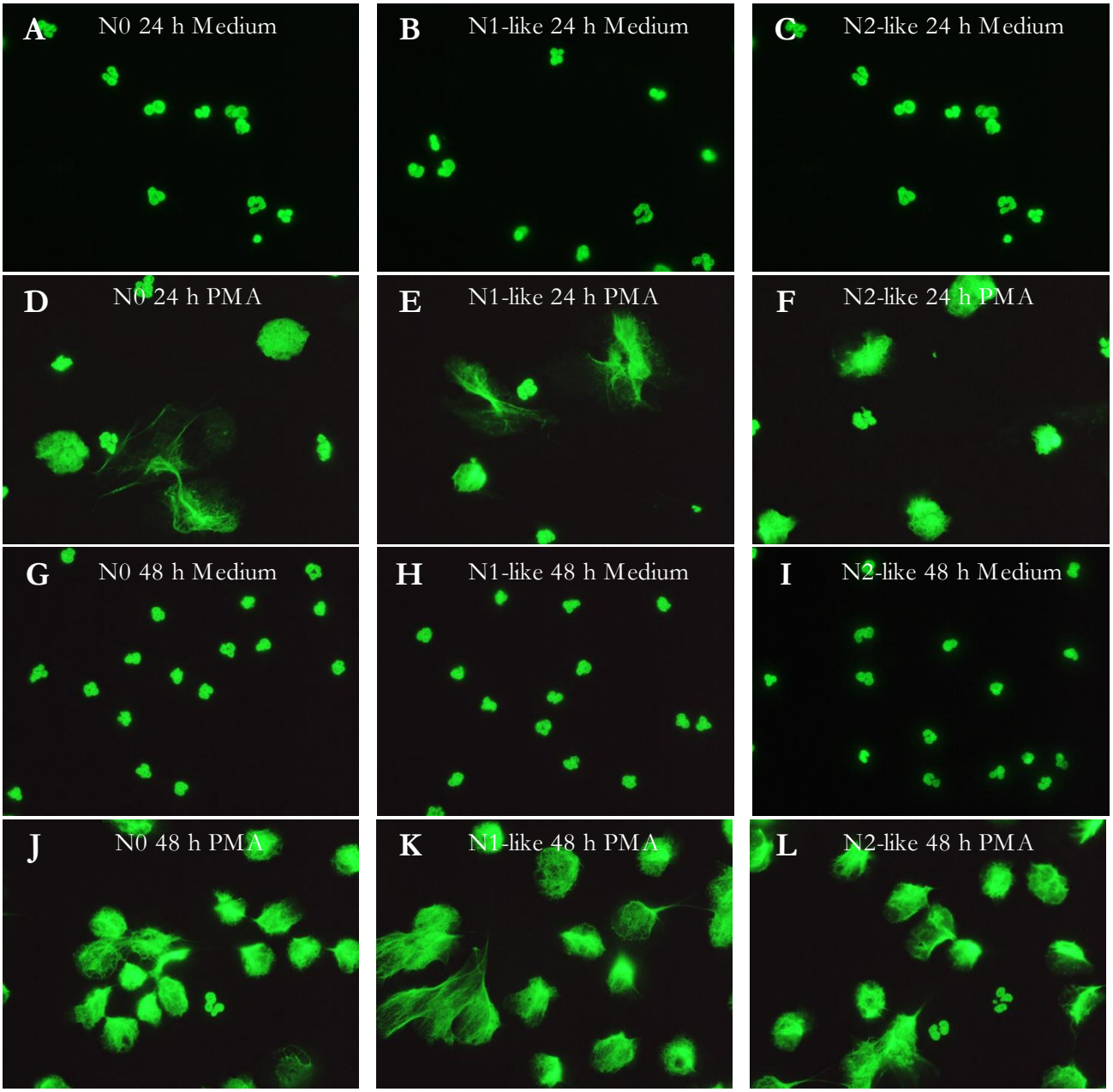

Figure 32. Visualization of NET formation by *in vitro* polarized neutrophils. Primary human neutrophils were incubated in the presence of a N1 or N2 polarization cocktail (N1- and N2-like, respectively) including the Pan-caspase inhibitor QVD-OPh. Neutrophils which were only treated with QVD-OPh (N0) served as control. After 24 h and 48 h NET release was induced by stimulation with 20 nM PMA. After 4 h incubation at 37°C and 5 % CO_2, the cells were fixed and the DNA was stained with 100 nM SYTOXGreen for visual assesment by fluorescence microscopy (FM). Representative FM images of unstimulated cells are shown in the panels **A**-**C** and **G**-**I** and representative FM images of PMA-treated cells are shown in the panels **D**-**F** and **J**-**L**.

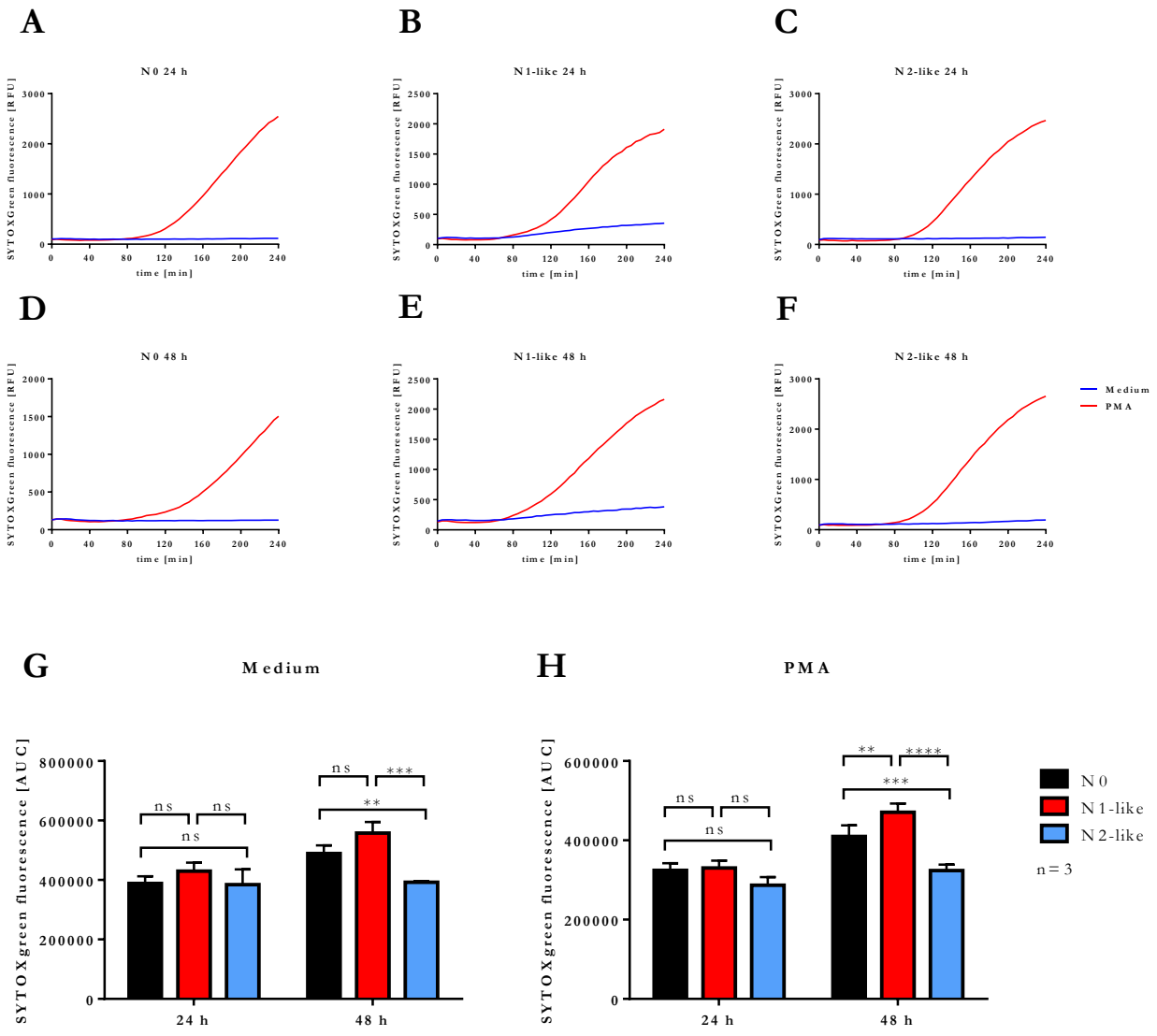

Figure 33. Extracellular DNA detection by SYTOXGreen staining of *in vitro* polarized neutrophils. Primary human neutrophils were incubated in the presence of a N1 or N2 polarization cocktail (N1- and N2-like, respectively) including the Pan-caspase inhibitor QVD-OPh. Neutrophils which were only treated with QVD-OPh (N0) served as control. After 24 h and 48 h, 5 µM SYTOXGreen was added to all samples. Stimulation with 20 nM PMA served as positive control. NET formation was monitored for a period of 4 h at 37°C and 5 % CO_2 by measurement of SYTOXGreen fluorescence. Representative real-time kinetics of NET formation is shown in the panels **A**-**F**. The bar diagrams (**G**, **H**) show the mean area under the curve (AUC) values ± SD (n=3), **p≤0.01, ***p≤0.001, ****p≤0.0001, ns = not significant.

N1-like neutrophils show higher expression of CD64 and CD89 but lower expression of CD16 and CD32 than N2-like neutrophils

ADCC is the most prominent anti-tumor activity of neutrophils. As the process of ADCC relies on the expression of Fc receptors on the effector cell surface, the expression of the of the Fc receptors FcRIIIγ (CD16), FcRIIγ (CD32), FcRIγ (CD64) and FcRα (CD89) on *in vitro* polarized neutrophils was assessed by flow cytometry. CD16 expression on N1-like neutrophils tended to be lower than on N0 and N2-like neutrophils after 24 h and was even significantly decreased on N1-like neutrophils compared to N0 and N2-like neutrophils after 48 h (**Figure 34**, **A**, **B**, **I**). Additionally, N1-like neutrophils showed significantly decreased CD32 expression compared to N2-like neutrophils after 24 h and also significantly decreased CD32 expression compared to N0

and N2-like neutrophils after 48 h (**Figure 34**, **C**, **D**, **J**). Further, N2-like neutrophils tended to express higher levels of CD32 on their cell surface compared to N0 after 24 h and 48 h (**Figure 34**, **C**, **D**, **J**). The expression of CD64 was significantly increased on N1-like neutrophils compared to N0 and N2-like neutrophils after 48 h (**Figure 34**, **E**, **F**, **K**). No differences regarding CD64 expression between N0, N1-like and N2-like neutrophils could be observed after 24 h (**Figure 34**, **E**, **F**, **K**). N1-like neutrophils showed increased expression of CD89 in comparison to N0 and N2-like neutrophils after 24 h (**Figure 34**, **G**, **H**, **L**). The expression of CD89 on N1-like neutrophils was significantly higher than on N0, but showed only a tendency of higher expression than on N2-like neutrophils. However, the expression of CD89 tended to be increased on N2-like neutrophils compared to N0 after 24 h and was even significantly increased compared to N0 after 48 h (**Figure 34**, **G**, **H**, **L**). Unfortunately, these data did not confirm that all Fc receptors involved in ADCC were upregulated on N1-like neutrophils as expected due to their so far well matching properties with N1 TANs. However, as CD89 is regarded as the most potent Fc receptor in ADCC, the obtained data indicated that N1-like neutrophils might be capable of ADCC.

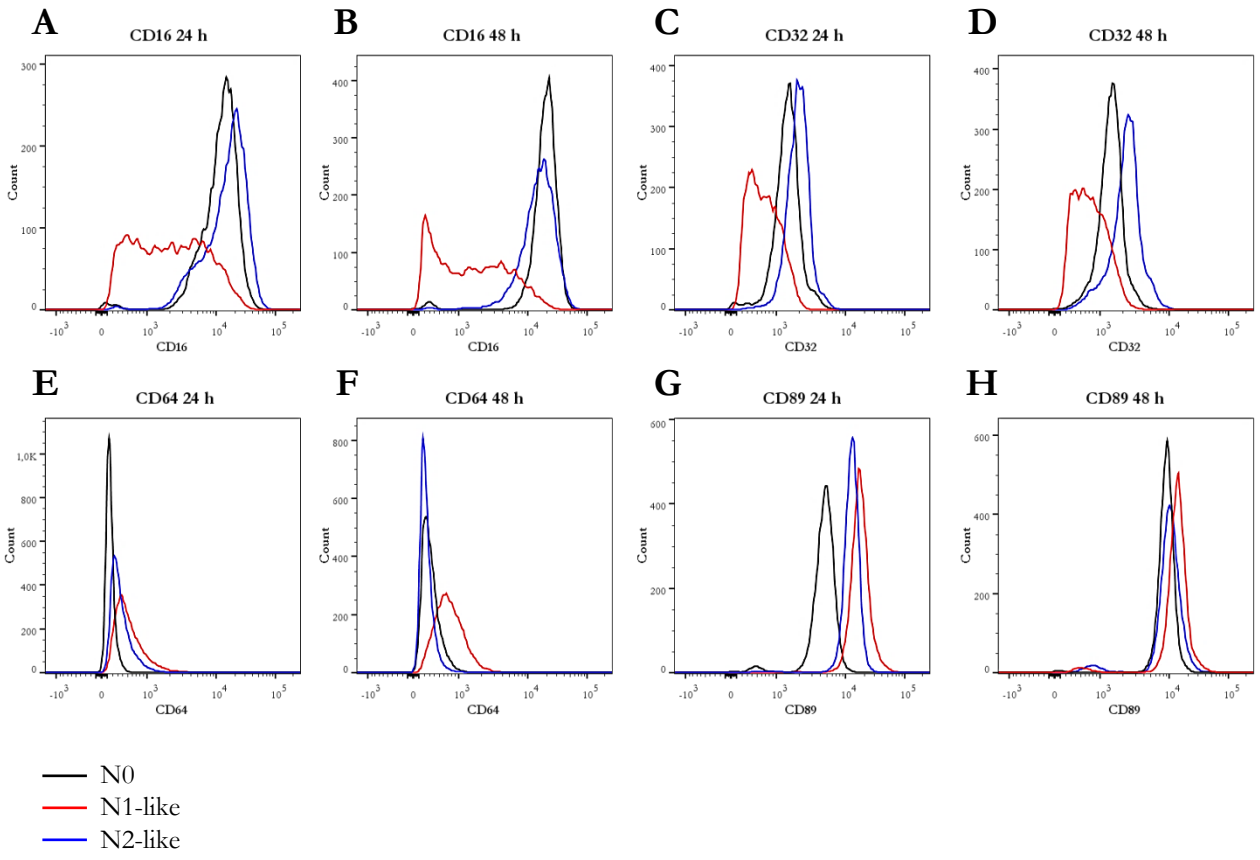

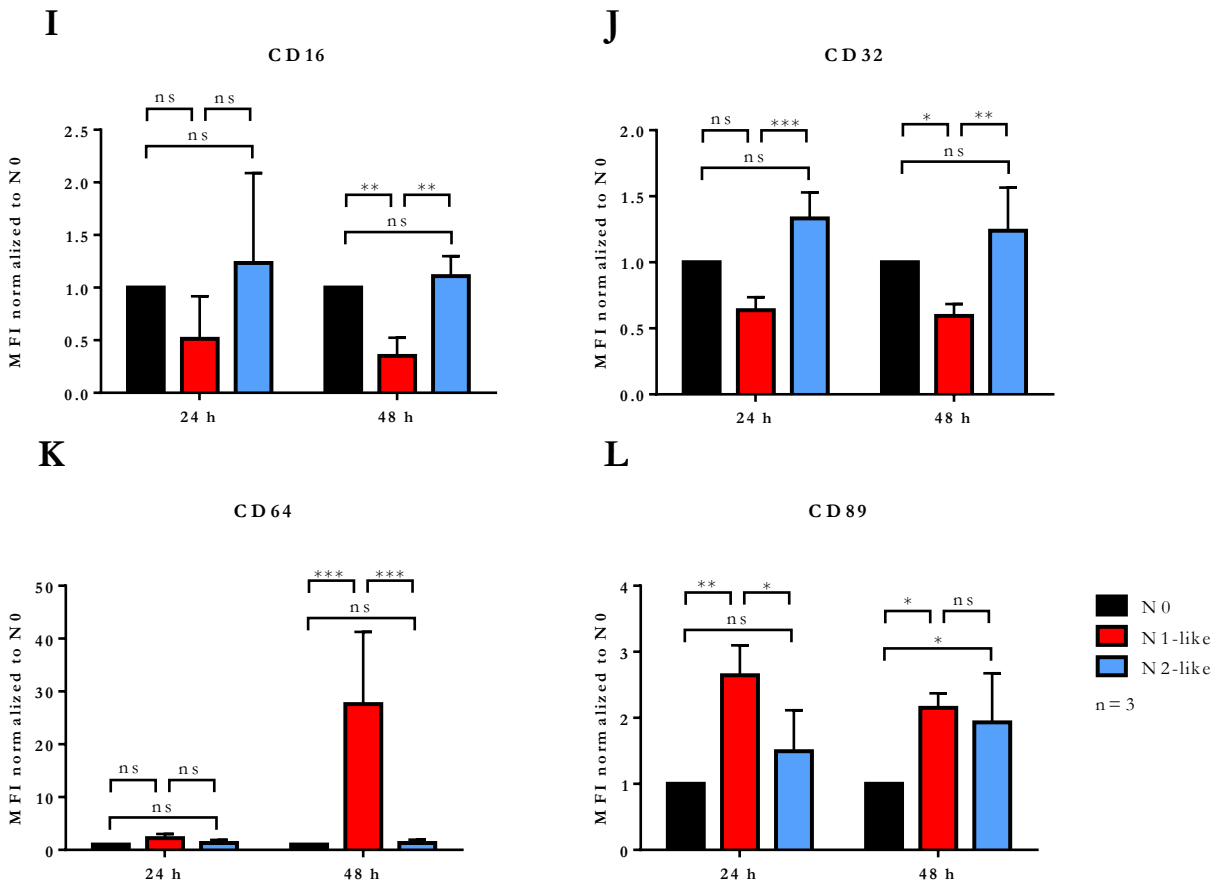

Figure 34. Cell surface expression of Fc receptors on *in vitro* polarized neutrophils. Primary human neutrophils were incubated in the presence of a N1 or N2 polarization cocktail (N1- and N2-like, respectively) including the Pan-caspase inhibitor QVD-OPh. Neutrophils which were only treated with QVD-OPh (N0) served as control. The cell surface expression of the Fc receptors FcRIIIγ (CD16), FcRIIγ (CD32), FcRIγ (CD64) and FcRα (CD89) was assessed by flow cytometry. Representative histograms show the Fc receptor expression on N0, N1-like and N2-like neutrophils after 24 h (**A**, **C**, **E**, **G**) and 48 h (**B**, **D**, **F**, **H**). The bar diagrams (**I**-**L**) show the mean fluorescence intensity (MFI) ± SD normalized to N0 (n=3), *p≤0.05, **p≤0.01, ns = not significant.

Taken together, the results obtained for the *in vitro* polarization demonstrated that it is feasible to polarize primary human neutrophils towards distinct phenotypes showing typical markers observed for N1 and N2 TANs *in vivo*. Despite rather unexpected results regarding the bacterial killing ability and the NET formation of polarized neutrophils, the majority of tested properties was in line with the literature. Further, decreased killing ability of *L. donovani* promastigotes by N2-like neutrophils supported the initially hypothesized idea that *Leishmania* are capable of polarizing neutrophils towards an immunosuppressive phenotype to prevent their elimination.

Part II: Metabolic phenotyping of *L. donovani*-infected neutrophils

Metabolic reprogramming of host cells is an integral component of the life cycle of intracellular pathogens to meet their extensive need for nutritional supplies and to avoid immune response. Although a study on murine *L. infantum*-infected macrophages indicated metabolic manipulation of the host mitochondrial energy metabolism, no data on the metabolism of neutrophils under *Leishmania* infection are available yet. However, neutrophils as host cells of *Leishmania* play a rather controversial role in protecting or promoting the disease. In order to overcome the high need for new therapies against leishmaniasis due to rising cases of drug resistance, this project aims for the identification of metabolic nodes in *L. donovani*-infected neutrophils for host-directed therapies as

future strategies against visceral leishmaniasis. For this purpose the energy metabolism of *L. donovani*-infected neutrophils was characterized by several metabolic assays, extracellular flux analysis and a transcriptome analysis. Furthermore, the main energy pathways in neutrophils were targeted with metabolic inhibitors and the anti-leishmanial capacity and the ROS production as relevant effector mechanism against *Leishmania* was measured.

Oxidative metabolism of *L. donovani*-infected neutrophils

During the establishment of infection, *Leishmania* are able to inhibit the oxidative metabolism of infected neutrophils in order to survive in the host. One study showed that during *L. major* infection of human neutrophils superoxide generation or mobilization of tertiary and specific granules was inhibited (Mollinedo et al., 2010). Contrary to these observations, *L. major* and *L. mexicana* promastigotes have been found to induce significant respiratory burst in rabbit peritoneal neutrophils upon infection (Mallinson et al., 1989). To investigate general changes in ROS production, including intracellular ROS production and extracellular superoxide formation, the luminol-based chemiluminescence assay was used to measure MPO-derived ROS production. To test exclusively intracellular ROS production that can eliminate the intracellular parasite the DHR assay was used. Extracellular ROS production, superoxide formation, was tested because I assumed that neutrophils can eliminate this way non-phagocytosed parasites and prevent the dissemination of the parasite.

Contact with *L. donovani* promastigotes upregulates ROS production of neutrophils

To test how the oxidative metabolism of neutrophils is already altered by direct contact with *L. donovani* promastigotes, freshly isolated neutrophils were kept unstimulated or were stimulated with *L. donovani* promastigotes in a 1:10 ratio that is also used for infection experiments. Subsequently, MPO-derived ROS production and superoxide formation were measured with the luminol- or lucigenin-based chemiluminescence assay, respectively. Additionally, intracellular ROS production upon initial parasite contact was measure by using the DHR assay. A statistically significant increase in MPO-derived ROS production and superoxide formation by neutrophils stimulated with *L. donovani* promastigotes was observed when compared with neutrophils not exposed to the parasite (**Figure 35**, **A**-**D**).

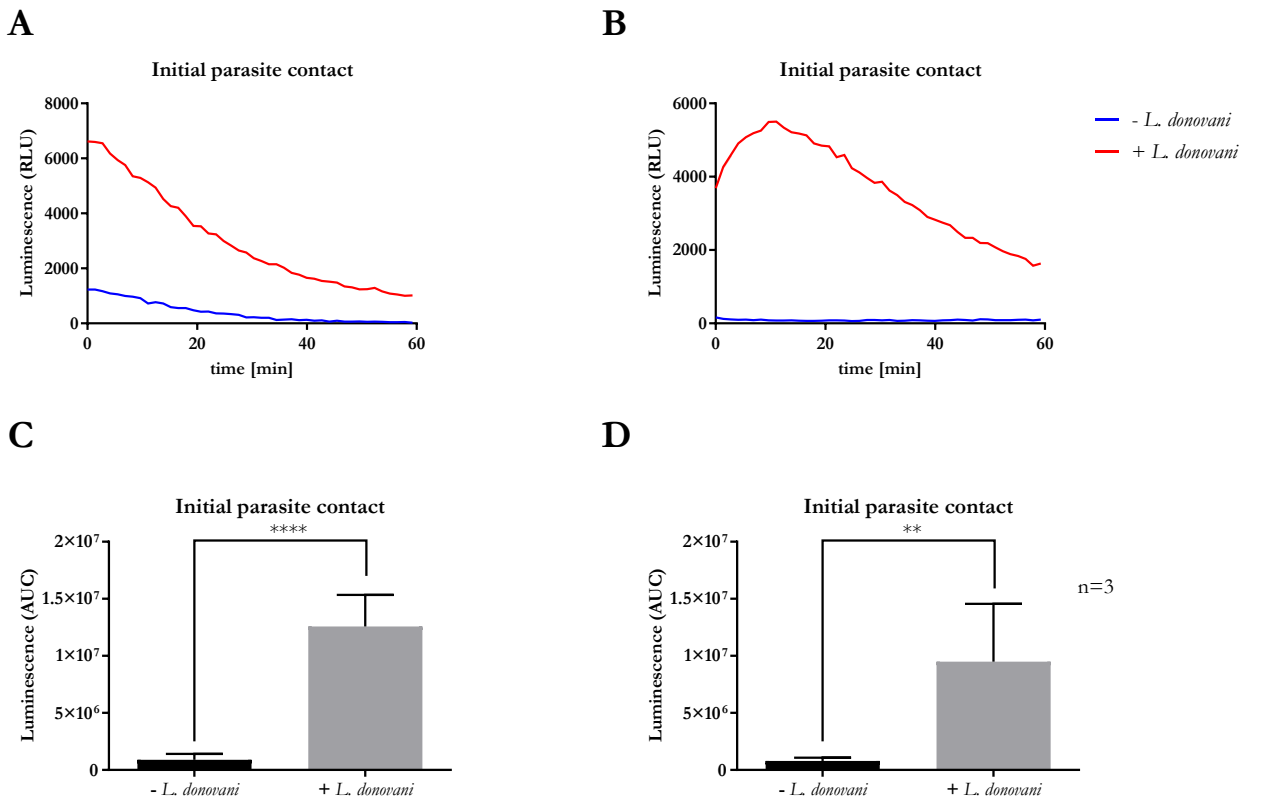

Figure 35. MPO-derived ROS production and superoxide formation of neutrophils upon *L. donovani* promastigote contact. Primary human neutrophils were co-incubated with *L. donovani* promastigotes (ratio 1:10). MPO-derived ROS production was measured for 60 min at 37°C and 5 % CO_2 in the presence or absence of *L. donovani* promastigotes by using the luminol-based chemiluminescence assay. Superoxide formation was measured for 60 min at 37°C and 5 % CO_2 in the presence or absence of *L. donovani* promastigotes by using the lucigenin-based chemiluminescence assay. A representative curve of luminol chemiluminescence is shown in panel **A**. A representative curve of lucigenin chemiluminescence is shown in panel **B**. The bar diagrams show the mean area under the curve (AUC) values ± SD for luminol chemiluminescence (**C**) and mean area under the curve (AUC) values ± SD for lucigenin chemiluminescence (**D**) (n=3), **p≤0.01, ****p≤0.0001.

Additionally, intracellular ROS production of neutrophils in the presence of *L. donovani* promastigotes was significantly higher than intracellular ROS production of neutrophils without *L. donovani* promastigotes (**Figure 36, A, B**). These data demonstrated that the contact of neutrophils with *L. donovani* promastigotes is sufficient to trigger ROS production.

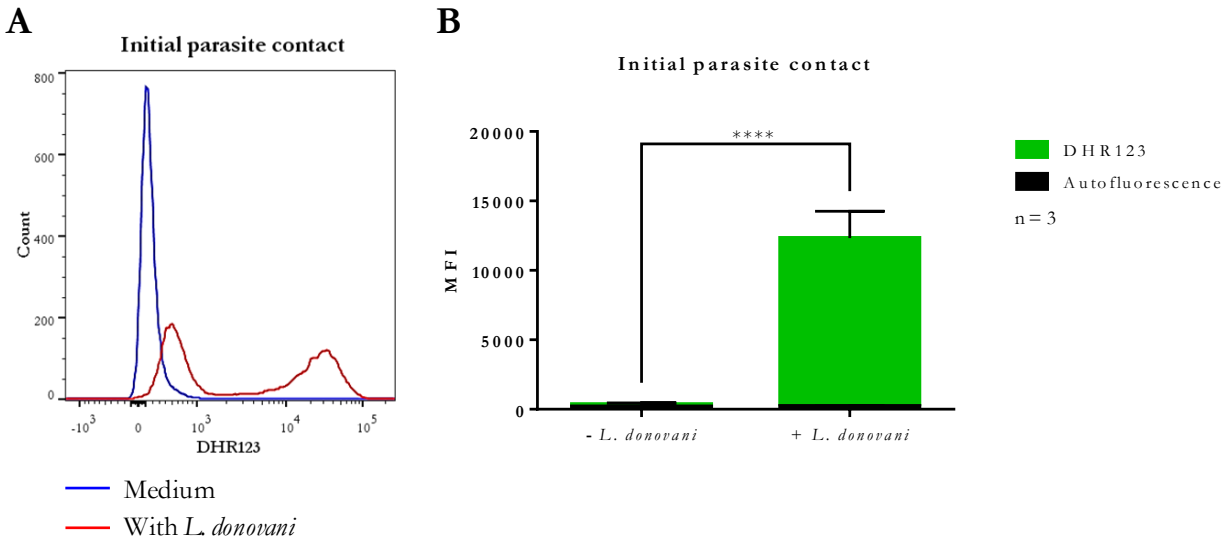

Figure 36. Intracellular ROS production of neutrophils upon *L. donovani* promastigote contact. Primary human neutrophils were co-incubated with *L. donovani* promastigotes (ratio 1:10). Intracellular ROS production was assessed after 30 min in the presence or absence of *L. donovani* promastigotes with flow cytometry by using DHR123. A representative curve of intracellular ROS production is shown in panel **A**. The bar diagram shows the mean fluorescence intensity (MFI) ± SD (n=3), autofluorescence in the DHR123 channel is depicted in black but was not included in statistical analysis, *p≤0.05.

MPO-derived ROS production of *L. donovani*-infected neutrophils is upregulated after PMA stimulation

Next, the MPO-derived ROS production of *L. donovani*-infected neutrophils after 6 hpi and 24 hpi was assessed by using the luminol-based chemiluminescence assay in the absence of stimuli or in the presence of PMA, LPS or fMLP. *L. donovani*-infected neutrophils showed a significant higher MPO-derived ROS production after stimulation with PMA but not fMLP compared to the medium control after 6 hpi and 24 hpi (**Figure 37**, **I**, **J**). In contrast, uninfected neutrophils reacted with significantly increased MPO-derived ROS production after PMA or fMLP stimulation compared to the medium control for both time points (**Figure 37**, **G**, **H**). Unstimulated *L. donovani*-infected neutrophils produced significantly more MPO-derived ROS than uninfected neutrophils after 6 hpi, whereas no differences between the two groups could be observed after 24 hpi (**Figure 37**, **A**, **D**, **K**). No differences in MPO-derived ROS production between *L. donovani*-infected and uninfected neutrophils could be observed after the stimulation with PMA or fMLP (**Figure 37**, **B**, **C**, **E**, **F**, **L**, **M**). These data demonstrated that the MPO-derived ROS production of *L. donovani*-infected neutrophils is higher than that of uninfected neutrophils. In addition, *L. donovani*-infected neutrophils produced more MPO-derived ROS upon PMA stimulation.

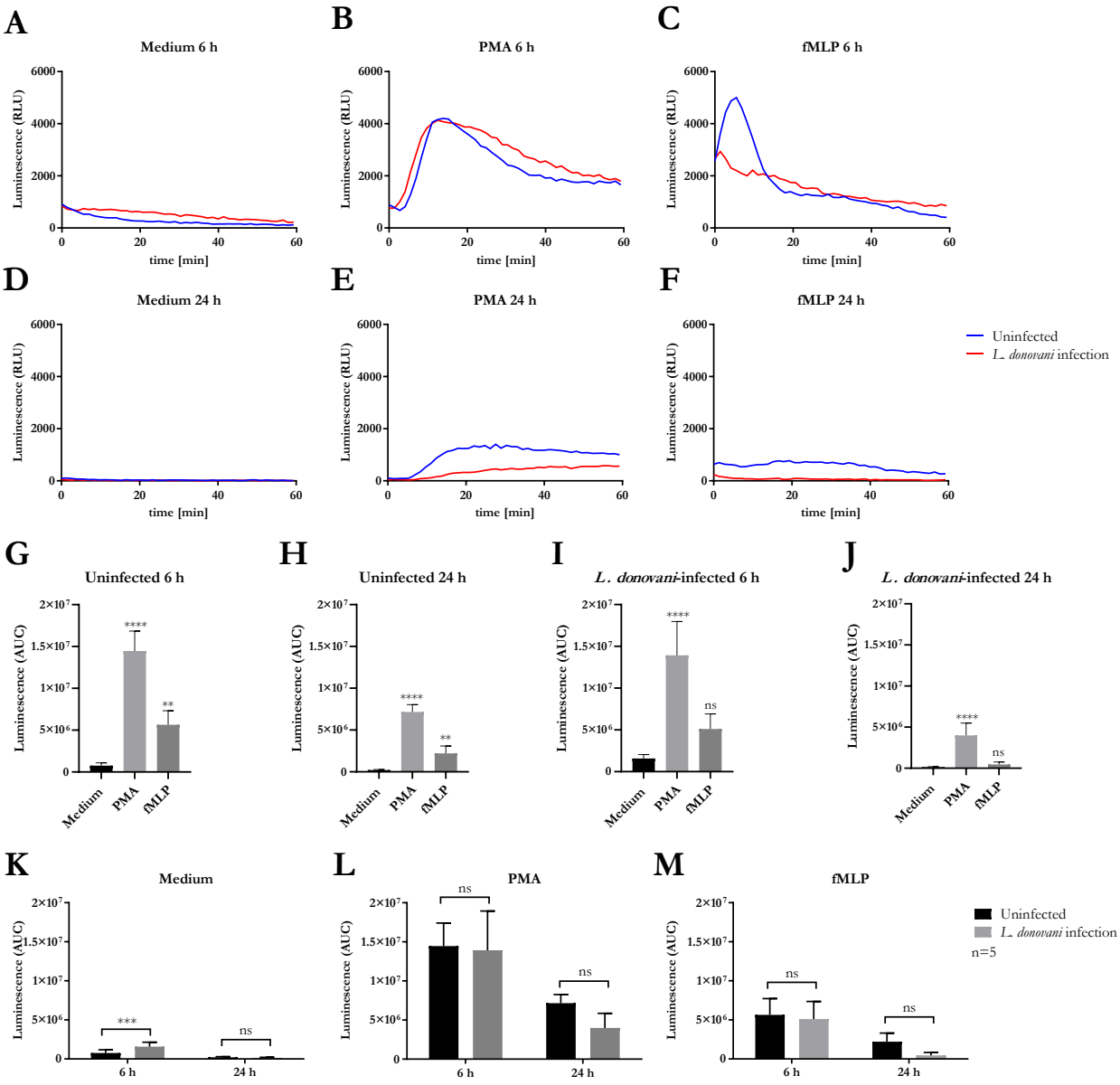

Figure 37. MPO-derived ROS production of *L. donovani*-infected neutrophils. Primary human neutrophils were infected with *L. donovani* promastigotes (ratio 1:10) for 3 h at 37°C and 5 % CO_2. Uninfected cells served as control. The infection rate was determined by Giemsa staining of cytocentrifuged samples. Subsequently, free, non-ingested parasites were removed by washing. MPO-derived ROS production was measured after 6 h and 24 h post infection for 60 min at 37°C and 5 % CO_2 after the addition of medium as negative control, 20 nM PMA, 100 ng/ml LPS, 10 nM LTB4, 10 nM C5a or 1 µM fMLP by using the luminol-based chemiluminescence assay. Representative curves of luminol chemiluminescence after 6 h and 24 h post infection, respectively are shown in panels **A**-**F**. The bar diagrams (**G**-**M**) show the mean area under the curve (AUC) values ± SD (n=5), *p≤0.05, ***p≤0.001, ****p≤0.0001, ns = not significant.

Superoxide production of *L. donovani*-infected neutrophils is increased after PMA stimulation

In addition to the MPO-derived ROS production also the superoxide formation of *L. donovani*-infected neutrophils after 6 hpi and 24 hpi was assessed by using the lucigenin-based chemiluminescence assay in the absence of stimuli or in the presence of PMA, LPS or fMLP. *L. donovani*-infected and uninfected neutrophils

showed a significantly increased superoxide production after stimulation with PMA but not fMLP compared to the medium control after 6 hpi and 24 hpi (**Figure 38**, **G – J**). No differences in superoxide formation between unstimulated *L. donovani*-infected and uninfected neutrophils were observed after 6 hpi and 24 hpi (**Figure 38**, **A**, **D**, **K**). Upon PMA stimulation *L. donovani*-infected neutrophils showed a significantly decreased superoxide formation compared to uninfected neutrophils after 6 hpi and the tendency to produce less superoxide than uninfected neutrophils after 24 hpi (**Figure 38**, **B**, **E**, **L**). Stimulation with fMLP resulted differences in superoxide production between *L. donovani*-infected and uninfected neutrophils after 6 hpi and 24 hpi (**Figure 38**, **C**, **F**, **M**). These data indicated that only PMA-stimulated *L. donovani*-infected neutrophils produce superoxide anions but less than uninfected neutrophils.

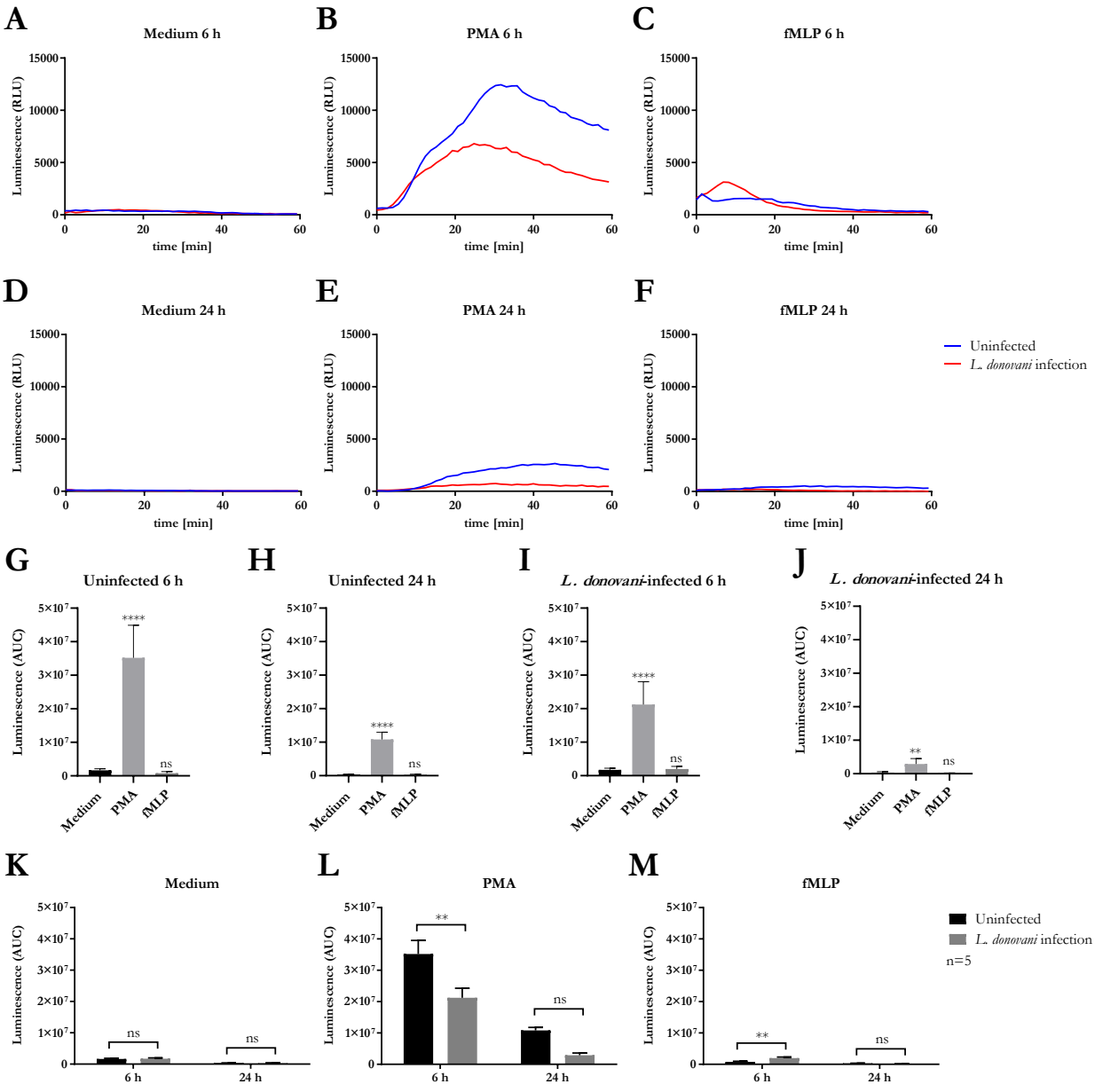

Figure 38. Superoxide formation of *L. donovani*-infected neutrophils. Primary human neutrophils were infected with *L. donovani* promastigotes (ratio 1:10) for 3 h at 37°C and 5 % CO_2. Uninfected cells served as control. The infection rate was determined by Giemsa staining of cytocentrifuged samples. Subsequently, free, non-ingested parasites were removed by washing. Superoxide formation was measured after 6 h and 24 h post infection for 60 min at 37°C and 5 % CO_2 after the addition of medium as negative control, 20 nM PMA, 100 ng/ml LPS, 10 nM LTB4, 10 nM C5a or 1 µM fMLP by using the lucigenin-based chemiluminescence assay. Representative curves of lucigenin chemiluminescence after 6 h and 24 h post infection, respectively are shown in panels **A**-**F**. The bar diagrams (**G**-**M**) show the mean area under the curve (AUC) values ± SD (n=5), *p≤0.05, **p≤0.01, ns = not significant.

L. donovani-infected neutrophils produce more intracellular ROS after stimulation with PMA or fMLP

In addition to MPO-derived ROS production and superoxide formation also intracellular ROS production during *L. donovani* infection of neutrophils was assessed by using the DHR assay in the absence or presence of the stimuli PMA or fMLP. *L. donovani*-infected neutrophils produced significantly more intracellular ROS after stimulation with PMA or fMLP compared to the medium control after 6 hpi (**Figure 39**, **I**). Uninfected neutrophils produced significantly more intracellular ROS after stimulation with fMLP but not PMA compared to the medium control after 6 h (**Figure 39**, **G**). Unstimulated *L. donovani*-infected neutrophils tended to produce more intracellular ROS than uninfected neutrophils after 6 hpi and 24 hpi (**Figure 39**, **A**, **D**, **K**, **N**). *L. donovani*-infected neutrophils produced more intracellular ROS after PMA or fMLP stimulation than uninfected neutrophils under the same conditions after 6 hpi (**Figure 39**, **B**, **C**, **L**, **M**). These results indicated that stimulation with PMA or fMLP upregulates the intracellular ROS production of *L. donovani*-infected neutrophils, which is compared to uninfected neutrophils.

Q **R**

K **L**

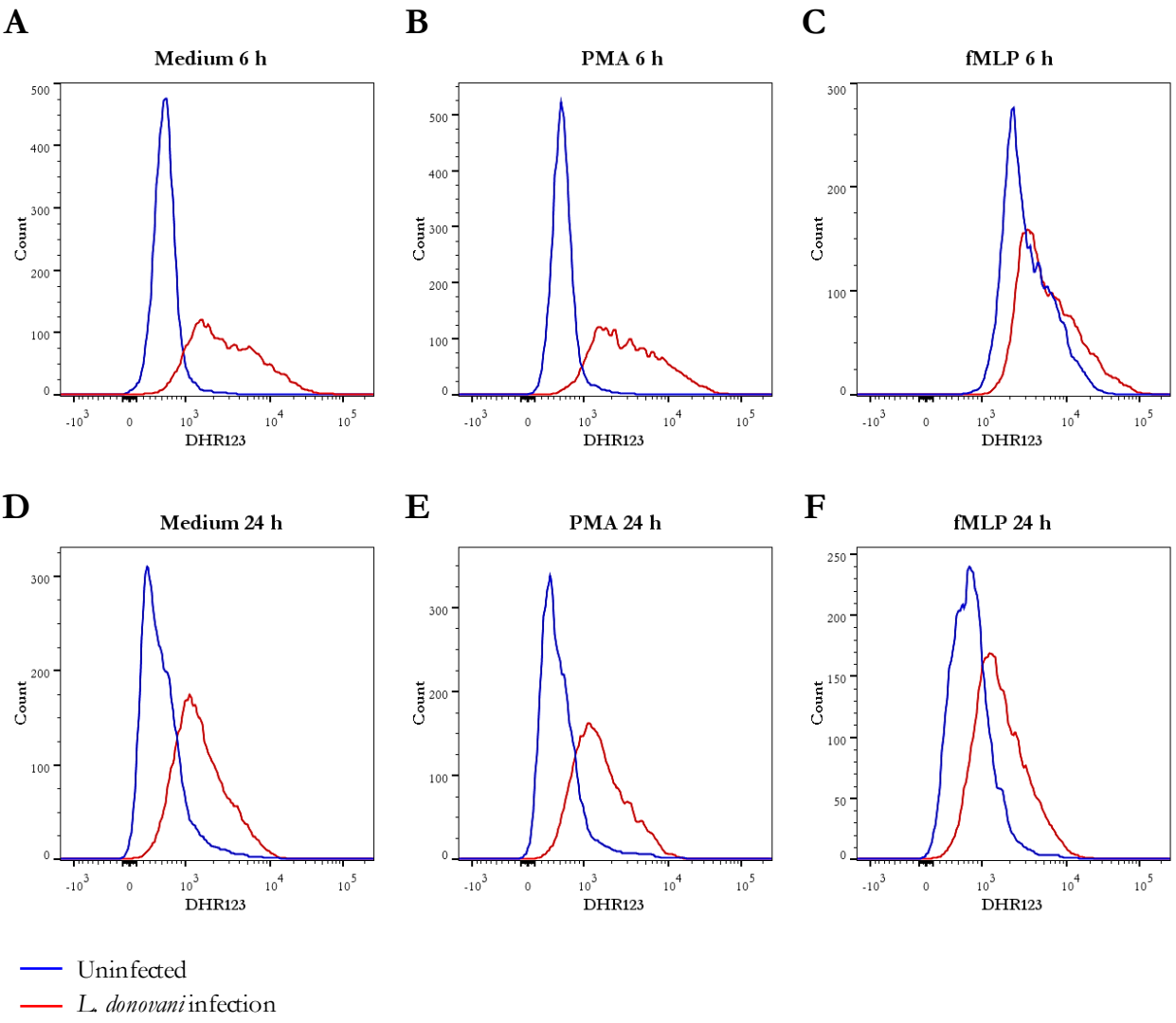
A
Medium 6 h
B
PMA 6 h
C
fMLP 6 h
D
Medium 24 h
E
PMA 24 h
F
fMLP 24 h
Count
DHR123
Uninfected
L. donovani infection

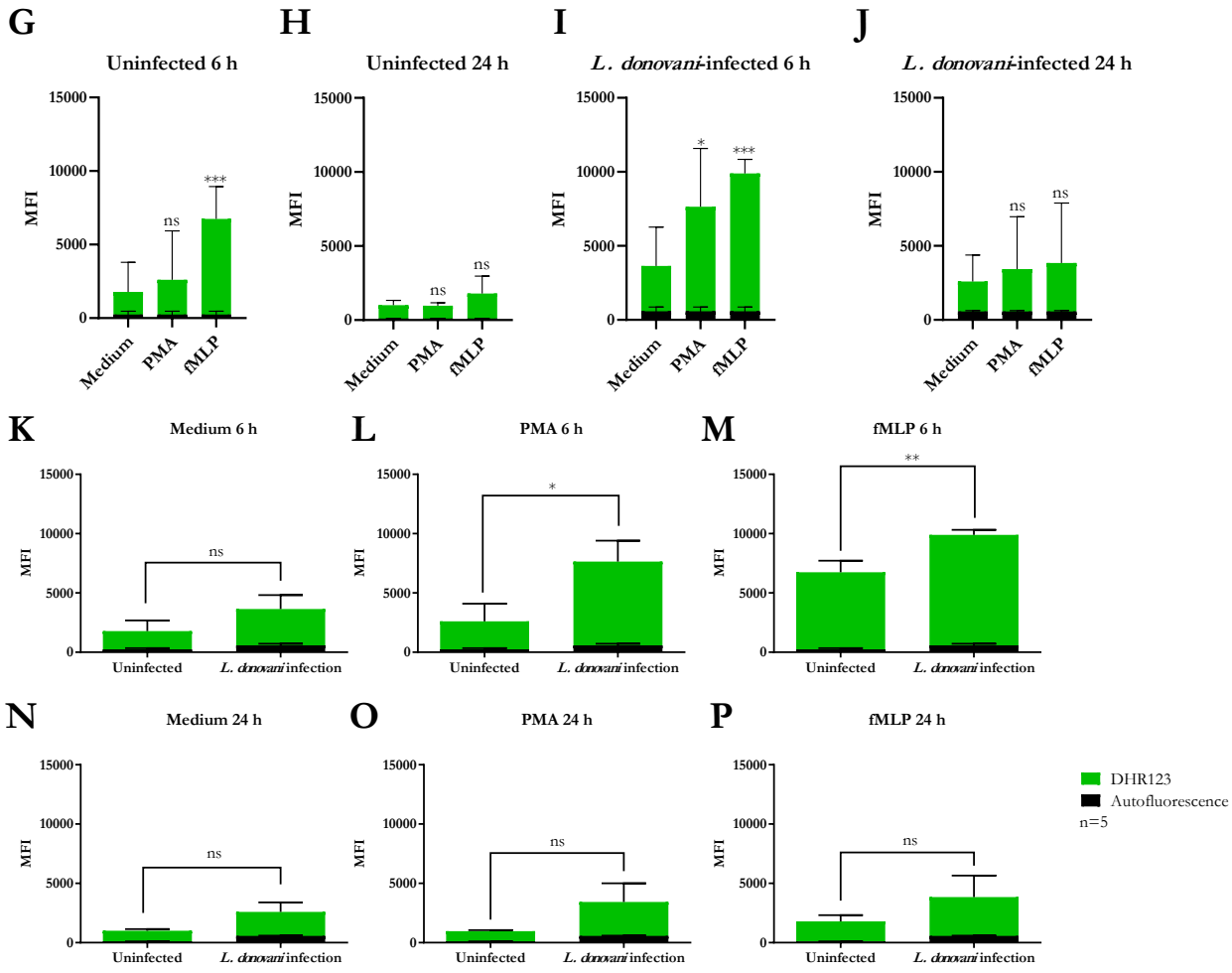

Figure 39. Intracellular ROS production of *L. donovani*-infected neutrophils. Primary human neutrophils were infected with *L. donovani* promastigotes (ratio 1:10) for 3 h at 37°C and 5 % CO_2. Uninfected cells served as control. The infection rate was determined by Giemsa staining of cytocentrifuged samples. Subsequently, free, non-ingested parasites were removed by washing. Intracellular ROS production was assessed 6 h and 24 h post infection immediately after the addition of medium as negative control, 4 µM PMA or 1 µM fMLP for 30 min with flow cytometry by using DHR123. Representative curves of intracellular ROS production after 6 h and 24 h post infection, respectively are shown in panels **A**-**F**. The bar diagrams (**G**-**P**) show the mean fluorescence intensity (MFI) ± SD (n=5), autofluorescence in the DHR123 channel is depicted in black but was not included in statistical analysis, *p≤0.05, **p≤0.01, ns = not significant.

L. donovani-infected neutrophils show increased mitochondrial ROS production

Apart from the NADPH oxidase complex another important source of ROS are mitochondria. Mitochondrial ROS contribute to the oxidative burst and fulfill regulatory functions in immune signaling. Further, a study with murine *L. donovani*-infected macrophages showed that *Leishmania* are capable of neutralizing mitochondrial ROS to persist in their host cells (Basu Ball et al., 2011). In order to address mitochondrial ROS production in primary human neutrophils infected with *L. donovani* promastigotes a MitoSox Red staining was performed and analyzed by flow cytometry after 6 hpi and 24 hpi. Autofluorescence of *L. donovani*-infected and uninfected neutrophils in the MitoSox Red channel was also assessed by flow cytometry (**Figure 40**, **A**, **B**) and was excluded from the statistical analysis. Mitochondrial ROS production of *L. donovani*-infected neutrophils tended to be increased compared to uninfected neutrophils after 6 hpi and was significantly increased compared to uninfected

neutrophils after 24 hpi (**Figure 40, C-F**). These data demonstrated that *L. donovani*-infected neutrophils produce more mitochondrial ROS than uninfected neutrophils.

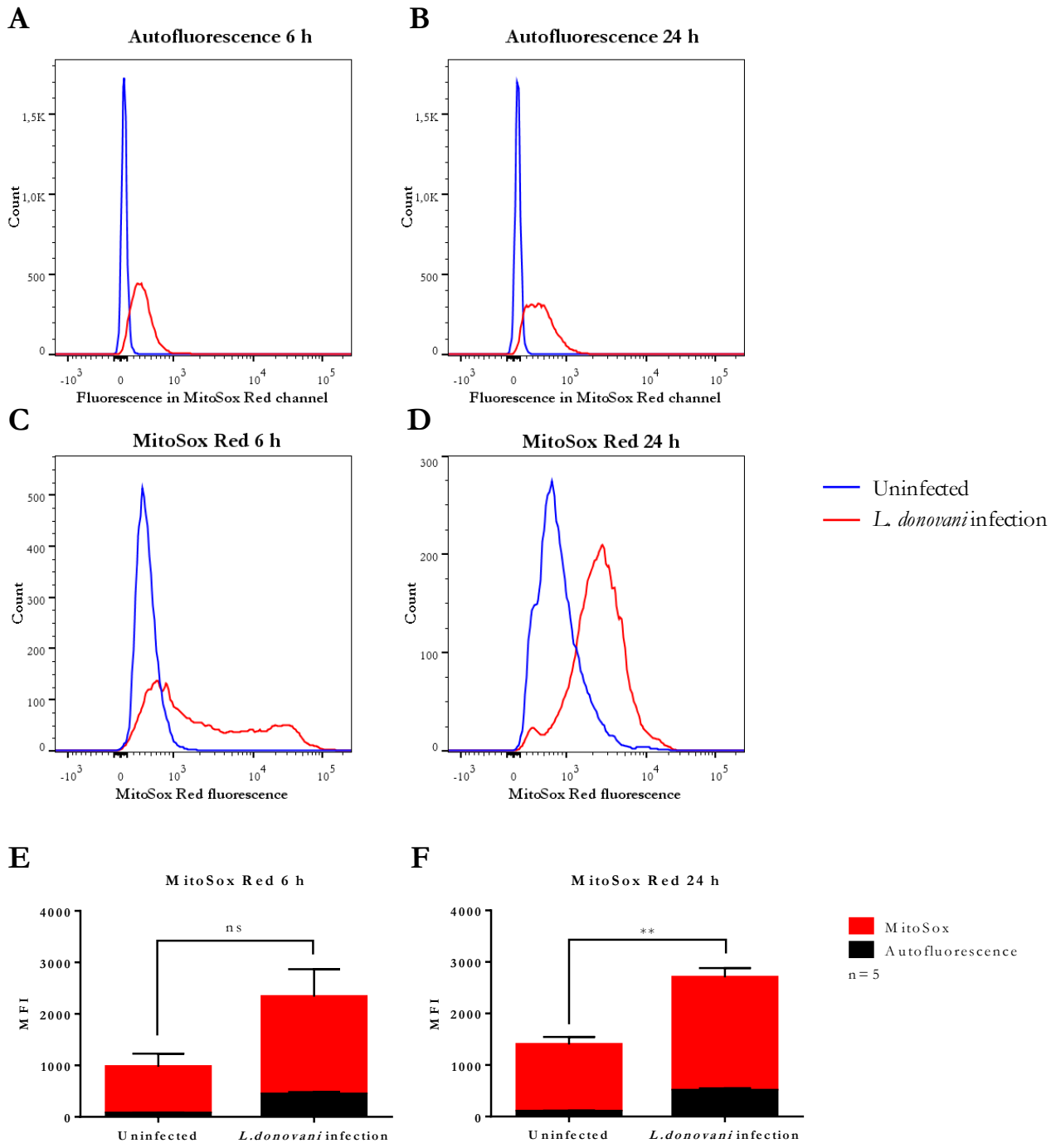

Figure 40. Detection of mitochondrial ROS of *L. donovani*-infected neutrophils. Primary human neutrophils were infected with *L. donovani* promastigotes (ratio 1:10) for 3 h at 37°C and 5 % CO_2. Uninfected cells served as control. The infection rate was determined by Giemsa staining of cytocentrifuged samples. Subsequently, free, non-ingested parasites were removed by washing. Mitochondrial ROS production was assessed 6 h and 24 h post infection after addition of MitoSox Red by flow cytometry. Autofluorescence of infected neutrophils in the same channel as MitoSox Red is shown in representative curves in panel **A** and **B**. Representative curves of mitochondrial ROS production are shown in panel **C** and **D**. Bar diagrams

(**E**, **F**) show the autofluorescence corrected mean fluorescence intensity (MFI) of MitoSox Red ± SD (n=5), autofluorescence in the DHR123 channel is depicted in black but was not included in statistical analysis, **p≤0.01, ns = not significant.

L. donovani-infected neutrophils secrete high levels of IL-8 and TNF but release no IP-10 upon IFNγ/LPS stimulation

Metabolism and immune response are two fundamental biological processes that are tightly intertwined. As intracellular pathogen *Leishmania* manipulate the metabolism of their host cells which leads to alterations in the cytokine response. In return, cytokines can affect the metabolism of infected host cells via metabolic reprogramming. To address the most important cytokines during *Leishmania* infection of neutrophils, namely TNF, IP-10 and IL-8, and to possibly cross-link the cytokine profile of infected cells with simultaneously occurring metabolic alterations ELISAs were performed. Cell-free supernatants of *L. donovani*-infected and uninfected neutrophils were collected after 6 hpi and 24 hpi and tested for TNF, IP-10 and IL-8. To induce IP-10 secretion the cells were treated with IFNγ and LPS for 6 h and 24 h. *L. donovani*-infected neutrophils produced more TNF than uninfected neutrophils after 6 hpi (**Figure 41**, **A**). The IP-10 levels of IFNγ/LPS-stimulated *L. donovani*-infected neutrophils were significantly decreased compared to uninfected neutrophils after 24 hpi (**Figure 41**, **B**). *L. donovani*-infected neutrophils secreted significantly more IL-8 than uninfected neutrophils after both time points (**Figure 41**, **C**). These data showed that *L. donovani*-infected neutrophils secrete high levels of TNF and IL-8, but are not capable to produce IP-10 upon IFNγ/LPS stimulation.

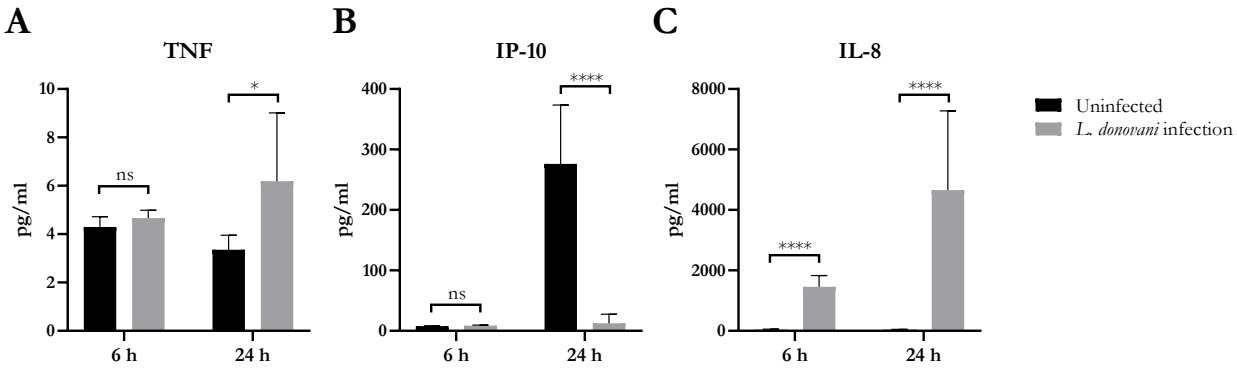

Figure 41. Secretion of TNF, IP-10 and IL-8 by *L. donovani*-infected neutrophils. Primary human neutrophils were infected with *L. donovani* promastigotes (ratio 1:10) for 3 h at 37°C and 5 % CO_2. Uninfected cells served as control. Successful infection was determined by Giemsa staining of cytocentrifuged samples. Subsequently, free, non-ingested parasites were removed by washing and cells were either cultured untreated for detection of TNF and IL-8 or treated with 200 U/ml IFNγ and 100 ng/ml LPS to induce IP-10 production. Cell-free culture supernatants were collected after 6 h and 24 h post infection. The concentrations of TNF (**A**), IP-10 (**B**) and IL-8 (**C**) were measured by ELISA. Bar diagrams show mean ± SD (n=3), *p≤0.05, ****p≤0.0001, ns = not significant.

L. donovani-infected neutrophils have an increased glycolytic metabolism

To address how *L. donovani* infection impacts on neutrophil metabolism and bioenergetics state, the glycolytic metabolism was assessed by measuring the extracellular acidification rate (ECAR), a consequence of lactate production, was quantified by using live cell extracellular flux analysis. After 6 h and 24 h post infection, higher basal ECAR levels were observed in *L. donovani*-infected neutrophils compared to uninfected neutrophils (**Figure 42**, **A**, **B**). As glycolysis is the main pathway used to supply ATP for the energy requirements of neutrophils, the key glycolytic parameters of *L. donovani*-infected neutrophils, namely glycolysis, glycolytic capacity and glycolytic reserve, were calculated from ECAR values. Glycolysis and glycolytic capacity of *L. donovani*-infected neutrophils

were increased after 6 h compared to uninfected neutrophils, whereas no difference in the glycolytic reserve were observed between the two groups (**Figure 42**, **C-E**). Compared to 6 hpi, glycolysis, glycolytic capacity and glycolytic reserve of *L. donovani*-infected neutrophils were significantly decreased after 24 hpi (**Figure 42**, **F- H**). This decrease could only be observed for glycolytic reserve in uninfected neutrophils (**Figure 42**, **H**). These data indicated that neutrophils rely highly on glycolysis during the early phase of infection with *L. donovani*.

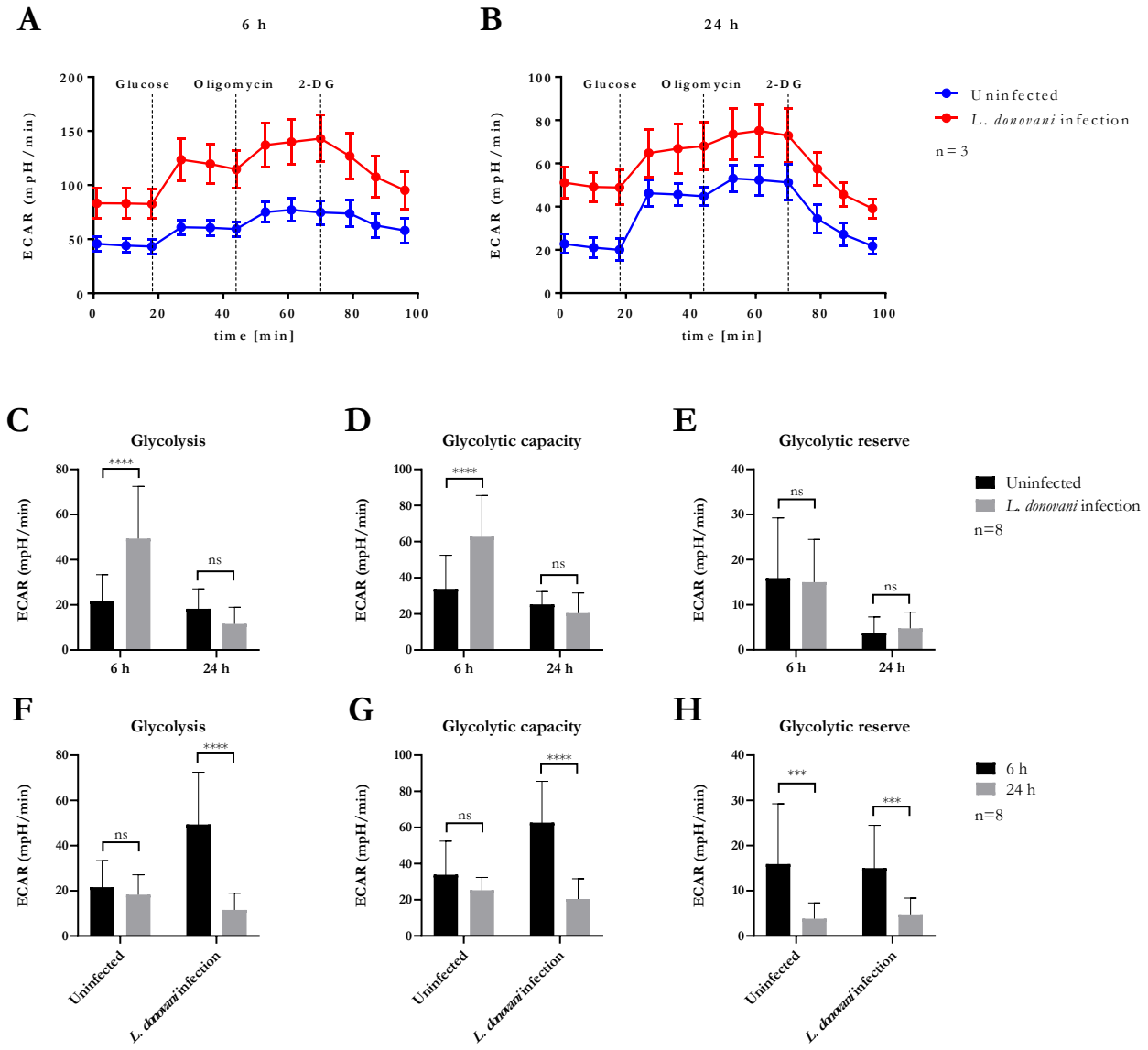

Figure 42. Glycolysis stress test profile of *L. donovani*-infected neutrophils. Primary human neutrophils were infected with *L. donovani* promastigotes (ratio 1:10) for 3 h at 37°C and 5 % CO_2. Uninfected cells served as control. The infection rate was determined by Giemsa staining of cytocentrifuged samples. Subsequently, free, non-ingested parasites were removed by washing. After 6 h and 24 h post infection the glycolysis stress test profile was determined by using the Seahorse extracellular flux analyzer. Extracellular acidification rate (ECAR) measurements following the sequential injection of 5 mM glucose, 1 µM oligomycin and 10 mM 2-DG (dotted lines indicate injection time) were used to calculate key parameters of glycolytic function. The ECAR curves of *L. donovani*-infected neutrophils and uninfected neutrophils represent the mean of three independent experiments (**A**, **B**). Glycolysis (**C**, **F**) was calculated by subtraction of 2-DG-mediated ECAR from glucose-mediated ECAR. Glycolytic capacity (**D**, **G**) was calculated by subtraction of 2-DG-mediated ECAR from

oligomycin-mediated ECAR. Glycolytic reserve (**E**, **H**) was calculated by subtraction of glucose-mediated ECAR. Bar graphs show mean ± SD (n=8), *p≤0.05, **p≤0.01, ns = not significant.

L. donovani-infected neutrophils show increased respiratory parameters

To examine the effect of *L. donovani* infection on host oxidative phosphorylation, an extracellular flux analysis of a mitochondrial stress test was used to determine key respiratory parameters, including non-mitochondrial respiration, basal respiration, maximal respiration, proton leak, ATP production and spare respiratory capacity. As the oxygen consumption rate (OCR) of neutrophils after 24 h barely reached the detection limit of the extracellular flux analyzer, only data of the 6 h time point were collected. The initial OCR of *L. donovani*-infected neutrophils was higher compared to uninfected neutrophils (**Figure 43**, **A**). Additionally, non-mitochondrial respiration, basal respiration, maximal respiration and proton leak of *L. donovani*-infected neutrophils were significantly increased compared to uninfected neutrophils (**Figure 43**, **B**-**E**). In contrast, ATP production and spare respiratory capacity in *L. donovani*-infected neutrophils showed no significant difference to uninfected neutrophils (**Figure 43**, **F**, **G**). These results indicated that *L. donovani*-infected neutrophils consume more oxygen that is most likely used to fuel their oxidative bust to eliminate the intracellular pathogen.

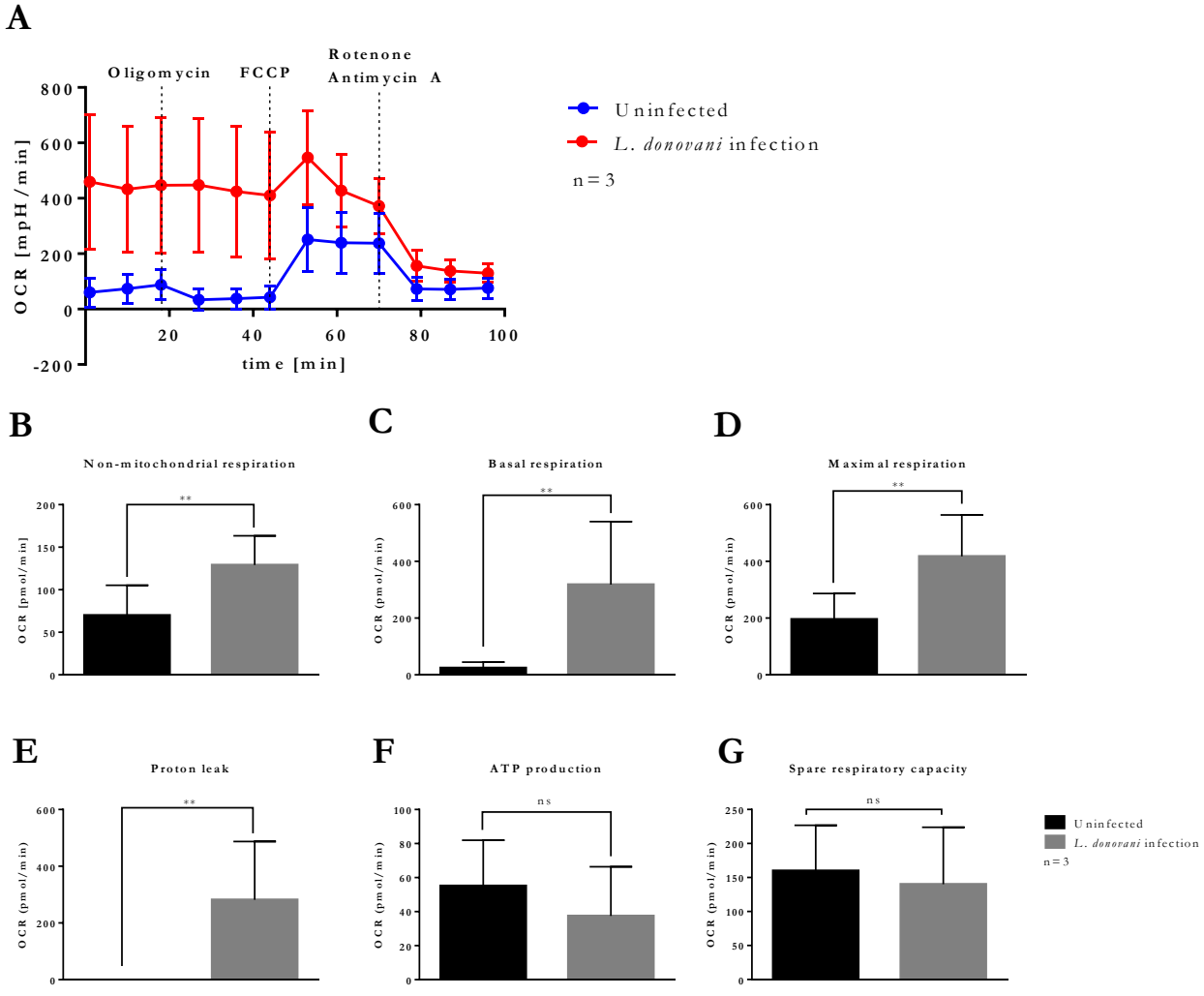

Figure 43. Mitochondrial stress test profile of *L. donovani*-infected neutrophils. Primary human neutrophils were infected with *L. donovani* promastigotes (ratio 1:10) for 3 h at 37°C and 5 % CO_2. Uninfected cells served as control. Successful infection was determined by Giemsa staining of cytocentrifuged samples. Subsequently, free, non-ingested

parasites were removed by washing. After 6 h post infection the mitochondrial stress test profile was determined by using the Seahorse extracellular flux analyzer. The measurement of basal oxygen consumption rate (OCR) was followed by sequential injections of 1 µM oligomycin, 1.5 µM FCCP, and 1 µM rotenone/antimycin A (dotted lines indicate injection time). OCR measurements were used to calculate key parameters of mitochondrial function. The OCR curves of *L. donovani*-infected neutrophils and uninfected neutrophils represent the mean of three independent experiments (**A**). Non-mitochondrial respiration (**B**) was calculated as OCR after rotenone/antimycin A injection. Basal respiration (**C**) was calculated by subtraction of rotenone/antimycin A-mediated OCR from basal OCR. Maximal respiration (**D**) was calculated by subtraction of rotenone/antimycin A-mediated OCR from FCCP-mediated OCR. Proton leak (**E**) was calculated by subtraction of non-mitochondrial respiration from oligomycin-mediated OCR. ATP production (**F**) was calculated by subtraction of oligomycin-mediated OCR from basal OCR. Spare respiratory (**G**) was calculated by subtraction of basal OCR from FCCP-mediated OCR. Bar graphs show mean ± SD (n=3), **p≤0.01, ns = not significant.

L. donovani-infected neutrophils exhibit increased levels of lactate and pyruvate

As extracellular flux analysis indicated an increased glycolytic metabolism in *L. donovani*-infected neutrophils, the metabolic end products of glycolysis under aerobic settings, pyruvate, and under anaerobic conditions, lactate, were determined by a pyruvate assay kit and a lactate assay kit, respectively. As shown in **Figure 44 A** and **B**, the lactate secretion as well as the pyruvate content of *L. donovani*-infected neutrophils was significantly increased compared to uninfected neutrophils. The accumulation of the glucose end products lactate and pyruvate in the supernatant of *L. donovani*-infected neutrophils highlighted the important role of the glycolytic metabolism in neutrophils during *L. donovani* infection.

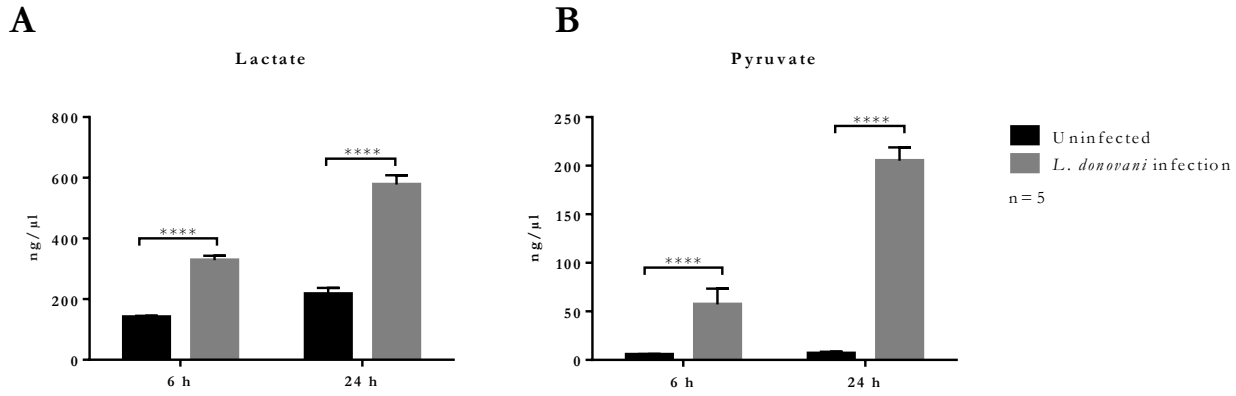

Figure 44. Lactate secretion and pyruvate content of *L. donovani*-infected neutrophils. Primary human neutrophils were infected with *L. donovani* promastigotes (ratio 1:10) for 3 h at 37°C and 5 % CO_2. Uninfected cells served as control. The infection rate was determined by Giemsa staining of cytocentrifuged samples. Subsequently, free, non-ingested parasites were removed by washing. Whole cell lysates were generated after 6 h and 24 h post infection by boiling cells at 90°C for 5 min. Cell-free supernatants were collected after 6 h and 24 h. Lactate was detected in culture supernatants by using a lactate assay kit. Pyruvate was detected in whole cell lysates by using a pyruvate assay kit. Bar diagrams show mean concentration of lactate (**A**) and pyruvate (**B**) calculated after subtraction of the medium blanks by interpolation from standard curve ± SD (n=5), ****p≤0.0001.

L. donovani infection upregulates the glucose uptake of neutrophils

Before glycolysis begins glucose must be transported from the extracellular milieu into the cells. This task is accomplished either by sodium coupled glucose transporters (SGLTs) or by glucose facilitative transporters, the GLUT family. Therefore another option to quantify the glycolytic flux of cells in culture is to measure the glucose uptake. For this purpose the uptake of the fluorescent glucose analog 2-NBDG in glucose-free medium by *L. donovani*-infected neutrophils and uninfected neutrophils was determined by flow cytometry. After 6 hpi *L. donovani*-infected neutrophils showed a significantly higher glucose uptake compared to uninfected neutrophils

(**Figure 45**, **C**, **E**). However after 24 hpi, *L. donovani*-infected neutrophils showed a significantly decreased glucose uptake compared to uninfected neutrophils (**Figure 45**, **D**, **F**). Autofluorescence of *L. donovani*-infected and uninfected neutrophils in the 2-NBDG channel was also assessed by flow cytometry (**Figure 45**, **A**, **B**) and was excluded from the statistical analysis. The increased glucose uptake of neutrophils during *L. donovani* infection supported the idea that neutrophils mainly rely on glycolysis during the infection with the intracellular parasite.

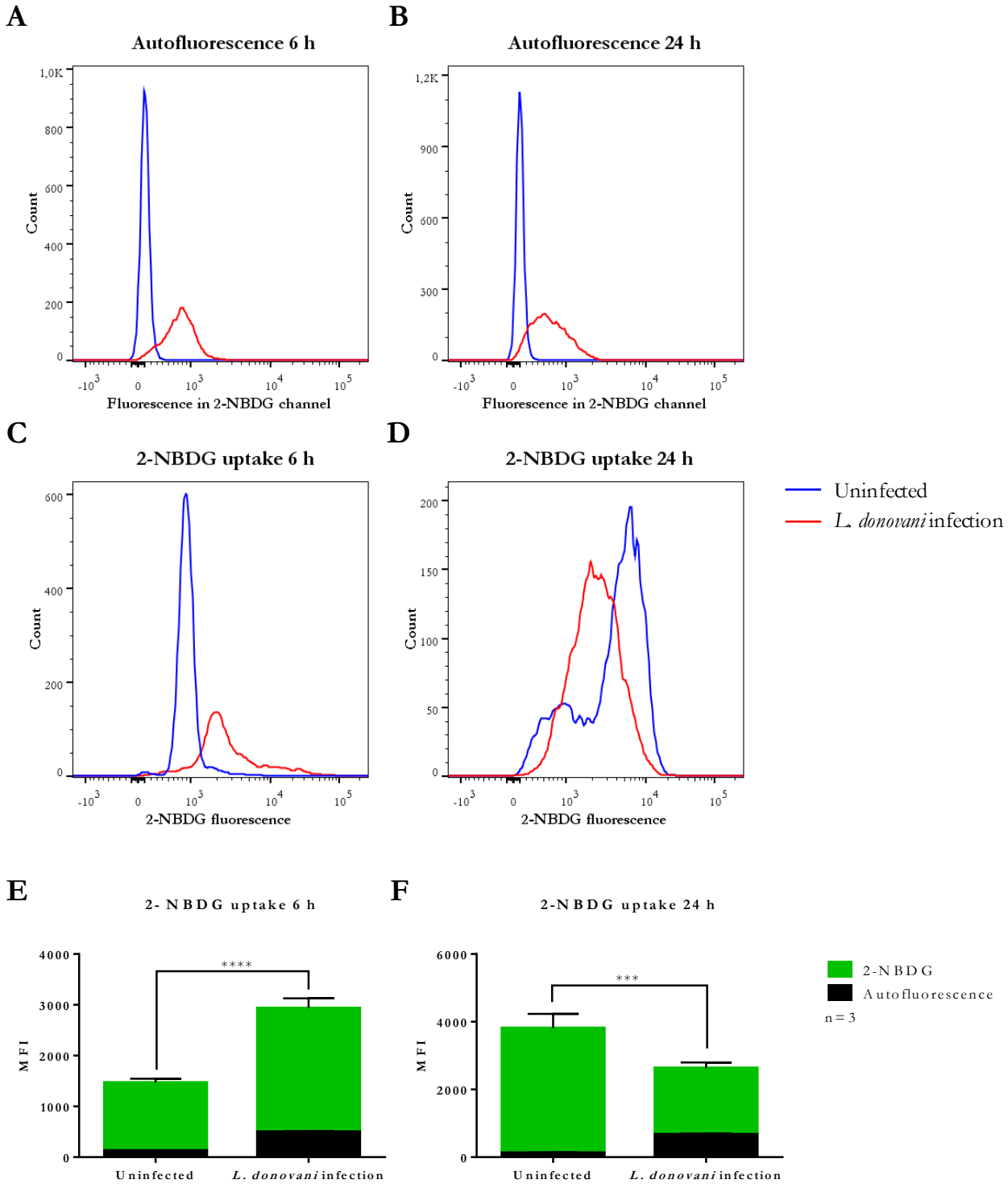

Figure 45. Glucose uptake of *L. donovani*-infected neutrophils. Primary human neutrophils were infected with *L. donovani* promastigotes (ratio 1:10) for 3 h at 37°C and 5 % CO_2. Uninfected cells served as control. The infection rate was determined by Giemsa staining of cytocentrifuged samples. Subsequently, free, non-ingested parasites were removed by washing. After 6 h and 24 h post infection the fluorescent glucose analog 2-NBDG was added to the cells in glucose-free medium. Autofluorescence of infected neutrophils in the same fluorescence channel as 2-NBDG is shown as representative curves in panel **A** and **B**. Representative curves of 2-NBDG uptake are shown in panel **C** and **D**. Bar diagrams (**E**, **F**) show the autofluorescence corrected mean fluorescence intensity (MFI) of 2-NBDG uptake ± SD (n=3), ***p≤0.001, ****p≤0.0001.

The ATP content of *L. donovani*-infected neutrophils decreases upon glycolysis and oxidative phosphorylation inhibition

To clarify which metabolic pathway, glycolysis or oxidative phosphorylation, supplies neutrophils during *L. donovani* infection with energy, the ATP concentration in *L. donovani*-infected neutrophils was determined upon treatment with 2-DG, a glycolysis inhibitor, and oligomycin or rotenone/antimycin A, inhibitors of oxidative phosphorylation. After 6 hpi 2-DG, oligomycin or rotenone/antimycin A treatment equally resulted in significantly decreased ATP concentrations of *L. donovani*-infected and uninfected neutrophils (**Figure 46**, **A**, **C**). For the 24 h time point uninfected neutrophils still reacted on 2-DG, oligomycin or rotenone/antimycin A treatment with significantly decreased ATP levels (**Figure 46**, **B**), whereas only the rotenone/antimycin A treatment resulted in significantly decreased ATP levels in *L. donovani*-infected neutrophils (**Figure 46**, **D**). The observed decrease in the ATP concentration after 2-DG treatment complemented the previous results and highlighted the importance of glycolysis during *L. donovani* infection. However, the decrease in ATP concentration after inhibition of oxidative phosphorylation did not match the expected the negligible role of oxidative phosphorylation in neutrophils I assumed so far.

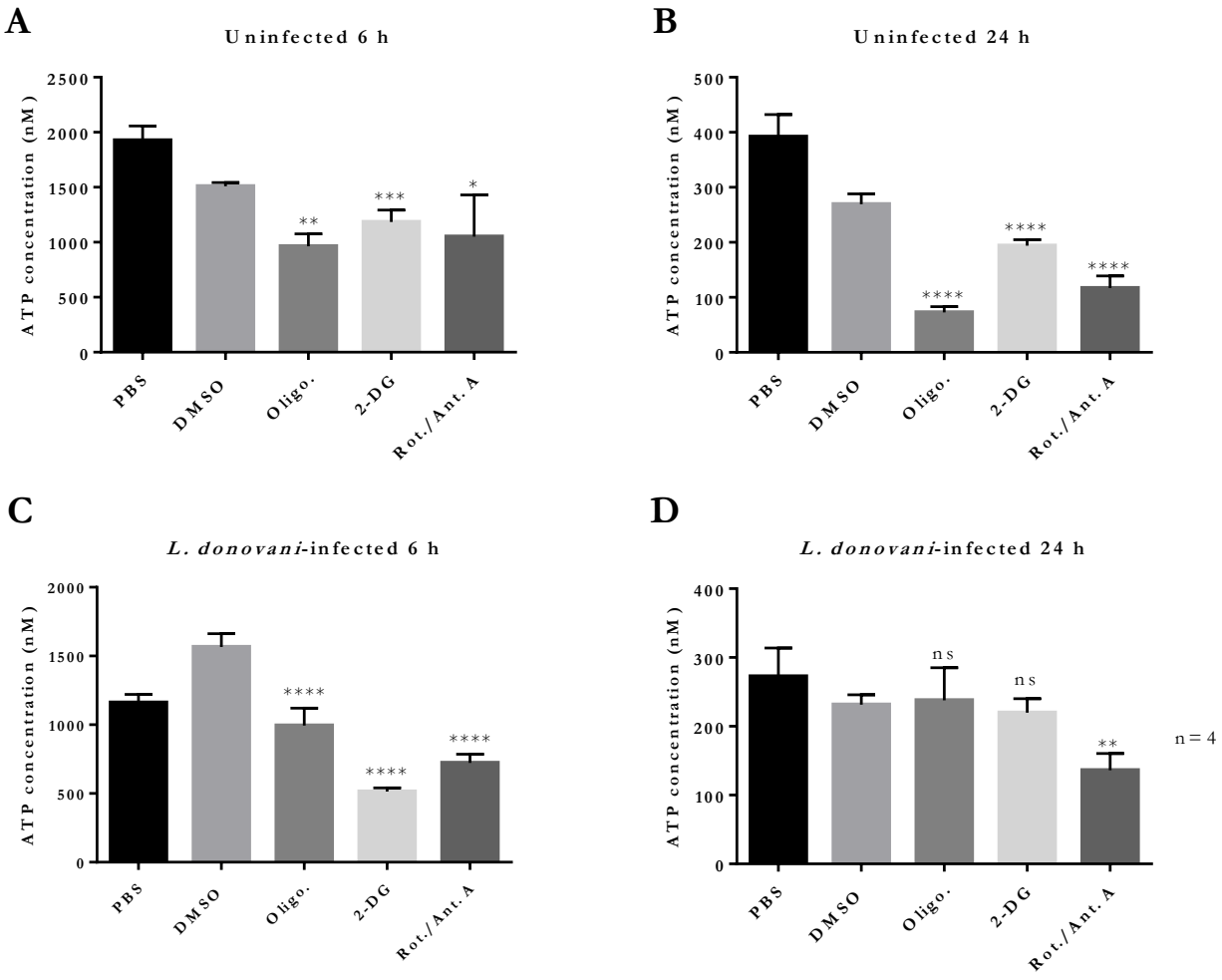

Figure 46. ATP concentration in *L. donovani*-infected neutrophils as response to metabolic inhibitors. Primary human neutrophils were infected with *L. donovani* promastigotes (ratio 1:10) for 3 h at 37°C and 5 % CO_2. Uninfected cells served as control. The infection rate was determined by Giemsa staining of cytocentrifuged samples. Subsequently, free, non-ingested parasites were removed by washing. After 6 h and 24 h post infection cells were treated with 10 mM 2-DG, 1 µM oligomycin or 1 µM rotenone/antimycin A for 3 h at 37°C and 5 % CO2. PBS and DMSO served as solvent controls. Whole cell lysates were prepared and the ATP concentration was determined by using the ATP determination kit. Bar diagrams (**A-D**) show the mean ATP concentration ± SD (n=4), whereby 2-DG-treated cells were compared to PBS-treated control cells and oligomycin- and rotenone A-treated cells were compared to the DMSO vehicle control, *p≤0.05, **p≤0.01, ***p≤0.001, ****p≤0.0001, ns = not significant.

L. donovani-infected neutrophils show an increased NAD^+/NADH ratio after 24 hpi

Pyridine nucleotides like nicotinamide adenine dinucleotides (NAD^+/NADH) are electron shuttling agents that act as co-factors in enzymatic reduction-oxidation (redox) reactions and play a central role in the mitochondrial energy metabolism to maintain the optimal redox status. For example NADH acts as principal electron donor in the respiratory chain and is oxidized to NAD^+ at complex I to drive mitochondrial oxidative phosphorylation. Mitochondrial NADH is maintained by the reduction of NAD^+ to NADH in the TCA cycle and via the import of NADH-derived reducing equivalents driven by the malate/aspartate-shuttle. Further, NAD^+ can also be consumed by poly(ADP-ribose) polymerase (PARP) enzymes or sirtuins. As changes in the metabolism are often underlined by modifications of the cellular redox potential in form of the NAD^+/NADH ratio, the content of

NAD+ and NADH as well as their ratio was determined by a luminescence-based assay for *L. donovani*-infected and uninfected neutrophils. *L. donovani*-infected neutrophils showed an increase in NAD+ and NADH levels after 6 hpi, which is reflected by the significantly higher NAD+/NADH ratio compared to uninfected neutrophils at this time point (**Figure 47**, **A**, **C**, **E**). After 24 hpi NAD+ and NADH levels of *L. donovani*-infected and uninfected neutrophils approached, therefore resulting in no significant differences between the groups (**Figure 47**, **B**, **D**, **E**). These data indicated that *L. donovani*-infected neutrophils have an elevated NAD+/NADH ratio compared to uninfected neutrophils.

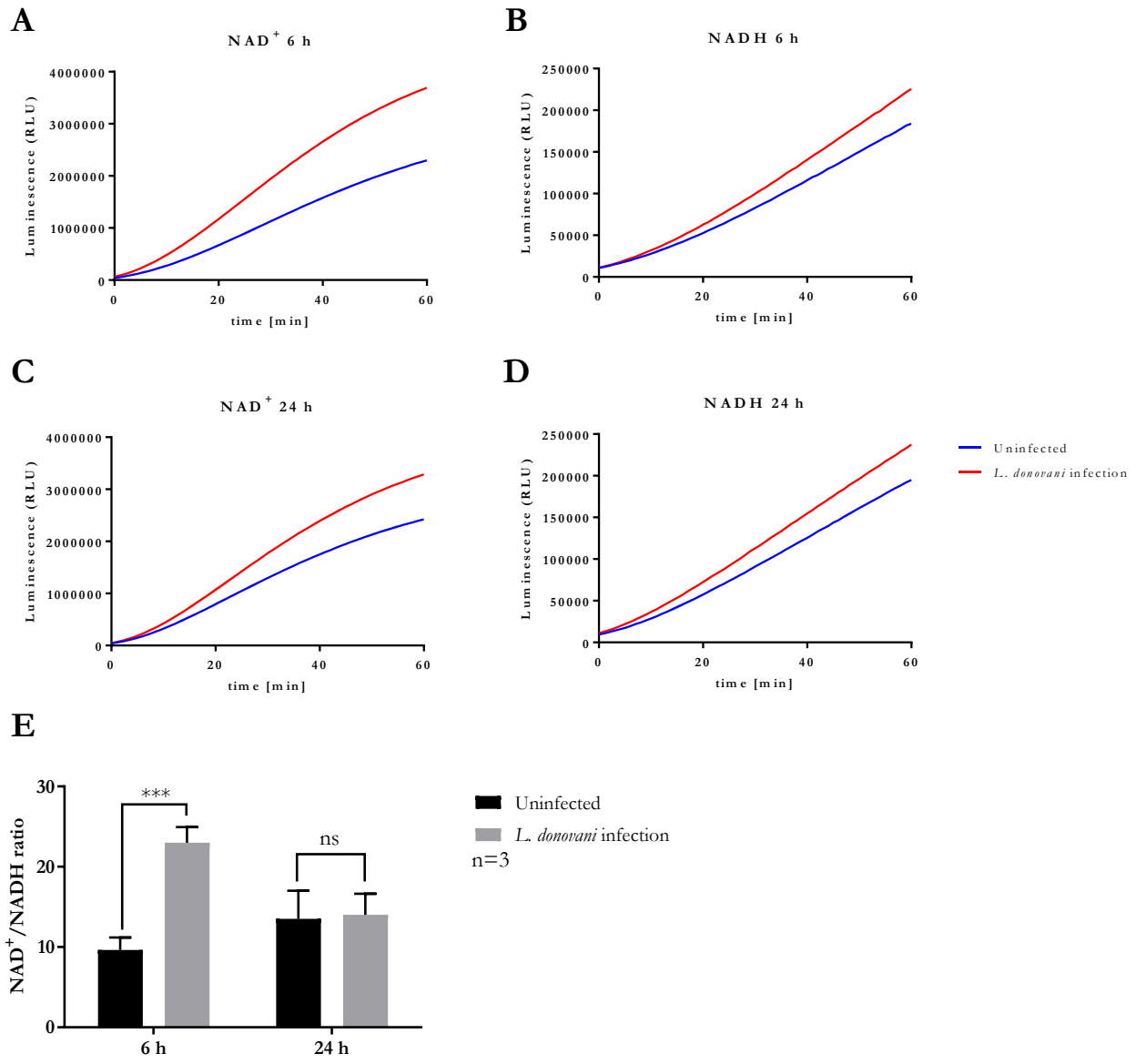

Figure 47. Detection of NAD+, NADH and NAD+/NADH ratio in *L. donovani*-infected neutrophils. Primary human neutrophils were infected with *L. donovani* promastigotes (ratio 1:10) for 3 h at 37°C and 5 % CO_2. Uninfected cells served as control. The infection rate was determined by Giemsa staining of cytocentrifuged samples. Subsequently, free, non-ingested parasites were removed by washing and whole cell lysates were prepared in accordance with the manufacturer's instructions. The amount of NAD+ and NADH was proportional to the luminescence generated by the ultra-Glo™ recombinant luciferase. After 6 h and 24 h post infection the luminescence was measured for 60 min at 37°C using the NAD/NADH-Glo™ assay. Representative curves for NAD+ and NADH, respectively are shown in panels **A**-**D**. The bar

diagram (**E**) shows the mean NAD^+/NADH ratio of the NAD^+ and NADH area under the curve (AUC) values ± SD (n=3), ***p≤0.001, ns = not significant.

L. donovani infection upregulates the fatty acid uptake of neutrophils after 24 hpi

In addition to glycolysis and oxidative phosphorylation, fatty acid oxidation is a primary means of producing energy in cells that have a particularly high need of energy supply. So far no data on fatty acid oxidation regarding *Leishmania* infection in neutrophils are available. Nonetheless, it cannot be excluded that *L. donovani* infection affects the fatty acid oxidation in neutrophils, and therefore the determination of fatty acid uptake during *L. donovani* infection was used to obtain data on this bioenergetic pathway. To be oxidized in the mitochondria fatty acids need to reach the mitochondria matrix. Fatty acids with chain length of 12 carbons or less enter the mitochondria without the help of a membrane transporter. Fatty acids with 14 or more carbons in length require membrane transporters to enter the mitochondrial matrix (Lehner and Quiroga, 2016). To test the uptake of both fatty acid types the uptake of the fluorescent fatty acid analoga BODIPY C12 and C16 was assessed by flow cytometry. *L. donovani*-infected neutrophils took up more BODIPY C16 after 24 hpi compared to 6 hpi (**Figure 48**, **J**). The uptake of BODIPY C12 and C16 by *L. donovani*-infected neutrophils was significantly increased after 24 hpi compared to uninfected neutrophils (**Figure 48**, **D**, **F**, **M**, **N**). Autofluorescence of *L. donovani*-infected and uninfected neutrophils in the BODIPY C12 and C16 channel was also assessed by flow cytometry (**Figure 48**, **A**, **B**) and was deducted from the values used for the statistical analysis. The data indicated that *L. donovani*-infected neutrophils take up more fatty acids than uninfected neutrophils after 24 hpi. Whether the increased fatty acid uptake is used for energy metabolism of the host cells or the parasite or might be involved in membrane modifications has to be further elucidated.

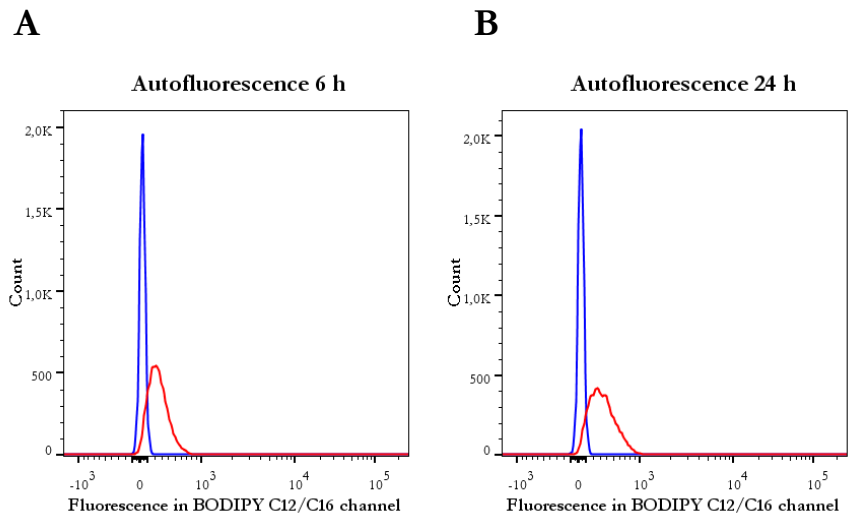

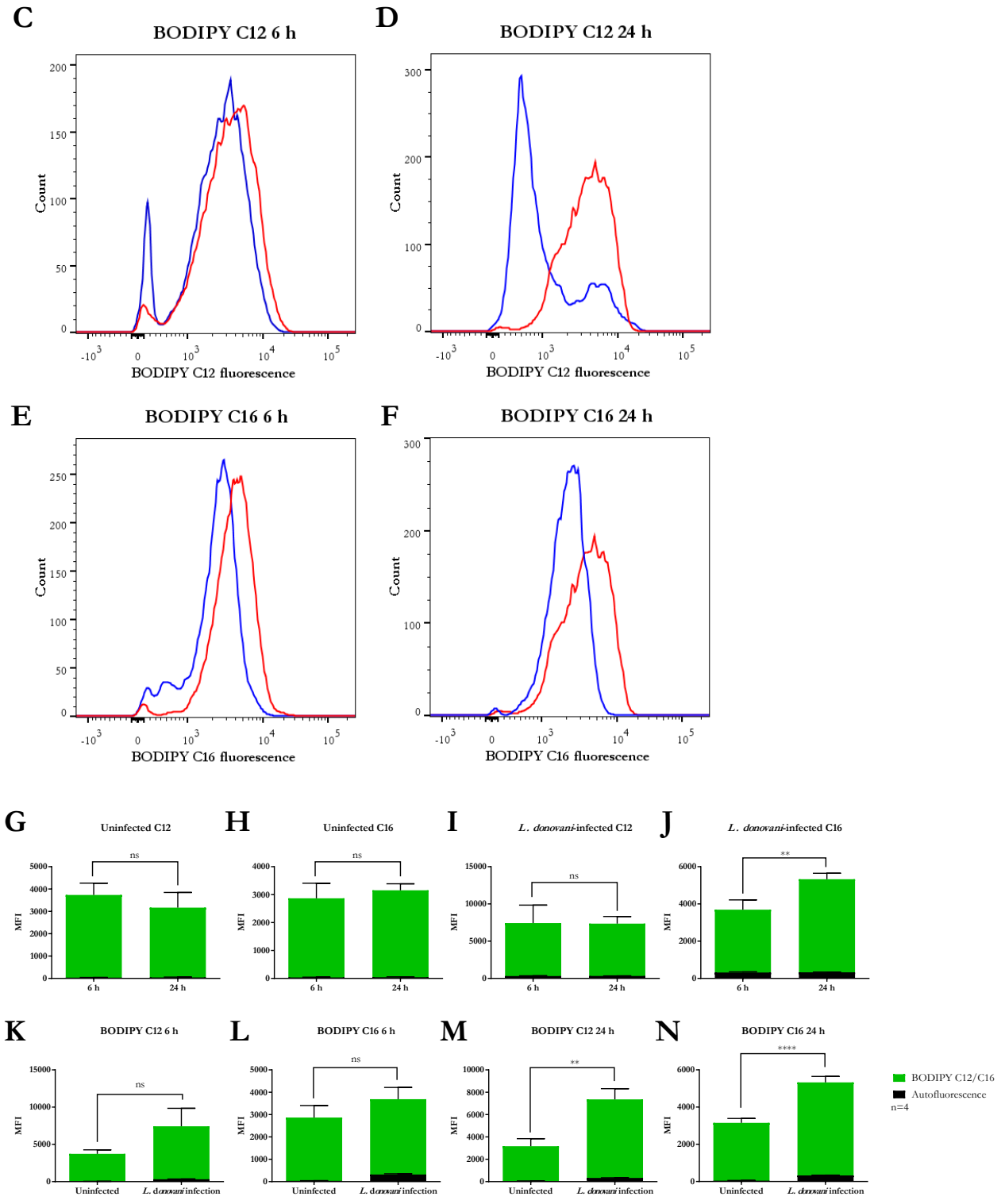

Figure 48. Fatty acid uptake of *L. donovani*-infected neutrophils. Primary human neutrophils were infected with *L. donovani* promastigotes (ratio 1:10) for 3 h at 37°C and 5 % CO_2. Uninfected cells served as control. The infection rate was determined by Giemsa staining of cytocentrifuged samples. Subsequently, free, non-ingested parasites were removed by washing. After 6 h and 24 h post infection the fluorescent fatty acid analog BODIPY™ C12 or C16 were added to the cells. Autofluorescence of infected neutrophils in the same fluorescence channel as BODIPY™ C12 and C16 is shown as

representative curves in panel **A** and **B**. Representative curves of BODIPY™ C12 and C16 uptake are shown in panels **C**-**F**. Bar diagrams (**G**-**J**) show the autofluorescence corrected mean fluorescence intensity (MFI) of BODIPY™ C12 and C16 uptake ± SD (n=4), **p≤0.01, ****p≤0.0001, ns = not significant.

Survival of *L. donovani* promastigotes in 2-DG treated neutrophils is decreased

To investigate the effects of glycolysis inhibition on the anti-leishmanial capacity of neutrophils, *L. donovani*-infected neutrophils were treated with 5 mM, 50 mM or 100 mM 2-DG and the survival of *L. donovani* promastigotes was assessed by using the limiting dilution assay after 6 hpi and 24 hpi. The non-toxic concentration range of 2-DG was previously determined by annexin-V PI staining (**Supplementary Figure S1**). As shown in **Figure 49 A**, the treatment of *L. donovani*-infected neutrophils with 5 mM or 50 mM 2-DG resulted in a significantly reduced survival rate of *L. donovani* promastigotes after 6 hpi. The same observation was made after 24 hpi for a treatment with 5 mM, 50 mM or 100 mM 2-DG (**Figure 49 A**). These data indicated that the inhibition of glycolysis by 2-DG in *L. donovani*-infected neutrophils either upregulates elimination of the parasite or has a cytotoxic effect on the *L. donovani* promastigotes.

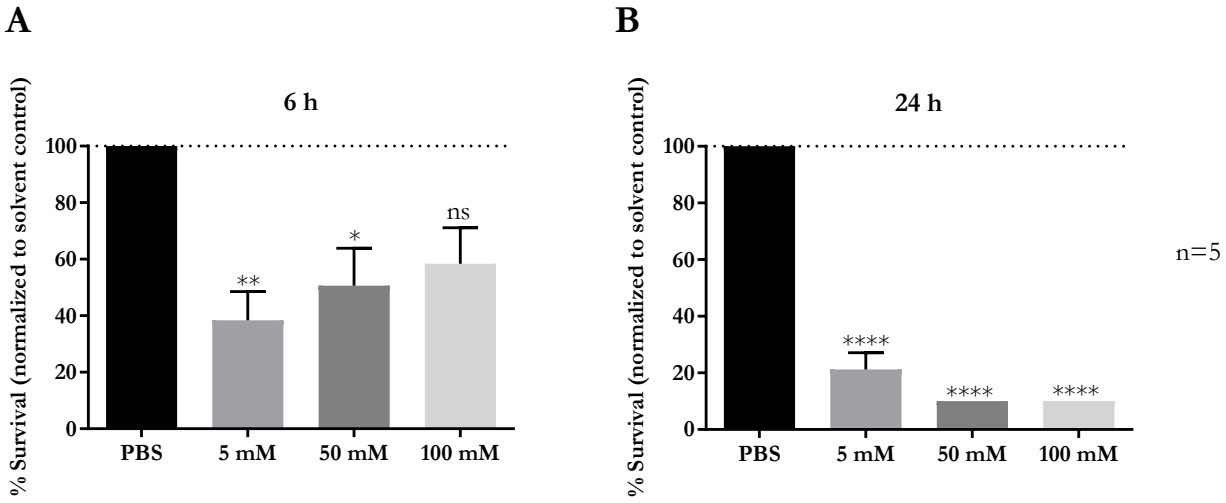

Figure 49. Survival of *L. donovani* promastigotes in 2-DG-treated neutrophils. Primary human neutrophils were infected with *L. donovani* promastigotes (ratio 1:10) for 3 h at 37°C, 5 % CO_2. The infection rate was determined by Giemsa staining of cytocentrifuged samples. After removing the free, non-ingested parasites the infected cells were treated with 5 mM, 50 mM or 100 mM 2-DG. Survival of parasites was assessed after 6 h and 24 h post infection by using the limiting dilution assay. Bar diagrams (**A**, **B**) show the mean survival rates (%) normalized to PBS-treated control cells ± SD (n=3), *p≤0.05, **p≤0.01, **** p≤0.0001, ns = not-significant.

2-DG treatment reduces ROS production of *L. donovani*-infected neutrophils after 24 hpi

To test whether the decreased survival of *L. donovani* promastigotes in 2-DG-treated neutrophils is linked to enhanced ROS production, a luminol-based chemiluminescence assay of 2-DG treated *L. donovani*-infected and uninfected neutrophils was performed after 6 hpi and 24 hpi in the presence or absence of the stimulus PMA. Unstimulated or PMA-stimulated *L. donovani*-infected neutrophils showed no significant differences in ROS production after 2-DG treatment (**Figure 50**, **C**, **D**, **K**, **L**). In contrast, unstimulated uninfected neutrophils produced significantly lower amounts of ROS production after 2-DG treatment compared to untreated cells (**Figure 50**, **A**, **I**). However, this effect could not be observed for PMA-stimulated uninfected neutrophils which after treatment with 5 mM or 50 mM 2-DG showed a significantly increased ROS production (**Figure 50**, **B**, **J**). After 24 hpi unstimulated as well as PMA-stimulated *L. donovani*-infected and uninfected neutrophils showed

significantly reduced ROS production after treatment with 5 mM, 50 mM or 100 mM 2-DG compared to untreated cells (**Figure 50**, **E**-**H**, **M**-**P**). These data demonstrated that the inhibition of glycolysis by 2-DG in *L. donovani*-infected neutrophils does not increase the elimination of the parasite through ROS production.

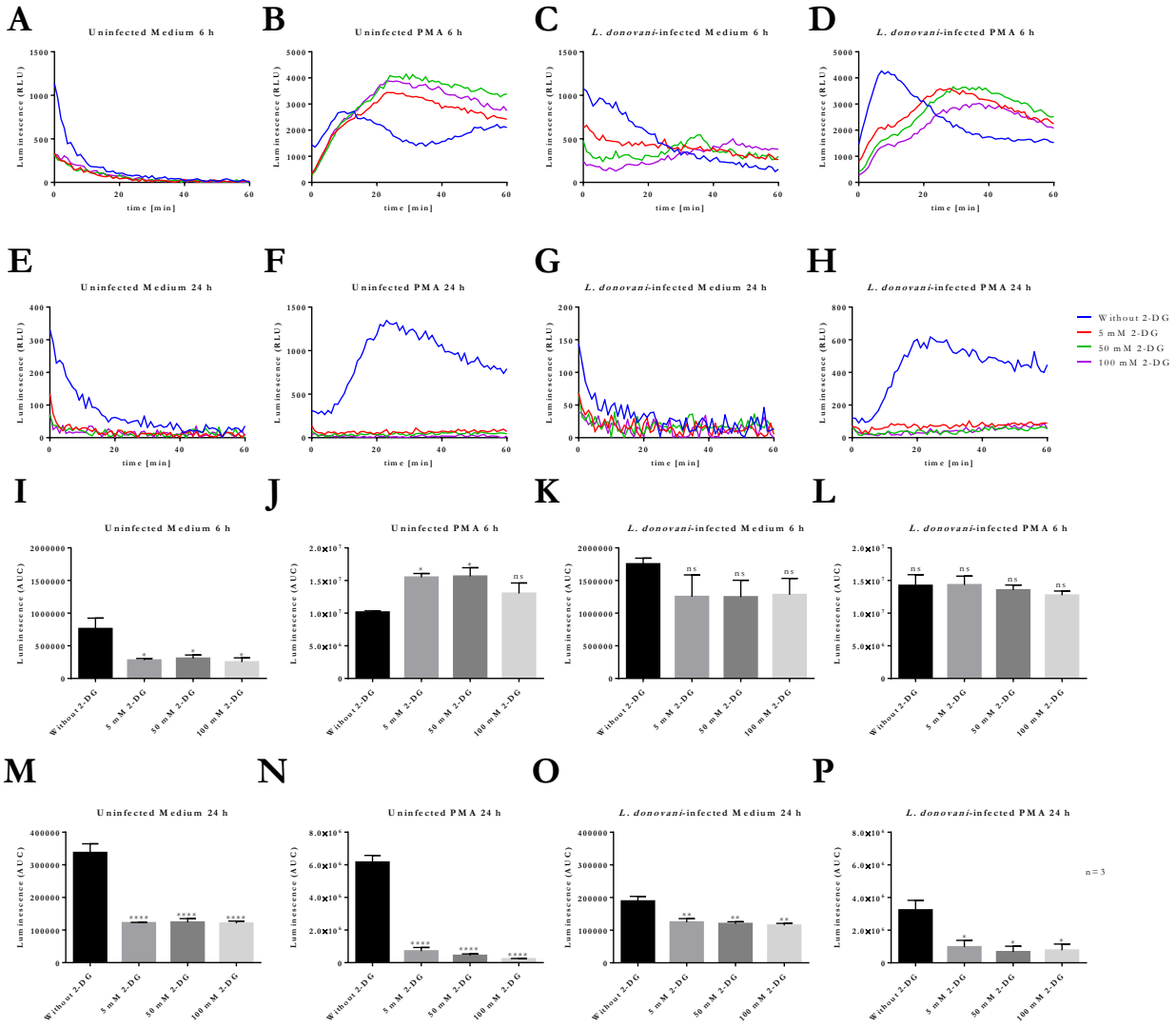

Figure 50. MPO-derived ROS production of 2-DG-treated *L.donovani*-infected neutrophils. Primary human neutrophils were infected with *L. donovani* promastigotes (ratio 1:10) for 3 h at 37°C, 5 % CO_2. Uninfected cells served as control. The infection rate was determined by Giemsa staining of cytocentrifuged samples. After removing the free, non-ingested parasites the infected and uninfected cells were treated with 5 mM, 50 mM or 100 mM 2-DG. After 6 h and 24 h post infection the MPO-derived ROS production was measured for 1 h at 37°C and 5 % CO_2 in medium alone or in the presence or absence of 20 nM PMA by using the luminol-based chemiluminescence assay. Representative curves of luminol chemiluminescence are shown in panels **A**-**H**. The bar diagrams (**I**-**P**) show the mean area under the curve (AUC) values ± SD (n=3), *p≤0.05, **p≤0.01, ****p≤0.0001, ns = not significant.

2-DG treatment reduces the survival of *L. donovani* promastigotes in culture

Next, it was tested if the reduced survival of *L. donowani* promastigotes in neutrophils was due to the cytotoxicity of 2-DG towards the parasite itself, as 2-DG due to its structural similarity to glucose is taken up by glucose transporters of cells. As quantified by microscopical analysis of Giemsa-stained cytocentrifuged samples, a neutrophil takes up on average five *L. donovani* promastigotes after 3h. Therefore $25 \cdot 10^6$/ml, five times the

concentration of neutrophils ($5 \cdot 10^6$/ml), was the concentration of *L. donovani* promastigotes used to determine the cytotoxicity of 2-DG on the parasites. *L. donovani* promastigotes were treated with 5 mM, 50 mM or 100 mM 2-DG at 37°C and 5 % CO_2 and their survival was assessed by using the limiting dilution assay after 3 h and 24 h. As shown in **Figure 51 A**, the treatment with 50 mM or 100 mM 2-DG had no effect on the survival of *L. donovani* promastigotes after 3 h. However, after 24 h the treatment with 50 mM or 100 mM 2-DG resulted in a significantly reduced survival of *L. donovani* promastigotes (**Figure 51, B**). These data demonstrated that 2-DG is cytotoxic for *L. donovani* promastigotes and therefore not suited for a HDT.

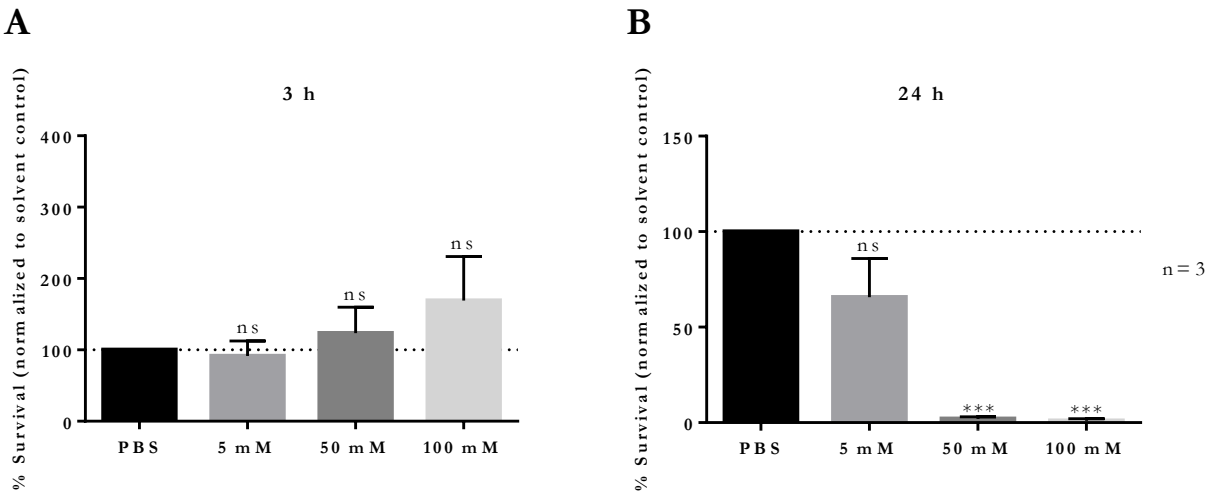

Figure 51. Survival of *L. donovani* promastigotes in the presence of 2-DG. *L. donovani* promastigotes were adjusted to $25 \cdot 10^6$ cells/ml in complete medium and treated with 5 mM, 50 mM or 100 mM 2-DG for 3 h and 24 h at 37°C and 5 % CO_2. PBS treatment served as solvent control. Survival of parasites was assessed after 3 h and 24 h by using the limiting dilution assay. Bar diagrams (**A**, **B**) show the mean normalized to PBS-treated control cells ± SD (n=3), *** $p \leq 0.001$, ns = not-significant.

Survival of *L. donovani* promastigotes in 3PO-treated neutrophils is reduced

To investigate another option to inhibit glycolysis the selective inhibitor 3PO of the 6-phosphofructo-2 kinase/fructose-2,6-bisphosphatase was tested. Furthermore, 3PO has the advantage that glucose is still transformed into glucose-6-phosphate by the hexokinase during the first step of glycolysis which in contrast is inhibited by 2-DG. Glucose-6-phosphate can also enter the pentose-phosphate pathway which fuels the NADPH-derived ROS production (**Figure 14**). To test the effect of 3PO as inhibitor of glycolysis on the anti-leishmanial capacity of neutrophils, *L. donovani*-infected neutrophils were treated with 1 µM, 30 µM or 100 µM 3PO and the survival of *L. donovani* promastigotes was assessed by using the limiting dilution assay after 6 hpi and 24 hpi. A non-toxic concentration range of 3PO was determined by annexin-V PI staining (**Supplementary Figure S2**). As shown in **Figure 52 A**, the treatment of *L. donovani*-infected neutrophils with 100 µM 3PO resulted in a significantly reduced survival rate of *L. donovani* promastigotes after 6 hpi. Moreover, the treatment with 30 µM or 100 µM 3PO of *L. donovani*-infected neutrophils significantly reduced the survival rate of *L. donovani* promastigotes after 24 hpi (**Figure 52, B**). These data indicated that the inhibition of glycolysis by 3PO in *L. donovani*-infected neutrophils either upregulates elimination of the parasite or has a cytotoxic effect on the *L. donovani* promastigotes.

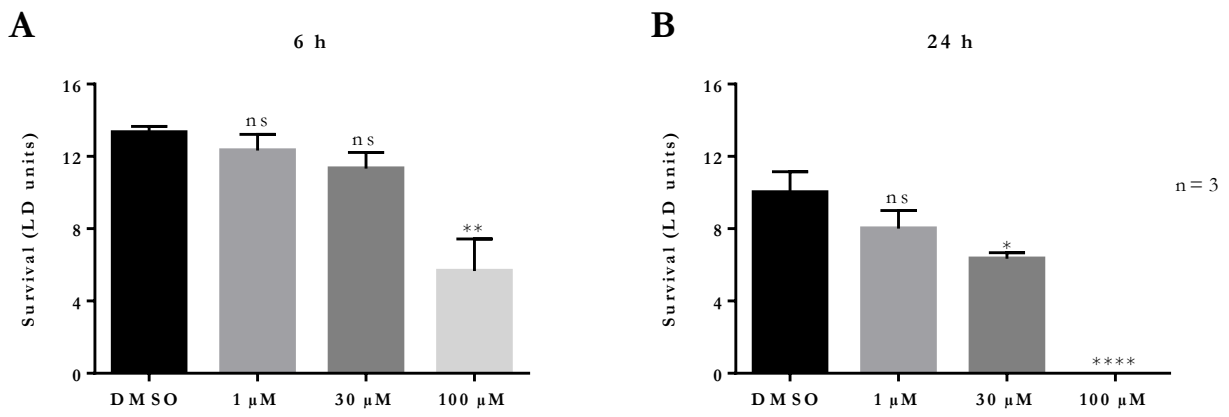

Figure 52. Survival of *L. donovani* promastigotes in 3PO-treated neutrophils. Primary human neutrophils were infected with *L. donovani* promastigotes (ratio 1:10) for 3 h at 37°C, 5 % CO_2. The infection rate was determined by Giemsa staining of cytocentrifuged samples. After removing the free, non-ingested parasites the infected cells were treated with 1 µM, 30 µM or 100 µM 3PO. Survival of parasites was assessed after 6 h and 24 h post infection by using the limiting dilution assay. Bar diagrams (**A**, **B**) show the mean survival rate ± SD (n=3), *p≤0.05, **p≤0.01, **** p≤0.0001, ns = not-significant.

3PO treatment reduces ROS production of *L. donovani*-infected neutrophils

To test whether the decreased survival of *L. donovani* promastigotes in 3PO-treated neutrophils is linked to enhanced ROS production, a luminol-based chemiluminescence assay of 3PO-treated *L. donovani*-infected and uninfected neutrophils was performed after 6 hpi and 24 hpi in the presence or absence of the stimulus PMA. Unstimulated or PMA-stimulated *L. donovani*-infected and uninfected neutrophils showed significantly decreased ROS production after treatment with 100 µM 3PO after 6 hpi (**Figure 53**, **A**-**C**, **I**-**L**). The same observation was made for PMA-stimulated *L. donovani*-infected and uninfected neutrophils after 24 hpi (**Figure 53**, **F**, **H**, **N**, **P**). However, unstimulated *L. donovani*-infected and uninfected neutrophils showed after treatment with 100 µM 3PO the tendency to produce less ROS than untreated cells (**Figure 53**, **E**, **G**, **M**, **O**). These data were rather unexpected as 3PO should not lead to an abrogation of the pentose-phosphate pathway by stalling the glucose-6-phosphate production. Therefore, 3PO treatment should not affect ROS production by the NADPH oxidase. Moreover, these data demonstrated that the inhibition of glycolysis by 3PO in *L. donovani*-infected neutrophils does not increase the elimination of the parasite through ROS production.

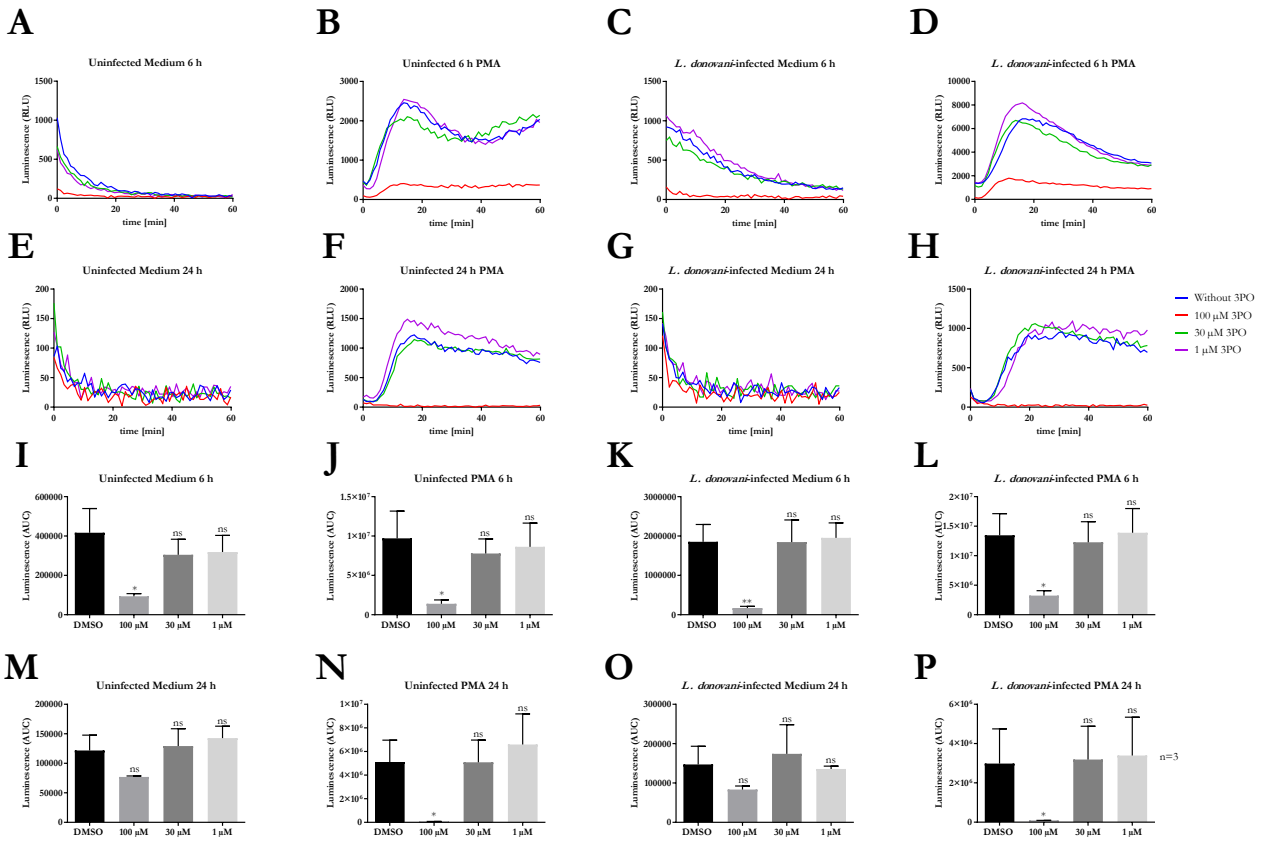

Figure 53. MPO-derived ROS production of 3PO-treated *L.donovani*-infected neutrophils. Primary human neutrophils were infected with *L. donovani* promastigotes (ratio 1:10) for 3 h at 37°C, 5 % CO_2. Uninfected cells served as control. The infection rate was determined by Giemsa staining of cytocentrifuged samples. After removing the free, non-ingested parasites the infected and uninfected cells were treated with 1µM, 30 µM or 100 µM 3PO. After 6 h and 24 h post infection the MPO-derived ROS production was measured for 1 h at 37°C and 5 % CO_2 in medium alone or in the presence or absence of 20 nM PMA by using the luminol-based chemiluminescence assay. Representative curves of luminol chemiluminescence are shown in panels **A**-**H**. The bar diagrams (**I**-**P**) show the mean area under the curve (AUC) values ± SD (n=3), *p≤0.05, **p≤0.01, ****p≤0.0001, ns = not significant.

3PO treatment seems to reduce the survival of *L. donovani* promastigotes in culture

Next, the direct cytotoxicity of 3PO towards *L. donovani* promastigotes was assessed by using the limiting dilution assay. As shown in **Figure 54**, treatment with 30 µM or 100 µM 3PO tended to reduce the survival of *L. donovani* promastigotes in culture. These data demonstrated that 3PO is cytotoxic for *L. donovani* promastigotes and therefore not suited for a HDT. Furthermore, these data in addition to the results obtained for glycolysis inhibition by 2-DG highlight the importance of glycolysis for the survival of *L. donovani* promastigotes.

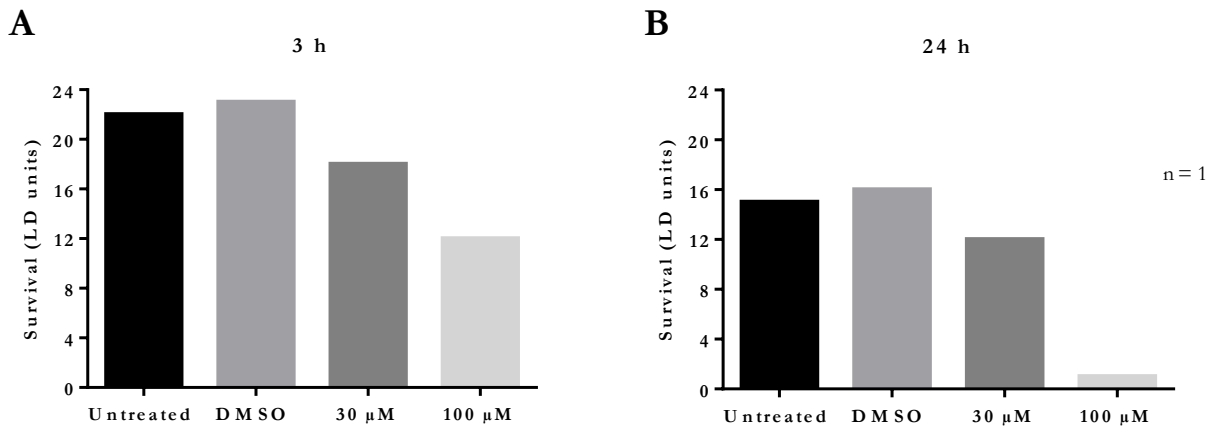

Figure 54. Survival of *L. donovani* promastigotes in the presence of 3PO. *L. donovani* promastigotes were adjusted to $25 \cdot 10^6$ cells/ml in complete medium and treated with 30 µM or 100 µM 3PO for 3 h and 24 h at 37°C and 5 % CO_2. DMSO treatment served as solvent control. Survival of parasites was assessed after 3 h and 24 h by using the limiting dilution assay. Bar diagrams (**A**, **B**) show the survival rate (LD units) (n=1).

Glucose replacement by galactose does neither affect anti-leishmanial capacity nor ROS production of neutrophils

One tool to switch the cellular metabolism from glycolysis to enhanced mitochondrial oxidative phosphorylation is the exchange of glucose for galactose in the culture medium. Whereas the production of pyruvate via glycolytic metabolism of glucose yields 2 net ATP, the production of pyruvate via glycolytic metabolism of galactose yields no net ATP, forcing the cells to have an increased reliance on oxidative phosphorylation for energy (Aguer et al., 2011). To test whether a switch from the preferred glycolysis to oxidative phosphorylation resulted in changes in the anti-leishmanial capacity of neutrophils, the culture medium was exchanged by a medium containing dialyzed FCS and 11.1 mM galactose instead of the usual 11.1 mM glucose. Dialyzed FCS was ultracentrifugated with a 10.000 Dalton exclusion membrane against physiological saline solution until the glucose content was below 10 mg/dl. As control served medium supplemented with 11.1 mM glucose, 11.1 mM glucose and 11.1 mM galactose or no supplementation at all. The listed culture conditions were confiremed as non-toxic after 3 h and 24 h incubation by annexin-V PI staining (**Supplementary Figure S3**). The different conditions did not result in changes in the viability of neutrophils compared to cells cultured in complete medium, except the medium with 11.1 mM galactose instead of 11.1 mM glucose which led to a significant lower viability of neutrophils compared to cells cultured in complete medium (**Supplementary Figure S3**, **K**). To assess the survival rate of *L. donovani* promastigotes in neutrophils after the exchange of glucose by galactose a limiting dilution assay was performed after 6 hpi and 24 hpi. To exclude the option that the dialyzed FCS contains components that would still allow the cells to prefer glycolysis over mitochondrial oxidative phosphorylation, the experiment was also conducted in medium without any FCS. As shown in **Supplementary Figure S4**, none of the different conditions resulted in changes in the survival rate of *L. donovani* promastigotes compared to medium supplemented with glucose. As shown in **Supplementary Figure S4** the presence or absence of glucose or galactose in medium supplemented with dialyzed FCS did not lead to changes in the ROS production of unstimulated or PMA-stimulated *L. donovani*-infected or uninfected neutrophils.

Moreover, the survival rate of *L. donovani* promastigotes cultured under the listed conditions was assessed by using the limiting dilution assay after 3 h and 24 h. As shown in **Supplementary Figure S6 A** the survival rate of *L. donovani* promastigotes in medium with dialyzed FCS was not changed compared to culture in complete

medium. After 24 h, medium containing dialyzed FCS but neither glucose nor galactose seemed to reduce the survival rate of *L. donovani* promastigotes (**Supplementary Figure S6 B**). These results indicated that it is either not possible to induce a shift from glycolysis to oxidative phosphorylation by exchanging glucose with galactose in the culture medium of *L. donovani*-infected neutrophils or that such an induced shift has no effect on the ROS production and anti-leishmanial capacity of neutrophils.

Glutaminolysis inhibition neither affects the anti-leishmanial capacity nor the ROS production of neutrophils

Glutaminolysis is a mitochondrial pathway that generates energy from the degradation of glutamine. When cells are confronted with low glucose levels in the extracellular milieu, they shift to glutaminolysis to fuel the TCA cycle by transforming glutamine to α-ketoglutarate via glutaminase to keep ATP and NADPH production up. To test whether glutaminolysis is a pathway used for energy generation during *L. donovani* infection the culture medium was changed after infection with *L. donovani* promastigotes to glucose-free medium supplemented with dialyzed FCS and 100 nM, 1 μM or 10 μM of the selective glutaminase inhibitor BPTES were added. Dialyzed FCS was used to prevent the metabolization of glucose and to drive glutaminolysis instead. The non-toxic concentration range of BPTES was previously confirmed by annexin-V PI staining (**Supplementary Figure S7**). Assessment of the survival rate of *L. donovani* promastigotes in BPTES-treated neutrophils in medium with or without dialyzed FCS resulted in no significant differences compared to the solvent control (**Supplementary Figure S8**). Additionally, the ROS production of BPTES-treated *L. donovani*-infected and uninfected neutrophils in the presence or absence of the stimulus PMA was determined after 6 hpi and 24 hpi by the luminol-based chemiluminescence assay. No differences between BPTES-treated and untreated *L. donovani*-infected or uninfected neutrophils could be observed in the presence or absence of the stimulus PMA compared to the solvent control (**Supplementary Figure S9**). Moreover, the effect of BPTES treatment on the survival rate of *L. donovani* promastigotes was assessed by using the limiting dilution assay. As shown in **Supplementary Figure S10**, the culture in glucose-free medium after 3 h and 24 h tended to decrease the survival rate of *L. donovani* promastigotes independent of the BPTES treatment compared to culture in complete medium. These data demonstrated that glutaminolysis plays no specific role for the anti-leishmanial capacity and ROS production of neutrophils. Further, the lack of glucose in the culture medium of *L. donovani* promastigotes impairs their survival highlighting the importance of the glucose metabolism for the parasite.

L. donovani-infected neutrophils use glycogen storages upon glucose deprivation

Electron microscopy studies have revealed the presence of glycogen stores within resting neutrophils(Robinson et al., 1982). Furthermore, it has been described that neutrophil apoptosis is regulated through glycogen availability (Sadiku et al., 2017). As neither glucose deprivation nor inhibition of glutaminolysis had a significant effect on the anti-leishmanial capacity of neutrophils it could be speculated that glycogenolysis fuels the missing glucose from the medium. To examine the role of glycogenolysis, the anti-leishmanial capacity as well as the ROS production of *L. donovani*-infected and uninfected neutrophils in glucose-free medium supplemented with dialyzed FCS was assessed after treatment with 50 μM of the glycogen phosphorylase inhibitor (GPI) for 6 hpi and 24 hpi. Dialyzed FCS was used to prevent the metabolization of glucose and to drive glycogenolysis instead. As shown in **Supplementary Figure S11**, no significant changes in the survival rate of *L. donovani* promastigotes from neutrophils in glucose-free medium supplemented with dialyzed FCS treated with 50 μM GPI or a combination of 50 μM GPI and 10 μM BPTES could be observed compared to neutrophils cultured in complete medium. Moreover, a treatment with 50 μM GPI did not induce significant changes in ROS production production of unstimulated or PMA-stimulated *L. donovani*-infected or uninfected neutrophils when compared to untreated cells in the corresponding medium (**Supplementary Figure S12**). Additionally, assessment of the survival rate of *L. donovani* promastigotes treated with 50 μM GPI or a combination of 50 μM GPI and 10 μM

BPTES revealed that the culture in glucose-free medium tended to decrease the survival rate of *L. donovani* (**Supplementary Figure S13**). To obtain information on the stability of the glycogen storage upon glucose deprivation a PAS staining of *L. donovani*-infected and uninfected neutrophils in complete medium and glucose-free medium supplemented with dialyzed FCS was performed after 6 hpi. The PAS reaction stains polysaccharides like glycogen, glycoproteins, glycolipids and mucins as purple-magenta color. The visualization by bright field microscopy as well as the quantification of microscopy images showed that the glycogen content of *L. donovani*-infected and uninfected neutrophils cultured in glucose-free medium supplemented with dialyzed FCS is significantly decreased compared to those culture in complete medium (**Figure 55**, **A**-**F**). These data indicated that *L. donovani*-infected neutrophils degrade glycogen in the absence of glucose. However, an inhibition of glycogenolysis had no impact on the anti-leishmanial capacity and ROS production of neutrophils. Therefore, it is very likely that neutrophils have either enough intracellular glucose to eliminate the parasites in a short period of time or use another metabolic pathway to fuel their need for energy.

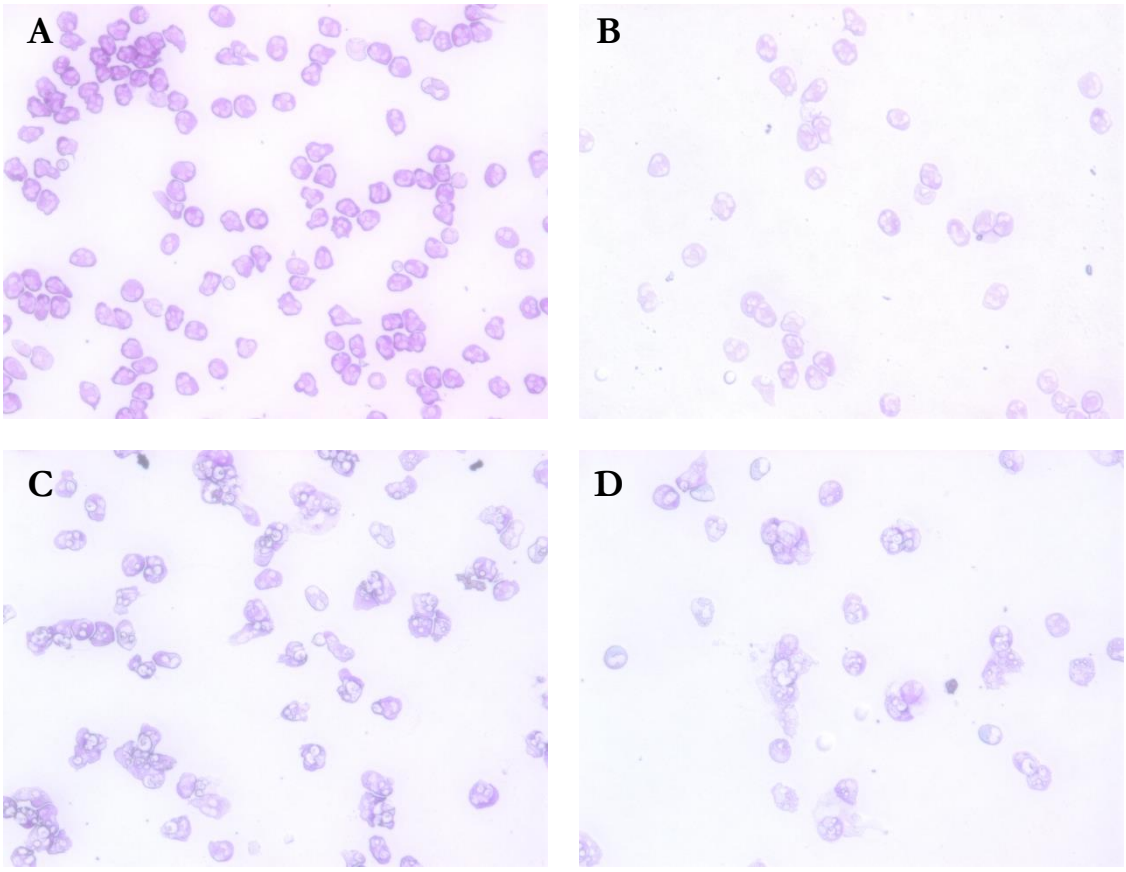

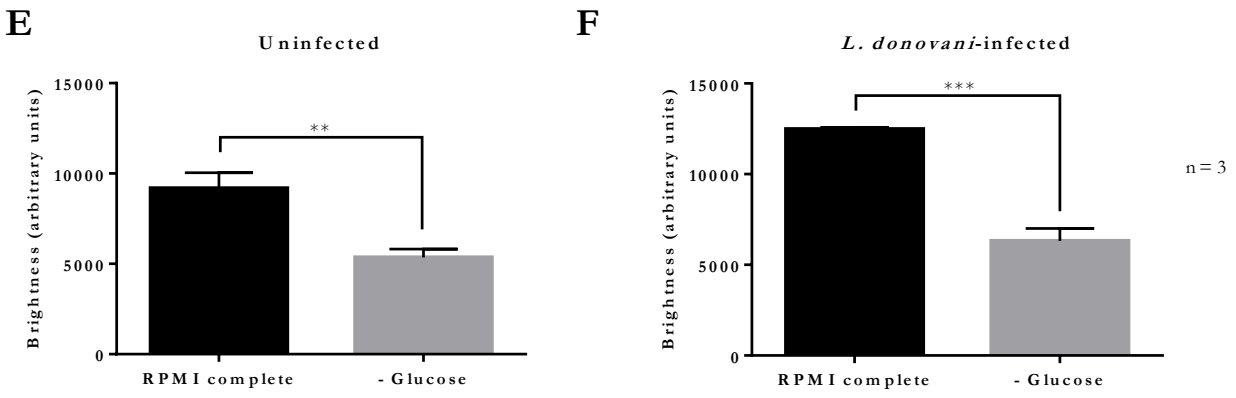

Figure 55. PAS staining of *L. donovani*-infected neutrophils in glucose-free medium. Primary human neutrophils were infected with *L. donovani* promastigotes (ratio 1:10) for 3 h at 37°C, 5 % CO_2. Uninfected cells served as control. The infection rate was determined by Giemsa staining of cytocentrifuged samples. After removing the free, non-ingested parasites the infected and uninfected cells were either cultured in complete medium or in glucose-free medium supplemented with dialyzed FCS. After 6 hpi cytospins were generated, the cells were fixated and a PAS staining was performed. Subsequently, bright field microscopy was used for visualization of cells (**A**-**D**). For quantification of microscopy images the colors of the bright field were turned into 16-bit grayscale and the brightness of individual cells was measured with ImageJ. For each sample 5 cells of three donors were evaluated. A cell-free area on the image was chosen to subtract the brightness of the background. Bar diagrams (**E**, **F**) show the background-corrected mean intensity of five individual cells ± SD (n=3), ** $p \leq 0.01$, *** $p \leq 0.001$.

Taken together, the data acquired on the metabolism of *L. donovani*-infected neutrophils including extracellular flux analysis, glucose uptake, glycolytic end product measurement and PAS staining indicate that the glycolytic metabolism plays an important role during the infection of neutrophils with *L. donovani*.

Part III: Transcriptomic profiling of *L. donovani*-infected neutrophils

In the present study, I examined the transcriptome of human neutrophils infected with *L. donovani* after 6 hpi and 24 hpi. I aimed to identify signaling pathways which are crucial for *L. donovani* persistence and survival in human neutrophil and to make them candidates of future host-directed therapies (HDTs).

To visualize how well RNA expression differed for *L. donovani*-infected and uninfected neutrophils over time, a dimensionality reduction by principal component analysis (PCA) based on the 1000 most variable genes was performed. **Supplementary Figure S14** shows the human transcriptomes over the course of the experiments and reveals that *L. donovani*-infected and uninfected neutrophils separated in the principal component space. Moreover, the PCA shows that the samples separated by time forming distinct clusters for 0 h, 6 h and 24 h.

In order to predict potential therapeutic drug candidates against VL and to target underlying pathways, a connectivity map (CMAP) analysis was performed on the transcriptome of *L. donovani*-infected neutrophils (**Supplementary Figure S15 A**). Using a reference database containing drug-specific gene expression reference profiles were compared to the gene expression signature of *L. donovani*-infected neutrophils after 6 and 24 hpi. The ten top-scoring drugs were selected by sorting all connectivity scores in descending order and identifying a relevance threshold. A positive correlation denotes the degree of similarity and a negative correlation reflects an inverse similarity between the query signature and the reference profile derived from an individual chemical perturbation, meaning the exposure to a certain drug or compound can mimic or reverse the observed expression pattern. I observed the most significant positive correlation between the transcriptomic profile of *L. donovani*-infected neutrophils and the reference profile for trichostatin A, thioridazine and 15-delta prostaglandin J2

(**Supplementary Figure S15 B**). The most significant negative correlation was identified for LY-294002, wortmannin and sirolimus (**Supplementary Figure S15 C**).

To utilize the transcriptome data of *L. donovani*-infected neutrophils for the identification of potential key nodes as targets for future HDTs, a protein-protein interaction (PPI) analysis was performed. The PPI network of 9039 nodes with 125337 protein interactions pairs was constructed to identify hub genes in *L. donovani* infected neutrophils. A hub gene codes a protein that plays a vital role in biological processes and regulates other proteins in a pathway network. The most significant modules of the PPI network are shown in Figure 8, in which the top hub genes after 6 hpi were centered around Jun and MAPK (**Supplementary Figure S16 A**), whereas signaling nodes including RICTOR, SYK and AKT1 were downregulated. After 24 hpi the signaling around the key node CASP8 was downregulated (**Supplementary Figure S16 B**).

These results demonstrated that the transcriptome of *L. donovani*-infected neutrophils differs from that of uninfected neutrophils and contains several metabolic nodes that could be targeted by HDTs. Unfortunately, the analysis of the functional enrichment analysis is not completed yet, but could provide further information on potential therapeutic targets in the future.

Discussion

Part I: Polarization of primary human neutrophils toward N1 and N2 phenotypes *in vitro*

Neutrophils are traditionally considered to be short-lived, terminally differentiated cells that form the host´s first line of defense against invading pathogens. However, the modern era of immunology has revealed the existence of distinct neutrophil subsets with functional and phenotypic heterogeneity. Especially, the pro-inflammatory N1 phenotype and the anti-inflammatory N2 phenotype which were first described as two divergent identities of tumor-associated neutrophils (TANs) can be regarded as representatives of the broad spectrum of neutrophil subsets reflecting the huge plasticity neutrophils can acquire.

Leishmania parasites are the causative agents of leishmaniasis, a neglected tropical disease that causes substantial morbidity and considerable mortality in many areas of the world. Visceral leishmaniasis caused by the *L. donovani* complex is the most severe form of leishmaniasis and universally fatal without treatment. Although the parasite grows and divides preferentially in macrophages also neutrophils serve as host cells for *Leishmania* and appear to be especially important after the parasites are introduced into the skin where they serve as "Trojan Horse" or "Trojan Rabbit" to enable successful infection of macrophages (Carlsen et al., 2015; Peters et al., 2009; Laskay et al., 2008; Müller et al., 2001). However, neutrophils fulfill either a protective or a permissive role during the establishment of leishmaniasis which might be explained by the acquisition of a N1-like or N2-like phenotype.

Until now major findings of N1 and N2 TANs are derived from murine cancer models. An *in vitro* model based on human cells would be the optimal option to overcome fundamental species differences between mouse and human without the ethical difficulties to get access to patient material. In the present work an *in vitro* polarization model for N1-like and N2-like neutrophils was developed to test the permissiveness of pro- and anti-inflammatory neutrophil phenotypes for *L. donovani* as those phenotypes might be the explanation for the contrary roles neutrophils fulfill in the development of VL. For a N1-like polarization a pro-inflammatory microenvironment was created by addition of IFNβ, IFNγ and LPS to the culture medium. To achieve a polarization towards the N2-like phenotype the tumor microenvironment was mimicked by addition of the immunosuppressive mediators IL-10, G-CSF, PGE_2, TGFβ, L-lactate and adenine to the culture medium as well as an acidification and oxygen deprivation of the extracellular milieu.

As the lifespan of neutrophils infiltrating the tumor tissues *in vivo* is generally considered to be extended to a few days, in this work the apoptosis of primary human neutrophils from the circulation was suppressed by addition of Pan-caspase inhibitor QVD-OPh to both the N1 and N2 polarization cocktail. As shown in **Figure 17** and **18** the QVD-OPh treatment suppressed apoptosis of neutrophils *in vitro* up to 48 h. Furthermore, the QVD-OPh treatment did not lead to CD62L shedding or ROS production (**Figure 19, 20**). Therefore the neutrophils were not activated through the QVD-OPh treatment. Prolongation of the neutrophil lifespan is critical for effective host defense and targeted by many pathogens. Also ingested *Leishmania* prolong the neutrophil lifespan for up to 24 h by upregulating phosphorylation of the ERK1/2 pathway and decreasing caspase-3 activity (Aga et al., 2002; Sarkar et al., 2013). Despite its artificial character, QVD-OPh treatment was efficiently able to suppress the apoptosis of neutrophils without altering their activation status.

To evaluate the effectiveness of the developed *in vitro* polarization model typical N1 and N2 TAN markers and neutrophil effector mechanisms were tested. As expected, neutrophils co-incubated with the N1 polarization cocktail were highly activated and showed strong degranulation (**Figure 21 – 23**). Responsible for this is likely an additive of the N1 polarization cocktail, LPS, which has been shown to increase the amount of CD11b (Nogare and Yarbrough, 1990) and CD66b (Schmidt et al., 2015) on the surface of human neutrophils and to induce CD62L shedding (Pédron et al., 2001). Furthermore, it is noteworthy that N2-like neutrophils showed less

CD62L shedding compared to N1-like and N0 neutrophils. This observation underlines again that the activation status of N1-like and N2-like polarized neutrophils differs and indicates that indeed two different neutrophil subsets were generated during this *in vitro* attempt. For N1-like neutrophils the typical surface markers FasR (CD95), ICAM-1 (CD54) and neprilysin (CD10) were investigated (Marini et al., 2017; Fridlender and Albelda, 2012). As shown in **Figure 24** N1-like neutrophils showed a high expression of all three markers which was also significantly increased compared to N2-like and N0 neutrophils. The surface expression of the typical N2 marker CXCR2 (CD182) (Chao et al., 2016; Nywening et al., 2018) was significantly increased on N2-like neutrophils compared to N1-like and N0 neutrophils (**Figure 24**, **C**, **D**, **M**). The surface expression of CXCR2 on N1-like neutrophils was low, an observation which is in accordance with the literature (Fridlender et al., 2009). The expression of all mentioned surface markers corresponded to the published profiles of N1 and N2 TANs. However, lectin-type oxidized LDL receptor 1 (LOX-1), a specific marker of G-MDSCs and LDGs (Chai et al., 2019; Condamine et al., 2016), was expected to be highly expressed on N2-like neutrophils as N2 TANs, G-MDSCs and LDNs share similar properties. Contrary to this expectation N1-like neutrophils showed a significantly increased expression of LOX-1 on their surface compared to N2-like and N0 neutrophils (**Figure 24**, **I**, **J**, **O**). However, some studies report the upregulation of LOX-1 on pro-inflammatory neutrophils in a murine sepsis model (Al-Banna and Lehmann, 2013; Condamine et al., 2016) which would explain the increased expression of LOX-1 on the surface of N1-like neutrophils as they represent also a pro-inflammatory phenotype. Furthermore, it it is questionable if LOX-1 is a suitable marker for N2-like neutrophils as one study showed that all neutrophils express LOX-1 on their surface (Lecot et al., 2019). In addition, the assumption that N2 TANs, G-MDSCs and LDGs show the same surface markers is an oversimplification as it is not known yet to which extent these populations overlap.

In addition to surface markers the secretion of typical N1 and N2 mediators described by Fridlender and Albeda was investigated (Fridlender and Albelda, 2012). Typical soluble mediators of N1 TANs include TNF and IP-10, whereas N2 TANs are characterized by the secretion of VEGF, MCP-1, IL-8 and MMP-9 (Fridlender and Albelda, 2012). Indeed, N1-like neutrophils secreted high amounts of IP-10 and TNF, cytokines that are involved in the anti-tumor immune response (**Figure 25**, **A**, **D**). IP-10 and TNF were shown to act in synergy to induce antitumor effects (Enderlin et al., 2009). IP-10 serves as key driver chemokine by attracting CD8+ and CD4+ T cells to tumor sites and potentiating their function (Karin and Razon, 2018). In addition, IP-10 is a major chemokine recruiting natural killer (NK) cells and exerts antitumor effects also by inhibiting angiogenesis (Strieter et al., 1995), making IP-10 a potent antitumor factor (Giese et al., 2002). Neutrophils treated with the N2 polarization cocktail secreted elevated levels of IL-8 (**Figure 25**, **E**). The IL-8/IL-8R axis is a signaling pathway used by tumor cells to recruit neutrophils initially to the tumor site. As N2 neutrophils are a potent source of IL-8, the entrapping influx of neutrophils into the tumor is established as a positive feedback loop (David et al., 2016). It is interesting to note that IFN-γ treatment of neutrophils has been shown to downregulate IL-8 production (Cassatella et al., 1993a, 1993b), indicating that IFN-γ may act as a signal to halt PMN recruitment and infiltration. However, this downregulation of the IL-8 production was correlated with an upregulated production of the pro-inflammatory cytokines TNF and IL-1β in neutrophils. *In vitro* experiments have shown that neutrophils incubated with IFN-γ demonstrate a transient downregulation of IL-8 production for the first few hours of incubation. Extended incubation of neutrophils with IFN-γ leads to production of TNF and IL-1β. This new cytokine milieu then acts in an autocrine manner to override the signal from IFN-γ and reactivates IL-8 synthesis, explaining the increased levels of IL-8 found in the supernatant of N1-like neutrophils (**Figure 25**, **E**).

The secretion of the typical N2 mediators VEGF, MMP-9 and MCP-1 by N2-like neutrophils was not increased, instead N1-like neutrophils showed elevated levels of these soluble mediators (**Figure 25**, **B**, **C**, **F**). VEGF has a central role in tumor angiogenesis and is stored intracellularly in human neutrophils to be released as response to various stimuli. Already 1998 a study reported that activated human neutrophils secrete high levels of VEGF

(Webb et al., 1998). Moreover, it was shown that TNF-activated murine neutrophils in an *in vivo* model of corneal angiogenesis produced and released VEGF (Gong and Koh, 2010). Considering these data, it is not surprising that the highly activated N1-like polarized neutrophils secrete elevated levels of VEGF.

MMP-9 plays an important role in neutrophil extravasation and migration by its ability to degrade the major components of the basement membrane (Nagaoka and Hirota, 2000). However, MMP-9 is also one of the major angiogenesis-inducing factor and supplied to the tumor microenvironment by infiltrating TANs (Deryugina et al., 2014). MMPs regulate acute and chronic inflammation likewise. As shown in a guinea pig model of peritoneal inflammation an acute inflammatory milieu increased the MMP-9 secretion of neutrophils (Nagaoka and Hirota, 2000). The N1 polarization cocktail contains with IFNβ, IFNγ and LPS key regulators of pro-inflammatory events, and is therefore probably increasing the MMP-9 secretion similarly as in the guinea pig model of acute peritoneal inflammation. Especially LPS seems to trigger MMP-9 production of neutrophils (Kanai et al., 2004), whereas IFNγ and IFNβ treatment of murine neutrophils resulted in reduced MMP-9 expression (Jablonska et al., 2010; Sun et al., 2014). However, it cannot be excluded, that the negative effect of IFNγ and IFNβ on the MMP-9 expression is outweighed by LPS or that the combination of all three components in the used polarization setting activates the signaling pathway PI3/Akt/NFκB upstream of MMP-9 (Cheng et al., 2012). As also the N2-like neutrophils acquired the property to release MMP-9 after 48 h polarization (**Figure 25**, **F**) it is possible that the N2 polarization cocktail has the potential to induce MMP-9 secretion but is probably delayed compared to the highly pro-inflammatory microenvironment created by the N1 polarization cocktail.

N2 TANs are amongst other chemokines characterized by the secretion of MCP-1 (Fridlender and Albelda, 2012). However, in my study N1-like neutrophils secreted high levels of MCP-1 (**Figure 25**, **C**), whereas N2-like neutrophils did not release any MCP-1. Responsible for this observation might be the composition of the N1 polarization cocktail which contains IFNγ which has been shown to induce the production of MCP-1 in response to activation by TLR ligands like e.g. the here used LPS (Yoshimura and Takahashi, 2007). Although, the role of MCP-1 in recruitment and activation of N2 TANs is known, an anti-tumor role of MCP-1 in neutrophil-mediated tumor killing through ROS production has also been stated (Lavender et al., 2017). Considered in this context, the increased MCP-1 levels measured for N1-like neutrophils support the success of the used polarization strategy.

One of the major hallmarks of N2 TANs is the expression of arginase 1, a protein which inhibits T cell proliferation and modulates PD-L1/PD-1 signaling in order to regulate an immunosuppressive response (Masucci et al., 2019). Detection of arginase 1 activity revealed that N2-like neutrophils tended to have a higher arginase 1 activity (**Figure 31**), supporting their overall characterization as an immunosuppressive phenotype. However, arginase 1 is constantly expressed in human neutrophils (Munder, 2005) and activated neutrophils also release arginase 1 as shown in a murine ischemic stroke model (Sippel et al., 2011).

As important effector function, the ROS production of *in vitro* polarized neutrophils was measured. Whereas the N1-like neutrophils produced more intracellular ROS (**Figure 28**) and showed the tendency to produce more MPO-derived ROS (**Figure 26**) than N2-like neutrophils, the superoxide production of N2-like neutrophils was increased compared to N1-like neutrophils (**Figure 27**). These findings reflect the two-faced role of neutrophil-derived ROS in the context of tumor progression. Due to the fact that neutrophils are considered a source of genotoxic ROS, results from a mutatect murine tumor model strongly suggest that tumor-infiltrating neutrophils may be mutagenic and can contribute to the genetic abnormalities associated with tumor development (Sandhu et al., 2000). Moreover, N2 TANs suppress tumor-killing γδ T cells through oxidative stress induced by ROS production (Mensurado et al., 2018). However, there is evidence that ROS produced by neutrophils have also anti-tumor activity as ROS can directly damage and destroy tumor cells (Uribe-Querol and Rosales, 2015). The

high superoxide production of N2-like neutrophils might represent the genotoxic und immunosuppressive properties proclaimed for N2 TANs *in vivo*. As superoxide production measured by using the lucigin-amplified chemiluminescence assay is directed into the extracellular milieu it could affect the tumor cells or T cells directly. On the other hand the high intracellular ROS production of N1-like neutrophils is compliant with the assumption that neutrophils cultured in a N1 polarization cocktail obtain a rather pro-inflammatory phenotype. As intracellular ROS function as a powerful effector mechanism against phagocytosed pathogens, tumor cells will not be harmed by intracellular ROS as they cannot be phagocytosed by neutrophils.

The importance of NETs in cancer is just emerging. Links have been made between NETs and metastasis in some murine tumor models and in patients with breast and colon cancers (Yang et al., 2020a), and evidence of the presence of NETs in certain tumors have been reported (Arpinati et al., 2020; Snoderly et al., 2019; Yang et al., 2020b). In the present study I assessed the NET formation of *in vitro* polarized neutrophils by microscopy and measurement of DNA release upon PMA stimulation (**Figure 32**, **33**). Fluorescence microscopy revealed that both N1-like and N2-like neutrophils are capable of NET formation upon PMA stimulation. This shows that despite their artificial lifespan prolongation the *in vitro* polarized neutrophils still remained functional. Real-time kinetics of SYTOXGreen staining showed that N1-like neutrophils form more NETs than N2-like neutrophils. Actually based on the known tumor promoting role of both NETs and N2 TANs, I expected to find a higher NET formation by N2-like neutrophils. The finding, that N1-like neutrophils released more NETs than N2-like neutrophils, was unexpected but might be explained by the components of the N1 polarization cocktail as LPS (Khan et al., 2017) and type I IFNs can promote NET formation (Garcia-Romo et al., 2011).

The most effective anti-tumor mechanism of neutrophils is antibody-dependent cell mediated cytotoxicity (ADCC). Antibodies that bind to tumor antigens are recognized by Fc receptors on neutrophils. This binding activates a cytotoxic response against the tumor cell. Expression of Fc receptors on the effector cell that recognize the Fc portion of the bound antibody on the target cell initiates the ADCC. Human neutrophils express the Fc receptors FcRIIIγ (CD16), FcRIIγ (CD32), FcRIγ (CD64) and FcRα (CD89). Although all these Fc receptors induce ADCC, a recent study showed that FcαR-mediated binding of IgA is much stronger than FcRγ-mediated IgG binding at triggering tumor cell killing by neutrophils (Brandsma et al., 2019). Moreover, IgA-mediated binding of neutrophils is more stable compared to IgG. IgA engagement of neutrophils elicited stronger Fc receptor signaling than IgG as indicated by measuring the p-ERK signaling molecule (Brandsma et al., 2019). The findings from this study clearly show that N1-like neutrophils express more FcRα on their surface than N0 and N2-like neutrophils (**Figure 34**). Therefore, it can be speculated that N1-like neutrophils kill tumor cells more potently than N2-like neutrophils as they express high levels of the relevant receptor.

Next, I tested the anti-bacterial properties of *in vitro* polarized neutrophils. Although, no data regarding the bacterial killing abilities of TANs have been confirmed yet, I assumed that the killing of bacteria is comparable to the killing of tumor cells. Despite the fact that the differences between N0, N1-like and N2-like neutrophils were not significant, N1-like neutrophils tended to kill fewer bacteria compared to the other two groups (**Figure 29**). This finding surprised me, as the data so far showed that N1-like neutrophils are highly activated, and I expected that activated neutrophils would kill more bacteria due to their potentiated effector mechanisms. However, some studies indicate that neutrophils, when excessively stimulated undergo exhaustion. ROS generation is also greatly decreased by the desensitization of intracellular signaling molecules due to excessive stimulation. This observation is known as immune paralysis of neutrophils (Alves-Filho et al., 2010; Lacy, 2006; Ward, 2004). This phenomenon could also explain the lower superoxide production of N1-like neutrophils compared to N2-like neutrophils. As the bacterial killing was measured 24 h and 48 h after polarization, the strong stimulation of N1-like neutrophils might have caused the already mentioned immune paralysis.

To address the hypothesis that N2-like neutrophils are permissive for *L. donovani*, the anti-leishmanial capacity of *in vitro* polarized neutrophils was assessed (**Figure 30**). The results showed that *in vitro* polarized N2-like neutrophils exert a decreased killing ability for *L. donovani* promastigotes compared to N1-like neutrophils which eliminated the majority of parasites. As neutrophils are the first innate immune cells at the site of *Leishmania* infection (Beil et al., 1992; Laufs et al., 2002; Müller et al., 2001), it would be of advantage for the parasite to polarize the neutrophils toward a favorable phenotype. Although the N2 polarization cocktail is based on conditions present in the tumor microenvironment, the results obtained in this study point towards the existence of an immunosuppressive N2-like phenotype that is permissive for *L. donovani*. This idea is further supported by the presence of several factors in the N2 polarization cocktail that are characteristic for the tumor microenvironment such as hypoxia (Mahnke et al., 2014; Singh et al., 2012a) or the cytokines IL-10 (Kane and Mosser, 2001b; Noben-Trauth et al., 2003), TGF-β (Anderson et al., 2008; Wilson et al., 1998), and the lipid mediator PGE_2 (Kane and Mosser, 2001b; Noben-Trauth et al., 2003) that are also found in tissues infected with *Leishmania*.

In this work I described for the first time that mature human neutrophils have the plasticity to acquire properties of N1 and N2 TANs *in vitro*. Nonetheless, also deviations from the current findings for TANs were observed, including the expression of LOX-1 on N1-like neutrophils, the secretion of VEGF, MMP-9 and MCP-1 by N1-like neutrophils as well as the NET formation of N2-like neutrophils. However, the reliance on published markers of TANs is rather insecure as many markers stated for N1 and N2 TANs were investigated by RT-PCR (Fridlender et al., 2009) not considering the discrepancy between transcriptome and proteome. Moreover, there are limitations in translating murine tumor models to human pathology and plack of human data, highlighting again the urgent need for an applicable model based on human neutrophils to elicit the properties of neutrophil subsets in health and disease. Additionally, it has to be mentioned that the rigid binary N1/N2 classification of neutrophils is likely an oversimplification. It is more likely that N1 and N2 represent extremes of a biological continuum that overlap with the G-MDSC and LDG phenotypes depending on the local microenvironment. Overall my attempt to polarize neutrophils towards specific subsets *in vitro* can be regarded as pioneer work. Further optimization and variation of polarization conditions can bring the phenotype of polarized neutrophils even closer to the aimed subsets. Future polarization strategies should consider the co-culture of neutrophils with tumor cells. The exhibited tumor microenvironment generated this way is, however, a certain black box compared to the well-defined composition of the polarization cocktails used in this study. Still, the direct contact between tumor cells and neutrophils may be a driving force of polarization into N1 or N2 TANs. Taken together, the *in vitro* polarization model developed in this study is just a first step in the development of a suitable *in vitro* model for the investigation of neutrophil subsets in health and disease.

Part II: Metabolic characterization of *L. donovani*-infected neutrophils

Intracellular pathogens like *Leishmania* can actively manipulate the host cell metabolism for their benefit. Conventionally, the effects of intracellular pathogens on host metabolism have been assumed to be downstream consequences of pathogenesis. However, increasing evidence suggests that these pathogen-induced disturbances may instead be strategies to evade immune response. Furthermore, intracellular pathogens, including *Trypanosoma cruzi*, *Plasmodium falciparum* and *Bordetella pertussis*, deprive nutrients from the host cell and trigger metabolic host cell responses which promote pathogen growth and persistence (Freyberg and Harvill, 2017). The host cell defense often includes general metabolic reactions, like the generation of reactive oxygen and/or nitrogen species and measures to prevent access to essential nutrients for the respective pathogen (Eisenreich et al., 2013). Moreover, a link between immune cell polarization and metabolic reprogramming exists. As shown for M1 and M2 macrophages, the metabolic adaption to the surrounding microenvironment instructs the polarization of macrophages with functionally distinct phenotypes (Thapa and Lee, 2019). Here, I investigated the effect of *L.*

donovani infection on the metabolism of host neutrophils as more knowledge about the metabolic manipulation and polarization of neutrophils by *Leishmania* may provide new targets for host-directed therapies.

First, the oxidative metabolism of *L. donovani*-infected neutrophils was investigated as it has been reported that ROS contribute to the killing of intracellular parasites like *L. donovani* or *L. major* (Laufs et al., 2002; Pearson and Steigbigel, 1981). Screwing the oxidative metabolism of neutrophils during infection might be a strategy of the parasite to evade elimination by ROS. Moreover, neutrophils from VL patients showed impaired ROS production (Yizengaw et al., 2016). It has been shown that *L. major* did not elicit the generation of ROS upon phagocytosis by human neutrophils. In contrast, other studies showed that *L. braziliensis* induces high levels of ROS production upon infection of human and murine neutrophils but ROS generation in human neutrophils did not affect parasite survival (McFarlane et al., 2008). Moreover, mid-log phase and metacyclic promastigotes of *L. major* have been found to induce significant respiratory burst in rabbit peritoneal neutrophils upon infection (Mallinson et al, 1989).

The findings in this study show that simple contact between *L. donovani* promastigotes and neutrophils triggered ROS production as well as intracellular and extracellular ROS production (**Figure 35**, **36**). Intracellular ROS are a potent effector mechanism against intracellular pathogens like *L. donovani* and I expected them to be increased in neutrophils capable of killing the phagocytosed *L. donovani* promastigotes. Although extracellular ROS do not harm the intracellular parasite, I wondered if they also increased during infection to stop the spreading of non-phagocytosed *Leishmania*. Overall ROS production measured by the luminol-based chemiluminescence assay was increased by *L. donovani*-infected neutrophils compared to uninfected neutrophils (**Figure 37**). Intracellular ROS production of *L. donovani*-infected neutrophils tended to be increased compared to uninfected neutrophils (**Figure 39**). My findings show that *L. donovani*-infected neutrophils produce more ROS which can kill the intracellular parasite. Although extracellular ROS production was increased after primary contact to the parasite, it was not increased 6 hpi and 24 hpi (**Figure 38**). Probably, neutrophils could sense that no extracellular parasites remained after the washing and stopped extracellular ROS production as it was no longer effective against the parasite. Further, it could be speculated that phagocytosis of the parasite shuts down extracellular ROS production as it is better strategy to use resources and energy for the production of intracellular ROS. *L. donovani*-infected neutrophils showed increased intra- und extracellular ROS production after the stimulation with PMA or fMLP (**Figure 37 – 39**). These results indicate that the oxidative metabolism of neutrophils is not decreased by *L. donovani* to prevent its elimination and remains a potent effector mechanism to kill the parasite.

Apart from NADPH oxidase, another important source of ROS is mitochondria. Mitochondria are major producers of ROS and hence contribute greatly to the cellular oxidative burst. To persist within the host cells, apart from phagosomal ROS, *Leishmania* can also neutralize mitochondrial ROS production in neutrophils (Basu and Das, 2019). To address the role of mitochondrial ROS during *L. donovani* infection of neutrophils a MitoSox Red staining of *L. donovani*-infected neutrophils was performed and analyzed by flow cytometry (**Figure 40**). The results showed that mitochondrial ROS production of *L. donovani*-infected neutrophils was significantly increased compared to uninfected neutrophils. These findings are not in line with the negative impact *Leishmania* infection had on the mitochondrial ROS production in macrophages (Basu and Das, 2019). However, apart from cell specific differences macrophages and neutrophils fulfill different roles in the life cycle of *Leishmania*. Therefore it is not possible to simply transfer findings from one cell type to the other. The data from this work indicate that the oxidative metabolism of human neutrophils is not negatively affected by *L. donovani* infection.

As metabolic reprogramming regulates cytokine response of immune cells during infection and *vice versa*, the cytokines TNF, IP-10 and IL-8 were monitored during *L. donovani* infection of human neutrophils (**Figure 41**). The secretion of TNF and IL-8 by *L. donovani*-infected neutrophils was evaluated compared to uninfected

neutrophils. Several studies reported that exposure and infection of neutrophils to *Leishmania* results in high production of IL-8 (Laufs et al., 2002; Safaiyan et al., 2011; van Zandbergen et al., 2002). The chemoattractant IL-8 enhances the early recruitment of neutrophils to the site of infection (Müller et al., 2001) and activates their functions, such as the phagocytosis (Scapini et al., 2000). Moreover, previous studies have shown that *Leishmania spp.* trigger the TNF secretion of human (Safaiyan et al., 2011) and murine neutrophils (Falcão et al., 2015). TNF produced by neutrophils plays an important role for leukocyte migration and for DC and macrophage activation and differentiation (Nathan, 2006). Furthermore, it can induce neutrophil degranulation at the site of infection, thus it influences the development of an efficient defense against the parasite (Nathan, 2006).

As already shown for *L. major* (van Zandbergen et al., 2002), I observed that *L. donovani* infection inhibited the IFNγ/LPS-inducible IP-10 production of human neutrophils. The chemokine IP-10 is a potent mediator of NK-cell recruitment which via the production of IFN-γ promotes the development a protective Th1-mediated cellular immune response. It is possible to correlate the findings from this study regarding the secreted cytokines of *L. donovani*-infected neutrophils with metabolic effects of the measured cytokines. Lately, IL-8 secretion has been associated with an increased glucose consumption, a high lactate production and overexpression of glycolytic enzymes in colorectal cancer cells (Xu et al., 2017). TNF as pro-inflammatory cytokine increased the glucose uptake in L6 myoblasts and is associated with obesity linked insulin resistance (Borst, 2004; Yamasaki et al., 1996). The plasma IP-10 levels of patients with pulmonary tuberculosis correlated positively with the blood glucose concentration and were increased under hyperglycemia (Devaraj and Jialal, 2009; Zhao et al., 2018). Transferring these findings on the here studied model, my results point towards an increased glycolytic metabolism in *L. donovani*-infected neutrophils. Taken into account the pro-inflammatory nature of IL-8, TNF and IP-10, it can be assumed that glycolysis as key player of inflammation is increased in *L. donovani*-infected neutrophil by just considering the cytokine profile determined here.

In the next step, I investigated glycolysis in *L. donovani*-infected neutrophils by extracellular flux analysis. *L. donovani*-infected neutrophils showed indeed increased glycolysis and glycolytic capacity compared to uninfected neutrophils after 6 hpi (**Figure 42**). After 24 hpi *L. donovani*-infected neutrophils showed decreased glycolysis compared to uninfected neutrophils. This observation could remind one of the metabolic switch of *L. infantum*-infected macrophages from early glycolysis to late oxidative phosphorylation as observed by Moreira et al. (Moreira et al., 2015). However, the increased oxidative phosphorylation of *L. donovani*-infected neutrophils compared to uninfected neutrophils was linked to increased respiration but not to ATP production (**Figure 43**). These results do not support the theory of a metabolic switch in *L. donovani*-infected neutrophils. Instead the data from the extracellular flux analysis indicate that glycolysis in *L. donovani*-infected neutrophils is the preferred energy metabolism and that the increased oxidative phosphorylation fuels the previously confirmed increased ROS production. Moreover, the finding that glycolysis is decreased after 24 hpi in *L. donovani*-infected neutrophils has to be interpreted with caution. Although, the 24 h time point was measured, data acquired for this time point are difficult to interpret as many neutrophils are already apoptotic at this time point. Furthermore, the high lactate secretion and pyruvate content (**Figure 44**) as well as elevated glucose uptake of *L. donovani*-infected neutrophils (**Figure 45**) support the view of an enhanced glycolytic metabolism of neutrophils during *L. donovani* infection.

Although all data on the metabolism of *L. donovani*-infected neutrophils pointed towards the predominant role glycolysis, the results of the assay used to determine the ATP content of *L. donovani*-infected neutrophils were not in line with the these findings. Inhibition of glycolysis by 2-DG treatment as well as inhibition of oxidative phosphorylation reduced the ATP content of *L. donovani*-infected (**Figure 46**). These findings are in direct contrast to the data obtained from the extracellular flux analysis, namely the increased glycolytic metabolism in *L. donovani*-infected neutrophils. Evaluating the two techniques, extracellular flux analysis is considered to be the gold standard to measure glycolysis and oxidative phosphorylation of cells. In contrast, the ATP determination

kit used in this study is a mere end point measurement providing less informational content and making the results of the extracellular flux analysis more trustworthy.

The coenzyme NAD plays a major role as a key redox carrier and signaling molecule. The NAD^+/NADH ratio is therefore an useful indicator for the metabolic capacities of a cell. The NAD^+/NADH ratio of *L. donovani*-infected neutrophils and uninfected neutrophils did not differ after 6 hpi (**Figure 47**). It can be speculated that the increased NAD^+/NADH ratio of *L. donovani*-infected neutrophils after 24 hpi, is derived from the parasite and not the host neutrophil. Further, data for the 24 h time point are difficult to interpret as a lot of cells underwent already apoptosis.

So far only little is known on the fatty acid oxidation of neutrophils. Here, it was demonstrated that *L. donovani*-infected neutrophils showed an increased uptake of fatty acids compared to uninfected neutrophils (**Figure 48**). If this serves ATP production or is a strategy of the parasite to acquire nutrients enabling it to survive in its host cell, still has to be elucidated.

As the data collected so far mainly pointed towards an increased glycolytic metabolism of *L. donovani*-infected neutrophils, the question remained whether this preference for glycolysis was linked to the anti-leishmanial capacities of the neutrophils or was induced by the parasite to guarantee its survival. In case of the latter, glycolysis might be, similarly, as in cancer therapy, a promising target of host-directed therapy. To test this option the anti-leishmanial capacity of 2-DG treated neutrophils was determined. Indeed, the survival of *L. donovani* promastigotes in 2-DG-treated neutrophils was decreased (**Figure 49**). To find out if this result could be traced back to an increased ROS production which eliminates the parasite, the ROS production of 2-DG-treated *L. donovani*-infected and uninfected neutrophils was measured. The data indicated that 2-DG treatment instead of triggering the ROS production induced significant abrogation of ROS production (**Figure 50**). Taking a closer look on the inhibited step in the glycolysis pathway, the underlying reason for these findings became obvious. 2-DG, due to its structural similarity with glucose, is a competitive inhibitor of the hexokinase, the first rate-limiting enzyme of the glycolysis pathway. The hexokinase catalyzes the conversion of glucose to glucose-6-phosphate, a metabolite which also enters the pentose-phosphate pathway where its further processing generates NADPH. The coenzyme NADPH is in turn the substrate of the NADPH oxidase, the protein complex mainly responsible for the ROS production in neutrophils. Nevertheless, the reduced survival of *L. donovani* promastigotes in 2-DG-treated neutrophils could not be explained by decreased ROS production through the 2-DG treatment. So there was still the possibility, that 2-DG was directly toxic for the *L. donovani*. A limiting dilution assay of *L. donovani* promastigotes cultured in the presence of 2-DG revealed that 2-DG alone reduced the survival rate of *L. donovani* promastigotes and is, therefore, toxic for the parasite (**Figure 51**). 2-DG was taken up by neutrophils and *L. donovani* promastigotes likewise as both cell types have very similar glucose transporters due to their eukaryotic nature. To target other steps of glycolysis, experiments were repeated with the selective 6-phosphofructo-2-kinase/fructose-2,6-bisphosphatase inhibitor 3PO. Targeting the phosphofructokinase blocks the second rate-limiting step of glycolysis, the conversion of fructo-6-phosphate to fructose-1,6-bisphosphate. As no direct link from this reaction to the pentose-phosphate pathway exists, NADPH oxidase-derived ROS production should not be altered by this treatment. As already observed for 2-DG also the survival of *L. donovani* promastigotes in 3PO-treated neutrophils was reduced (**Figure 52**). This was specifically effective when 100 μM 3PO were applied. However, ROS production of *L. donovani*-infected and uninfected neutrophils was decreased after the treatment with 100 μM 3PO. This observation was rather surprising as 3PO treatment should not affect the ROS production. As also the viability of neutrophils was not affected by 3PO treatment (**Supplementary Figure S2**), it can only be speculated that neutrophils may enter a resting or quiescent state once their major ATP source, glycolysis, is abrogated. Overall, also 3PO seemed to reduce the survival of *L. donovani* promastigotes (**Figure 54**). This suggests that glycolytic enzymes of neutrophils and the parasite have a high phylogentic similarity. The

important role of glycolysis for *Leishmania* is further highlighted by the presence of glycosomes, specialized organelles which contain most of the peroxisomal enzymes. In addition, they also possess nine glycolytic enzymes (Jamdhade et al., 2015). An inhibition of the glycolytic metabolism also hits the parasite and is therefore very likely to affect its viability.

Whereas *L. infantum*-infected macrophages experience a metabolic switch from glycolysis towards oxidative phosphorylation, such a change in the energy metabolism of *L. donovani*-infected neutrophils has not been demonstrated. However, this raises the question what would happen if neutrophils were forced to switch from glycolysis towards oxidative phosphorylation. A tool to switch the metabolism of cells from glycolysis to enhanced oxidative phosphorylation is the exchange of glucose for galactose in the culture medium. As the glycolytic metabolism of galactose leads to less ATP than the catabolization of glucose, the cell will compensate the ATP loss by oxidative phosphorylation. In my experiments the exchange of glucose by galactose in the culture medium had neither an impact on the survival of *L. donovani* promastigotes in neutrophils nor on the ROS production of neutrophils (**Supplementary Figure S4**, **S5**). On the contrary, glucose deprivation without an exchange through galactose tended to impair the survival of *L. donovani* promastigotes alone.

To test whether neutrophils in the absence of glucose rely on glutaminolysis to make up ATP supply via TCA cycle, a glutaminase inhibitor was applied. However, also inhibition of glutaminolysis in the absence of glucose did neither alter the survival of *L. donovani* promastigotes nor had an impact on the ROS production of neutrophils (**Supplementary Figure S8**, **S9**). As the survival of *L. donovani* promastigotes tended to be very low in the absence of glucose a further decrease through BPTES treatment could not be observed.

As neutrophils also contain high amounts of glycogen the possibility existed that glycogen was degraded in the absence of glucose and fueled glycolysis. To test this hypothesis the survival of *L. donovani* in neutrophils treated with a glycogen phosphorylase inhibitor (GPI) in glucose-free medium was measured. The respective results indicated that neither GPI treatment nor a combination of GPI and a glutaminase inhibitor treatment led to a reduced survival of *L. donovani* in neutrophils. Moreover, GPI treatment did not affect ROS production of *L. donovani*-infected or uninfected neutrophils. To evaluate the glycogen content after glucose deprivation as PAS staining which visualizes polysaccharides of *L. donovani*-infected and uninfected neutrophils was performed. Indeed, the intensity of the PAS staining was reduced of those cells cultured in glucose-free medium (**Figure 55**). This demonstrates that *L. donovani*-infected and uninfected neutrophils degrade glycogen when confronted with low glucose conditions. An explanation for the lacking effect of GPI on the anti-leishmanial capacity and MPO-derived ROS production of neutrophils is still missing. One explanation might be the presence of intracellular glucose which could be used by neutrophils in the absence of glucose from the culture medium. As the PAS staining detects all polysaccharides including glycogen, glycolipids, glycoproteins and mucins, a specific quantification of only glycogen by this experiment is simply not possible.

In conclusion, the findings regarding the metabolic characterization of *L. donovani*-infected neutrophils obtained in this study support the view that glycolysis is the main energy pathway in neutrophils. However, as *Leishmania* parasites are also highly dependent on glycolysis a host-directed therapy of leishmaniasis does not appear to be a promising approach. In addition, it is very likely that host cell and parasite metabolism are strongly intertwined. Nevertheless, the obtained information could be used to develop an anti-parasitic therapy against visceral leishmaniasis as drugs targeting glycolysis used in the context of cancer therapy might be repurposed for visceral leishmaniasis.

Part III: Transcriptomic profiling of *L. donovani*-infected neutrophils

The number of studies analyzing transcriptional responses in neutrophils is rather limited, thus, little is known on the transcriptional changes that are caused by the infection with the intracellular protozoan parasite *L. donovani*. In the present study, I therefore investigated the transcriptional response of neutrophils during *L. donovani* infection with the goal to identify signaling pathways engaged in parasite persistence to make them future targets of HDTs. To investigate general trends in the data, principal component analysis (PCA) was carried out for neutrophil transcriptomes over the course of the experiment (**Supplementary Figure 14**). A high similarity between biological replicates was evident in the PCA plots. In general, similar samples clustered together by infection status and time point. For the prediction of potential drugs targeting signaling pathways which are elevated in VL, I performed a connectivity map (CMAP) analysis of *L. donovani*-infected neutrophils. The highest positive correlation was identified for the antifungal antibiotic trichostatin A, the antipsychotic drug thioridazin and the anti-inflammatory lipid mediator 15-delta prostaglandin J2 (**Supplemenatry Figure 15 B**). The latter has been confirmed to induce ROS-mediated apoptosis of *L. donovani* promastigotes and amastigotes in an rodent model of VL (Vishwakarma et al., 2016). Also isoforms of trichostatin A which inhibits histone deacetylases showed an antileishmanial activity against *L. donovani* (Sodji et al., 2014). Moreover, thioridazin has recently attracted interest as potent drug candidate against malaria, leishmaniasis and Chagas disease (Thanacoody, 2007). The highest negative CMAP correlation for *L. donovani*-infected neutrophils was obtained for PI3K inhibitors LY-294002 and wortmannin as well as for the mTOR inhibitor sirolimus (**Supplementary Figure 15 C**). Based on the RNA seq data obtained on *L. donovani*-infected neutrophils a protein-protein interaction (PPI) network was generated to provide information on the most important protein hub nodes (**Supplementary Figure 16**). The PPI network after 6 hpi showed that interactions centered around Jun and MAPK making them a potential target for HDTs. In contrast, protein hub nodes around RICTOR, Syk and Akt were downregulated. After 24 hpi a downregulation of CASP8 was observed. This finding is in line with the observation that *Leishmania* parasites can extend the lifespan of neutrophils to prolong their presence in these cells (Aga et al., 2002; Regli et al., 2017).

The next step of this project involves the targeting of the metabolic nodes identified in the transcriptome analysis in *L. donovani*-infected neutrophils. In addition, functional enrichment analysis, which has not been completed yet, will give even deeper insight into differentially regulated signaling pathways in *L. donovani*-infected neutrophils that will help to understand the role of neutrophils in VL better and to develop new therapies against VL.

Summary

Visceral leishmaniasis (VL) is a systemic protozoan disease that is endemic in countries that are among the least developed in the world. There are approximately 500.000 new cases of VL and more than 50.000 deaths from the disease each year, a death toll that is only surpassed among parasitic infections by malaria. The widespread emergence of resistance in VL reaching epidemic dimensions in India demonstrates the urgent need for more research and development to improve the drug pipeline for VL. In this context host-directed therapy that targets host pathways required for pathogen survival or its clearance is a promising approach for treating VL. The function of neutrophils in leishmaniasis was reported to be either beneficial by contributing to parasite elimination or detrimental by providing a transient safe shelter for the parasite prior to its entry into the definite host cells, macrophages. However, so far no satisfactory explanation for the controversial roles of neutrophils during leishmaniasis has been found.

Neutrophil heterogeneity has become an emerging focus with accumulating evidence of neutrophil subsets with distinct functions under both steady-state and pathologic conditions. A shift in the balance between pro-inflammatory and anti-inflammatory neutrophils, like the N1 and N2 tumor-associated neutrophils (TANs), can decisively determine disease outcome. To test the hypothesis that an infection with *Leishmania donovani* drives neutrophils towards an anti-inflammatory phenotype, I attempted to generate N1-like and N2-like neutrophils *in vitro*. Primary human neutrophils were cultured in a N1 or N2 polarization cocktail that either mimicked a pro-inflammatory or tumor microenvironment, respectively. On the one hand it was investigated whether *in vitro* polarized neutrophils gained N1 or N2 TAN properties and on the other hand how the acquired phenotypes correlated with permissiveness for *L. donovani*. After exposure to the N1 polarization cocktail neutrophils became highly activated and showed increased degranulation. Additionally, N1-like neutrophils expressed neprilysin, FasR and ICAM-1 at a high level on their surface and secreted high levels of TNF and IP-10. Moreover, the expression of FcαRI was elevated on N1-like neutrophils suggesting a higher capacity antibody-dependent cell-mediated cytotoxicity. Neutrophils which were cultured with the N2 polarization cocktail showed a high expression of CXCR2 on their surface as well as secreted IL-8 which is typical for N2 neutrophils. The increased extracellular ROS production of N2-like neutrophils compared to N1-like neutrophils reflects the acquired pro-tumor properties of N2-like neutrophils as extracellular ROS can induce genotoxicity of tumor cells and suppress CD8+ T cells. The assessment of the anti-leishmanial capacity of *in vitro* polarized neutrophils clearly showed that N2-like neutrophils harbored significantly more viable parasites as compared to N1-like neutrophils, this way I could prove the hypothesis of the decreased killing ability of N2-like neutrophils for *L. donovani*.

The second part of this study dealt with the metabolic characterization of *L. donovani*-infected neutrophils with the aid of extracellular flux analysis and metabolic assays to identify metabolic nodes essential for the parasite survival. In the future those metabolic nodes could be used as targets for the development of host-directed therapies. As important defense mechanism against intracellular pathogens, the oxidative metabolism of neutrophils during *L. donovani* infection was assessed. In summary the ROS production of *L. donovani*-infected neutrophils was increased compared to uninfected neutrophils. As cytokines can affect the metabolism and *vice versa*, the secretion of TNF, IL-8 and IP-10 of *L. donovani*-infected neutrophils was assessed. *L. donovani*-infected neutrophils showed high levels of TNF and IL-8, whereas the IP-10 production was abrogated. Since these cytokines are known to be associated with glycolysis, next I investigated the glycolytic metabolism. Extracellular flux analysis of *L. donovani*-infected neutrophils showed indeed that glycolysis was the preferred bioenergetics pathway. This result was further supported by the observation that the glycolytic end products, lactate or pyruvate, accumulated in the supernatant and in the cytosol of *L. donovani*-infected neutrophils. Moreover, glucose uptake of *L. donovani*-infected neutrophils was elevated compared to uninfected neutrophils. Inhibition of glycolysis reduced the survival of *L. donovani* promastigotes in neutrophils. Due to the direct cytotoxicity of

glycolysis inhibitors on *L. donovani* promastigotes, a host-directed therapy based on glycolysis inhibition is not possible but might serve as anti-parasitic therapy against VL.

The transcriptome analysis of *L. donovani*-infected neutrophils revealed several metabolic nodes those potential as candidates for host-directed therapies against VL will be investigated in the future.

Together the whole thesis showed that the presence of N1-like and N2-like neutrophils might explain the contrary roles of neutrophils in the development of VL and that glycolysis is the major bioenergetics pathway in *L. donovani*-infected neutrophils.

Zusammenfassung

Viszerale Leishmaniose (VL) ist eine systemische von Protozoen hervorgerufene Erkrankung, die in Ländern endemisch ist, die zu den am wenigsten entwickelten der Welt gehören. Jährlich gibt es etwa 500.000 Neuinfektionen und 50.000 Todesfälle, eine Zahl, die bei parasitären Erkrankungen nur durch Malaria übertroffen wird. Das weit verbreitete Auftreten von Resistenzen bei VL, die in Indien epidemische Ausmaße erreichen, zeigt, dass dringend mehr Forschung und Entwicklung erforderlich sind, um die Azneimittelversorgung für VL zu verbessern. In diesem Zusammenhang ist eine wirtsgerichtete Therapie, die auf Signalwege des Wirts abzielt, die für das Überleben oder die Eliminierung eines Erregers nötig sind, ein vielversprechender Ansatz für die Behandlung von VL. Es ist bekannt, dass Neutrophile entweder eine vorteilhafte Rolle bei der Eliminierung des Parasiten spielen oder eine nachteilige Funktion einnehmen, indem sie dem Parasiten vorübergehend Schutz bieten, bevor dieser in seine finalen Wirtszellen, Makrophagen, gelangt. Bislang wurde keine zufriedenstellende Erklärung für diese ambivalente Rolle von Neutrophilen während der Leishmaniose gefunden.

Die Heterogenität von Neutrophilen ist ein Interessensschwerpunkt geworden, der darauf hinweist, dass Neutrophil-Teilgruppen unterschiedliche Funktionen unter homöostatischen und pathologischen Bedingungen erfüllen. Eine Verschiebung des Gleichgewichts zwischen proinflammatorischen und antiinflammatorischen Phänotypen, wie bei N1 und N2 Tumor-assoziierten Neutrophilen (TANs), kann den Verlauf von Krankheiten entscheidend mitbestimmen. Um die Hypothese zu testen, dass eine Infektion mit *L. donovani* Neutrophile einen antiinflammatorischen Phänotyp annehmen lässt, versuchte ich, N1 und N2 Neutrophile *in vitro* zu erzeugen. Primäre humane Neutrophile wurden mit einem N1 oder N2 Polarisationscocktail kultiviert, der entweder ein proinflammatorisches Milieu oder die Tumormikroumgebung imitierte. Einerseits wurde so untersucht, ob *in vitro* polarisierte Neutrophile die Eigenschaften von N1 und N2 TANs annehmen können, und andererseits, wie die erlangten Phänotypen mit der Permissivität für *L. donovani* korrelieren. Nach Inkubation mit dem N1 Polarisationscocktail waren die Neutrophile stark aktiviert und zeigten verstärkte Degranulation. Außerdem exprimierten N1-ähnliche Neutrophile hohe Mengen an Neprilysin, FasR und ICAM-1 auf ihrer Oberfläche und sekretierten viel TNF und IP-10. Darüber hinaus war die Expression von FcαRI auf N1-ähnlichen Neutrophilen erhöht, was auf eine höhere Kapazität für antikörperabhängige zelluläre Zytotoxizität hinweist. Die erhöhte extrazelluläre ROS-Produktion von N2-ähnlichen Neutrophilen im Vergleich zu N1-ähnlichen Neutrophilen spiegelt die erworbenen pro-tumorigenen Eigenschaften von N2-ähnlichen Neutrophilen wider, da extrazelluläre ROS die Genotoxizität von Tumorzellen induzieren und CD8 + T-Zellen unterdrücken können. Die antimikrobielle Kapazität von *in vitro* polarisierten Neutrophilen gegen Leishmanien zeigt deutlich, dass N2-ähnliche Neutrophile im Vergleich zu N1-ähnlichen Neutrophilen mehr lebensfähige Parasiten enthielten, wodurch ich die Hypothese beweisen konnte, dass N2 Neutrophilen eine verminderte Abtötungsfähigkeit für *L. donovani* aufweisen.

Der zweite Teil dieses Projektes befasste sich mit der metabolischen Charakterisierung von *L. donovani*-infizierten Neutrophilen unter Zuhilfenahme von extrazellulärer Flussanalyse und metabolischen Assays, um für das Überleben der Leishmanien essentielle metabolische Knotenpunkte zu identifizieren. In Zukunft könnten diese metabolischen Knotenpunkte als Angriffsziele für die Entwicklung von wirtsgerichtete Therapien dienen. Als wichtiger Abwehrmechanismus gegen intrazelluläre Erreger wurde der oxidative Metabolismus von Neutrophilen während einer *L. donovani* Infektion untersucht. Zusammenfassend war die ROS Produktion von *L. donovani*-infizierten Neutrophilen im Vergleich zu nicht infizierten Neutrophilen erhöht. Da Zytokine den Metabolismus beeinflussen können und umgekehrt, wurde die Sekretion von TNF, IL-8 und IP-10 von *L. donovani*-infizierten Neutrophilen gemessen. *L. donovani*-infizierten Neutrophilen zeigten hohe Werte für TNF und IL-8, während die Produktion von IP-10 aufgehoben wurde. Da diese Zytokine dafür bekannt sind, mit der Glykolyse assoziiert zu sein, habe ich als nächstes den glykolytischen Stoffwechsel untersucht. Die extrazelluläre Flussanalyse von *L.*

donovani-infizierten Neutrophilen ergab, dass Glykolyse der bevorzugte bioenergetische Stoffwechselweg ist. Dieses Ergebnis wurde zudem durch die Beobachtung gestützt, dass sich die glykolytischen Endprodukte, Laktat oder Pyruvat, im Überstand und im Zytosol von *L. donovani*-infizierten Neutrophilen anreicherten. Darüber hinaus war die Glukoseaufnahme von *L. donovani*-infizierten Neutrophilen im Vergleich zu nicht infizierten Neutrophilen erhöht. Die Inhibition der Glykolyse verringerte das Überleben von *L. donovani* Promastigoten in Neutrophilen. Aufgrund der direkten Zytotoxizität von Glykolyse-Inhibitoren auf *L. donovani* Promastigoten, ist eine wirtsgerichtete Therapie, die auf der Inhibition der Glykolyse basiert eher ungeeignet, könnte aber als anti-parasitäre Therapie gegen VL eingesetzt werden.

Die Transkriptomanalyse von *L. donovani*-infizierten Neutrophilen ergab mehrere metabolische Knotenpunkte, die als Kandidaten für wirtsgerichtete Therapien gegen VL in der Zukunft untersucht werden.

Zusammenfassend zeigte diese Arbeit, dass das Vorhandensein von N1-ähnlichen und N2-ähnlichen Neutrophilen die gegensätzlichen Rollen von Neutrophilen bei der Entwicklung von VL erklären könnte und dass Glykolyse der wichtigste bioenergetische Stoffwechselweg bei *L. donovani*-infizierten Neutrophilen ist.

References

Abadie, V., Badell, E., Douillard, P., Ensergueix, D., Leenen, P.J.M., Tanguy, M., Fiette, L., Saeland, S., Gicquel, B., and Winter, N. (2005). Neutrophils rapidly migrate via lymphatics after Mycobacterium bovis BCG intradermal vaccination and shuttle live bacilli to the draining lymph nodes. Blood *106*, 1843–1850.

Abi Abdallah, D.S., Egan, C.E., Butcher, B.A., and Denkers, E.Y. (2011). Mouse neutrophils are professional antigen-presenting cells programmed to instruct Th1 and Th17 T-cell differentiation. Int. Immunol. *23*, 317–326.

Adler-Moore, J., and Proffitt, R.T. (2002). AmBisome: liposomal formulation, structure, mechanism of action and pre-clinical experience. J. Antimicrob. Chemother. *49 Suppl 1*, 21–30.

Aga, E., Katschinski, D.M., van Zandbergen, G., Laufs, H., Hansen, B., Müller, K., Solbach, W., and Laskay, T. (2002). Inhibition of the Spontaneous Apoptosis of Neutrophil Granulocytes by the Intracellular Parasite *Leishmania major*. J Immunol *169*, 898–905.

Aguer, C., Gambarotta, D., Mailloux, R.J., Moffat, C., Dent, R., McPherson, R., and Harper, M.-E. (2011). Galactose Enhances Oxidative Metabolism and Reveals Mitochondrial Dysfunction in Human Primary Muscle Cells. PLoS ONE *6*, e28536.

Aguilar-Be, I., da Silva Zardo, R., Paraguai de Souza, E., Borja-Cabrera, G.P., Rosado-Vallado, M., Mut-Martin, M., García-Miss, M. del R., Palatnik de Sousa, C.B., and Dumonteil, E. (2005). Cross-protective efficacy of a prophylactic Leishmania donovani DNA vaccine against visceral and cutaneous murine leishmaniasis. Infect. Immun. *73*, 812–819.

Akbay, E.A., Koyama, S., Liu, Y., Dries, R., Bufe, L.E., Silkes, M., Alam, M.M., Magee, D.M., Jones, R., Jinushi, M., et al. (2017). Interleukin-17A Promotes Lung Tumor Progression through Neutrophil Attraction to Tumor Sites and Mediating Resistance to PD-1 Blockade. J Thorac Oncol *12*, 1268–1279.

Akhoundi, M., Kuhls, K., Cannet, A., Votýpka, J., Marty, P., Delaunay, P., and Sereno, D. (2016). A Historical Overview of the Classification, Evolution, and Dispersion of Leishmania Parasites and Sandflies. PLoS Negl Trop Dis *10*, e0004349.

Akkoyunlu, M., Malawista, S.E., Anguita, J., and Fikrig, E. (2001). Exploitation of interleukin-8-induced neutrophil chemotaxis by the agent of human granulocytic ehrlichiosis. Infect. Immun. *69*, 5577–5588.

Al-Banna, N., and Lehmann, C. (2013). Oxidized LDL and LOX-1 in Experimental Sepsis. Mediators of Inflammation *2013*, 1–6.

Albrengues, J., Shields, M.A., Ng, D., Park, C.G., Ambrico, A., Poindexter, M.E., Upadhyay, P., Uyeminami, D.L., Pommier, A., Küttner, V., et al. (2018). Neutrophil extracellular traps produced during inflammation awaken dormant cancer cells in mice. Science *361*.

Aleman, C. (1969). Finestructure of cultured Leishmania brasiliensis. Experimental Parasitology *24*, 259–264.

Aliaga, L., Cobo, F., Mediavilla, J.D., Bravo, J., Osuna, A., Amador, J.M., Martín-Sánchez, J., Cordero, E., and Navarro, J.M. (2003). Localized mucosal leishmaniasis due to Leishmania (Leishmania) infantum: clinical and microbiologic findings in 31 patients. Medicine (Baltimore) *82*, 147–158.

Allen, L.A., and Aderem, A. (1996). Molecular definition of distinct cytoskeletal structures involved in complement- and Fc receptor-mediated phagocytosis in macrophages. J. Exp. Med. *184*, 627–637.

Alvar, J., Vélez, I.D., Bern, C., Herrero, M., Desjeux, P., Cano, J., Jannin, J., Boer, M. den, and the WHO Leishmaniasis Control Team (2012). Leishmaniasis Worldwide and Global Estimates of Its Incidence. PLoS ONE *7*, e35671.

Alves-Filho, J.C., Spiller, F., and Cunha, F.Q. (2010). NEUTROPHIL PARALYSIS IN SEPSIS: Shock *34*, 15–21.

Amankulor, N.M., Kim, Y., Arora, S., Kargl, J., Szulzewsky, F., Hanke, M., Margineantu, D.H., Rao, A., Bolouri, H., Delrow, J., et al. (2017). Mutant IDH1 regulates the tumor-associated immune system in gliomas. Genes Dev. *31*, 774–786.

Ambrosio, A.R., and De Messias-Reason, I.J.T. (2005). Leishmania (Viannia) braziliensis: interaction of mannose-binding lectin with surface glycoconjugates and complement activation. An antibody-independent defence mechanism. Parasite Immunol. *27*, 333–340.

Amulic, B., Cazalet, C., Hayes, G.L., Metzler, K.D., and Zychlinsky, A. (2012). Neutrophil Function: From Mechanisms to Disease. Annu. Rev. Immunol. *30*, 459–489.

Anderson, C.F., Lira, R., Kamhawi, S., Belkaid, Y., Wynn, T.A., and Sacks, D. (2008). IL-10 and TGF-β Control the Establishment of Persistent and Transmissible Infections Produced by *Leishmania tropica* in C57BL/6 Mice. J Immunol *180*, 4090–4097.

Andzinski, L., Kasnitz, N., Stahnke, S., Wu, C.-F., Gereke, M., von Köckritz-Blickwede, M., Schilling, B., Brandau, S., Weiss, S., and Jablonska, J. (2016). Type IIFNs induce anti-tumor polarization of tumor associated neutrophils in mice and human: TANs in tumorigenesis. Int. J. Cancer *138*, 1982–1993.

Aoyama, M., Kotani, J., and Usami, M. (2010). Butyrate and propionate induced activated or non-activated neutrophil apoptosis via HDAC inhibitor activity but without activating GPR-41/GPR-43 pathways. Nutrition *26*, 653–661.

Ardi, V.C., Kupriyanova, T.A., Deryugina, E.I., and Quigley, J.P. (2007). Human neutrophils uniquely release TIMP-free MMP-9 to provide a potent catalytic stimulator of angiogenesis. Proc. Natl. Acad. Sci. U.S.A. *104*, 20262–20267.

Ardi, V.C., Van den Steen, P.E., Opdenakker, G., Schweighofer, B., Deryugina, E.I., and Quigley, J.P. (2009). Neutrophil MMP-9 proenzyme, unencumbered by TIMP-1, undergoes efficient activation in vivo and catalytically induces angiogenesis via a basic fibroblast growth factor (FGF-2)/FGFR-2 pathway. J. Biol. Chem. *284*, 25854–25866.

Arena, E.T., Tinevez, J.-Y., Nigro, G., Sansonetti, P.J., and Marteyn, B.S. (2017). The infectious hypoxia: occurrence and causes during Shigella infection. Microbes Infect. *19*, 157–165.

Arpinati, L., Shaul, M.E., Kaisar-Iluz, N., Mali, S., Mahroum, S., and Fridlender, Z.G. (2020). NETosis in cancer: a critical analysis of the impact of cancer on neutrophil extracellular trap (NET) release in lung cancer patients vs. mice. Cancer Immunol Immunother *69*, 199–213.

Arruda-Silva, F., Bianchetto-Aguilera, F., Gasperini, S., Polletti, S., Cosentino, E., Tamassia, N., and Cassatella, M.A. (2017). Human Neutrophils Produce CCL23 in Response to Various TLR-Agonists and TNFα. Front. Cell. Infect. Microbiol. *7*, 176.

Atri, C., Guerfali, F., and Laouini, D. (2018). Role of Human Macrophage Polarization in Inflammation during Infectious Diseases. IJMS *19*, 1801.

Azevedo, E.P., Rochael, N.C., Guimarães-Costa, A.B., de Souza-Vieira, T.S., Ganilho, J., Saraiva, E.M., Palhano, F.L., and Foguel, D. (2015). A Metabolic Shift toward Pentose Phosphate Pathway Is Necessary for Amyloid Fibril- and Phorbol 12-Myristate 13-Acetate-induced Neutrophil Extracellular Trap (NET) Formation. J. Biol. Chem. *290*, 22174–22183.

Bai, M., Grieshaber-Bouyer, R., Wang, J., Schmider, A.B., Wilson, Z.S., Zeng, L., Halyabar, O., Godin, M.D., Nguyen, H.N., Levescot, A., et al. (2017). CD177 modulates human neutrophil migration through activation-mediated integrin and chemoreceptor regulation. Blood *130*, 2092–2100.

Baillet, A., Hograindleur, M.-A., El Benna, J., Grichine, A., Berthier, S., Morel, F., and Paclet, M.-H. (2017). Unexpected function of the phagocyte NADPH oxidase in supporting hyperglycolysis in stimulated neutrophils: key role of 6-phosphofructo-2-kinase. FASEB J. *31*, 663–673.

Banerjee, R., Anguita, J., Roos, D., and Fikrig, E. (2000). Cutting edge: infection by the agent of human granulocytic ehrlichiosis prevents the respiratory burst by down-regulating gp91phox. J. Immunol. *164*, 3946–3949.

Bao, Y., Ledderose, C., Graf, A.F., Brix, B., Birsak, T., Lee, A., Zhang, J., and Junger, W.G. (2015). mTOR and differential activation of mitochondria orchestrate neutrophil chemotaxis. J. Cell Biol. *210*, 1153–1164.

Barcellos-de-Souza, P., Canetti, C., Barja-Fidalgo, C., and Arruda, M.A. (2012). Leukotriene B4 inhibits neutrophil apoptosis via NADPH oxidase activity: Redox control of NF-κB pathway and mitochondrial stability. Biochimica et Biophysica Acta (BBA) - Molecular Cell Research *1823*, 1990–1997.

Barksdale, A.R., Bernard, A.C., Maley, M.E., Gellin, G.L., Kearney, P.A., Boulanger, B.R., Tsuei, B.J., and Ochoa, J.B. (2004). Regulation of arginase expression by T-helper II cytokines and isoproterenol. Surgery *135*, 527–535.

Basu, M., and Das, P.K. (2019). Role of Reactive Oxygen Species in Infection by the Intracellular Leishmania Parasites. In Oxidative Stress in Microbial Diseases, S. Chakraborti, T. Chakraborti, D. Chattopadhyay, and C. Shaha, eds. (Singapore: Springer Singapore), pp. 297–311.

Basu, R., Bhaumik, S., Basu, J.M., Naskar, K., De, T., and Roy, S. (2005). Kinetoplastid membrane protein-11 DNA vaccination induces complete protection against both pentavalent antimonial-sensitive and -resistant strains of Leishmania donovani that correlates with inducible nitric oxide synthase activity and IL-4 generation: evidence for mixed Th1- and Th2-like responses in visceral leishmaniasis. J. Immunol. *174*, 7160–7171.

Basu Ball, W., Kar, S., Mukherjee, M., Chande, A.G., Mukhopadhyaya, R., and Das, P.K. (2011). Uncoupling Protein 2 Negatively Regulates Mitochondrial Reactive Oxygen Species Generation and Induces Phosphatase-Mediated Anti-Inflammatory Response in Experimental Visceral Leishmaniasis. J.I. *187*, 1322–1332.

Bauer, S., Abdgawad, M., Gunnarsson, L., Segelmark, M., Tapper, H., and Hellmark, T. (2007). Proteinase 3 and CD177 are expressed on the plasma membrane of the same subset of neutrophils. J. Leukoc. Biol. *81*, 458–464.

Beauvillain, C., Cunin, P., Doni, A., Scotet, M., Jaillon, S., Loiry, M.-L., Magistrelli, G., Masternak, K., Chevailler, A., Delneste, Y., et al. (2011). CCR7 is involved in the migration of neutrophils to lymph nodes. Blood *117*, 1196–1204.

Beil, W.J., Meinardus-Hager, G., Neugebauer, D.C., and Sorg, C. (1992). Differences in the onset of the inflammatory response to cutaneous leishmaniasis in resistant and susceptible mice. J. Leukoc. Biol. *52*, 135–142.

Belkaid, Y., Piccirillo, C.A., Mendez, S., Shevach, E.M., and Sacks, D.L. (2002). CD4+CD25+ regulatory T cells control Leishmania major persistence and immunity. Nature *420*, 502–507.

Beyrau, M., Bodkin, J.V., and Nourshargh, S. (2012). Neutrophil heterogeneity in health and disease: a revitalized avenue in inflammation and immunity. Open Biol. *2*, 120134.

Bhattacharyya, S., Ghosh, S., Dasgupta, B., Mazumder, D., Roy, S., and Majumdar, S. (2002). Chemokine-induced leishmanicidal activity in murine macrophages via the generation of nitric oxide. J. Infect. Dis. *185*, 1704–1708.

Bhowmick, S., and Ali, N. (2009). Identification of novel Leishmania donovani antigens that help define correlates of vaccine-mediated protection in visceral leishmaniasis. PLoS ONE *4*, e5820.

Bianchi, M., Hakkim, A., Brinkmann, V., Siler, U., Seger, R.A., Zychlinsky, A., and Reichenbach, J. (2009). Restoration of NET formation by gene therapy in CGD controls aspergillosis. Blood *114*, 2619–2622.

Bodduluru, L.N., Kasala, E.R., Madhana, R.M.R., and Sriram, C.S. (2015). Natural killer cells: the journey from puzzles in biology to treatment of cancer. Cancer Lett. *357*, 454–467.

Bodmer, J.L., Holler, N., Reynard, S., Vinciguerra, P., Schneider, P., Juo, P., Blenis, J., and Tschopp, J. (2000). TRAIL receptor-2 signals apoptosis through FADD and caspase-8. Nat. Cell Biol. *2*, 241–243.

Bogdan, C. (2012). Natural killer cells in experimental and human leishmaniasis. Front Cell Infect Microbiol *2*, 69.

Bogdan, C., Donhauser, N., Döring, R., Röllinghoff, M., Diefenbach, A., and Rittig, M.G. (2000). Fibroblasts as Host Cells in Latent Leishmaniosis. Journal of Experimental Medicine *191*, 2121–2130.

Bokoch, G.M., and Zhao, T. (2006). Regulation of the phagocyte NADPH oxidase by Rac GTPase. Antioxid. Redox Signal. *8*, 1533–1548.

Borregaard, N., and Herlin, T. (1982). Energy metabolism of human neutrophils during phagocytosis. J. Clin. Invest. *70*, 550–557.

Borregaard, N., Sørensen, O.E., and Theilgaard-Mönch, K. (2007). Neutrophil granules: a library of innate immunity proteins. Trends Immunol. *28*, 340–345.

Borst, S.E. (2004). The Role of TNF-α in Insulin Resistance. ENDO *23*, 177–182.

Bourreau, E., Ronet, C., Couppié, P., Sainte-Marie, D., Tacchini-Cottier, F., and Launois, P. (2007). IL-10 producing CD8+ T cells in human infection with Leishmania guyanensis. Microbes Infect. *9*, 1034–1041.

Böyum, A. (1968). Isolation of mononuclear cells and granulocytes from human blood. Isolation of monuclear cells by one centrifugation, and of granulocytes by combining centrifugation and sedimentation at 1 g. Scand. J. Clin. Lab. Invest. Suppl. *97*, 77–89.

Bozonet, S.M., Carr, A.C., Pullar, J.M., and Vissers, M.C.M. (2015). Enhanced human neutrophil vitamin C status, chemotaxis and oxidant generation following dietary supplementation with vitamin C-rich SunGold kiwifruit. Nutrients *7*, 2574–2588.

Brandau, S., Dumitru, C.A., and Lang, S. (2013). Protumor and antitumor functions of neutrophil granulocytes. Semin Immunopathol *35*, 163–176.

Brandonisio, O., Panaro, M.A., Fumarola, I., Sisto, M., Leogrande, D., Acquafredda, A., Spinelli, R., and Mitolo, V. (2002). Macrophage chemotactic protein-1 and macrophage inflammatory protein-1 alpha induce nitric oxide release and enhance parasite killing in Leishmania infantum-infected human macrophages. Clin. Exp. Med. *2*, 125–129.

Brandsma, A.M., Bondza, S., Evers, M., Koutstaal, R., Nederend, M., Jansen, J.H.M., Rösner, T., Valerius, T., Leusen, J.H.W., and Ten Broeke, T. (2019). Potent Fc Receptor Signaling by IgA Leads to Superior Killing of Cancer Cells by Neutrophils Compared to IgG. Front Immunol *10*, 704.

Bratton, D.L., and Henson, P.M. (2011). Neutrophil clearance: when the party is over, clean-up begins. Trends in Immunology *32*, 350–357.

Brincks, E.L., Risk, M.C., and Griffith, T.S. (2013). PMN and anti-tumor immunity--the case of bladder cancer immunotherapy. Semin. Cancer Biol. *23*, 183–189.

Brinkmann, V. (2004). Neutrophil Extracellular Traps Kill Bacteria. Science *303*, 1532–1535.

Brinkmann, V. (2018). Neutrophil Extracellular Traps in the Second Decade. J Innate Immun *10*, 414–421.

Brunelli, L., Crow, J.P., and Beckman, J.S. (1995). The Comparative Toxicity of Nitric Oxide and Peroxynitrite to Escherichia coli. Archives of Biochemistry and Biophysics *316*, 327–334.

Brunton, J., Steele, S., Ziehr, B., Moorman, N., and Kawula, T. (2013). Feeding uninvited guests: mTOR and AMPK set the table for intracellular pathogens. PLoS Pathog. *9*, e1003552.

Bubeník, J., Perlmann, P., Helmstein, K., and Moberger, G. (1970). Cellular and humoral immune responses to human urinary bladder carcinomas. Int. J. Cancer *5*, 310–319.

Cadet, J., and Wagner, J.R. (2013). DNA base damage by reactive oxygen species, oxidizing agents, and UV radiation. Cold Spring Harb Perspect Biol *5*.

Cairns, R., Papandreou, I., and Denko, N. (2006). Overcoming physiologic barriers to cancer treatment by molecularly targeting the tumor microenvironment. Mol. Cancer Res. *4*, 61–70.

Carlsen, E.D., Liang, Y., Shelite, T.R., Walker, D.H., Melby, P.C., and Soong, L. (2015). Permissive and protective roles for neutrophils in leishmaniasis: Complex roles for neutrophils in leishmaniasis. Clin Exp Immunol *182*, 109–118.

Cassatella, M.A. (1999). Neutrophil-Derived Proteins: Selling Cytokines by the Pound. In Advances in Immunology, (Elsevier), pp. 369–509.

Cassatella, M.A., Guasparri, I., Ceska, M., Bazzoni, F., and Rossi, F. (1993a). Interferon-gamma inhibits interleukin-8 production by human polymorphonuclear leucocytes. Immunology *78*, 177–184.

Cassatella, M.A., Aste, M., Calzetti, F., Constantin, G., Guasparri, I., Ceska, M., and Rossi, F. (1993b). Studies on the Regulatory Mechanisms of Interleukin-8 Gene Expression in Resting and IFN-γ-Treated Neutrophils: Evidence on the Capability of Staurosporine of Inducing the Production of Interleukin-8 by Human Neutrophils. Biochemical and Biophysical Research Communications *190*, 660–667.

Ceccarelli, M., Galluzzi, L., Migliazzo, A., and Magnani, M. (2014). Detection and Characterization of Leishmania (Leishmania) and Leishmania (Viannia) by SYBR Green-Based Real-Time PCR and High Resolution Melt Analysis Targeting Kinetoplast Minicircle DNA. PLoS ONE *9*, e88845.

Chai, E., Zhang, L., and Li, C. (2019). LOX-1+ PMN-MDSC enhances immune suppression which promotes glioblastoma multiforme progression. CMAR *Volume 11*, 7307–7315.

Chakraborty, D., Banerjee, S., Sen, A., Banerjee, K.K., Das, P., and Roy, S. (2005). Leishmania donovani affects antigen presentation of macrophage by disrupting lipid rafts. J. Immunol. *175*, 3214–3224.

Chang, K.-P. (1981). Leishmanicidal Mechanisms of Human Polymorphonuclear Phagocytes *. The American Journal of Tropical Medicine and Hygiene *30*, 322–333.

Chao, T., Furth, E.E., and Vonderheide, R.H. (2016). CXCR2-Dependent Accumulation of Tumor-Associated Neutrophils Regulates T-cell Immunity in Pancreatic Ductal Adenocarcinoma. Cancer Immunology Research *4*, 968–982.

Chen, Y., Corriden, R., Inoue, Y., Yip, L., Hashiguchi, N., Zinkernagel, A., Nizet, V., Insel, P.A., and Junger, W.G. (2006). ATP release guides neutrophil chemotaxis via P2Y2 and A3 receptors. Science *314*, 1792–1795.

Cheng, C.-Y., Hsieh, H.-L., Hsiao, L.-D., and Yang, C.-M. (2012). PI3-K/Akt/JNK/NF-κB is essential for MMP-9 expression and outgrowth in human limbal epithelial cells on intact amniotic membrane. Stem Cell Research *9*, 9–23.

Choi, K.-S., Garyu, J., Park, J., and Dumler, J.S. (2003). Diminished adhesion of Anaplasma phagocytophilum-infected neutrophils to endothelial cells is associated with reduced expression of leukocyte surface selectin. Infect. Immun. *71*, 4586–4594.

Choi, K.-S., Park, J.T., and Dumler, J.S. (2005). Anaplasma phagocytophilum Delay of Neutrophil Apoptosis through the p38 Mitogen-Activated Protein Kinase Signal Pathway. Infection and Immunity *73*, 8209–8218.

Christoffersson, G., and Phillipson, M. (2018). The neutrophil: one cell on many missions or many cells with different agendas? Cell Tissue Res *371*, 415–423.

Christoffersson, G., Vågesjö, E., Vandooren, J., Lidén, M., Massena, S., Reinert, R.B., Brissova, M., Powers, A.C., Opdenakker, G., and Phillipson, M. (2012). VEGF-A recruits a proangiogenic MMP-9-delivering neutrophil subset that induces angiogenesis in transplanted hypoxic tissue. Blood *120*, 4653–4662.

Clemmensen, S.N., Bohr, C.T., Rørvig, S., Glenthøj, A., Mora-Jensen, H., Cramer, E.P., Jacobsen, L.C., Larsen, M.T., Cowland, J.B., Tanassi, J.T., et al. (2012). Olfactomedin 4 defines a subset of human neutrophils. J. Leukoc. Biol. *91*, 495–500.

Coffelt, S.B., Kersten, K., Doornebal, C.W., Weiden, J., Vrijland, K., Hau, C.-S., Verstegen, N.J.M., Ciampricotti, M., Hawinkels, L.J.A.C., Jonkers, J., et al. (2015). IL-17-producing γδ T cells and neutrophils conspire to promote breast cancer metastasis. Nature *522*, 345–348.

Coffelt, S.B., Wellenstein, M.D., and de Visser, K.E. (2016). Neutrophils in cancer: neutral no more. Nat Rev Cancer *16*, 431–446.

Coler, R.N., and Reed, S.G. (2005). Second-generation vaccines against leishmaniasis. Trends Parasitol. *21*, 244–249.

Collin, N., Gomes, R., Teixeira, C., Cheng, L., Laughinghouse, A., Ward, J.M., Elnaiem, D.-E., Fischer, L., Valenzuela, J.G., and Kamhawi, S. (2009). Sand fly salivary proteins induce strong cellular immunity in a natural reservoir of visceral leishmaniasis with adverse consequences for Leishmania. PLoS Pathog. *5*, e1000441.

Condamine, T., Dominguez, G.A., Youn, J.-I., Kossenkov, A.V., Mony, S., Alicea-Torres, K., Tcyganov, E., Hashimoto, A., Nefedova, Y., Lin, C., et al. (2016). Lectin-type oxidized LDL receptor-1 distinguishes population of human polymorphonuclear myeloid-derived suppressor cells in cancer patients. Sci. Immunol. *1*, aaf8943–aaf8943.

Cools-Lartigue, J., Spicer, J., McDonald, B., Gowing, S., Chow, S., Giannias, B., Bourdeau, F., Kubes, P., and Ferri, L. (2013). Neutrophil extracellular traps sequester circulating tumor cells and promote metastasis. J. Clin. Invest.

Couto, D.V., Hans Filho, G., Medeiros, M.Z., Vicari, C.F.S., Barbosa, A.B., and Takita, L.C. (2014). American tegumentary leishmaniasis - a case of therapeutic challenge. An. Bras. Dermatol. *89*, 974–976.

Croft, S.L., and Brazil, R.P. (1982). Effect of pentamidine isethionate on the ultrastructure and morphology of Leishmania mexicana amazonensis in vitro. Ann Trop Med Parasitol *76*, 37–43.

Croft, S.L., and Coombs, G.H. (2003). Leishmaniasis– current chemotherapy and recent advances in the search for novel drugs. Trends in Parasitology *19*, 502–508.

Cross, A.R., and Segal, A.W. (2004). The NADPH oxidase of professional phagocytes—prototype of the NOX electron transport chain systems. Biochimica et Biophysica Acta (BBA) - Bioenergetics *1657*, 1–22.

Cummings, H.E., Barbi, J., Reville, P., Oghumu, S., Zorko, N., Sarkar, A., Keiser, T.L., Lu, B., Rückle, T., Varikuti, S., et al. (2012). Critical role for phosphoinositide 3-kinase gamma in parasite invasion and disease progression of cutaneous leishmaniasis. Proc. Natl. Acad. Sci. U.S.A. *109*, 1251–1256.

Curi, T.C., de Melo, M.P., de Azevedo, R.B., and Curi, R. (1997). Glutamine utilization by rat neutrophils. Biochem. Soc. Trans. *25*, 249S.

Dallegri, F., Ottonello, L., Ballestrero, A., Dapino, P., Ferrando, F., Patrone, F., and Sacchetti, C. (1991). Tumor cell lysis by activated human neutrophils: analysis of neutrophil-delivered oxidative attack and role of leukocyte function-associated antigen 1. Inflammation *15*, 15–30.

Dancey, J.T., Deubelbeiss, K.A., Harker, L.A., and Finch, C.A. (1976). Neutrophil kinetics in man. J. Clin. Invest. *58*, 705–715.

David, J.M., Dominguez, C., Hamilton, D.H., and Palena, C. (2016). The IL-8/IL-8R Axis: A Double Agent in Tumor Immune Resistance. Vaccines (Basel) *4*.

De Larco, J.E., Wuertz, B.R.K., and Furcht, L.T. (2004). The potential role of neutrophils in promoting the metastatic phenotype of tumors releasing interleukin-8. Clin. Cancer Res. *10*, 4895–4900.

De Martinis, M., Modesti, M., and Ginaldi, L. (2004). Phenotypic and functional changes of circulating monocytes and polymorphonuclear leucocytes from elderly persons. Immunol. Cell Biol. *82*, 415–420.

De Muylder, G., Vanhollebeke, B., Caljon, G., Wolfe, A.R., McKerrow, J., and Dujardin, J.-C. (2016). Naloxonazine, an Amastigote-Specific Compound, Affects Leishmania Parasites through Modulation of Host-Encoded Functions. PLoS Negl Trop Dis *10*, e0005234.

Delgado-Rizo, V., Martínez-Guzmán, M.A., Iñiguez-Gutierrez, L., García-Orozco, A., Alvarado-Navarro, A., and Fafutis-Morris, M. (2017). Neutrophil Extracellular Traps and Its Implications in Inflammation: An Overview. Front. Immunol. *8*.

Denny, M.F., Yalavarthi, S., Zhao, W., Thacker, S.G., Anderson, M., Sandy, A.R., McCune, W.J., and Kaplan, M.J. (2010). A Distinct Subset of Proinflammatory Neutrophils Isolated from Patients with Systemic Lupus Erythematosus Induces Vascular Damage and Synthesizes Type I IFNs. J.I. *184*, 3284–3297.

Deryugina, E.I., Zajac, E., Juncker-Jensen, A., Kupriyanova, T.A., Welter, L., and Quigley, J.P. (2014). Tissue-Infiltrating Neutrophils Constitute the Major In Vivo Source of Angiogenesis-Inducing MMP-9 in the Tumor Microenvironment. Neoplasia *16*, 771–788.

Devaraj, S., and Jialal, I. (2009). Increased secretion of IP-10 from monocytes under hyperglycemia is via the TLR2 and TLR4 pathway. Cytokine *47*, 6–10.

Dubovsky, J.A., Beckwith, K.A., Natarajan, G., Woyach, J.A., Jaglowski, S., Zhong, Y., Hessler, J.D., Liu, T.-M., Chang, B.Y., Larkin, K.M., et al. (2013). Ibrutinib is an irreversible molecular inhibitor of ITK driving a Th1-selective pressure in T lymphocytes. Blood *122*, 2539–2549.

Dumitru, C.A., Lang, S., and Brandau, S. (2013). Modulation of neutrophil granulocytes in the tumor microenvironment: Mechanisms and consequences for tumor progression. Seminars in Cancer Biology *23*, 141–148.

Eash, K.J., Greenbaum, A.M., Gopalan, P.K., and Link, D.C. (2010). CXCR2 and CXCR4 antagonistically regulate neutrophil trafficking from murine bone marrow. J. Clin. Invest. *120*, 2423–2431.

Ebrahem, Q., Chaurasia, S.S., Vasanji, A., Qi, J.H., Klenotic, P.A., Cutler, A., Asosingh, K., Erzurum, S., and Anand-Apte, B. (2010). Cross-talk between vascular endothelial growth factor and matrix metalloproteinases in the induction of neovascularization in vivo. Am. J. Pathol. *176*, 496–503.

Ehrlich, P. (1880). Methodologische Beiträge zur Physiologie und Pathologie der verschiedenen Formen der Leukocyten. (Z. Klin. Med.).

Ehrlich, A., Castilho, T.M., Goldsmith-Pestana, K., Chae, W.-J., Bothwell, A.L.M., Sparwasser, T., and McMahon-Pratt, D. (2014). The immunotherapeutic role of regulatory T cells in Leishmania (Viannia) panamensis infection. J. Immunol. *193*, 2961–2970.

Eisenreich, W., Heesemann, J., Rudel, T., and Goebel, W. (2013). Metabolic host responses to infection by intracellular bacterial pathogens. Front. Cell. Infect. Microbiol. *3*.

Ekman, A.-K., and Cardell, L.O. (2010). The expression and function of Nod-like receptors in neutrophils. Immunology *130*, 55–63.

El Rayes, T., Catena, R., Lee, S., Stawowczyk, M., Joshi, N., Fischbach, C., Powell, C.A., Dannenberg, A.J., Altorki, N.K., Gao, D., et al. (2015). Lung inflammation promotes metastasis through neutrophil protease-mediated degradation of Tsp-1. Proc. Natl. Acad. Sci. U.S.A. *112*, 16000–16005.

Enderlin, M., Kleinmann, E.V., Struyf, S., Buracchi, C., Vecchi, A., Kinscherf, R., Kiessling, F., Paschek, S., Sozzani, S., Rommelaere, J., et al. (2009). TNF-alpha and the IFN-gamma-inducible protein 10 (IP-10/CXCL-10) delivered by parvoviral vectors act in synergy to induce antitumor effects in mouse glioblastoma. Cancer Gene Ther. *16*, 149–160.

Eruslanov, E.B., Singhal, S., and Albelda, S.M. (2017). Mouse versus Human Neutrophils in Cancer: A Major Knowledge Gap. Trends Cancer *3*, 149–160.

Esch, K.J., and Petersen, C.A. (2013). Transmission and Epidemiology of Zoonotic Protozoal Diseases of Companion Animals. Clin. Microbiol. Rev. *26*, 58–85.

Estúa-Acosta, G.A., Zamora-Ortiz, R., Buentello-Volante, B., García-Mejía, M., and Garfias, Y. (2019). Neutrophil Extracellular Traps: Current Perspectives in the Eye. Cells *8*, 979.

Falcão, S.A.C., Weinkopff, T., Hurrell, B.P., Celes, F.S., Curvelo, R.P., Prates, D.B., Barral, A., Borges, V.M., Tacchini-Cottier, F., and de Oliveira, C.I. (2015). Exposure to Leishmania braziliensis Triggers Neutrophil Activation and Apoptosis. PLoS Negl Trop Dis *9*, e0003601.

Faurschou, M., and Borregaard, N. (2003). Neutrophil granules and secretory vesicles in inflammation. Microbes Infect. *5*, 1317–1327.

Ferraz, R., Cunha, C.F., Pimentel, M.I.F., Lyra, M.R., Pereira-Da-Silva, T., Schubach, A.O., Da-Cruz, A.M., and Bertho, A.L. (2017). CD3+CD4negCD8neg (double negative) T lymphocytes and NKT cells as the main cytotoxic-related-CD107a+ cells in lesions of cutaneous leishmaniasis caused by Leishmania (Viannia) braziliensis. Parasit Vectors *10*, 219.

Finisguerra, V., Di Conza, G., Di Matteo, M., Serneels, J., Costa, S., Thompson, A.A.R., Wauters, E., Walmsley, S., Prenen, H., Granot, Z., et al. (2015). MET is required for the recruitment of anti-tumoural neutrophils. Nature *522*, 349–353.

Fischer, M.A., Davies, M.L., Reider, I.E., Heipertz, E.L., Epler, M.R., Sei, J.J., Ingersoll, M.A., Rooijen, N.V., Randolph, G.J., and Norbury, C.C. (2011). CD11b$^+$, Ly6G$^+$ cells produce type I interferon and exhibit tissue protective properties following peripheral virus infection. PLoS Pathog. *7*, e1002374.

Flannery, A.R., Renberg, R.L., and Andrews, N.W. (2013). Pathways of iron acquisition and utilization in Leishmania. Curr. Opin. Microbiol. *16*, 716–721.

Fossati, G., Moulding, D.A., Spiller, D.G., Moots, R.J., White, M.R.H., and Edwards, S.W. (2003). The mitochondrial network of human neutrophils: role in chemotaxis, phagocytosis, respiratory burst activation, and commitment to apoptosis. J. Immunol. *170*, 1964–1972.

Freyberg, Z., and Harvill, E.T. (2017). Pathogen manipulation of host metabolism: A common strategy for immune evasion. PLoS Pathog *13*, e1006669.

Fridlender, Z.G., and Albelda, S.M. (2012). Tumor-associated neutrophils: friend or foe? Carcinogenesis *33*, 949–955.

Fridlender, Z.G., Sun, J., Kim, S., Kapoor, V., Cheng, G., Ling, L., Worthen, G.S., and Albelda, S.M. (2009). Polarization of tumor-associated neutrophil phenotype by TGF-beta: "N1" versus "N2" TAN. Cancer Cell *16*, 183–194.

Fuchs, T.A., Abed, U., Goosmann, C., Hurwitz, R., Schulze, I., Wahn, V., Weinrauch, Y., Brinkmann, V., and Zychlinsky, A. (2007). Novel cell death program leads to neutrophil extracellular traps. J. Cell Biol. *176*, 231–241.

Fulda, S. (2014). Tumor-necrosis-factor-related apoptosis-inducing ligand (TRAIL). Adv. Exp. Med. Biol. *818*, 167–180.

Gabriel, Á., Valério-Bolas, A., Palma-Marques, J., Mourata-Gonçalves, P., Ruas, P., Dias-Guerreiro, T., and Santos-Gomes, G. (2019). Cutaneous Leishmaniasis: The Complexity of Host's Effective Immune Response against a Polymorphic Parasitic Disease. Journal of Immunology Research *2019*, 1–16.

Gabriel, C., McMaster, W.R., Girard, D., and Descoteaux, A. (2010). *Leishmania donowani* Promastigotes Evade the Antimicrobial Activity of Neutrophil Extracellular Traps. J.I. *185*, 4319–4327.

Gabrilovich, D.I., Ostrand-Rosenberg, S., and Bronte, V. (2012). Coordinated regulation of myeloid cells by tumours. Nat. Rev. Immunol. *12*, 253–268.

Gaffen, S.L., Jain, R., Garg, A.V., and Cua, D.J. (2014). The IL-23–IL-17 immune axis: from mechanisms to therapeutic testing. Nat Rev Immunol *14*, 585–600.

Gaida, M.M., Steffen, T.G., Günther, F., Tschaharganeh, D.F., Felix, K., Bergmann, F., Schirmacher, P., and Hänsch, G.M. (2012). Polymorphonuclear neutrophils promote dyshesion of tumor cells and elastase-mediated degradation of E-cadherin in pancreatic tumors. Eur. J. Immunol. *42*, 3369–3380.

Gallin, J.I. (1984). Human neutrophil heterogeneity exists, but is it meaningful? Blood *63*, 977–983.

Garcia-Romo, G.S., Caielli, S., Vega, B., Connolly, J., Allantaz, F., Xu, Z., Punaro, M., Baisch, J., Guiducci, C., Coffman, R.L., et al. (2011). Netting Neutrophils Are Major Inducers of Type I IFN Production in Pediatric Systemic Lupus Erythematosus. Science Translational Medicine *3*, 73ra20-73ra20.

Gatenby, R.A., and Gillies, R.J. (2004). Why do cancers have high aerobic glycolysis? Nat. Rev. Cancer *4*, 891–899.

Geraci, N.S., Tan, J.C., and McDowell, M.A. (2015). Characterization of microRNA expression profiles in Leishmania-infected human phagocytes. Parasite Immunol. *37*, 43–51.

Gershkovitz, M., Fainsod-Levi, T., Zelter, T., Sionov, R.V., and Granot, Z. (2019). TRPM2 modulates neutrophil attraction to murine tumor cells by regulating CXCL2 expression. Cancer Immunol. Immunother. *68*, 33–43.

Ghorbani, M., and Farhoudi, R. (2017a). Leishmaniasis in humans: drug or vaccine therapy? DDDT *Volume 12*, 25–40.

Ghorbani, M., and Farhoudi, R. (2017b). Leishmaniasis in humans: drug or vaccine therapy? DDDT *Volume 12*, 25–40.

Ghosh, J., Das, S., Guha, R., Ghosh, D., Naskar, K., Das, A., and Roy, S. (2012). Hyperlipidemia offers protection against *Leishmania donovani* infection: role of membrane cholesterol. J. Lipid Res. *53*, 2560–2572.

Giese, N.A., Raykov, Z., DeMartino, L., Vecchi, A., Sozzani, S., Dinsart, C., Cornelis, J.J., and Rommelaere, J. (2002). Suppression of metastatic hemangiosarcoma by a parvovirus MVMp vector transducing the IP-10 chemokine into immunocompetent mice. Cancer Gene Ther. *9*, 432–442.

Gonçalves-de-Albuquerque, S. da C., Pessoa-E-Silva, R., Trajano-Silva, L.A.M., de Goes, T.C., de Morais, R.C.S., da C Oliveira, C.N., de Lorena, V.M.B., and de Paiva-Cavalcanti, M. (2017). The Equivocal Role of Th17 Cells and Neutrophils on Immunopathogenesis of Leishmaniasis. Front Immunol *8*, 1437.

Gong, Y., and Koh, D.-R. (2010). Neutrophils promote inflammatory angiogenesis via release of preformed VEGF in an in vivo corneal model. Cell Tissue Res *339*, 437–448.

Görgens, A., Radtke, S., Möllmann, M., Cross, M., Dürig, J., Horn, P.A., and Giebel, B. (2013). Revision of the Human Hematopoietic Tree: Granulocyte Subtypes Derive from Distinct Hematopoietic Lineages. Cell Reports *3*, 1539–1552.

Gradoni, L., Foglia Manzillo, V., Pagano, A., Piantedosi, D., De Luna, R., Gramiccia, M., Scalone, A., Di Muccio, T., and Oliva, G. (2005). Failure of a multi-subunit recombinant leishmanial vaccine (MML) to protect dogs from Leishmania infantum infection and to prevent disease progression in infected animals. Vaccine *23*, 5245–5251.

Granot, Z., Henke, E., Comen, E.A., King, T.A., Norton, L., and Benezra, R. (2011). Tumor Entrained Neutrophils Inhibit Seeding in the Premetastatic Lung. Cancer Cell *20*, 300–314.

Grecian, R., Whyte, M.K.B., and Walmsley, S.R. (2018). The role of neutrophils in cancer. British Medical Bulletin *128*, 5–14.

Green, S.J., Crawford, R.M., Hockmeyer, J.T., Meltzer, M.S., and Nacy, C.A. (1990). Leishmania major amastigotes initiate the L-arginine-dependent killing mechanism in IFN-gamma-stimulated macrophages by induction of tumor necrosis factor-alpha. J. Immunol. *145*, 4290–4297.

Grunewald, M., Avraham, I., Dor, Y., Bachar-Lustig, E., Itin, A., Yung, S., Chimenti, S., Landsman, L., Abramovitch, R., and Keshet, E. (2006). VEGF-Induced Adult Neovascularization: Recruitment, Retention, and Role of Accessory Cells. Cell *124*, 175–189.

Guimarães-Costa, A.B., Nascimento, M.T.C., Froment, G.S., Soares, R.P.P., Morgado, F.N., Conceição-Silva, F., and Saraiva, E.M. (2009). Leishmania amazonensis promastigotes induce and are killed by neutrophil extracellular traps. Proc. Natl. Acad. Sci. U.S.A. *106*, 6748–6753.

Gullberg, U., Andersson, E., Garwicz, D., Lindmark, A., and Olsson, I. (2009). Biosynthesis, processing and sorting of neutrophil proteins: insight into neutrophil granule development. European Journal of Haematology *58*, 137–153.

Gutiérrez-Fernández, A., Fueyo, A., Folgueras, A.R., Garabaya, C., Pennington, C.J., Pilgrim, S., Edwards, D.R., Holliday, D.L., Jones, J.L., Span, P.N., et al. (2008). Matrix metalloproteinase-8 functions as a metastasis suppressor through modulation of tumor cell adhesion and invasion. Cancer Res. *68*, 2755–2763.

Hajishengallis, G., and Chavakis, T. (2013). Endogenous modulators of inflammatory cell recruitment. Trends in Immunology *34*, 1–6.

Hata, K., Andoh, A., Shimada, M., Fujino, S., Bamba, S., Araki, Y., Okuno, T., Fujiyama, Y., and Bamba, T. (2002). IL-17 stimulates inflammatory responses via NF-kappaB and MAP kinase pathways in human colonic myofibroblasts. Am. J. Physiol. Gastrointest. Liver Physiol. *282*, G1035-1044.

Hayashi, F., Means, T.K., and Luster, A.D. (2003). Toll-like receptors stimulate human neutrophil function. Blood *102*, 2660–2669.

Hill, J., and Samuel, J.E. (2011). Coxiella burnetii acid phosphatase inhibits the release of reactive oxygen intermediates in polymorphonuclear leukocytes. Infect. Immun. *79*, 414–420.

Hirai, Y., Iyoda, M., Shibata, T., Kuno, Y., Kawaguchi, M., Hizawa, N., Matsumoto, K., Wada, Y., Kokubu, F., and Akizawa, T. (2012). IL-17A stimulates granulocyte colony-stimulating factor production via ERK1/2 but not p38 or JNK in human renal proximal tubular epithelial cells. American Journal of Physiology-Renal Physiology *302*, F244–F250.

Homburg, C.H., de Haas, M., von dem Borne, A.E., Verhoeven, A.J., Reutelingsperger, C.P., and Roos, D. (1995). Human neutrophils lose their surface Fc gamma RIII and acquire Annexin V binding sites during apoptosis in vitro. Blood *85*, 532–540.

Hong, C.-W. (2017). Current Understanding in Neutrophil Differentiation and Heterogeneity. Immune Netw *17*, 298.

Hoover, D.L., Berger, M., Nacy, C.A., Hockmeyer, W.T., and Meltzer, M.S. (1984). Killing of Leishmania tropica amastigotes by factors in normal human serum. J. Immunol. *132*, 893–897.

Hoppenbrouwers, T., Autar, A.S.A., Sultan, A.R., Abraham, T.E., van Cappellen, W.A., Houtsmuller, A.B., van Wamel, W.J.B., van Beusekom, H.M.M., van Neck, J.W., and de Maat, M.P.M. (2017). In vitro induction of NETosis: Comprehensive live imaging comparison and systematic review. PLoS ONE *12*, e0176472.

Hossain, F., Al-Khami, A.A., Wyczechowska, D., Hernandez, C., Zheng, L., Reiss, K., Valle, L.D., Trillo-Tinoco, J., Maj, T., Zou, W., et al. (2015). Inhibition of Fatty Acid Oxidation Modulates Immunosuppressive Functions of Myeloid-Derived Suppressor Cells and Enhances Cancer Therapies. Cancer Immunol Res *3*, 1236–1247.

Howard, R., Kanetsky, P.A., and Egan, K.M. (2019). Exploring the prognostic value of the neutrophil-to-lymphocyte ratio in cancer. Sci Rep *9*, 19673.

Hu, X., Zhou, Y., Dong, K., Sun, Z., Zhao, D., Wang, W., Yu, G., Liu, W., Xu, G., Han, Z., et al. (2014). Programming of the Development of Tumor-Promoting Neutrophils by Mesenchymal Stromal Cells. Cell Physiol Biochem *33*, 1802–1814.

Hurrell, B.P., Schuster, S., Grün, E., Coutaz, M., Williams, R.A., Held, W., Malissen, B., Malissen, M., Yousefi, S., Simon, H.-U., et al. (2015). Rapid Sequestration of Leishmania mexicana by Neutrophils Contributes to the Development of Chronic Lesion. PLoS Pathog *11*, e1004929.

Hurrell, B.P., Regli, I.B., and Tacchini-Cottier, F. (2016). Different Leishmania Species Drive Distinct Neutrophil Functions. Trends in Parasitology *32*, 392–401.

Iborra, S., Soto, M., Carrión, J., Nieto, A., Fernández, E., Alonso, C., and Requena, J.M. (2003). The Leishmania infantum acidic ribosomal protein P0 administered as a DNA vaccine confers protective immunity to Leishmania major infection in BALB/c mice. Infect. Immun. *71*, 6562–6572.

Iliopoulos, D., Ernst, C., Steplewski, Z., Jambrosic, J.A., Rodeck, U., Herlyn, M., Clark, W.H., Koprowski, H., and Herlyn, D. (1989). Inhibition of metastases of a human melanoma xenograft by monoclonal antibody to the GD2/GD3 gangliosides. J. Natl. Cancer Inst. *81*, 440–444.

Imai, Y., Kubota, Y., Yamamoto, S., Tsuji, K., Shimatani, M., Shibatani, N., Takamido, S., Matsushita, M., and Okazaki, K. (2005). Neutrophils enhance invasion activity of human cholangiocellular carcinoma and hepatocellular carcinoma cells: an in vitro study. J. Gastroenterol. Hepatol. *20*, 287–293.

Imlay, J.A. (2008). Cellular Defenses against Superoxide and Hydrogen Peroxide. Annu. Rev. Biochem. *77*, 755–776.

Iniesta, V., Gómez-Nieto, L.C., Molano, I., Mohedano, A., Carcelén, J., Mirón, C., Alonso, C., and Corraliza, I. (2002). Arginase I induction in macrophages, triggered by Th2-type cytokines, supports the growth of intracellular Leishmania parasites. Parasite Immunol. *24*, 113–118.

Injarabian, L., Devin, A., Ransac, S., and Marteyn, B.S. (2019). Neutrophil Metabolic Shift during their Lifecycle: Impact on their Survival and Activation. Int J Mol Sci *21*.

Inoki, K., Kim, J., and Guan, K.-L. (2012). AMPK and mTOR in cellular energy homeostasis and drug targets. Annu. Rev. Pharmacol. Toxicol. *52*, 381–400.

Jablonska, J., Leschner, S., Westphal, K., Lienenklaus, S., and Weiss, S. (2010). Neutrophils responsive to endogenous IFN-β regulate tumor angiogenesis and growth in a mouse tumor model. J. Clin. Invest. *120*, 1151–1164.

Jamdhade, M.D., Pawar, H., Chavan, S., Sathe, G., Umasankar, P.K., Mahale, K.N., Dixit, T., Madugundu, A.K., Prasad, T.S.K., Gowda, H., et al. (2015). Comprehensive Proteomics Analysis of Glycosomes from *Leishmania donovani*. OMICS: A Journal of Integrative Biology *19*, 157–170.

Jankowski, A., Scott, C.C., and Grinstein, S. (2002). Determinants of the phagosomal pH in neutrophils. J. Biol. Chem. *277*, 6059–6066.

Jaramillo, M., Gomez, M.A., Larsson, O., Shio, M.T., Topisirovic, I., Contreras, I., Luxenburg, R., Rosenfeld, A., Colina, R., McMaster, R.W., et al. (2011). Leishmania repression of host translation through mTOR cleavage is required for parasite survival and infection. Cell Host Microbe *9*, 331–341.

Jeong, H., Kim, S., Hong, B.-J., Lee, C.-J., Kim, Y.-E., Bok, S., Oh, J.-M., Gwak, S.-H., Yoo, M.Y., Lee, M.S., et al. (2019). Tumor-Associated Macrophages Enhance Tumor Hypoxia and Aerobic Glycolysis. Cancer Res. *79*, 795–806.

Jesaitis, A.J., Buescher, E.S., Harrison, D., Quinn, M.T., Parkos, C.A., Livesey, S., and Linner, J. (1990). Ultrastructural localization of cytochrome b in the membranes of resting and phagocytosing human granulocytes. J. Clin. Invest. *85*, 821–835.

Ji, J., Sun, J., and Soong, L. (2003). Impaired expression of inflammatory cytokines and chemokines at early stages of infection with Leishmania amazonensis. Infect. Immun. *71*, 4278–4288.

Jones, R., McDonald, K.E., Willson, J.A., Ghesquière, B., Sammut, D., Daniel, E., Harris, A.J., Lewis, A., Thompson, A.A.R., Dickinson, R.S., et al. (2016). Mutations in succinate dehydrogenase B (SDHB) enhance neutrophil survival independent of HIF-1α expression. Blood *127*, 2641–2644.

Justus, C.R., Dong, L., and Yang, L.V. (2013). Acidic tumor microenvironment and pH-sensing G protein-coupled receptors. Front Physiol *4*, 354.

Kamhawi, S. (2006). Phlebotomine sand flies and Leishmania parasites: friends or foes? Trends in Parasitology *22*, 439–445.

Kanai, K.-I., Asano, K., Hisamitsu, T., and Suzaki, H. (2004). Suppression of matrix metalloproteinase-9 production from neutrophils by a macrolide antibiotic, roxithromycin, in vitro. Mediators of Inflammation *13*, 313–319.

Kane, M.M., and Mosser, D.M. (2001a). The role of IL-10 in promoting disease progression in leishmaniasis. J. Immunol. *166*, 1141–1147.

Kane, M.M., and Mosser, D.M. (2001b). The Role of IL-10 in Promoting Disease Progression in Leishmaniasis. J Immunol *166*, 1141–1147.

Kaplan, M.J., and Radic, M. (2012). Neutrophil Extracellular Traps: Double-Edged Swords of Innate Immunity. J.I. *189*, 2689–2695.

Karin, N., and Razon, H. (2018). Chemokines beyond chemo-attraction: CXCL10 and its significant role in cancer and autoimmunity. Cytokine *109*, 24–28.

Karinch, A.M., Pan, M., Lin, C.M., Strange, R., and Souba, W.W. (2001). Glutamine metabolism in sepsis and infection. J. Nutr. *131*, 2535S-8S; discussion 2550S-1S.

Karlsson, A., and Dahlgren, C. (2002). Assembly and activation of the neutrophil NADPH oxidase in granule membranes. Antioxid. Redox Signal. *4*, 49–60.

Kautz-Neu, K., Noordegraaf, M., Dinges, S., Bennett, C.L., John, D., Clausen, B.E., and von Stebut, E. (2011). Langerhans cells are negative regulators of the anti-Leishmania response. J. Exp. Med. *208*, 885–891.

Kedzierski, L. (2010). Leishmaniasis Vaccine: Where are We Today? J Glob Infect Dis *2*, 177–185.

Kennedy, A.D., Willment, J.A., Dorward, D.W., Williams, D.L., Brown, G.D., and DeLeo, F.R. (2007). Dectin-1 promotes fungicidal activity of human neutrophils. Eur. J. Immunol. *37*, 467–478.

Khan, M.A., Farahvash, A., Douda, D.N., Licht, J.-C., Grasemann, H., Sweezey, N., and Palaniyar, N. (2017). JNK Activation Turns on LPS- and Gram-Negative Bacteria-Induced NADPH Oxidase-Dependent Suicidal NETosis. Sci Rep *7*, 3409.

Khan, M.A., Philip, L.M., Cheung, G., Vadakepeedika, S., Grasemann, H., Sweezey, N., and Palaniyar, N. (2018). Regulating NETosis: Increasing pH Promotes NADPH Oxidase-Dependent NETosis. Front Med (Lausanne) *5*, 19.

Kim, H.K., De La Luz Sierra, M., Williams, C.K., Gulino, A.V., and Tosato, G. (2006). G-CSF down-regulation of CXCR4 expression identified as a mechanism for mobilization of myeloid cells. Blood *108*, 812–820.

Kirchner, T., Möller, S., Klinger, M., Solbach, W., Laskay, T., and Behnen, M. (2012). The Impact of Various Reactive Oxygen Species on the Formation of Neutrophil Extracellular Traps. Mediators of Inflammation *2012*, 1–10.

Knaapen, A.M., Güngör, N., Schins, R.P.F., Borm, P.J.A., and Van Schooten, F.J. (2006). Neutrophils and respiratory tract DNA damage and mutagenesis: a review. Mutagenesis *21*, 225–236.

Kobets, T., Grekov, I., and Lipoldova, M. (2012). Leishmaniasis: prevention, parasite detection and treatment. Curr. Med. Chem. *19*, 1443–1474.

Köhler, A., De Filippo, K., Hasenberg, M., van den Brandt, C., Nye, E., Hosking, M.P., Lane, T.E., Männ, L., Ransohoff, R.M., Hauser, A.E., et al. (2011). G-CSF–mediated thrombopoietin release triggers neutrophil motility and mobilization from bone marrow via induction of Cxcr2 ligands. Blood *117*, 4349–4357.

Kolaczkowska, E., and Kubes, P. (2013). Neutrophil recruitment and function in health and inflammation. Nat Rev Immunol *13*, 159–175.

Kousis, P.C., Henderson, B.W., Maier, P.G., and Gollnick, S.O. (2007). Photodynamic therapy enhancement of antitumor immunity is regulated by neutrophils. Cancer Res. *67*, 10501–10510.

Kruger, P., Saffarzadeh, M., Weber, A.N.R., Rieber, N., Radsak, M., von Bernuth, H., Benarafa, C., Roos, D., Skokowa, J., and Hartl, D. (2015). Neutrophils: Between host defence, immune modulation, and tissue injury. PLoS Pathog. *11*, e1004651.

Kuhlencord, A., Maniera, T., Eibl, H., and Unger, C. (1992). Hexadecylphosphocholine: oral treatment of visceral leishmaniasis in mice. Antimicrob. Agents Chemother. *36*, 1630–1634.

Kumar, G.A., Roy, S., Jafurulla, M., Mandal, C., and Chattopadhyay, A. (2016). Statin-induced chronic cholesterol depletion inhibits Leishmania donovani infection: Relevance of optimum host membrane cholesterol. Biochim. Biophys. Acta *1858*, 2088–2096.

Kushner, B.H., and Cheung, N.K. (1992). Absolute requirement of CD11/CD18 adhesion molecules, FcRII and the phosphatidylinositol-linked FcRIII for monoclonal antibody-mediated neutrophil antihuman tumor cytotoxicity. Blood *79*, 1484–1490.

Lacy, P. (2005). The role of Rho GTPases and SNAREs in mediator release from granulocytes. Pharmacol. Ther. *107*, 358–376.

Lacy, P. (2006). Mechanisms of Degranulation in Neutrophils. Allergy, Asthma & Clinical Immunology *2*, 98.

Lal, C.S., Kumar, A., Kumar, S., Pandey, K., Kumar, N., Bimal, S., Sinha, P.K., and Das, P. (2007). Hypocholesterolemia and increased triglyceride in pediatric visceral leishmaniasis. Clinica Chimica Acta *382*, 151–153.

Lambeth, J.D. (2004). NOX enzymes and the biology of reactive oxygen. Nat Rev Immunol *4*, 181–189.

Laskay, T., Wittmann, I., Diefenbach, A., Röllinghoff, M., and Solbach, W. (1997). Control of Leishmania major infection in BALB/c mice by inhibition of early lymphocyte entry into peripheral lymph nodes. J. Immunol. *158*, 1246–1253.

Laskay, T., van Zandbergen, G., and Solbach, W. (2008). Neutrophil granulocytes as host cells and transport vehicles for intracellular pathogens: Apoptosis as infection-promoting factor. Immunobiology *213*, 183–191.

Laufs, H., Müller, K., Fleischer, J., Reiling, N., Jahnke, N., Jensenius, J.C., Solbach, W., and Laskay, T. (2002). Intracellular Survival of Leishmania major in Neutrophil Granulocytes after Uptake in the Absence of Heat-Labile Serum Factors. IAI *70*, 826–835.

Laurenti, M.D., Orn, A., Sinhorini, I.L., and Corbett, C.E.P. (2004). The role of complement in the early phase of Leishmania (Leishmania) amazonensis infection in BALB/c mice. Braz. J. Med. Biol. Res. *37*, 427–434.

Lavender, N., Yang, J., Chen, S.-C., Sai, J., Johnson, C.A., Owens, P., Ayers, G.D., and Richmond, A. (2017). The Yin/Yan of CCL2: a minor role in neutrophil anti-tumor activity in vitro but a major role on the outgrowth of metastatic breast cancer lesions in the lung in vivo. BMC Cancer *17*, 88.

Le Cabec, V., Cowland, J.B., Calafat, J., and Borregaard, N. (1996). Targeting of proteins to granule subsets is determined by timing and not by sorting: The specific granule protein NGAL is localized to azurophil granules when expressed in HL-60 cells. Proceedings of the National Academy of Sciences *93*, 6454–6457.

Lee, W.L., Harrison, R.E., and Grinstein, S. (2003). Phagocytosis by neutrophils. Microbes Infect. *5*, 1299–1306.

Lehner, R., and Quiroga, A.D. (2016). Fatty Acid Handling in Mammalian Cells. In Biochemistry of Lipids, Lipoproteins and Membranes, (Elsevier), pp. 149–184.

Ley, K., Laudanna, C., Cybulsky, M.I., and Nourshargh, S. (2007). Getting to the site of inflammation: the leukocyte adhesion cascade updated. Nat Rev Immunol *7*, 678–689.

Li, S., Wang, W., Fu, S., Wang, J., Liu, H., Xie, S., Liu, B., Li, Y., Lv, Q., Li, Z., et al. (2013). IL-21 modulates release of proinflammatory cytokines in LPS-stimulated macrophages through distinct signaling pathways. Mediators Inflamm. *2013*, 548073.

Li, T.-J., Jiang, Y.-M., Hu, Y.-F., Huang, L., Yu, J., Zhao, L.-Y., Deng, H.-J., Mou, T.-Y., Liu, H., Yang, Y., et al. (2017). Interleukin-17-Producing Neutrophils Link Inflammatory Stimuli to Disease Progression by Promoting Angiogenesis in Gastric Cancer. Clin. Cancer Res. *23*, 1575–1585.

Li, Y., Wang, W., Yang, F., Xu, Y., Feng, C., and Zhao, Y. (2019). The regulatory roles of neutrophils in adaptive immunity. Cell Commun Signal *17*, 147.

Lichtenstein, A., and Kahle, J. (1985). Anti-tumor effect of inflammatory neutrophils: characteristics of in vivo generation and in vitro tumor cell lysis. Int. J. Cancer *35*, 121–127.

Lieke, T., Nylén, S., Eidsmo, L., McMaster, W.R., Mohammadi, A.M., Khamesipour, A., Berg, L., and Akuffo, H. (2008). Leishmania surface protein gp63 binds directly to human natural killer cells and inhibits proliferation. Clin. Exp. Immunol. *153*, 221–230.

Liew, F.Y., Li, Y., Moss, D., Parkinson, C., Rogers, M.V., and Moncada, S. (1991). Resistance to Leishmania major infection correlates with the induction of nitric oxide synthase in murine macrophages. Eur. J. Immunol. *21*, 3009–3014.

Lin, M., Jackson, P., Tester, A.M., Diaconu, E., Overall, C.M., Blalock, J.E., and Pearlman, E. (2008). Matrix metalloproteinase-8 facilitates neutrophil migration through the corneal stromal matrix by collagen degradation and production of the chemotactic peptide Pro-Gly-Pro. Am. J. Pathol. *173*, 144–153.

Liou, G.-Y., and Storz, P. (2010). Reactive oxygen species in cancer. Free Radic. Res. *44*, 479–496.

Liu, Y., Hu, Y., Gu, F., Liang, J., Zeng, Y., Hong, X., Zhang, K., and Liu, L. (2017). Phenotypic and clinical characterization of low density neutrophils in patients with advanced lung adenocarcinoma. Oncotarget *8*, 90969–90978.

Lockwood, D., and Moore, E. (2010). Treatment of visceral leishmaniasis. J Global Infect Dis *2*, 151.

Lodhi, I.J., Wei, X., Yin, L., Feng, C., Adak, S., Abou-Ezzi, G., Hsu, F.-F., Link, D.C., and Semenkovich, C.F. (2015). Peroxisomal lipid synthesis regulates inflammation by sustaining neutrophil membrane phospholipid composition and viability. Cell Metab. *21*, 51–64.

Lopes, M.F., Costa-da-Silva, A.C., and DosReis, G.A. (2014). Innate immunity to Leishmania infection: within phagocytes. Mediators Inflamm. *2014*, 754965.

Lyden, D., Hattori, K., Dias, S., Costa, C., Blaikie, P., Butros, L., Chadburn, A., Heissig, B., Marks, W., Witte, L., et al. (2001). Impaired recruitment of bone-marrow–derived endothelial and hematopoietic precursor cells blocks tumor angiogenesis and growth. Nat Med *7*, 1194–1201.

Mahdy, M.A.K., Al-Mekhlafi, A.M., Abdul-Ghani, R., Saif-Ali, R., Al-Mekhlafi, H.M., Al-Eryani, S.M., Lim, Y.A.L., and Mahmud, R. (2016). First Molecular Characterization of Leishmania Species Causing Visceral Leishmaniasis among Children in Yemen. PLoS ONE *11*, e0151265.

Mahnke, A., Meier, R.J., Schatz, V., Hofmann, J., Castiglione, K., Schleicher, U., Wolfbeis, O.S., Bogdan, C., and Jantsch, J. (2014). Hypoxia in Leishmania major Skin Lesions Impairs the NO-Dependent Leishmanicidal Activity of Macrophages. Journal of Investigative Dermatology *134*, 2339–2346.

Maianski, N.A., Geissler, J., Srinivasula, S.M., Alnemri, E.S., Roos, D., and Kuijpers, T.W. (2004). Functional characterization of mitochondria in neutrophils: a role restricted to apoptosis. Cell Death Differ. *11*, 143–153.

Mallinson, D.J., Lackie, J.M., and Coombs, G.H. (1989). The oxidative response of rabbit peritoneal neutrophils to leishmanias and other trypanosomatids. Int. J. Parasitol. *19*, 639–645.

Maran, N., Gomes, P.S., Freire-de-Lima, L., Freitas, E.O., Freire-de-Lima, C.G., and Morrot, A. (2016). Host resistance to visceral leishmaniasis: prevalence and prevention. Expert Rev Anti Infect Ther *14*, 435–442.

Maratou, E., Dimitriadis, G., Kollias, A., Boutati, E., Lambadiari, V., Mitrou, P., and Raptis, S.A. (2007). Glucose transporter expression on the plasma membrane of resting and activated white blood cells. Eur. J. Clin. Invest. *37*, 282–290.

Marini, O., Costa, S., Bevilacqua, D., Calzetti, F., Tamassia, N., Spina, C., De Sabata, D., Tinazzi, E., Lunardi, C., Scupoli, M.T., et al. (2017). Mature CD10+ and immature CD10- neutrophils present in G-CSF-treated donors display opposite effects on T cells. Blood *129*, 1343–1356.

Marovich, M.A., Lira, R., Shepard, M., Fuchs, G.H., Kruetzer, R., Nutman, T.B., and Neva, F.A. (2001). Leishmaniasis recidivans recurrence after 43 years: a clinical and immunologic report after successful treatment. Clin. Infect. Dis. *33*, 1076–1079.

Martinez, F.O., Helming, L., and Gordon, S. (2009). Alternative activation of macrophages: an immunologic functional perspective. Annu. Rev. Immunol. *27*, 451–483.

Maslowski, K.M., Vieira, A.T., Ng, A., Kranich, J., Sierro, F., Yu, D., Schilter, H.C., Rolph, M.S., Mackay, F., Artis, D., et al. (2009). Regulation of inflammatory responses by gut microbiota and chemoattractant receptor GPR43. Nature *461*, 1282–1286.

Masucci, M.T., Minopoli, M., and Carriero, M.V. (2019). Tumor Associated Neutrophils. Their Role in Tumorigenesis, Metastasis, Prognosis and Therapy. Front. Oncol. *9*, 1146.

Matlung, H.L., Babes, L., Zhao, X.W., van Houdt, M., Treffers, L.W., van Rees, D.J., Franke, K., Schornagel, K., Verkuijlen, P., Janssen, H., et al. (2018). Neutrophils Kill Antibody-Opsonized Cancer Cells by Trogoptosis. Cell Reports *23*, 3946-3959.e6.

Mattner, J., Donhauser, N., Werner-Felmayer, G., and Bogdan, C. (2006). NKT cells mediate organ-specific resistance against Leishmania major infection. Microbes Infect. *8*, 354–362.

Mauro, C., Leow, S.C., Anso, E., Rocha, S., Thotakura, A.K., Tornatore, L., Moretti, M., De Smaele, E., Beg, A.A., Tergaonkar, V., et al. (2011). NF-*κ*B controls energy homeostasis and metabolic adaptation by upregulating mitochondrial respiration. Nat. Cell Biol. *13*, 1272–1279.

Mayadas, T.N., and Cullere, X. (2005). Neutrophil β2 integrins: moderators of life or death decisions. Trends in Immunology *26*, 388–395.

Mayadas, T.N., Cullere, X., and Lowell, C.A. (2014). The Multifaceted Functions of Neutrophils. Annu. Rev. Pathol. Mech. Dis. *9*, 181–218.

McFarlane, E., Perez, C., Charmoy, M., Allenbach, C., Carter, K.C., Alexander, J., and Tacchini-Cottier, F. (2008). Neutrophils Contribute to Development of a Protective Immune Response during Onset of Infection with Leishmania donovani. IAI *76*, 532–541.

McGuinness, W.A., Kobayashi, S.D., and DeLeo, F.R. (2016). Evasion of Neutrophil Killing by Staphylococcus aureus. Pathogens *5*.

McGwire, B.S., and Satoskar, A.R. (2014). Leishmaniasis: clinical syndromes and treatment. QJM *107*, 7–14.

Meda, L., Gasperini, S., Ceska, M., and Cassatella, M.A. (1994). Modulation of Proinflammatory Cytokine Release from Human Polymorphonuclear Leukocytes by Gamma Interferon. Cellular Immunology *157*, 448–461.

Mencacci, A., Montagnoli, C., Bacci, A., Cenci, E., Pitzurra, L., Spreca, A., Kopf, M., Sharpe, A.H., and Romani, L. (2002). CD80+Gr-1+ myeloid cells inhibit development of antifungal Th1 immunity in mice with candidiasis. J. Immunol. *169*, 3180–3190.

de Menezes, J.P.B., Guedes, C.E.S., Petersen, A.L. de O.A., Fraga, D.B.M., and Veras, P.S.T. (2015). Advances in Development of New Treatment for Leishmaniasis. BioMed Research International *2015*, 1–11.

Mensurado, S., Rei, M., Lança, T., Ioannou, M., Gonçalves-Sousa, N., Kubo, H., Malissen, M., Papayannopoulos, V., Serre, K., and Silva-Santos, B. (2018). Tumor-associated neutrophils suppress pro-tumoral IL-17+ γδ T cells through induction of oxidative stress. PLoS Biol *16*, e2004990.

Metzler, K.D., Goosmann, C., Lubojemska, A., Zychlinsky, A., and Papayannopoulos, V. (2014). A Myeloperoxidase-Containing Complex Regulates Neutrophil Elastase Release and Actin Dynamics during NETosis. Cell Reports *8*, 883–896.

Minero, M.A., Chinchilla, M., Guerrero, O.M., and Castro, A. (2014). Infección de fibroblastos de piel de animales con distinto grado de susceptibilidad a *Leishmania infantum y Leishmania mexicana* (Kinetoplastida: Trypanosomatidae). RBT *52*, 261.

Miralda, I., Uriarte, S.M., and McLeish, K.R. (2017). Multiple Phenotypic Changes Define Neutrophil Priming. Front. Cell. Infect. Microbiol. *7*, 217.

Miranda Lessa, M., Andrade Lessa, H., Castro, T.W.N., Oliveira, A., Scherifer, A., Machado, P., and Carvalho, E.M. (2007). Mucosal leishmaniasis: epidemiological and clinical aspects. Braz J Otorhinolaryngol *73*, 843–847.

Mishalian, I., Bayuh, R., Levy, L., Zolotarov, L., Michaeli, J., and Fridlender, Z.G. (2013). Tumor-associated neutrophils (TAN) develop pro-tumorigenic properties during tumor progression. Cancer Immunol Immunother *62*, 1745–1756.

Mitroulis, I., Kambas, K., Chrysanthopoulou, A., Skendros, P., Apostolidou, E., Kourtzelis, I., Drosos, G.I., Boumpas, D.T., and Ritis, K. (2011). Neutrophil Extracellular Trap Formation Is Associated with IL-1β and Autophagy-Related Signaling in Gout. PLoS ONE *6*, e29318.

Mohapatra, N.P., Soni, S., Rajaram, M.V.S., Strandberg, K.L., and Gunn, J.S. (2013). Type A Francisella tularensis acid phosphatases contribute to pathogenesis. PLoS ONE *8*, e56834.

Mollinedo, F., Janssen, H., de la Iglesia-Vicente, J., Villa-Pulgarin, J.A., and Calafat, J. (2010). Selective Fusion of Azurophilic Granules with *Leishmania*- containing Phagosomes in Human Neutrophils. J. Biol. Chem. *285*, 34528–34536.

Moreira, D., Rodrigues, V., Abengozar, M., Rivas, L., Rial, E., Laforge, M., Li, X., Foretz, M., Viollet, B., Estaquier, J., et al. (2015). Leishmania infantum Modulates Host Macrophage Mitochondrial Metabolism by Hijacking the SIRT1-AMPK Axis. PLoS Pathog *11*, e1004684.

Morgan, J.F., Morton, H.J., and Parker, R.C. (1950). Nutrition of animal cells in tissue culture; initial studies on a synthetic medium. Proc. Soc. Exp. Biol. Med. *73*, 1–8.

Morimoto-Kamata, R., Mizoguchi, S., Ichisugi, T., and Yui, S. (2012). Cathepsin G induces cell aggregation of human breast cancer MCF-7 cells via a 2-step mechanism: catalytic site-independent binding to the cell surface and enzymatic activity-dependent induction of the cell aggregation. Mediators Inflamm. *2012*, 456462.

Mu, X., Shi, W., Xu, Y., Xu, C., Zhao, T., Geng, B., Yang, J., Pan, J., Hu, S., Zhang, C., et al. (2018). Tumor-derived lactate induces M2 macrophage polarization via the activation of the ERK/STAT3 signaling pathway in breast cancer. Cell Cycle *17*, 428–438.

Mühling, J., Tussing, F., Nickolaus, K.A., Matejec, R., Henrich, M., Harbach, H., Wolff, M., Weismüller, K., Engel, J., Welters, I.D., et al. (2010). Effects of alpha-ketoglutarate on neutrophil intracellular amino and alpha-keto acid profiles and ROS production. Amino Acids *38*, 167–177.

Mukbel, R., Petersen, C.A., and Jones, D.E. (2006). Soluble factors from Leishmania major-specific CD4+T cells and B cells limit L. amazonensis amastigote survival within infected macrophages. Microbes Infect. *8*, 2547–2555.

Müller, I., Munder, M., Kropf, P., and Hänsch, G.M. (2009). Polymorphonuclear neutrophils and T lymphocytes: strange bedfellows or brothers in arms? Trends Immunol. *30*, 522–530.

Müller, K., van Zandbergen, G., Hansen, B., Laufs, H., Jahnke, N., Solbach, W., and Laskay, T. (2001). Chemokines, natural killer cells and granulocytes in the early course of Leishmania major infection in mice. Med. Microbiol. Immunol. *190*, 73–76.

Munder, M. (2005). Arginase I is constitutively expressed in human granulocytes and participates in fungicidal activity. Blood *105*, 2549–2556.

Muxel, S.M., Aoki, J.I., Fernandes, J.C.R., Laranjeira-Silva, M.F., Zampieri, R.A., Acuña, S.M., Müller, K.E., Vanderlinde, R.H., and Floeter-Winter, L.M. (2018). Arginine and Polyamines Fate in Leishmania Infection. Front. Microbiol. *8*, 2682.

Nagaoka, I., and Hirota, S. (2000). Increased expression of matrix metalloproteinase-9 in neutrophils in glycogen-induced peritoneal inflammation of guinea pigs. Inflammation Research *49*, 55–62.

Nagaraj, S., Gupta, K., Pisarev, V., Kinarsky, L., Sherman, S., Kang, L., Herber, D.L., Schneck, J., and Gabrilovich, D.I. (2007). Altered recognition of antigen is a mechanism of CD8+ T cell tolerance in cancer. Nat. Med. *13*, 828–835.

Nateghi Rostami, M., Keshavarz, H., Edalat, R., Sarrafnejad, A., Shahrestani, T., Mahboudi, F., and Khamesipour, A. (2010). CD8+ T cells as a source of IFN-γ production in human cutaneous leishmaniasis. PLoS Negl Trop Dis *4*, e845.

Nathan, C. (2006). Neutrophils and immunity: challenges and opportunities. Nat Rev Immunol *6*, 173–182.

Nayak, A., Akpunarlieva, S., Barrett, M., and Burchmore, R. (2018). A defined medium for Leishmania culture allows definition of essential amino acids. Experimental Parasitology *185*, 39–52.

Neufert, C., Pai, R.K., Noss, E.H., Berger, M., Boom, W.H., and Harding, C.V. (2001). Mycobacterium tuberculosis 19-kDa lipoprotein promotes neutrophil activation. J. Immunol. *167*, 1542–1549.

Newsholme, P., Curi, R., Pithon Curi, T.C., Murphy, C.J., Garcia, C., and Pires de Melo, M. (1999). Glutamine metabolism by lymphocytes, macrophages, and neutrophils: its importance in health and disease. J. Nutr. Biochem. *10*, 316–324.

Nguyen, G.T., Green, E.R., and Mecsas, J. (2017). Neutrophils to the ROScue: Mechanisms of NADPH Oxidase Activation and Bacterial Resistance. Front. Cell. Infect. Microbiol. *7*, 373.

Noazin, S., Modabber, F., Khamesipour, A., Smith, P.G., Moulton, L.H., Nasseri, K., Sharifi, I., Khalil, E.A.G., Bernal, I.D.V., Antunes, C.M.F., et al. (2008). First generation leishmaniasis vaccines: a review of field efficacy trials. Vaccine *26*, 6759–6767.

Noben-Trauth, N., Lira, R., Nagase, H., Paul, W.E., and Sacks, D.L. (2003). The Relative Contribution of IL-4 Receptor Signaling and IL-10 to Susceptibility to *Leishmania major*. J Immunol *170*, 5152–5158.

Nogare, A.R., and Yarbrough, W.C. (1990). A comparison of the effects of intact and deacylated lipopolysaccharide on human polymorphonuclear leukocytes. J. Immunol. *144*, 1404–1410.

Nomellini, V., Brubaker, A.L., Mahbub, S., Palmer, J.L., Gomez, C.R., and Kovacs, E.J. (2012). Dysregulation of neutrophil CXCR2 and pulmonary endothelial icam-1 promotes age-related pulmonary inflammation. Aging Dis *3*, 234–247.

Nüsse, O., and Lindau, M. (1988). The dynamics of exocytosis in human neutrophils. J. Cell Biol. *107*, 2117–2123.

Nywening, T.M., Belt, B.A., Cullinan, D.R., Panni, R.Z., Han, B.J., Sanford, D.E., Jacobs, R.C., Ye, J., Patel, A.A., Gillanders, W.E., et al. (2018). Targeting both tumour-associated CXCR2 $^{+}$ neutrophils and CCR2 $^{+}$ macrophages disrupts myeloid recruitment and improves chemotherapeutic responses in pancreatic ductal adenocarcinoma. Gut *67*, 1112–1123.

Oghumu, S., Varikuti, S., Saljoughian, N., Terrazas, C., Huntsman, A.C., Parinandi, N.L., Fuchs, J.R., Kinghorn, A.D., and Satoskar, A.R. (2017). Pentalinonsterol, a Constituent of Pentalinon andrieuxii, Possesses Potent Immunomodulatory Activity and Primes T Cell Immune Responses. J. Nat. Prod. *80*, 2515–2523.

Oklu, R., Sheth, R.A., Wong, K.H.K., Jahromi, A.H., and Albadawi, H. (2017). Neutrophil extracellular traps are increased in cancer patients but does not associate with venous thrombosis. Cardiovasc Diagn Ther *7*, S140–S149.

Oliveira, F., Rowton, E., Aslan, H., Gomes, R., Castrovinci, P.A., Alvarenga, P.H., Abdeladhim, M., Teixeira, C., Meneses, C., Kleeman, L.T., et al. (2015). A sand fly salivary protein vaccine shows efficacy against vector-transmitted cutaneous leishmaniasis in nonhuman primates. Sci Transl Med *7*, 290ra90.

Oliveira-Neto, M.P., Mattos, M., Souza, C.S., Fernandes, O., and Pirmez, C. (1998). Leishmaniasis recidiva cutis in New World cutaneous leishmaniasis. Int. J. Dermatol. *37*, 846–849.

O'Neill, L.A.J., Kishton, R.J., and Rathmell, J. (2016). A guide to immunometabolism for immunologists. Nat. Rev. Immunol. *16*, 553–565.

Orecchioni, M., Ghosheh, Y., Pramod, A.B., and Ley, K. (2019). Macrophage Polarization: Different Gene Signatures in M1(LPS+) vs. Classically and M2(LPS–) vs. Alternatively Activated Macrophages. Front. Immunol. *10*, 1084.

Ostrand-Rosenberg, S., and Fenselau, C. (2018). Myeloid-Derived Suppressor Cells: Immune-Suppressive Cells That Impair Antitumor Immunity and Are Sculpted by Their Environment. J. Immunol. *200*, 422–431.

Otten, M.A., Leusen, J.H.W., Rudolph, E., van der Linden, J.A., Beelen, R.H.J., van de Winkel, J.G.J., and van Egmond, M. (2007). FcR gamma-chain dependent signaling in immature neutrophils is mediated by FcalphaRI, but not by FcgammaRI. J. Immunol. *179*, 2918–2924.

Parekh, A., Das, S., Parida, S., Das, C.K., Dutta, D., Mallick, S.K., Wu, P.-H., Kumar, B.N.P., Bharti, R., Dey, G., et al. (2018). Multi-nucleated cells use ROS to induce breast cancer chemo-resistance in vitro and in vivo. Oncogene *37*, 4546–4561.

Patel, T.A., and Lockwood, D.N. (2009). Pentamidine as secondary prophylaxis for visceral leishmaniasis in the immunocompromised host: report of four cases. Trop. Med. Int. Health *14*, 1064–1070.

Pearson, R.D., and Schwartzman, J.D. (1985). The Interaction of Leishmania Donovani Promastigotes and Human Fibroblasts in Vitro *. The American Journal of Tropical Medicine and Hygiene *34*, 850–855.

Pearson, R.D., and Sousa, A.Q. (1996). Clinical spectrum of Leishmaniasis. Clin. Infect. Dis. *22*, 1–13.

Pearson, R.D., and Steigbigel, R.T. (1981). Phagocytosis and killing of the protozoan Leishmania donovani by human polymorphonuclear leukocytes. J. Immunol. *127*, 1438–1443.

Pédron, T., Girard, R., and Chaby, R. (2001). Down-Modulation of L-Selectin by Lipopolysaccharide Is Not Required for Lipopolysaccharide-Induced Expression of CD14 in Mouse Bone Marrow Granulocytes. Infect. Immun. *69*, 4287–4294.

Peniche, A.G., Bonilla, D.L., Palma, G.I., Melby, P.C., Travi, B.L., and Osorio, E.Y. (2017). A secondary wave of neutrophil infiltration causes necrosis and ulceration in lesions of experimental American cutaneous leishmaniasis. PLoS ONE *12*, e0179084.

Perkins, P.V., and Sacks, D.L. (1985). Development of Infective Stage Leishmania Promastigotes within Phlebotomine Sand Flies. The American Journal of Tropical Medicine and Hygiene *34*, 456–459.

Peters, N.C., Kimblin, N., Secundino, N., Kamhawi, S., Lawyer, P., and Sacks, D.L. (2009). Vector Transmission of Leishmania Abrogates Vaccine-Induced Protective Immunity. PLoS Pathog *5*, e1000484.

Petit, I., Szyper-Kravitz, M., Nagler, A., Lahav, M., Peled, A., Habler, L., Ponomaryov, T., Taichman, R.S., Arenzana-Seisdedos, F., Fujii, N., et al. (2002). G-CSF induces stem cell mobilization by decreasing bone marrow SDF-1 and up-regulating CXCR4. Nat Immunol *3*, 687–694.

Pham, N.-K., Mouriz, J., and Kima, P.E. (2005). Leishmania pifanoi amastigotes avoid macrophage production of superoxide by inducing heme degradation. Infect. Immun. *73*, 8322–8333.

Pillay, J., Ramakers, B.P., Kamp, V.M., Loi, A.L.T., Lam, S.W., Hietbrink, F., Leenen, L.P., Tool, A.T., Pickkers, P., and Koenderman, L. (2010). Functional heterogeneity and differential priming of circulating neutrophils in human experimental endotoxemia. J. Leukoc. Biol. *88*, 211–220.

Pillay, J., Kamp, V.M., van Hoffen, E., Visser, T., Tak, T., Lammers, J.-W., Ulfman, L.H., Leenen, L.P., Pickkers, P., and Koenderman, L. (2012). A subset of neutrophils in human systemic inflammation inhibits T cell responses through Mac-1. J. Clin. Invest. *122*, 327–336.

Pinto-Martinez, A.K., Rodriguez-Durán, J., Serrano-Martin, X., Hernandez-Rodriguez, V., and Benaim, G. (2017). Mechanism of Action of Miltefosine on Leishmania donovani Involves the Impairment of Acidocalcisome Function and the Activation of the Sphingosine-Dependent Plasma Membrane Ca2+ Channel. Antimicrob Agents Chemother *62*, e01614-17.

Powell, D.R., and Huttenlocher, A. (2016). Neutrophils in the Tumor Microenvironment. Trends Immunol. *37*, 41–52.

Puellmann, K., Kaminski, W.E., Vogel, M., Nebe, C.T., Schroeder, J., Wolf, H., and Beham, A.W. (2006). A variable immunoreceptor in a subpopulation of human neutrophils. Proc. Natl. Acad. Sci. U.S.A. *103*, 14441–14446.

Qiu, S.-L., Zhang, H., Tang, Q., Bai, J., He, Z.-Y., Zhang, J.-Q., Li, M.-H., Deng, J.-M., Liu, G.-N., and Zhong, X.-N. (2017). Neutrophil extracellular traps induced by cigarette smoke activate plasmacytoid dendritic cells. Thorax *72*, 1084–1093.

Queen, M.M., Ryan, R.E., Holzer, R.G., Keller-Peck, C.R., and Jorcyk, C.L. (2005). Breast Cancer Cells Stimulate Neutrophils to Produce Oncostatin M: Potential Implications for Tumor Progression. Cancer Res *65*, 8896–8904.

Quinnell, R.J., and Courtenay, O. (2009). Transmission, reservoir hosts and control of zoonotic visceral leishmaniasis. Parasitology *136*, 1915–1934.

van Raam, B.J., Sluiter, W., de Wit, E., Roos, D., Verhoeven, A.J., and Kuijpers, T.W. (2008). Mitochondrial membrane potential in human neutrophils is maintained by complex III activity in the absence of supercomplex organisation. PLoS ONE *3*, e2013.

Rabhi, I., Rabhi, S., Ben-Othman, R., Rasche, A., Daskalaki, A., Trentin, B., Piquemal, D., Regnault, B., Descoteaux, A., Guizani-Tabbane, L., et al. (2012). Transcriptomic signature of Leishmania infected mice macrophages: a metabolic point of view. PLoS Negl Trop Dis *6*, e1763.

Rada, B.K., Geiszt, M., Káldi, K., Timár, C., and Ligeti, E. (2004). Dual role of phagocytic NADPH oxidase in bacterial killing. Blood *104*, 2947–2953.

Rafati, S., Nakhaee, A., Taheri, T., Taslimi, Y., Darabi, H., Eravani, D., Sanos, S., Kaye, P., Taghikhani, M., Jamshidi, S., et al. (2005). Protective vaccination against experimental canine visceral leishmaniasis using a combination of DNA and protein immunization with cysteine proteinases type I and II of L. infantum. Vaccine *23*, 3716–3725.

Raina, A., and Jänne, J. (1968). Biosynthesis of putrescine: characterization of ornithine decarboxylase from regenerating rat liver. Acta Chem Scand *22*, 2375–2378.

Rajeeve, K., Das, S., Prusty, B.K., and Rudel, T. (2018). Chlamydia trachomatis paralyses neutrophils to evade the host innate immune response. Nat Microbiol *3*, 824–835.

Rath, M., Müller, I., Kropf, P., Closs, E.I., and Munder, M. (2014). Metabolism via Arginase or Nitric Oxide Synthase: Two Competing Arginine Pathways in Macrophages. Front Immunol *5*, 532.

Ribeiro-Gomes, F.L., Moniz-de-Souza, M.C.A., Alexandre-Moreira, M.S., Dias, W.B., Lopes, M.F., Nunes, M.P., Lungarella, G., and DosReis, G.A. (2007). Neutrophils Activate Macrophages for Intracellular Killing of *Leishmania major* through Recruitment of TLR4 by Neutrophil Elastase. J Immunol *179*, 3988–3994.

Rice, C.M., Davies, L.C., Subleski, J.J., Maio, N., Gonzalez-Cotto, M., Andrews, C., Patel, N.L., Palmieri, E.M., Weiss, J.M., Lee, J.-M., et al. (2018). Tumour-elicited neutrophils engage mitochondrial metabolism to circumvent nutrient limitations and maintain immune suppression. Nat Commun *9*, 5099.

Riedel, D.D., and Kaufmann, S.H. (1997). Chemokine secretion by human polymorphonuclear granulocytes after stimulation with Mycobacterium tuberculosis and lipoarabinomannan. Infect. Immun. *65*, 4620–4623.

Riffelmacher, T., Clarke, A., Richter, F.C., Stranks, A., Pandey, S., Danielli, S., Hublitz, P., Yu, Z., Johnson, E., Schwerd, T., et al. (2017). Autophagy-Dependent Generation of Free Fatty Acids Is Critical for Normal Neutrophil Differentiation. Immunity *47*, 466-480.e5.

Ritter, U., Frischknecht, F., and van Zandbergen, G. (2009). Are neutrophils important host cells for Leishmania parasites? Trends in Parasitology *25*, 505–510.

Robinson, J.M. (2008). Reactive oxygen species in phagocytic leukocytes. Histochem Cell Biol *130*, 281–297.

Robinson, J.M., Karnovsky, M.L., and Karnovsky, M.J. (1982). Glycogen accumulation in polymorphonuclear leukocytes, and other intracellular alterations that occur during inflammation. J. Cell Biol. *95*, 933–942.

Rodriguez, P.C., Quiceno, D.G., Zabaleta, J., Ortiz, B., Zea, A.H., Piazuelo, M.B., Delgado, A., Correa, P., Brayer, J., Sotomayor, E.M., et al. (2004). Arginase I production in the tumor microenvironment by mature myeloid cells inhibits T-cell receptor expression and antigen-specific T-cell responses. Cancer Res. *64*, 5839–5849.

Rodriguez, P.C., Quiceno, D.G., and Ochoa, A.C. (2007). L-arginine availability regulates T-lymphocyte cell-cycle progression. Blood *109*, 1568–1573.

Rodríguez-Espinosa, O., Rojas-Espinosa, O., Moreno-Altamirano, M.M.B., López-Villegas, E.O., and Sánchez-García, F.J. (2015). Metabolic requirements for neutrophil extracellular traps formation. Immunology *145*, 213–224.

Rogers, M.E., Chance, M.L., and Bates, P.A. (2002). The role of promastigote secretory gel in the origin and transmission of the infective stage of Leishmania mexicana by the sandfly Lutzomyia longipalpis. Parasitology *124*, 495–507.

Rørvig, S., Honore, C., Larsson, L.-I., Ohlsson, S., Pedersen, C.C., Jacobsen, L.C., Cowland, J.B., Garred, P., and Borregaard, N. (2009). Ficolin-1 is present in a highly mobilizable subset of human neutrophil granules and associates with the cell surface after stimulation with fMLP. Journal of Leukocyte Biology *86*, 1439–1449.

Rosales, C. (2018). Neutrophil: A Cell with Many Roles in Inflammation or Several Cell Types? Front. Physiol. *9*, 113.

Rossato, M., Cencig, S., Gasperini, S., Cassatella, M.A., and Bazzoni, F. (2007). IL-10 modulates cytokine gene transcription by protein synthesis-independent and dependent mechanisms in lipopolysaccharide-treated neutrophils. Eur. J. Immunol. *37*, 3176–3189.

Rossi, M., and Fasel, N. (2018). How to master the host immune system? Leishmania parasites have the solutions! International Immunology *30*, 103–111.

Roy, S., Dutta, D., Satyavarapu, E.M., Yadav, P.K., Mandal, C., Kar, S., and Mandal, C. (2017). Mahanine exerts in vitro and in vivo antileishmanial activity by modulation of redox homeostasis. Sci Rep *7*, 4141.

Rub, A., Dey, R., Jadhav, M., Kamat, R., Chakkaramakkil, S., Majumdar, S., Mukhopadhyaya, R., and Saha, B. (2009). Cholesterol depletion associated with Leishmania major infection alters macrophage CD40 signalosome composition and effector function. Nat. Immunol. *10*, 273–280.

Russell, D.G. (1987). The macrophage-attachment glycoprotein gp63 is the predominant C3-acceptor site on Leishmania mexicana promastigotes. Eur. J. Biochem. *164*, 213–221.

Russo, D.M., Burns, J.M., Carvalho, E.M., Armitage, R.J., Grabstein, K.H., Button, L.L., McMaster, W.R., and Reed, S.G. (1991). Human T cell responses to gp63, a surface antigen of Leishmania. J. Immunol. *147*, 3575–3580.

Sadiku, P., Willson, J.A., Dickinson, R.S., Murphy, F., Harris, A.J., Lewis, A., Sammut, D., Mirchandani, A.S., Ryan, E., Watts, E.R., et al. (2017). Prolyl hydroxylase 2 inactivation enhances glycogen storage and promotes excessive neutrophilic responses. J. Clin. Invest. *127*, 3407–3420.

Safaiyan, S., Bolhassani, A., Nylen, S., Akuffo, H., and Rafati, S. (2011). Contribution of human neutrophils in the development of protective immune response during in vitro Leishmania major infection: Contribution of human neutrophils in leishmaniasis. Parasite Immunology *33*, 609–620.

Sagiv, J.Y., Michaeli, J., Assi, S., Mishalian, I., Kisos, H., Levy, L., Damti, P., Lumbroso, D., Polyansky, L., Sionov, R.V., et al. (2015). Phenotypic Diversity and Plasticity in Circulating Neutrophil Subpopulations in Cancer. Cell Reports *10*, 562–573.

Saha, B., Bandyopadhyay, D., Roy, S., and Roy, D.S. (1995). Immunobiological Studies on Experimental Visceral Leishmaniasis IV. Kinetics of Evolution of Disease-Promoting Versus Host-Protective Cells of Monocyte-Macrophage Lineage and their Characterization. Scand J Immunol *42*, 540–546.

Saha, P., Bhattacharjee, S., Sarkar, A., Manna, A., Majumder, S., and Chatterjee, M. (2011). Berberine chloride mediates its anti-leishmanial activity via differential regulation of the mitogen activated protein kinase pathway in macrophages. PLoS ONE *6*, e18467.

Samant, M., Gupta, R., Kumari, S., Misra, P., Khare, P., Kushawaha, P.K., Sahasrabuddhe, A.A., and Dube, A. (2009). Immunization with the DNA-encoding N-terminal domain of proteophosphoglycan of Leishmania donovani generates Th1-type immunoprotective response against experimental visceral leishmaniasis. J. Immunol. *183*, 470–479.

Sandhu, J.K., Privora, H.F., Wenckebach, G., and Birnboim, H.C. (2000). Neutrophils, Nitric Oxide Synthase, and Mutations in the Mutatect Murine Tumor Model. The American Journal of Pathology *156*, 509–518.

Sandilands, G.P., Ahmed, Z., Perry, N., Davison, M., Lupton, A., and Young, B. (2005). Cross-linking of neutrophil CD11b results in rapid cell surface expression of molecules required for antigen presentation and T-cell activation. Immunology *114*, 354–368.

Sangaletti, S., Tripodo, C., Vitali, C., Portararo, P., Guarnotta, C., Casalini, P., Cappetti, B., Miotti, S., Pinciroli, P., Fuligni, F., et al. (2014). Defective stromal remodeling and neutrophil extracellular traps in lymphoid tissues favor the transition from autoimmunity to lymphoma. Cancer Discov *4*, 110–129.

Santiago, B., Calonge, E., Rey, M.J.D., Gutierrez-Cañas, I., Izquierdo, E., Usategui, A., Galindo, M., Alcamí, J., and Pablos, J.L. (2011). CXCL12 gene expression is upregulated by hypoxia and growth arrest but not by inflammatory cytokines in rheumatoid synovial fibroblasts. Cytokine *53*, 184–190.

Saravia, N.G., Hazbón, M.H., Osorio, Y., Valderrama, L., Walker, J., Santrich, C., Cortázar, T., Lebowitz, J.H., and Travi, B.L. (2005). Protective immunogenicity of the paraflagellar rod protein 2 of Leishmania mexicana. Vaccine *23*, 984–995.

Sarkar, A., Aga, E., Bussmeyer, U., Bhattacharyya, A., Möller, S., Hellberg, L., Behnen, M., Solbach, W., and Laskay, T. (2013). Infection of neutrophil granulocytes with Leishmania major activates ERK 1/2 and modulates multiple apoptotic pathways to inhibit apoptosis. Med Microbiol Immunol *202*, 25–35.

Sato, T., Hongu, T., Sakamoto, M., Funakoshi, Y., and Kanaho, Y. (2013). Molecular Mechanisms of N-Formyl-Methionyl-Leucyl-Phenylalanine-Induced Superoxide Generation and Degranulation in Mouse Neutrophils: Phospholipase D Is Dispensable. Molecular and Cellular Biology *33*, 136–145.

Sbarra, A.J., and Karnovsky, M.L. (1959). The biochemical basis of phagocytosis. I. Metabolic changes during the ingestion of particles by polymorphonuclear leukocytes. J. Biol. Chem. *234*, 1355–1362.

Scapini, P., Lapinet-Vera, J.A., Gasperini, S., Calzetti, F., Bazzoni, F., and Cassatella, M.A. (2000). The neutrophil as a cellular source of chemokines. Immunol. Rev. *177*, 195–203.

Scharton, T.M., and Scott, P. (1993). Natural killer cells are a source of interferon gamma that drives differentiation of CD4+ T cell subsets and induces early resistance to Leishmania major in mice. J. Exp. Med. *178*, 567–577.

Schmidt, T., Brodesser, A., Schnitzler, N., Grüger, T., Brandenburg, K., Zinserling, J., and Zündorf, J. (2015). CD66b Overexpression and Loss of C5a Receptors as Surface Markers for Staphylococcus aureus-Induced Neutrophil Dysfunction. PLoS ONE *10*, e0132703.

Schneider, I. (1972). Cell lines derived from late embryonic stages of Drosophila melanogaster. J Embryol Exp Morphol *27*, 353–365.

Sen, S., Roy, K., Mukherjee, S., Mukhopadhyay, R., and Roy, S. (2011). Restoration of IFNγR subunit assembly, IFNγ signaling and parasite clearance in Leishmania donovani infected macrophages: role of membrane cholesterol. PLoS Pathog. *7*, e1002229.

Shabani, F., McNeil, J., and Tippett, L. (1998). The oxidative inactivation of tissue inhibitor of metalloproteinase-1 (TIMP-1) by hypochlorous acid (HOCI) is suppressed by anti-rheumatic drugs. Free Radic. Res. *28*, 115–123.

Shadab, Md., and Ali, N. (2011). Evasion of Host Defence by *Leishmania donovani*: Subversion of Signaling Pathways. Molecular Biology International *2011*, 1–10.

Sheshachalam, A., Srivastava, N., Mitchell, T., Lacy, P., and Eitzen, G. (2014). Granule Protein Processing and Regulated Secretion in Neutrophils. Front. Immunol. *5*.

Silveira, F.T., Lainson, R., Gomes, C.M.C., Laurenti, M.D., and Corbett, C.E.P. (2008). Reviewing the role of the dendritic Langerhans cells in the immunopathogenesis of American cutaneous leishmaniasis. Trans. R. Soc. Trop. Med. Hyg. *102*, 1075–1080.

Silveira, F.T., Lainson, R., De Castro Gomes, C.M., Laurenti, M.D., and Corbett, C.E.P. (2009). Immunopathogenic competences of Leishmania (V.) braziliensis and L. (L.) amazonensis in American cutaneous leishmaniasis. Parasite Immunol. *31*, 423–431.

Silvestre-Roig, C., Hidalgo, A., and Soehnlein, O. (2016). Neutrophil heterogeneity: implications for homeostasis and pathogenesis. Blood *127*, 2173–2181.

Simsek, T., Kocabas, F., Zheng, J., Deberardinis, R.J., Mahmoud, A.I., Olson, E.N., Schneider, J.W., Zhang, C.C., and Sadek, H.A. (2010). The distinct metabolic profile of hematopoietic stem cells reflects their location in a hypoxic niche. Cell Stem Cell *7*, 380–390.

Singh, A.K., Mukhopadhyay, C., Biswas, S., Singh, V.K., and Mukhopadhyay, C.K. (2012a). Intracellular pathogen Leishmania donovani activates hypoxia inducible factor-1 by dual mechanism for survival advantage within macrophage. PLoS ONE *7*, e38489.

Singh, N., Kumar, M., and Singh, R.K. (2012b). Leishmaniasis: Current status of available drugs and new potential drug targets. Asian Pacific Journal of Tropical Medicine *5*, 485–497.

Sionov, R.V., Fridlender, Z.G., and Granot, Z. (2015). The Multifaceted Roles Neutrophils Play in the Tumor Microenvironment. Cancer Microenvironment *8*, 125–158.

Sippel, T.R., White, J., Nag, K., Tsvankin, V., Klaassen, M., Kleinschmidt-DeMasters, B.K., and Waziri, A. (2011). Neutrophil degranulation and immunosuppression in patients with GBM: restoration of cellular immune function by targeting arginase I. Clin. Cancer Res. *17*, 6992–7002.

Siripattanapipong, S., Boontanom, P., Leelayoova, S., Mungthin, M., and Tan-Ariya, P. (2019). In vitro growth characteristics and morphological differentiation of Leishmania martiniquensis promastigotes in different culture media. Acta Trop. *197*, 105039.

Skeiky, Y.A.W., Coler, R.N., Brannon, M., Stromberg, E., Greeson, K., Crane, R.T., Webb, J.R., Campos-Neto, A., and Reed, S.G. (2002). Protective efficacy of a tandemly linked, multi-subunit recombinant leishmanial vaccine (Leish-111f) formulated in MPL adjuvant. Vaccine *20*, 3292–3303.

Skokowa, J., Lan, D., Thakur, B.K., Wang, F., Gupta, K., Cario, G., Brechlin, A.M., Schambach, A., Hinrichsen, L., Meyer, G., et al. (2009). NAMPT is essential for the G-CSF-induced myeloid differentiation via a NAD(+)-sirtuin-1-dependent pathway. Nat. Med. *15*, 151–158.

Snoderly, H.T., Boone, B.A., and Bennewitz, M.F. (2019). Neutrophil extracellular traps in breast cancer and beyond: current perspectives on NET stimuli, thrombosis and metastasis, and clinical utility for diagnosis and treatment. Breast Cancer Res *21*, 145.

Soong, L., Duboise, S.M., Kima, P., and McMahon-Pratt, D. (1995). Leishmania pifanoi amastigote antigens protect mice against cutaneous leishmaniasis. Infect. Immun. *63*, 3559–3566.

Spencer, J.A., Ferraro, F., Roussakis, E., Klein, A., Wu, J., Runnels, J.M., Zaher, W., Mortensen, L.J., Alt, C., Turcotte, R., et al. (2014). Direct measurement of local oxygen concentration in the bone marrow of live animals. Nature *508*, 269–273.

Stäger, S., Smith, D.F., and Kaye, P.M. (2000). Immunization with a recombinant stage-regulated surface protein from Leishmania donovani induces protection against visceral leishmaniasis. J. Immunol. *165*, 7064–7071.

Stanton, R.C. (2012). Glucose-6-phosphate dehydrogenase, NADPH, and cell survival. IUBMB Life *64*, 362–369.

Stark, M.A., Huo, Y., Burcin, T.L., Morris, M.A., Olson, T.S., and Ley, K. (2005). Phagocytosis of Apoptotic Neutrophils Regulates Granulopoiesis via IL-23 and IL-17. Immunity *22*, 285–294.

Steven, J.L. (1892). Metchnikoff on the Comparative Pathology of Inflammation. Glasgow Med J *38*, 195–205.

Stevens, P., and Hong, D. (1984). The role of myeloperoxidase and superoxide anion in the luminol- and lucigenin-dependent chemiluminescence of human neutrophils. Microchemical Journal *30*, 135–146.

Stoiber, W., Obermayer, A., Steinbacher, P., and Krautgartner, W.-D. (2015). The Role of Reactive Oxygen Species (ROS) in the Formation of Extracellular Traps (ETs) in Humans. Biomolecules *5*, 702–723.

Stoppacciaro, A., Melani, C., Parenza, M., Mastracchio, A., Bassi, C., Baroni, C., Parmiani, G., and Colombo, M.P. (1993). Regression of an established tumor genetically modified to release granulocyte colony-stimulating factor requires granulocyte-T cell cooperation and T cell-produced interferon gamma. J. Exp. Med. *178*, 151–161.

Streit, J.A., Recker, T.J., Donelson, J.E., and Wilson, M.E. (2000). BCG expressing LCR1 of Leishmania chagasi induces protective immunity in susceptible mice. Exp. Parasitol. *94*, 33–41.

Strieter, R.M., Kunkel, S.L., Arenberg, D.A., Burdick, M.D., and Polverini, P.J. (1995). Interferon gamma-inducible protein 10 (IP-10), a member of the C-X-C chemokine family, is an inhibitor of angiogenesis. Biochem. Biophys. Res. Commun. *210*, 51–57.

Stroncek, D.F., Shankar, R.A., Noren, P.A., Herr, G.P., and Clement, L.T. (1996). Analysis of the expression of NB1 antigen using two monoclonal antibodies. Transfusion *36*, 168–174.

Summers, C., Rankin, S.M., Condliffe, A.M., Singh, N., Peters, A.M., and Chilvers, E.R. (2010). Neutrophil kinetics in health and disease. Trends in Immunology *31*, 318–324.

Sun, B., Qin, W., Song, M., Liu, L., Yu, Y., Qi, X., and Sun, H. (2018). Neutrophil Suppresses Tumor Cell Proliferation via Fas /Fas Ligand Pathway Mediated Cell Cycle Arrested. Int. J. Biol. Sci. *14*, 2103–2113.

Sun, R., Luo, J., Li, D., Shu, Y., Luo, C., Wang, S.-S., Qin, J., Zhang, G.-M., and Feng, Z.-H. (2014). Neutrophils with protumor potential could efficiently suppress tumor growth after cytokine priming and in presence of normal NK cells. Oncotarget *5*, 12621–12634.

Sundar, S., and Jaya, J. (2010). Liposomal amphotericin B and leishmaniasis: Dose and response. J Global Infect Dis *2*, 159.

Sunter, J., and Gull, K. (2017). Shape, form, function and *Leishmania* pathogenicity: from textbook descriptions to biological understanding. Open Biol. *7*, 170165.

Takei, H., Araki, A., Watanabe, H., Ichinose, A., and Sendo, F. (1996). Rapid killing of human neutrophils by the potent activator phorbol 12-myristate 13-acetate (PMA) accompanied by changes different from typical apoptosis or necrosis. J Leukoc Biol *59*, 229–240.

Tamassia, N., Cassatella, M.A., and Bazzoni, F. (2014). Fast and Accurate Quantitative Analysis of Cytokine Gene Expression in Human Neutrophils. In Neutrophil Methods and Protocols, M.T. Quinn, and F.R. DeLeo, eds. (Totowa, NJ: Humana Press), pp. 451–467.

Tamassia, N., Bianchetto-Aguilera, F., Arruda-Silva, F., Gardiman, E., Gasperini, S., Calzetti, F., and Cassatella, M.A. (2018). Cytokine production by human neutrophils: Revisiting the "dark side of the moon." Eur J Clin Invest *48*, e12952.

Tanaka, E., and Sendo, F. (1993). Abrogation of tumor-inhibitory MRC-OX8+ (CD8+) effector T-cell generation in rats by selective depletion of neutrophils in vivo using a monoclonal antibody. Int. J. Cancer *54*, 131–136.

Tewary, P., Jain, M., Sahani, M.H., Saxena, S., and Madhubala, R. (2005). A heterologous prime-boost vaccination regimen using ORFF DNA and recombinant ORFF protein confers protective immunity against experimental visceral leishmaniasis. J. Infect. Dis. *191*, 2130–2137.

Thalhofer, C.J., Chen, Y., Sudan, B., Love-Homan, L., and Wilson, M.E. (2011). Leukocytes infiltrate the skin and draining lymph nodes in response to the protozoan Leishmania infantum chagasi. Infect. Immun. *79*, 108–117.

Tillack, K., Breiden, P., Martin, R., and Sospedra, M. (2012). T Lymphocyte Priming by Neutrophil Extracellular Traps Links Innate and Adaptive Immune Responses. J.I. *188*, 3150–3159.

Tosello Boari, J., Amezcua Vesely, M.C., Bermejo, D.A., Ramello, M.C., Montes, C.L., Cejas, H., Gruppi, A., and Acosta Rodríguez, E.V. (2012). IL-17RA signaling reduces inflammation and mortality during Trypanosoma cruzi infection by recruiting suppressive IL-10-producing neutrophils. PLoS Pathog. *8*, e1002658.

Tsuda, Y., Takahashi, H., Kobayashi, M., Hanafusa, T., Herndon, D.N., and Suzuki, F. (2004). Three Different Neutrophil Subsets Exhibited in Mice with Different Susceptibilities to Infection by Methicillin-Resistant Staphylococcus aureus. Immunity *21*, 215–226.

Underhill, D.M., and Ozinsky, A. (2002). P HAGOCYTOSIS OF M ICROBES : Complexity in Action. Annu. Rev. Immunol. *20*, 825–852.

Urban, C.F., Lourido, S., and Zychlinsky, A. (2006). How do microbes evade neutrophil killing? Cell Microbiol *8*, 1687–1696.

Urdinguio, R.G., Fernandez, A.F., Moncada-Pazos, A., Huidobro, C., Rodriguez, R.M., Ferrero, C., Martinez-Camblor, P., Obaya, A.J., Bernal, T., Parra-Blanco, A., et al. (2013). Immune-dependent and independent antitumor activity of GM-CSF aberrantly expressed by mouse and human colorectal tumors. Cancer Res. *73*, 395–405.

Uribe-Querol, E., and Rosales, C. (2015). Neutrophils in Cancer: Two Sides of the Same Coin. Journal of Immunology Research *2015*, 1–21.

Valente, S.A., Fallon, W.F., Alexander, T.S., Tomas, E.R., Evancho-Chapman, M.M., Schmidt, S.P., Gorski, R., Pizov, O., DeFine, L., and Clark, A.J. (2009). Immunologic function in the elderly after injury--the neutrophil and innate immunity. J Trauma *67*, 968–974.

Valenzuela, J.G., Belkaid, Y., Garfield, M.K., Mendez, S., Kamhawi, S., Rowton, E.D., Sacks, D.L., and Ribeiro, J.M. (2001). Toward a defined anti-Leishmania vaccine targeting vector antigens: characterization of a protective salivary protein. J. Exp. Med. *194*, 331–342.

Valerius, T., Repp, R., de Wit, T.P., Berthold, S., Platzer, E., Kalden, J.R., Gramatzki, M., and van de Winkel, J.G. (1993). Involvement of the high-affinity receptor for IgG (Fc gamma RI; CD64) in enhanced tumor cell cytotoxicity of neutrophils during granulocyte colony-stimulating factor therapy. Blood *82*, 931–939.

Veglia, F., Tyurin, V.A., Blasi, M., De Leo, A., Kossenkov, A.V., Donthireddy, L., To, T.K.J., Schug, Z., Basu, S., Wang, F., et al. (2019). Fatty acid transport protein 2 reprograms neutrophils in cancer. Nature *569*, 73–78.

von Vietinghoff, S., and Ley, K. (2008). Homeostatic Regulation of Blood Neutrophil Counts. J Immunol *181*, 5183–5188.

Villanueva, E., Yalavarthi, S., Berthier, C.C., Hodgin, J.B., Khandpur, R., Lin, A.M., Rubin, C.J., Zhao, W., Olsen, S.H., Klinker, M., et al. (2011). Netting Neutrophils Induce Endothelial Damage, Infiltrate Tissues, and Expose Immunostimulatory Molecules in Systemic Lupus Erythematosus. J.I. *187*, 538–552.

Vinolo, M.A.R., Rodrigues, H.G., Hatanaka, E., Hebeda, C.B., Farsky, S.H.P., and Curi, R. (2009). Short-chain fatty acids stimulate the migration of neutrophils to inflammatory sites. Clin. Sci. *117*, 331–338.

Vissers, M.C.M., Gunningham, S.P., Morrison, M.J., Dachs, G.U., and Currie, M.J. (2007). Modulation of hypoxia-inducible factor-1 alpha in cultured primary cells by intracellular ascorbate. Free Radic. Biol. Med. *42*, 765–772.

Wada, Y., Yoshida, K., Hihara, J., Konishi, K., Tanabe, K., Ukon, K., Taomoto, J., Suzuki, T., and Mizuiri, H. (2006). Sivelestat, a specific neutrophil elastase inhibitor, suppresses the growth of gastric carcinoma cells by preventing the release of transforming growth factor-alpha. Cancer Sci. *97*, 1037–1043.

Walker, D.M., Oghumu, S., Gupta, G., McGwire, B.S., Drew, M.E., and Satoskar, A.R. (2014). Mechanisms of cellular invasion by intracellular parasites. Cell. Mol. Life Sci. *71*, 1245–1263.

Walmsley, S.R., Print, C., Farahi, N., Peyssonnaux, C., Johnson, R.S., Cramer, T., Sobolewski, A., Condliffe, A.M., Cowburn, A.S., Johnson, N., et al. (2005). Hypoxia-induced neutrophil survival is mediated by HIF-1alpha-dependent NF-kappaB activity. J. Exp. Med. *201*, 105–115.

Wang, L., Zhou, X., Yin, Y., Mai, Y., Wang, D., and Zhang, X. (2018). Hyperglycemia Induces Neutrophil Extracellular Traps Formation Through an NADPH Oxidase-Dependent Pathway in Diabetic Retinopathy. Front Immunol *9*, 3076.

Warburg, O. (1956). On the origin of cancer cells. Science *123*, 309–314.

Warburg, O., Wind, F., and Negelein, E. (1927). THE METABOLISM OF TUMORS IN THE BODY. J. Gen. Physiol. *8*, 519–530.

Ward, P.A. (2004). The dark side of C5a in sepsis. Nat Rev Immunol *4*, 133–142.

Webb, N.J.A., Myers, C.R., Watson, C.J., Bottomley, M.J., and Brenchley, P.E.C. (1998). ACTIVATED HUMAN NEUTROPHILS EXPRESS VASCULAR ENDOTHELIAL GROWTH FACTOR (VEGF). Cytokine *10*, 254–257.

Wetzel, D.M., McMahon-Pratt, D., and Koleske, A.J. (2012). The Abl and Arg kinases mediate distinct modes of phagocytosis and are required for maximal Leishmania infection. Mol. Cell. Biol. *32*, 3176–3186.

Wheeler, R.J., Gluenz, E., and Gull, K. (2015). Basal body multipotency and axonemal remodelling are two pathways to a 9+0 flagellum. Nat Commun *6*, 8964.

Wheeler, R.J., Sunter, J.D., and Gull, K. (2016). Flagellar pocket restructuring through the *Leishmania* life cycle involves a discrete flagellum attachment zone. J Cell Sci *129*, 854–867.

Wilson, M.E., Young, B.M., Davidson, B.L., Mente, K.A., and McGowan, S.E. (1998). The importance of TGF-beta in murine visceral leishmaniasis. J. Immunol. *161*, 6148–6155.

Wilson, T.J., Nannuru, K.C., Futakuchi, M., and Singh, R.K. (2010). Cathepsin G-mediated enhanced TGF-beta signaling promotes angiogenesis via upregulation of VEGF and MCP-1. Cancer Lett. *288*, 162–169.

Wislez, M., Rabbe, N., Marchal, J., Milleron, B., Crestani, B., Mayaud, C., Antoine, M., Soler, P., and Cadranel, J. (2003). Hepatocyte growth factor production by neutrophils infiltrating bronchioloalveolar subtype pulmonary adenocarcinoma: role in tumor progression and death. Cancer Res. *63*, 1405–1412.

Wood, A.J.T., Vassallo, A., Summers, C., Chilvers, E.R., and Conway-Morris, A. (2018). C5a anaphylatoxin and its role in critical illness-induced organ dysfunction. Eur J Clin Invest *48*, e13028.

Wu, Saxena, Awaji, and Singh (2019). Tumor-Associated Neutrophils in Cancer: Going Pro. Cancers *11*, 564.

Wylie, C.E., Carbonell-Antoñanzas, M., Aiassa, E., Dhollander, S., Zagmutt, F.J., Brodbelt, D.C., and Solano-Gallego, L. (2014). A systematic review of the efficacy of prophylactic control measures for naturally-occurring canine leishmaniosis, part I: vaccinations. Prev. Vet. Med. *117*, 7–18.

Xu, H., Zeng, Y., Liu, L., Gao, Q., Jin, S., Lan, Q., Lai, W., Luo, X., Wu, H., Huang, Y., et al. (2017). PRL-3 improves colorectal cancer cell proliferation and invasion through IL-8 mediated glycolysis metabolism. International Journal of Oncology *51*, 1271–1279.

Yamasaki, H., Yamaguchi, Y., Takino, H., Matsuo, H., Matsumoto, K., Uotani, S., Akazawa, S., Yamashita, S., and Nagataki, S. (1996). TNF-α stimulates glucose uptake in L6 myoblasts. Diabetes Research and Clinical Practice *32*, 11–18.

Yan, M., Mehta, J.L., Zhang, W., and Hu, C. (2011). LOX-1, oxidative stress and inflammation: a novel mechanism for diabetic cardiovascular complications. Cardiovasc Drugs Ther *25*, 451–459.

Yang, L. (2017). Tumor Microenvironment and Metabolism. IJMS *18*, 2729.

Yang, L., Liu, Q., Zhang, X., Liu, X., Zhou, B., Chen, J., Huang, D., Li, J., Li, H., Chen, F., et al. (2020a). DNA of neutrophil extracellular traps promotes cancer metastasis via CCDC25. Nature *583*, 133–138.

Yang, L.-Y., Luo, Q., Lu, L., Zhu, W.-W., Sun, H.-T., Wei, R., Lin, Z.-F., Wang, X.-Y., Wang, C.-Q., Lu, M., et al. (2020b). Increased neutrophil extracellular traps promote metastasis potential of hepatocellular carcinoma via provoking tumorous inflammatory response. J Hematol Oncol *13*, 3.

Yang, R., Zhong, L., Yang, X.-Q., Jiang, K.-L., Li, L., Song, H., and Liu, B.-Z. (2016). Neutrophil elastase enhances the proliferation and decreases apoptosis of leukemia cells via activation of PI3K/Akt signaling. Mol Med Rep *13*, 4175–4182.

Yipp, B.G., and Kubes, P. (2013). NETosis: how vital is it? Blood *122*, 2784–2794.

Yizengaw, E., Getahun, M., Tajebe, F., Cruz Cervera, E., Adem, E., Mesfin, G., Hailu, A., Van der Auwera, G., Yardley, V., Lemma, M., et al. (2016). Visceral Leishmaniasis Patients Display Altered Composition and Maturity of Neutrophils as well as Impaired Neutrophil Effector Functions. Front. Immunol. *7*.

YlÖstalo, J.H., Bartosh, T.J., Coble, K., and Prockop, D.J. (2012). Human Mesenchymal Stem/Stromal Cells Cultured as Spheroids are Self-activated to Produce Prostaglandin E2 that Directs Stimulated Macrophages into an Anti-inflammatory Phenotype: hMSC Spheroids Promote M2 Macrophage Phenotype. STEM CELLS *30*, 2283–2296.

Yoshimura, T., and Takahashi, M. (2007). IFN-γ-Mediated Survival Enables Human Neutrophils to Produce MCP-1/CCL2 in Response to Activation by TLR Ligands. J Immunol *179*, 1942–1949.

Yui, S., Osawa, Y., Ichisugi, T., and Morimoto-Kamata, R. (2014). Neutrophil cathepsin G, but not elastase, induces aggregation of MCF-7 mammary carcinoma cells by a protease activity-dependent cell-oriented mechanism. Mediators Inflamm. *2014*, 971409.

Zabaleta, J., McGee, D.J., Zea, A.H., Hernández, C.P., Rodriguez, P.C., Sierra, R.A., Correa, P., and Ochoa, A.C. (2004). Helicobacter pylori arginase inhibits T cell proliferation and reduces the expression of the TCR zeta-chain (CD3zeta). J. Immunol. *173*, 586–593.

van Zandbergen, G., Hermann, N., Laufs, H., Solbach, W., and Laskay, T. (2002). Leishmania promastigotes release a granulocyte chemotactic factor and induce interleukin-8 release but inhibit gamma interferon-inducible protein 10 production by neutrophil granulocytes. Infect. Immun. *70*, 4177–4184.

Zhang, W., Chen, Z., Li, F., Kamencic, H., Juurlink, B., Gordon, J.R., and Xiang, J. (2003). Tumour necrosis factor-alpha (TNF-alpha) transgene-expressing dendritic cells (DCs) undergo augmented cellular maturation and induce more robust T-cell activation and anti-tumour immunity than DCs generated in recombinant TNF-alpha. Immunology *108*, 177–188.

Zhang, X., Zhang, W., Yuan, X., Fu, M., Qian, H., and Xu, W. (2016). Neutrophils in cancer development and progression: Roles, mechanisms, and implications (Review). International Journal of Oncology *49*, 857–867.

Zhao, Y., Yang, X., Zhang, X., Yu, Q., Zhao, P., Wang, J., Duan, C., Li, J., Johnson, H., Feng, X., et al. (2018). IP-10 and RANTES as biomarkers for pulmonary tuberculosis diagnosis and monitoring. Tuberculosis *111*, 45–53.

Zhou, W., Cao, L., Jeffries, J., Zhu, X., Staiger, C.J., and Deng, Q. (2018). Neutrophil-specific knockout demonstrates a role for mitochondria in regulating neutrophil motility in zebrafish. Dis Model Mech *11*.

Zhu, Q., Zhang, X., Zhang, L., Li, W., Wu, H., Yuan, X., Mao, F., Wang, M., Zhu, W., Qian, H., et al. (2014). The IL-6–STAT3 axis mediates a reciprocal crosstalk between cancer-derived mesenchymal stem cells and neutrophils to synergistically prompt gastric cancer progression. Cell Death Dis *5*, e1295–e1295.

Zijlstra, E.E. (2016). The immunology of post-kala-azar dermal leishmaniasis (PKDL). Parasites Vectors *9*, 464.

Zijlstra, E., Musa, A., Khalil, E., El Hassan, I., and El-Hassan, A. (2003). Post-kala-azar dermal leishmaniasis. The Lancet Infectious Diseases *3*, 87–98.

Zivkovic, M., Poljak-Blazi, M., Egger, G., Sunjic, S.B., Schaur, R.J., and Zarkovic, N. (2005). Oxidative burst and anticancer activities of rat neutrophils. Biofactors *24*, 305–312.

Zmijewski, J.W., Lorne, E., Zhao, X., Tsuruta, Y., Sha, Y., Liu, G., Siegal, G.P., and Abraham, E. (2008). Mitochondrial respiratory complex I regulates neutrophil activation and severity of lung injury. Am. J. Respir. Crit. Care Med. *178*, 168–179.

Zmijewski, J.W., Lorne, E., Banerjee, S., and Abraham, E. (2009). Participation of mitochondrial respiratory complex III in neutrophil activation and lung injury. Am. J. Physiol. Lung Cell Mol. Physiol. *296*, L624-634.

Acknowledgements

Firstly, I would like to express my sincere gratitude to my advisor Prof. Dr. rer. nat. Tamás Laskay for the continuous support of my PhD study and related research, for his patience, motivation, and immense knowledge. His guidance helped me in all the time of research and writing of this thesis. Apart from my Supervisor, I won't forget to express the gratitude to rest of the team: Heidi Tackenberg, Sonja Möller and Daniel Dömer, for giving the encouragement and sharing insightful suggestions. They all have played a major role in polishing my research skills.

I would like to thank the members of the INLEISH consortium, Ricardo Silvestre (Braga, Portugal), Bhaskar Saha (Pune, India), Arup Sarkar (Bhubaneswar, India) and Jérome Estaquier *(*Paris, France) for guiding me through this project. The meetings and conversations were vital in inspiring me to think outside the box, from multiple perspectives to form a comprehensive and objective critique.

My sincere thanks also goes to Prof. Dr. med. Jan Rupp who provided me an opportunity to join the team of the Department of Infectious Diseases and Microbiology at the University of Lübeck, and who gave access to the laboratory and research facilities.

I would also like to thank all of the donors who gave their blood (and neutrophils) for this study.

I am also thankful to the graduate school IRTG1911, including my mentors PD Dr. rer. nat. Christina Zechel and PD Dr. rer. nat. Ulrike Schleicher as well as all its members for all the considerate guidance.

I would like to pay my special regards to the group of Dr. rer. nat. Daniel Rapoport, especially Ana Cristina Guerra de Souza, Miriam Voigt and Falk Nette, for the great exchange of knowledge and the support with laboratory materials.

To conclude, I cannot forget to thank my family and friends for all the unconditional support in this very intense academic years.

Supplementary Material

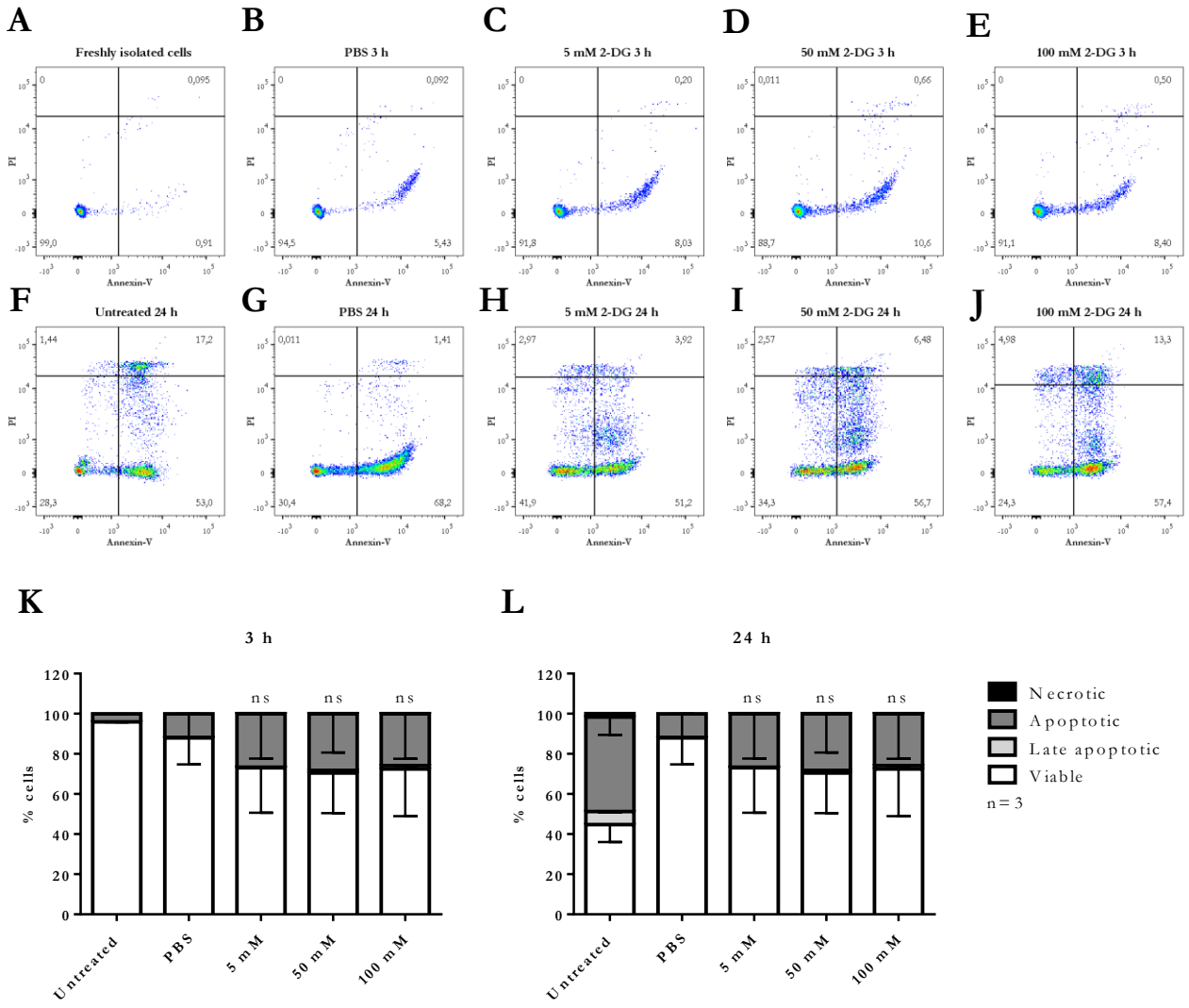

Supplementary Figure S1. Apoptosis and viability of 2-DG-treated neutrophils. Primary human neutrophils were treated with 5 mM, 50 mM or 100 mM 2-DG. PBS treatment served as solvent control. After 3 h and 24 h apoptosis and cell viability was assessed by annexin-V and PI staining and analyzed by flow cytometry. Annexin-V- and PI-negative cells (lower left quadrant) were regarded as viable, whereas annexin-V only positive cells (lower right quadrant) were considered as apoptotic, annexin-V- and PI-positive cells were defined as late apoptotic (upper right quadrant) and PI only positive cells were regarded necrotic (upper left quadrant). Representative dot plots are shown in the panels **A**-**J**. The ratio (%) of viable cells was used for statistical analysis by one-way ANOVA. Bar diagrams (**K**, **L**) show mean ± SD (n=3), ns = not-significant.

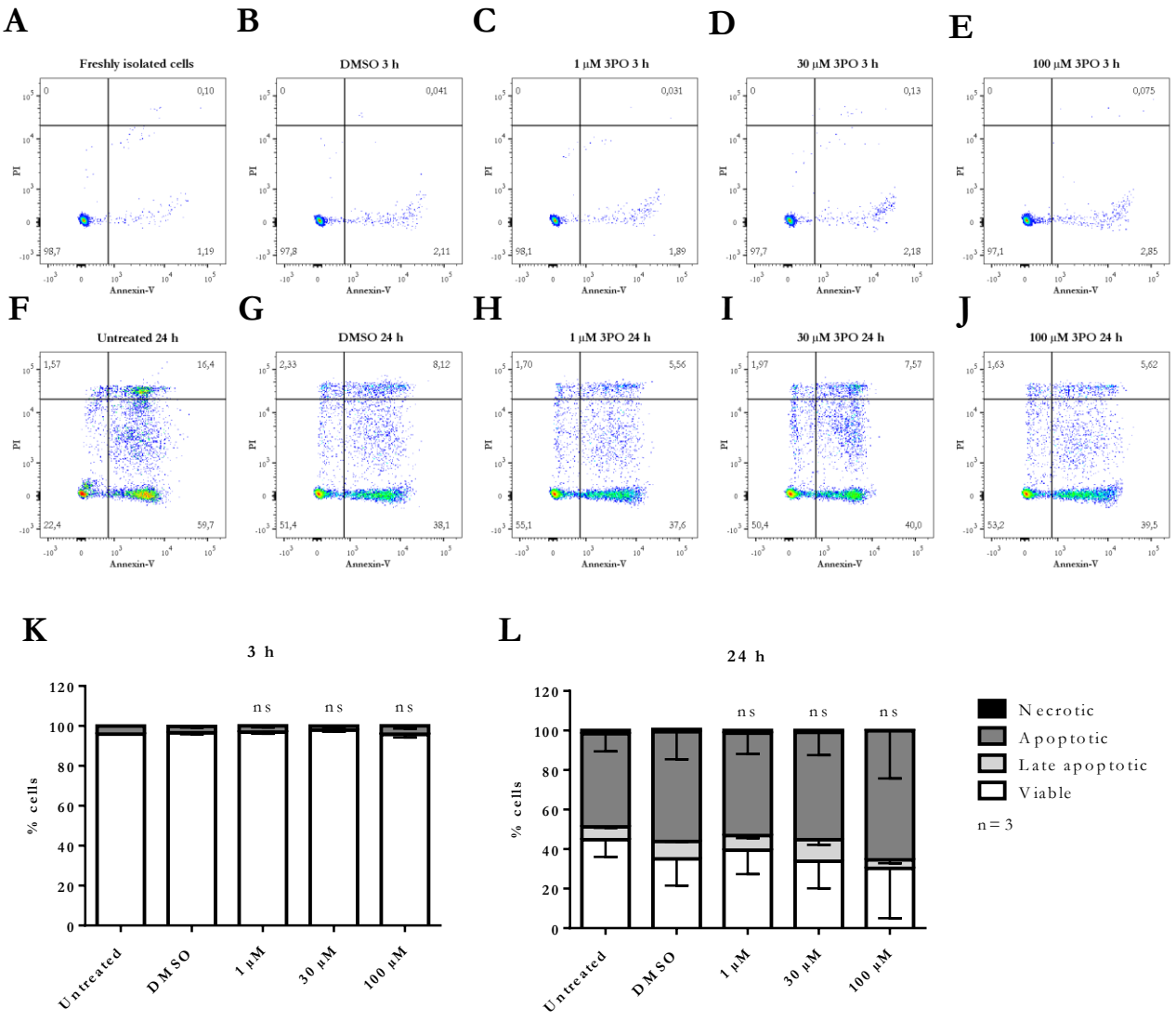

Supplementary Figure S2. Apoptosis and viability of 3PO-treated neutrophils. Primary human neutrophils were treated with 1 µM, 30 µM or 100 µM 3PO. DMSO treatment served as solvent control. After 3 h and 24 h apoptosis and cell viability was assessed by annexin-V and PI staining and analyzed by flow cytometry. Annexin-V- and PI-negative cells (lower left quadrant) were regarded as viable, whereas annexin-V only positive cells (lower right quadrant) were considered as apoptotic, annexin-V- and PI-positive cells were defined as late apoptotic (upper right quadrant) and PI only positive cells were regarded necrotic (upper left quadrant). Representative dot plots are shown in the panels **A**-**J**. The ratio (%) of viable cells was used for statistical analysis by one-way ANOVA. Bar diagrams (**K**, **L**) show mean ± SD (n=3), ns = not-significant.

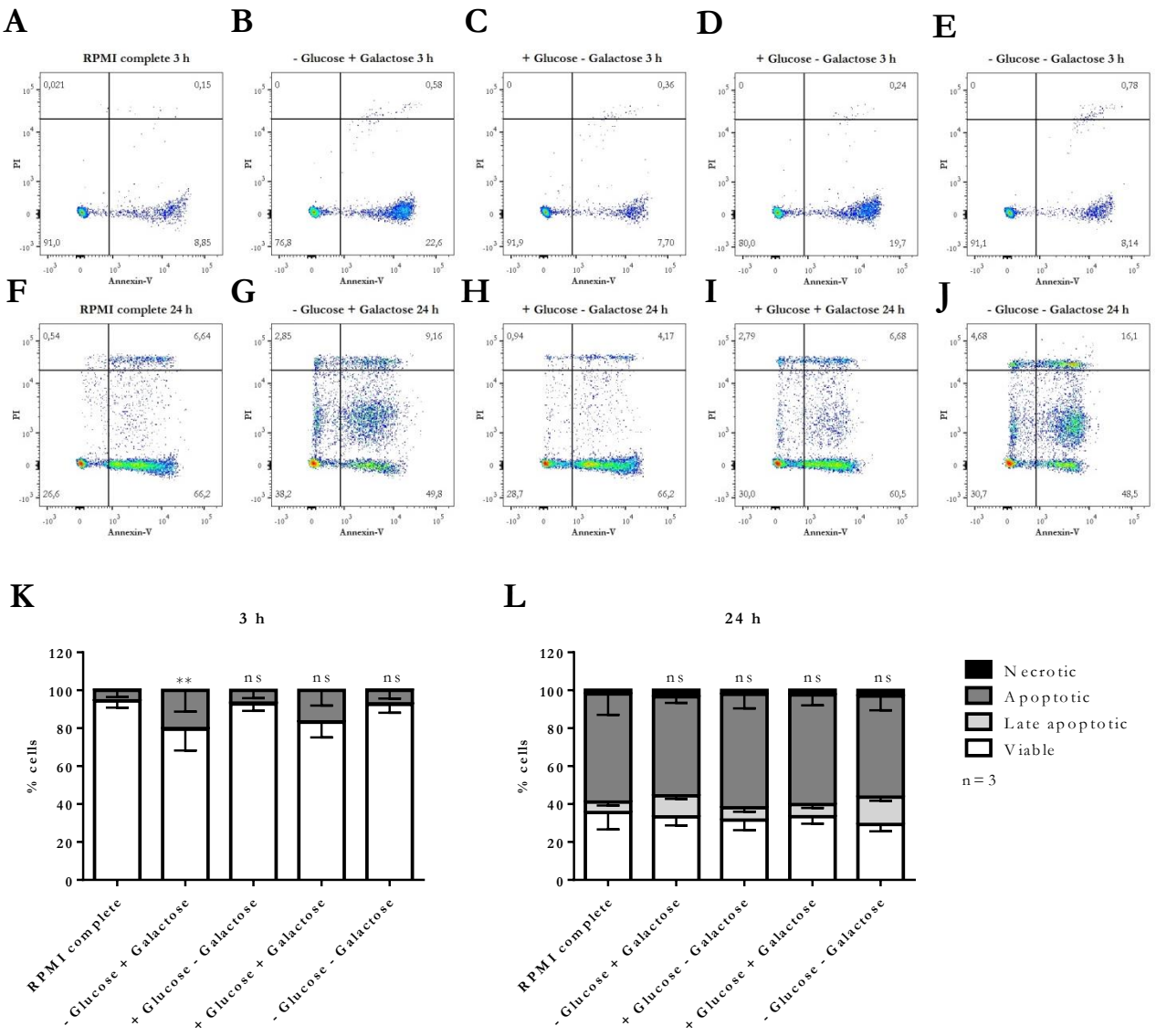

Supplementary Figure S3. Apoptosis and viability of neutrophils cultured in glucose-free medium enriched with galactose. Primary human neutrophils were cultured in medium yielding dialyzed FCS and 11.1 mM glucose, 11.1 mM galactose, 11.1 mM glucose and 11.1 mM galactose or neither glucose nor galactose. Cells cultured in RPMI complete served as control. After 3 h and 24 h apoptosis and cell viability was assessed by annexin-V and PI staining and analyzed by flow cytometry. Annexin-V- and PI-negative cells (lower left quadrant) were regarded as viable, whereas annexin-V only positive cells (lower right quadrant) were considered as apoptotic, annexin-V- and PI-positive cells were defined as late apoptotic (upper right quadrant) and PI only positive cells were regarded necrotic (upper left quadrant). Representative dot plots are shown in the panels **A**-**J**. The ratio (%) of viable cells was used for statistical analysis by one-way ANOVA. Bar diagrams (**K**, **L**) show mean ± SD (n=3), ns = not-significant.

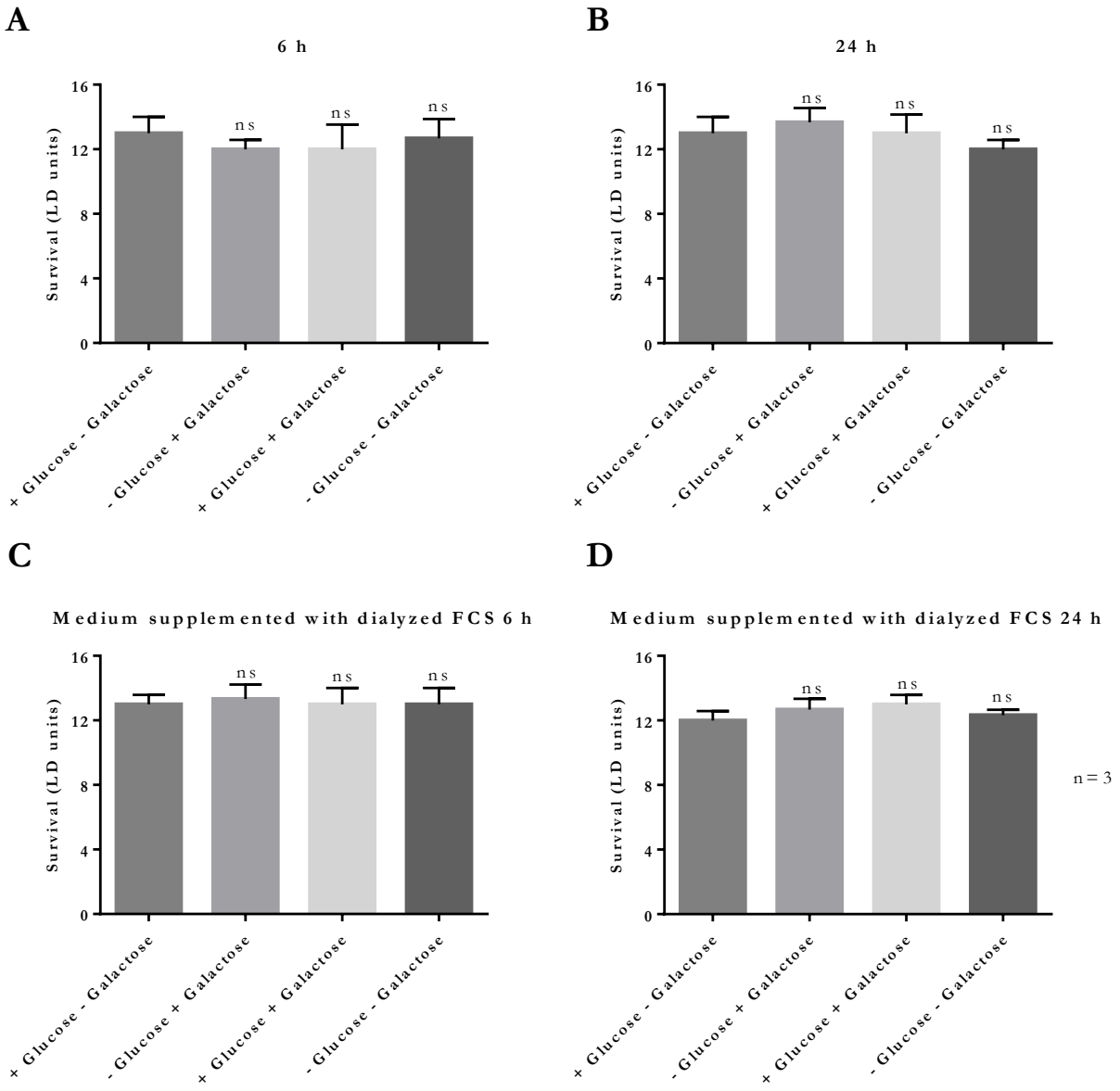

Supplementary Figure S4. Survival of *L. donovani* promastigotes in neutrophils cultured in glucose-free medium enriched with galactose. Primary human neutrophils were infected with *L. donovani* promastigotes (ratio 1:10) for 3 h at 37°C, 5 % CO_2. The infection rate was determined by Giemsa staining of cytocentrifuged samples. After removing the free, non-ingested parasites the infected cells were cultured in medium supplemented with or without dialyzed FCS and 11.1 mM glucose, galactose, glucose and galactose or no glucose and no galactose. Cells cultured in RPMI complete served as control. Survival of parasites was assessed after 6 h and 24 h post infection by using the limiting dilution assay. Bar diagrams (**A**-**D**) show the mean survival rate ± SD (n=3), ns = not-significant.

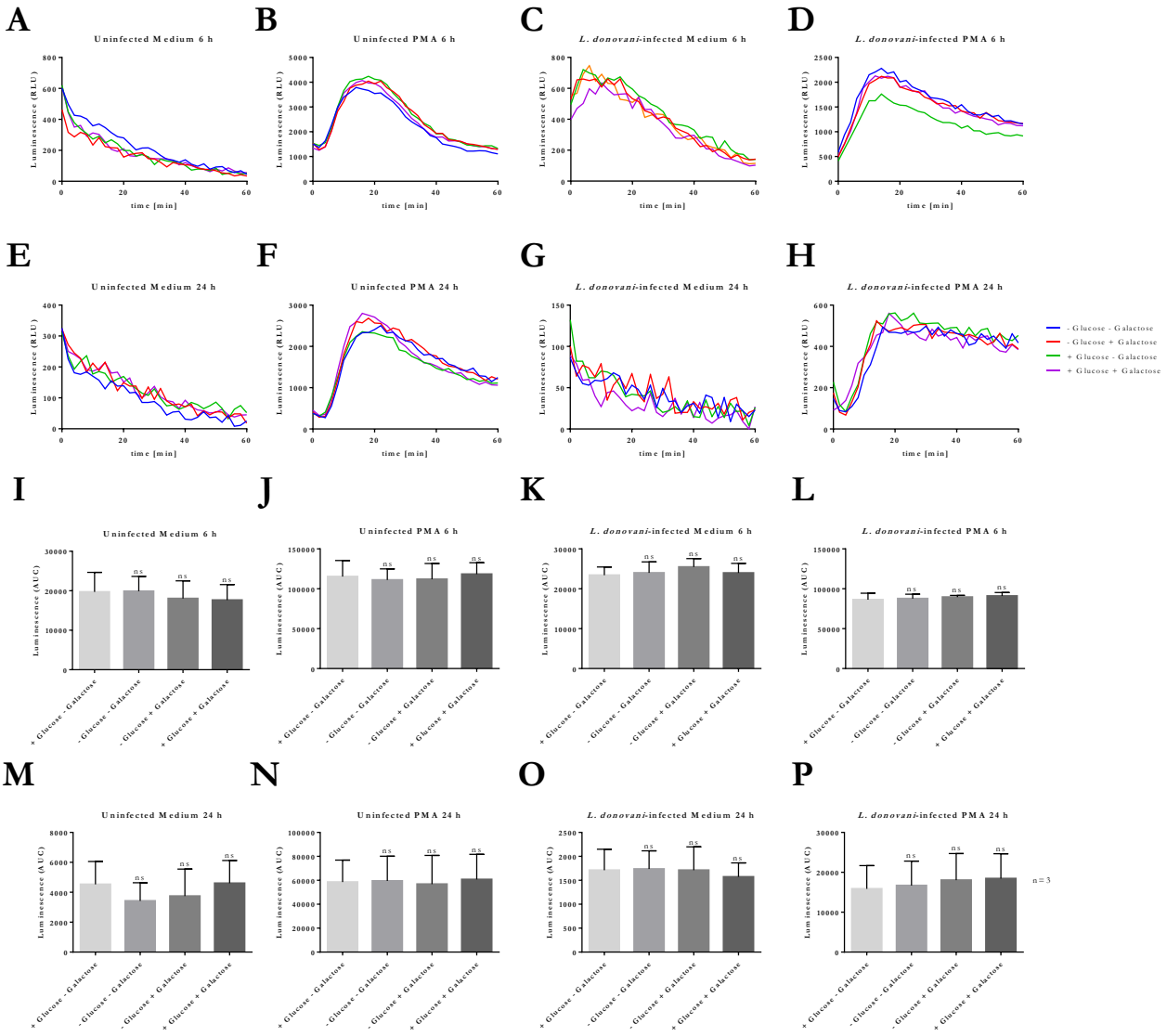

Supplementary Figure S5. MPO-derived ROS production of *L. donovani*-infected neutrophils cultured in glucose-free medium enriched with galactose. Primary human neutrophils were infected with *L. donovani* promastigotes (ratio 1:10) for 3 h at 37°C, 5 % CO_2. Uninfected cells served as control. The infection rate was determined by Giemsa staining of cytocentrifuged samples. After removing the free, non-ingested parasites infected and uninfected cells were cultured in medium yielding dialyzed FCS supplemented with 11.1 mM glucose, galactose, glucose and galactose or no glucose and no galactose. After 6 h and 24 h post infection the MPO-derived ROS production was measured for 60 min at 37°C and 5 % CO_2 in medium alone or in the presence of 20 nM PMA by using the luminol-based chemiluminescence assay. Representative curves of luminol chemiluminescence are shown in panels **A**-**H**. The bar diagrams (**I**-**P**) show the mean area under the curve (AUC) values ± SD (n=3), ns = not significant.

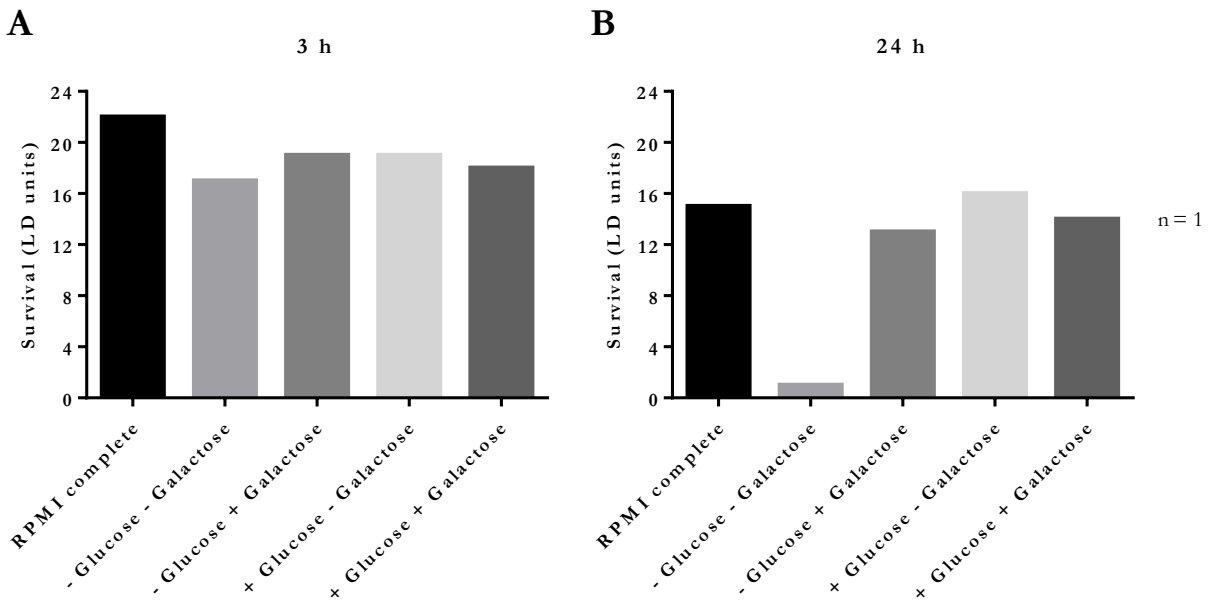

Supplementary Figure S6. Survival of *L. donovani* promastigotes in glucose-free medium enriched with galactose. *L. donovani* promastigotes were adjusted to $25 \cdot 10^6$ cells/ml in glucose-free medium and 11.1 mM galactose, 11.1 mM glucose, 11.1 mM galactose and 11.1 mM glucose or no supplements were added. The cells were cultured for 3 h or 24 h at 37°C and 5 % CO_2. Culture in RPMI complete served as assay control. Survival of parasites was assessed after 3 h and 24 h by using the limiting dilution assay. Bar diagrams (**A**, **B**) show the survival rate (LD units) (n=1).

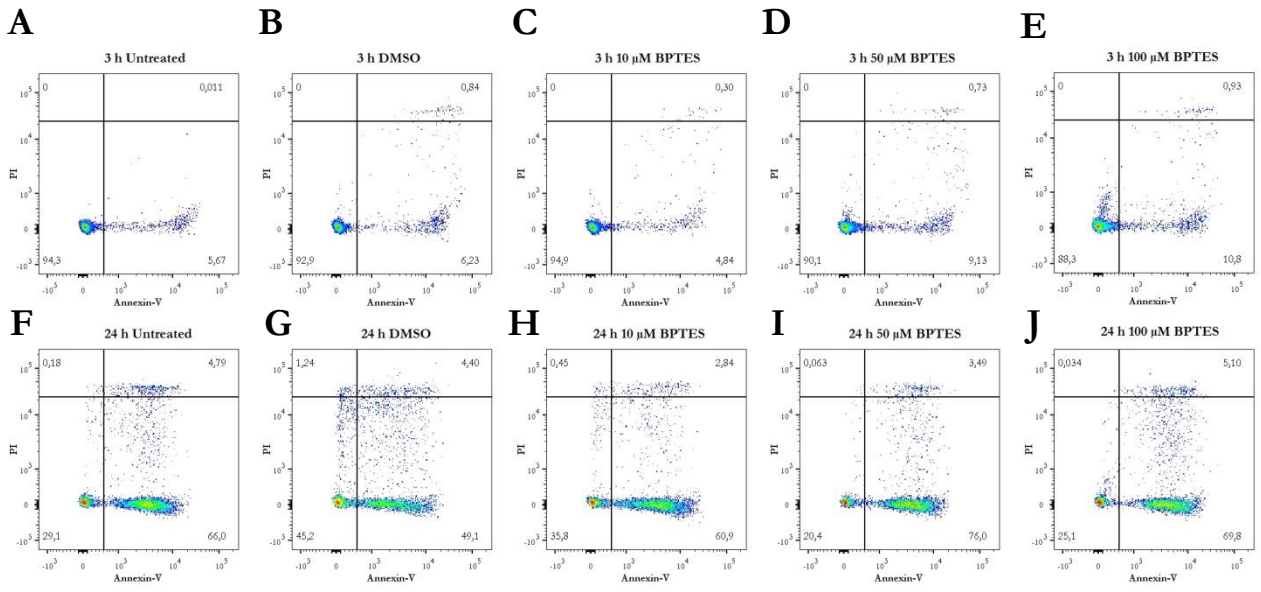

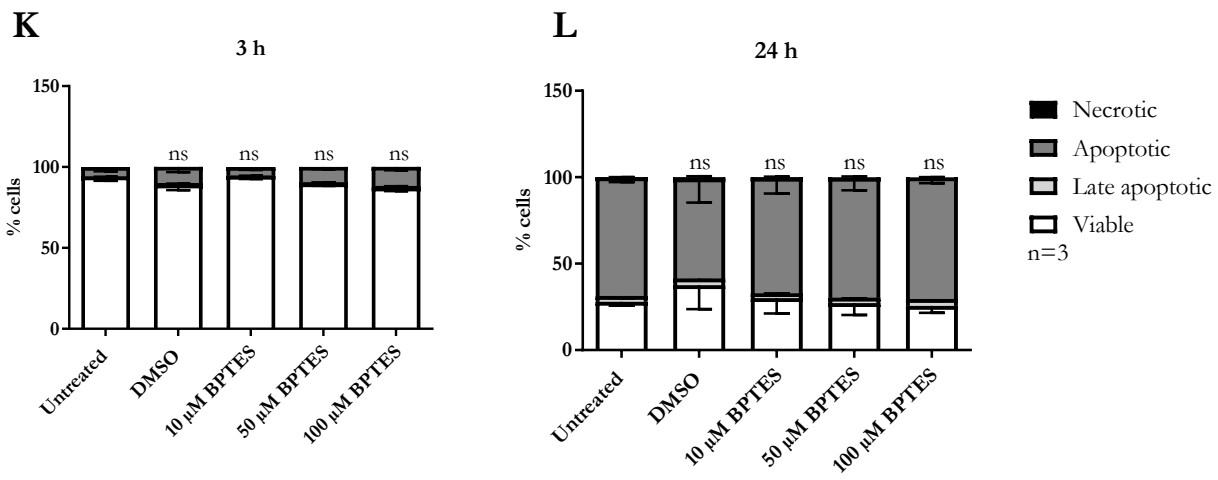

Supplementary Figure S7. Apoptosis and viability of BPTES-treated neutrophils cultured in glucose-free medium. Primary human neutrophils were cultured in glucose-free medium yielding dialyzed FCS and were treated with 10 µM, 50 µM or 100 µM BPTES. Cells cultured in RPMI complete served as control. After 3 h and 24 h apoptosis and cell viability was assessed by annexin-V and PI staining and analyzed by flow cytometry. Annexin-V- and PI-negative cells (lower left quadrant) were regarded as viable, whereas annexin-V only positive cells (lower right quadrant) were considered as apoptotic, annexin-V- and PI-positive cells were defined as late apoptotic (upper right quadrant) and PI only positive cells were regarded necrotic (upper left quadrant). Representative dot plots are shown in the panels **A**-**J**. The ratio (%) of viable cells was used for statistical analysis by one-way ANOVA. Bar diagrams (**K**, **L**) show mean ± SD (n=3), ns = not-significant.

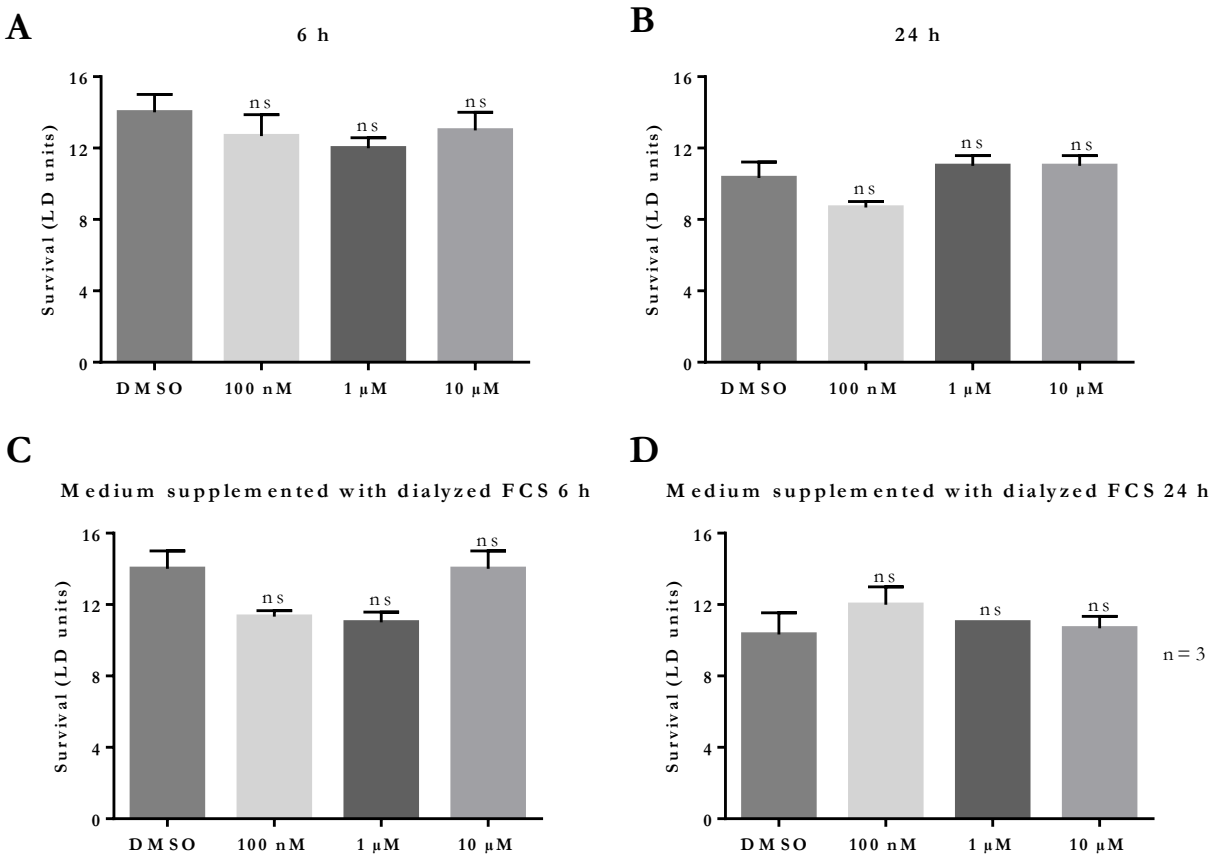

Supplementary Figure S8. Survival of *L. donovani* promastigotes in BPTES-treated neutrophils cultured in glucose-free medium. Primary human neutrophils were infected with *L. donovani* promastigotes (ratio 1:10) for 3 h at 37°C, 5 % CO_2. The infection rate was determined by Giemsa staining of cytocentrifuged samples. After removing the free, non-ingested parasites the infected cells were cultured in medium supplemented with or without dialyzed. Subsequently, the cells were treated with 100 nM, 1 µM or 10 µM BPTES. Survival of parasites was assessed after 6 h and 24 h post infection by using the limiting dilution assay. Bar diagrams (**A**-**D**) show the mean survival rate ± SD (n=3), ns = not-significant.

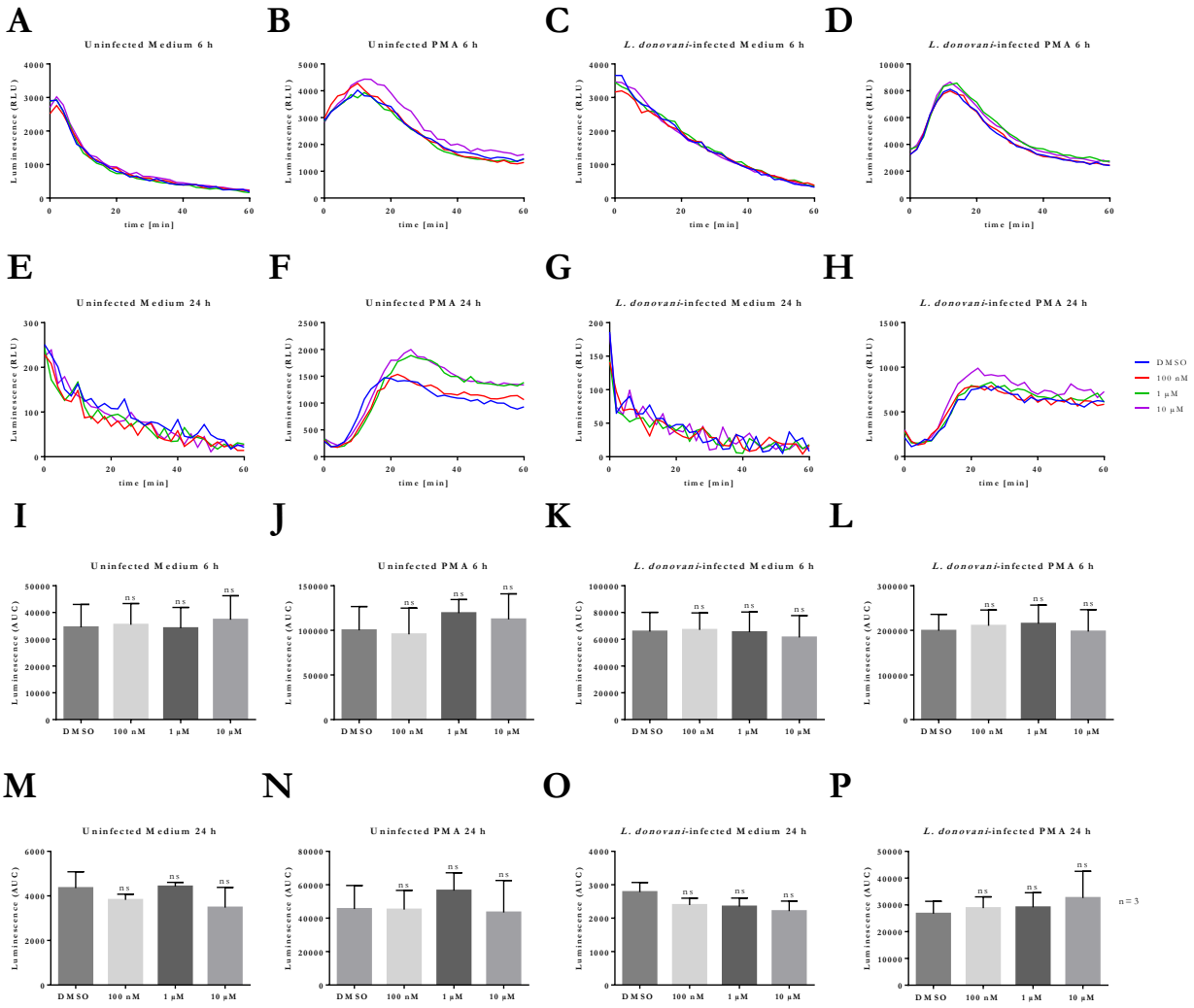

Supplementary Figure S9. MPO-derived ROS production of BPTES-treated *L. donovani*-infected neutrophils cultured in glucose-free medium. Primary human neutrophils were infected with *L. donovani* promastigotes (ratio 1:10) for 3 h at 37°C, 5 % CO_2. Uninfected cells served as control. The infection rate was determined by Giemsa staining of cytocentrifuged samples. After removing the free, non-ingested parasites infected and uninfected cells were cultured in medium containing neither FCS nor glucose. The cells were treated with 100 nM, 1 µM or 10 µM BPTES. After 6 h and 24 h post infection the MPO-derived ROS production was measured for 60 min at 37°C and 5 % CO_2 in medium alone or in the presence of 20 nM PMA by using the luminol-based chemiluminescence assay. Representative curves of luminol chemiluminescence are shown in panels **A**-**H**. The bar diagrams (**I**-**P**) show the mean area under the curve (AUC) values ± SD (n=3), ns = not significant.

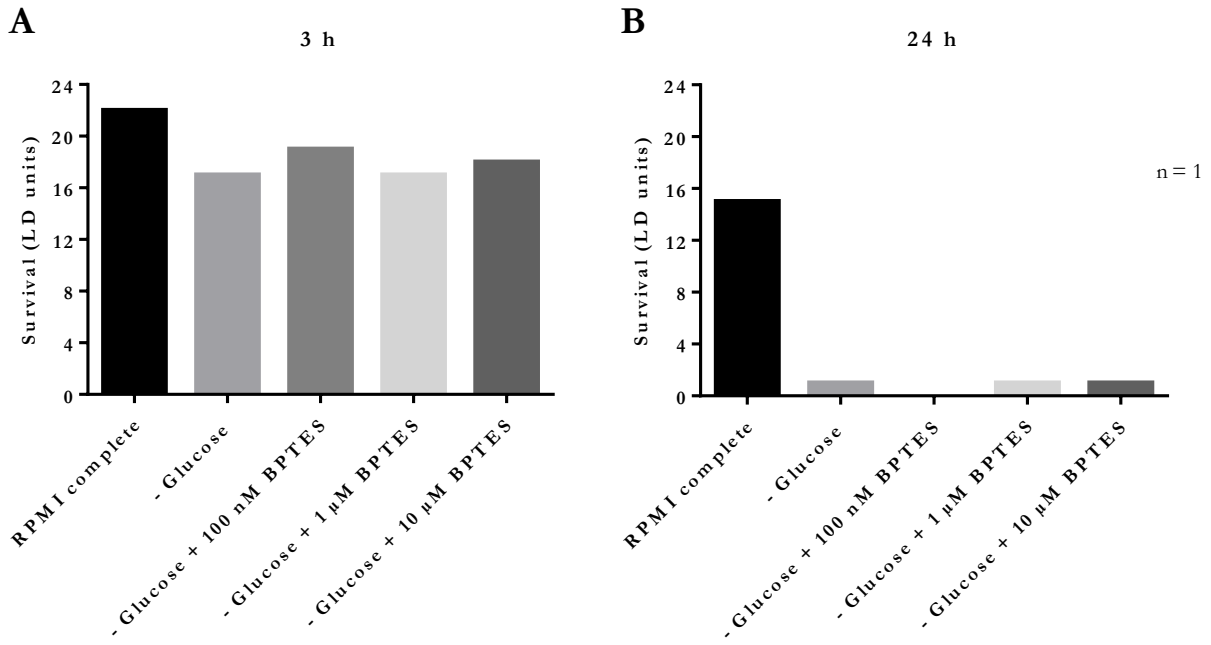

Supplementary Figure S10. Survival of *L. donovani* promastigotes in the presence of BPTES in glucose-free medium. *L. donovani* promastigotes were adjusted to $25 \cdot 10^6$ cells/ml in glucose-free medium and treated with 100 nM, 1 µM or 10 µM BPTES for 3 h or 24 h at 37°C and 5 % CO_2. Culture in RPMI complete served as assay control. Survival of parasites was assessed after 3 h and 24 h by using the limiting dilution assay. Bar diagrams (**A**, **B**) show the survival rate (LD units) (n=1).

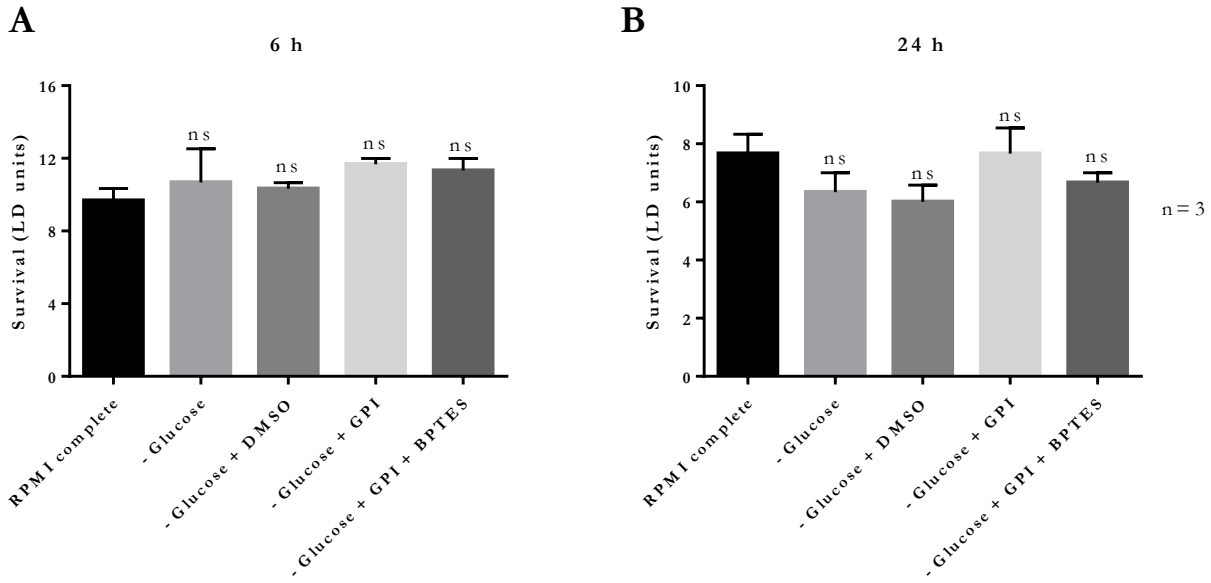

Supplementary Figure S11. Survival of *L. donovani* promastigotes in GPI-treated neutrophils. Primary human neutrophils were infected with *L. donovani* promastigotes (ratio 1:10) for 3 h at 37°C, 5 % CO_2. The infection rate was determined by Giemsa staining of cytocentrifuged samples. After removing the free, non-ingested parasites the infected cells were cultured in glucose-free medium supplemented with dialyzed. Subsequently, the cells were treated with 50 µM GPI or a

combination of 50 µM and 10 µM BPTES. Survival of parasites was assessed after 6 h and 24 h post infection by using the limiting dilution assay. Bar diagrams (**A**-**D**) show the mean survival rate ± SD (n=3), ns = not-significant.

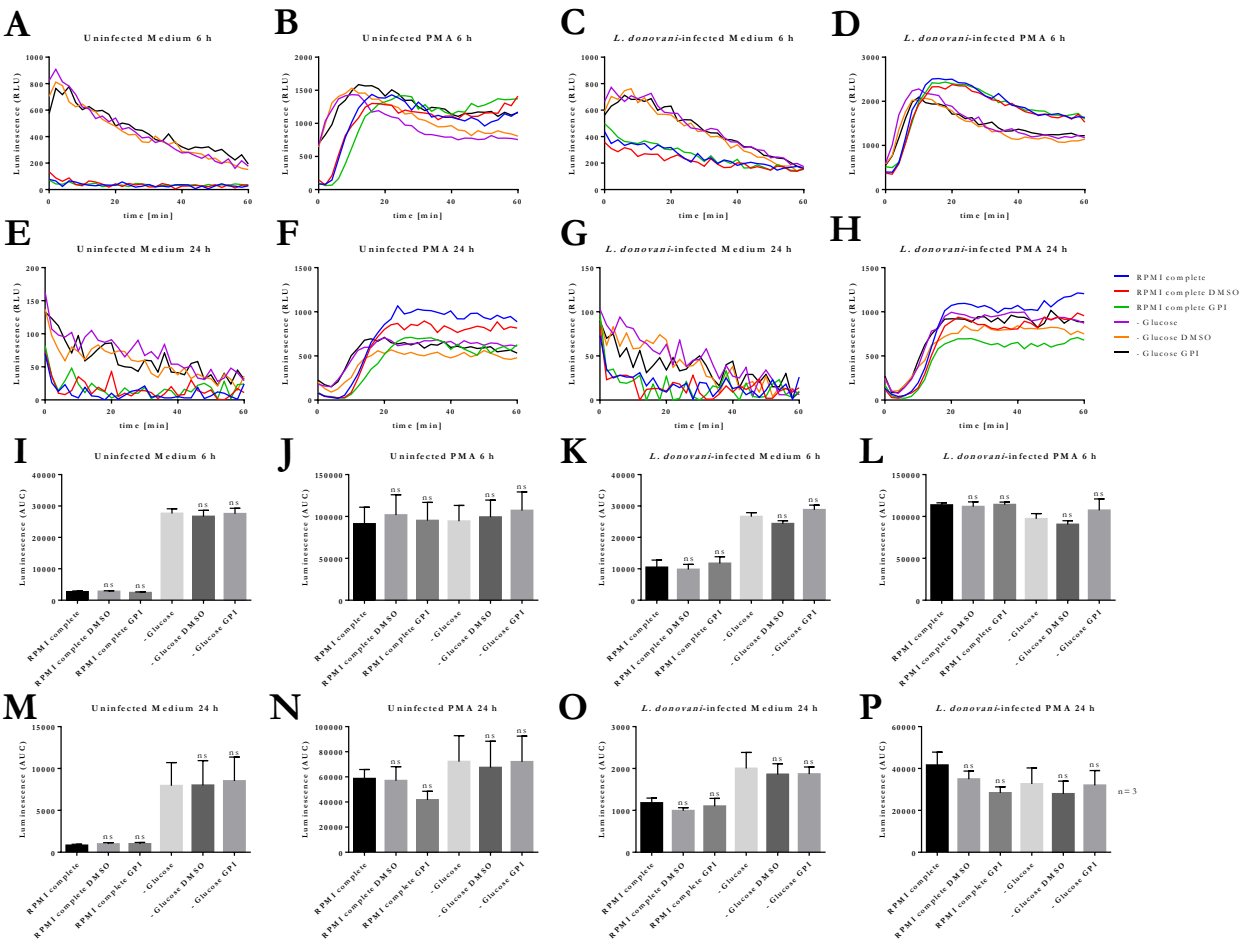

Supplementary Figure S12. MPO-derived ROS production of GPI-treated *L. donovani*-infected neutrophils cultured in glucose-free medium. Primary human neutrophils were infected with *L. donovani* promastigotes (ratio 1:10) for 3 h at 37°C, 5 % CO_2. Uninfected cells served as control. The infection rate was determined by Giemsa staining of cytocentrifuged samples. After removing the free, non-ingested parasites infected and uninfected cells were cultured in medium containing neither FCS nor glucose or RPMI complete as control. The cells were treated with 50 µM glycogen phosphorylase inhibitor (GPI) or DMSO as solvent control. After 6 h and 24 h post infection the MPO-derived ROS production was measured for 60 min at 37°C and 5 % CO_2 in medium alone or in the presence of 20 nM PMA by using the luminol-based chemiluminescence assay. Representative curves of luminol chemiluminescence are shown in panels **A**-**H**. The bar diagrams (**I**-**P**) show the mean area under the curve (AUC) values ± SD (n=3), for statistical analysis the samples were compared to the corresponding culture medium, ns = not significant.

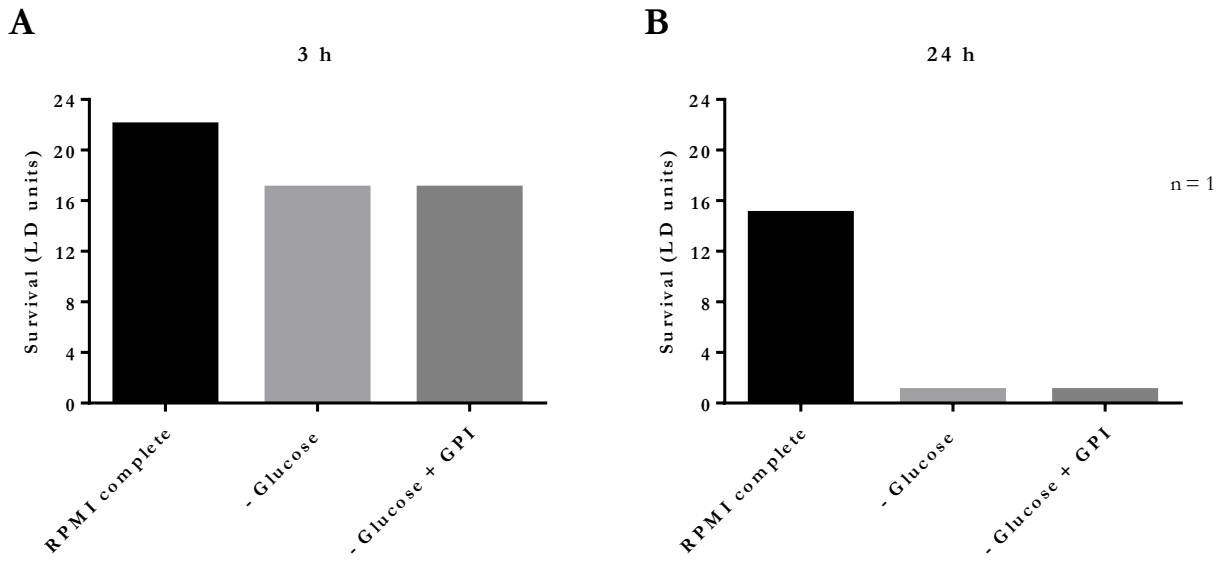

Supplementary Figure S13. Survival of *L. donovani* promastigotes in the presence of GPI in glucose-free medium. *L. donovani* promastigotes were adjusted to $25 \cdot 10^6$ cells/ml in glucose-free medium with or without 50 µM GPI as well as 10 µM BPTES for 3 h or 24 h at 37°C and 5 % CO_2. Culture in RPMI complete served as assay control. Survival of parasites was assessed after 3 h and 24 h by using the limiting dilution assay. Bar diagrams (**A**, **B**) show the survival rate (LD units) (n=1).

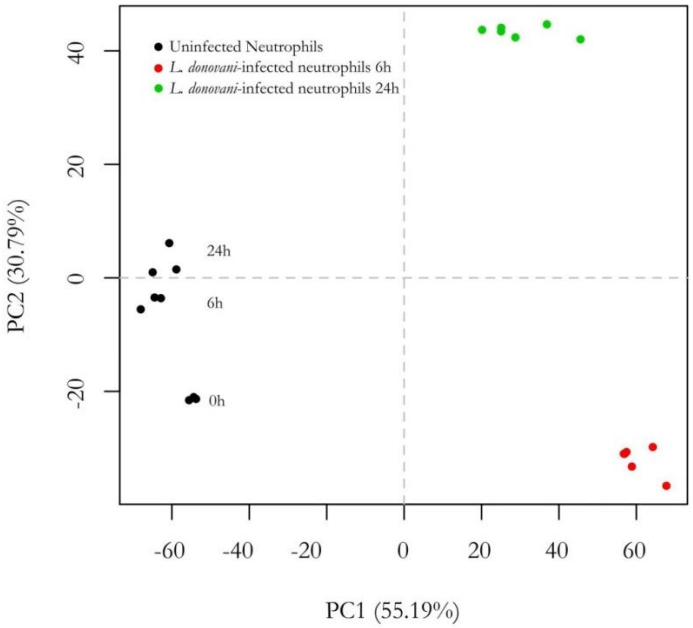

Supplementary Figure S14. Principal component analysis (PCA) of *L. donovani*-infected neutrophils. RNA-Seq was carried out on uninfected and *L. donovani*-infected neutrophils after 0 h, 6 h, 24 h. The PCA plot based on the 1000 most variable genes was generated in R using the prcomp function. The first two principal components are shown on the X and the Y axis, respectively, with the proportion of total variance attributable to that PC indicated. The distance along each axis represents the amount of variance in gene expression explained by the corresponding factor. Each individual sample is represented as a single point with color indicating sample type/time point as depicted in the legend.

A

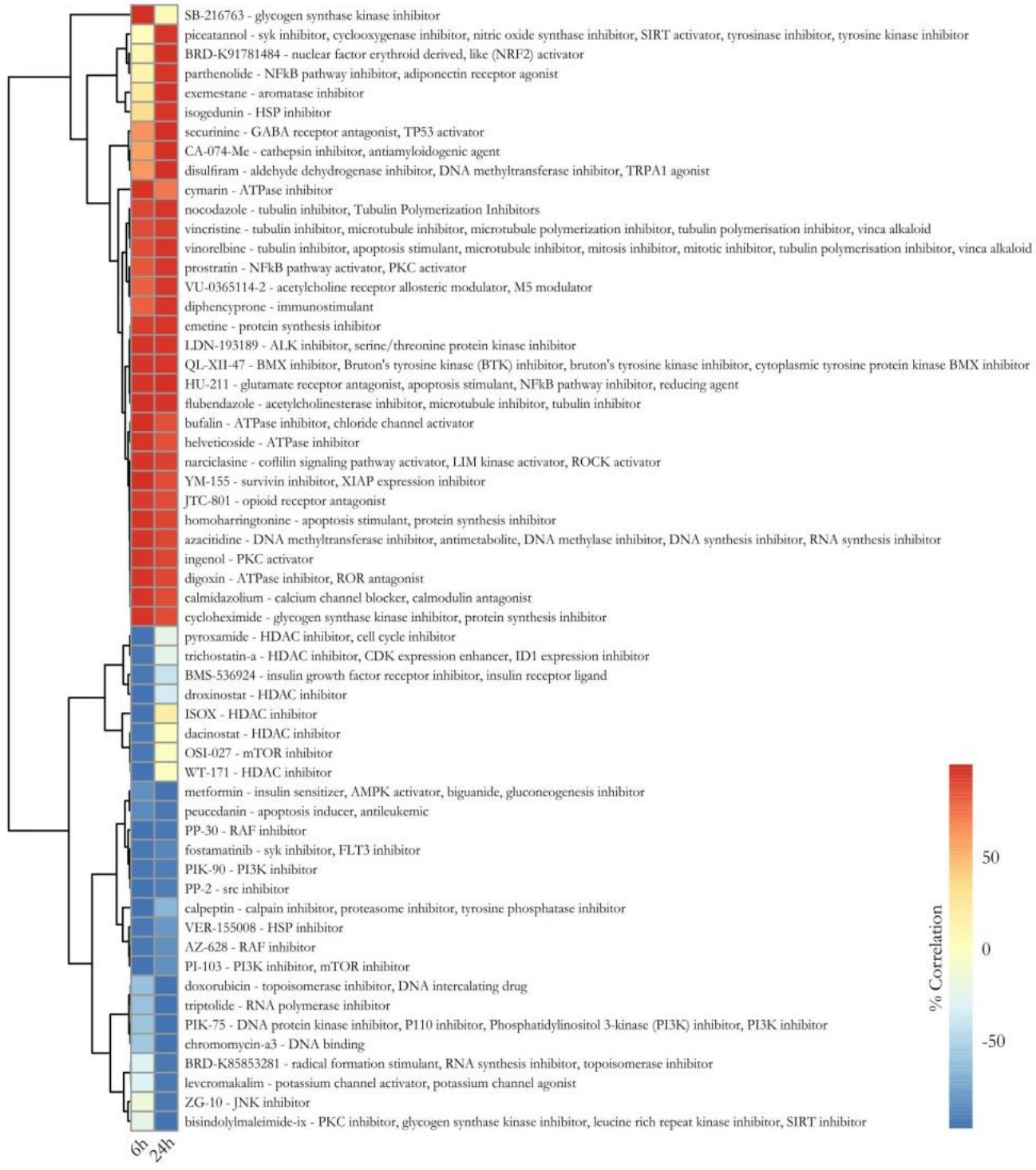
SB-216763 - glycogen synthase kinase inhibitor
piceatannol - syk inhibitor, cyclooxygenase inhibitor, nitric oxide synthase inhibitor, SIRT activator, tyrosinase inhibitor, tyrosine kinase inhibitor
BRD-K91781484 - nuclear factor erythroid derived, like (NRF2) activator
parthenolide - NFkB pathway inhibitor, adiponectin receptor agonist
exemestane - aromatase inhibitor
isogedunin - HSP inhibitor
securinine - GABA receptor antagonist, TP53 activator
CA-074-Me - cathepsin inhibitor, antiamyloidogenic agent
disulfiram - aldehyde dehydrogenase inhibitor, DNA methyltransferase inhibitor, TRPA1 agonist
cymarin - ATPase inhibitor
nocodazole - tubulin inhibitor, Tubulin Polymerization Inhibitors
vincristine - tubulin inhibitor, microtubule inhibitor, microtubule polymerization inhibitor, tubulin polymerisation inhibitor, vinca alkaloid
vinorelbine - tubulin inhibitor, apoptosis stimulant, microtubule inhibitor, mitosis inhibitor, mitotic inhibitor, tubulin polymerisation inhibitor, vinca alkaloid
prostratin - NFkB pathway activator, PKC activator
VU-0365114-2 - acetylcholine receptor allosteric modulator, M5 modulator
diphencyprone - immunostimulant
emetine - protein synthesis inhibitor
LDN-193189 - ALK inhibitor, serine/threonine protein kinase inhibitor
QL-XII-47 - BMX inhibitor, Bruton's tyrosine kinase (BTK) inhibitor, bruton's tyrosine kinase inhibitor, cytoplasmic tyrosine protein kinase BMX inhibitor
HU-211 - glutamate receptor antagonist, apoptosis stimulant, NFkB pathway inhibitor, reducing agent
flubendazole - acetylcholinesterase inhibitor, microtubule inhibitor, tubulin inhibitor
bufalin - ATPase inhibitor, chloride channel activator
helveticoside - ATPase inhibitor
narciclasine - cofilin signaling pathway activator, LIM kinase activator, ROCK activator
YM-155 - survivin inhibitor, XIAP expression inhibitor
JTC-801 - opioid receptor antagonist
homoharringtonine - apoptosis stimulant, protein synthesis inhibitor
azacitidine - DNA methyltransferase inhibitor, antimetabolite, DNA methylase inhibitor, DNA synthesis inhibitor, RNA synthesis inhibitor
ingenol - PKC activator
digoxin - ATPase inhibitor, ROR antagonist
calmidazolium - calcium channel blocker, calmodulin antagonist
cycloheximide - glycogen synthase kinase inhibitor, protein synthesis inhibitor
pyroxamide - HDAC inhibitor, cell cycle inhibitor
trichostatin-a - HDAC inhibitor, CDK expression enhancer, ID1 expression inhibitor
BMS-536924 - insulin growth factor receptor inhibitor, insulin receptor ligand
droxinostat - HDAC inhibitor
ISOX - HDAC inhibitor
dacinostat - HDAC inhibitor
OSI-027 - mTOR inhibitor
WT-171 - HDAC inhibitor
metformin - insulin sensitizer, AMPK activator, biguanide, gluconeogenesis inhibitor
peucedanin - apoptosis inducer, antileukemic
PP-30 - RAF inhibitor
fostamatinib - syk inhibitor, FLT3 inhibitor
PIK-90 - PI3K inhibitor
PP-2 - src inhibitor
calpeptin - calpain inhibitor, proteasome inhibitor, tyrosine phosphatase inhibitor
VER-155008 - HSP inhibitor
AZ-628 - RAF inhibitor
PI-103 - PI3K inhibitor, mTOR inhibitor
doxorubicin - topoisomerase inhibitor, DNA intercalating drug
triptolide - RNA polymerase inhibitor
PIK-75 - DNA protein kinase inhibitor, P110 inhibitor, Phosphatidylinositol 3-kinase (PI3K) inhibitor, PI3K inhibitor
chromomycin-a3 - DNA binding
BRD-K85853281 - radical formation stimulant, RNA synthesis inhibitor, topoisomerase inhibitor
levcromakalim - potassium channel activator, potassium channel agonist
ZG-10 - JNK inhibitor
bisindolylmaleimide-ix - PKC inhibitor, glycogen synthase kinase inhibitor, leucine rich repeat kinase inhibitor, SIRT inhibitor
6h
24h
% Correlation
50
0
-50

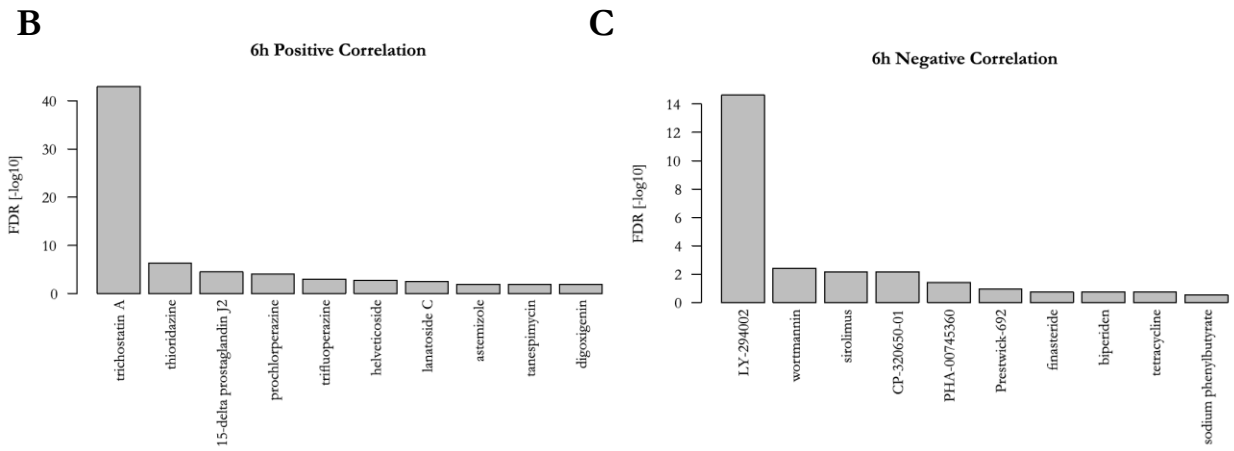

Supplementary Figure S15. Connectivity map (CMAP) analysis of *L. donovani*-infected neutrophils. RNA-Seq was carried out on uninfected and *L. donovani*-infected neutrophils after 0 h, 6 h, 24. The gene response of *L. donovani*-infected neutrophils after 6 h and 24 h was correlated with CMAP signatures. The heatmap (**A**) shows the GSVA enrichment scores. Samples and pathways in the columns and rows have been hierarchically clustered by a complete linkage method according to their Eudidean distance. Bar diagrams show the top-ranked 10 CMAP compounds/drugs that induce transcriptome alterations oppositional (negative correlation, **C**) or overlapping (positive correlation, **B**) with the gene response of *L. donovani*-infected neutrophils after 6 hpi, FDR = false discovery rate.

A

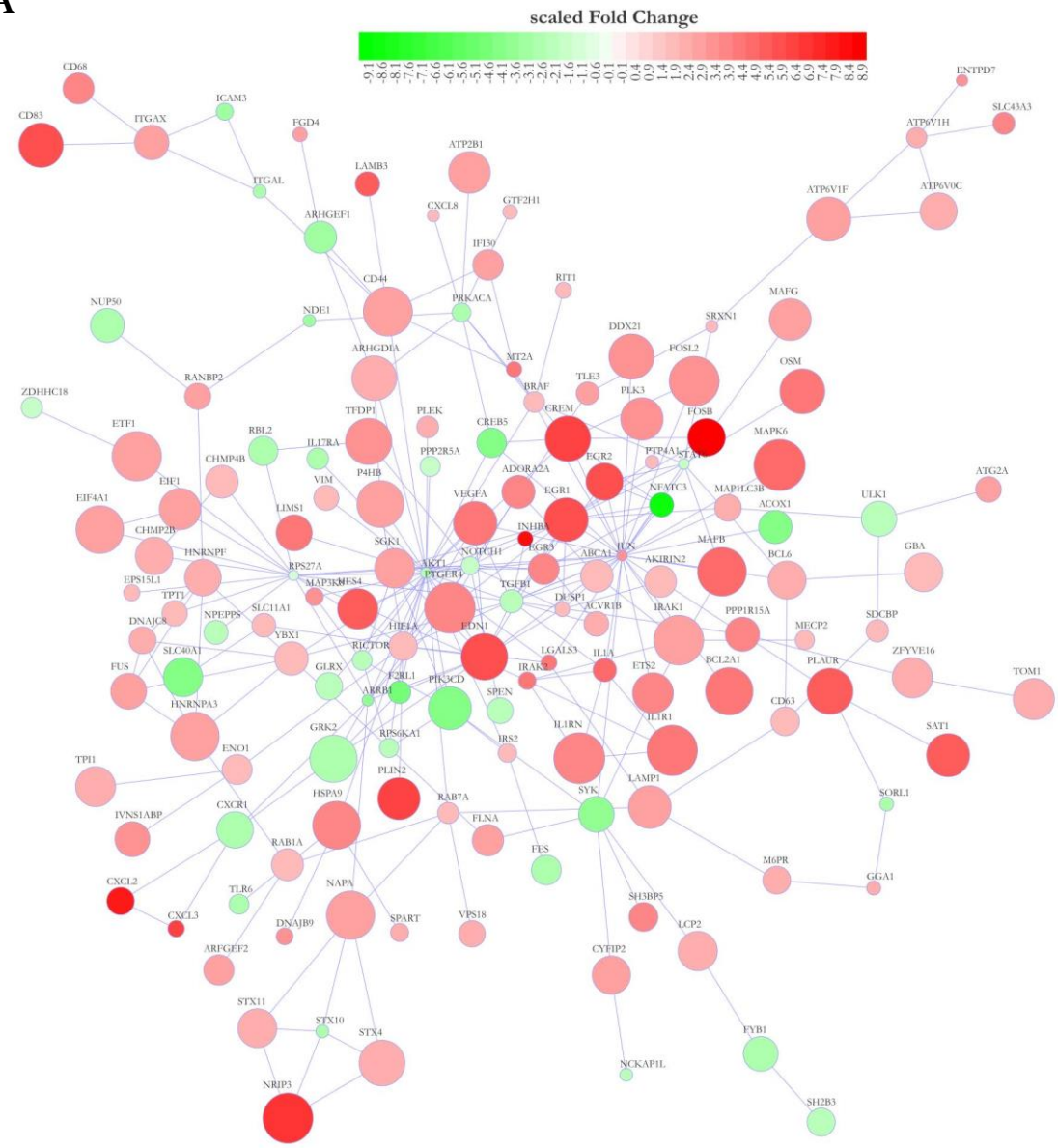
scaled Fold Change
-9.1 -8.6 -8.1 -7.6 -7.1 -6.6 -6.1 -5.6 -5.1 -4.6 -4.1 -3.6 -3.1 -2.6 -2.1 -1.6 -1.1 -0.6 -0.1 0.4 0.9 1.4 1.9 2.4 2.9 3.4 3.9 4.4 4.9 5.4 5.9 6.4 6.9 7.4 7.9 8.4 8.9
CD68
CD83
ITGAX
ICAM3
ITGAL
FGD4
LAMB3
ATP2B1
CXCL8
GTF2H1
ARHGEF1
IFI30
CD44
PRKACA
RIT1
NUP50
NDE1
ARHGDIA
MT2A
RANBP2
BRAF
TLE3
PLK3
CREM
ZDHHC18
ETF1
RBL2
IL17RA
TFDP1
PLEK
CREB5
PPP2R5A
FOSB
CHMP4B
P4HB
VIM
ADORA2A
EGR2
PTP4A1
STAT1
EIF1
EIF4A1
CHMP2B
LIMS1
VEGFA
EGR1
NFATC3
MAP1LC3B
ACOX1
ULK1
ATG2A
HNRNPF
SGK1
INHBA
EGR3
ABCA1
JUN
MAFB
BCL6
GBA
EPS15L1
TPT1
RPS27A
MAP3K14
AKT1
PTGER4
NOTCH1
TGFBI
AKIRIN2
DUSP1
ACVR1B
IRAK1
PPP1R15A
MECP2
SDCBP
DNAJC8
NPEPPS
SLC11A1
YBX1
HIF1A
EDN1
RICTOR
LGALS3
IL1A
ETS2
BCL2A1
PLAUR
ZFYVE16
TOM1
FUS
SLC40A1
GLRX
F2RL1
PIK3CD
IRAK2
SPEN
ABRA
HNRNPA3
CD63
IL1R1
SAT1
GRK2
ENO1
RPS6KA1
IRS2
IL1RN
TPI1
PLIN2
LAMP1
SYK
SORL1
HSPA9
RAB7A
IVNS1ABP
CXCR1
FLNA
RAB1A
FES
M6PR
GGA1
CXCL2
TLR6
NAPA
SH3BP5
CXCL3
DNAJB9
SPART
VPS18
LCP2
ARFGEF2
CYFIP2
STX11
STX10
STX4
EYB1
NRIP3
NCKAP1L
SH2B3
ENTPD7
SLC43A3
ATP6V1H
ATP6V1F
ATP6V0C
MAFG
SRXN1
DDX21
POSL2
OSM
MAPK6

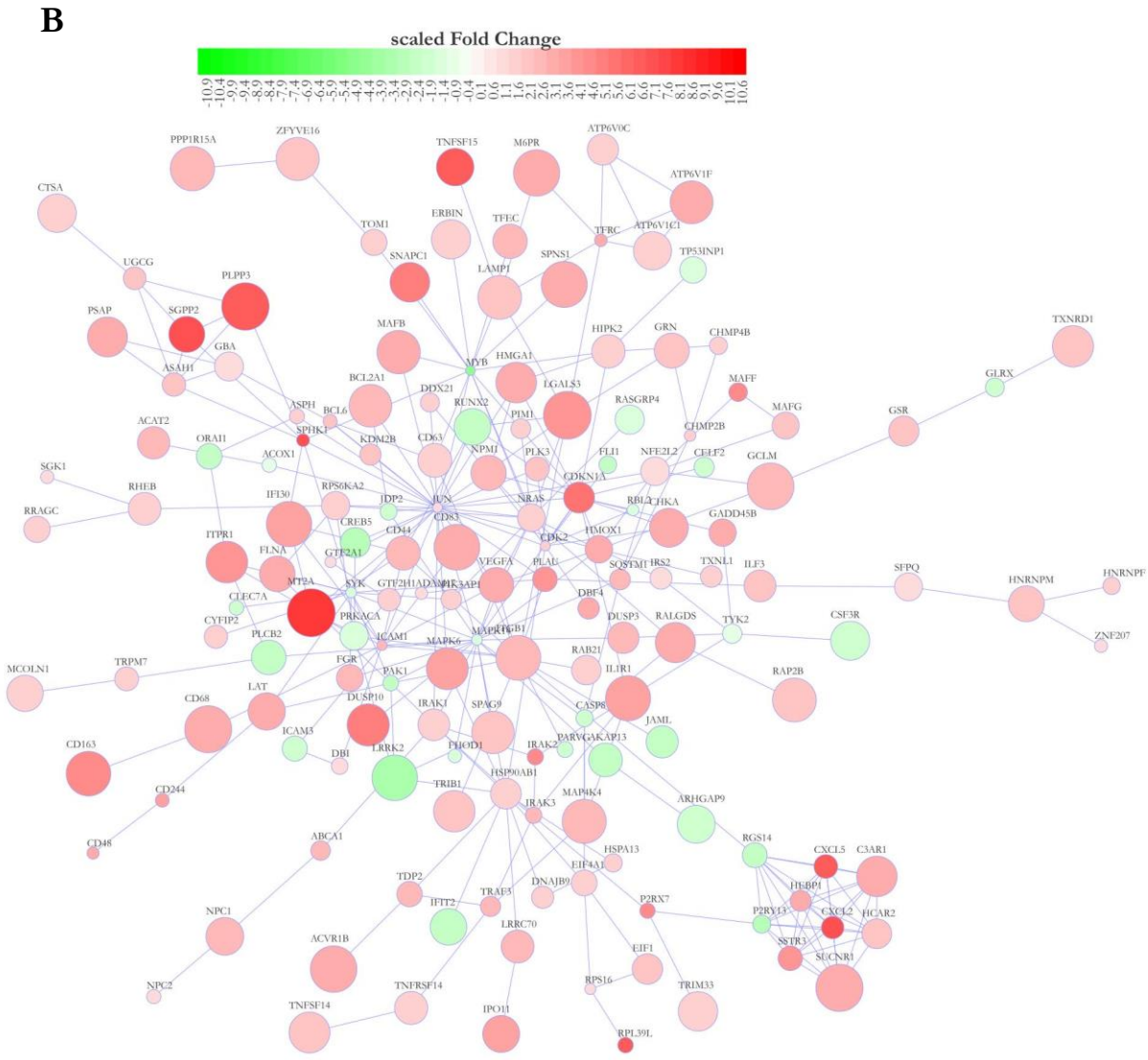

Supplementary Figure S16. Protein-Protein interaction (PPI) network of differentially expressed genes of *L. donovani*-infected neutrophils after 6 hpi. RNA-Seq was carried out on uninfected and *L. donovani*-infected neutrophils after 0 h, 6 h, 24 h. Differentially expressed genes (DEGs) of *L. donovani*-infected neutrophils after 6 hpi (**A**) and 24 hpi (**B**) were mapped onto a PPI on the basis of the STRING v.10.0a database with a confidence score ≤ 0.7. Proteins with more than 400 connections were exduded and a fully connected network of the most DEGs with 150 nodes was generated. Each node represents a protein and the edge between two nodes represents their interaction. The red nodes indicate the upregulated DEGs, while green nodes indicate the downregulated DEGs.

Curriculum vitae

Mareike Ohms
Neufresenburg 20
23843 Bad Oldesloe
Phone: 04531/8977153
E-Mail: ohms.mareike@gmx.de

Professional appointment

Scientific employee 2018 – now
University hospital Lübeck (UKSH)
Department of Infectiology and Microbiology
Research group of Prof. Dr. Tamás Laskay

Education

Master study 2015 – 2017
Molecular Life Science, University of Lübeck
Thesis title: Establishment of Siberian hamster (*Phodopus sungorus*)
ex vivo models to study seasonality dependent influenza A virus replication
Research group of Prof. Dr. Gülsah Gabriel, Heinrich-Pette institute Hamburg

Bachelor study 2012 – 2015
Molecular Life Science, University of Lübeck
Thesis title: Studies on the in vitro transport into the endoplasmic reticulum
and the heterologous expression of the protein Pex8p from the yeast *Saccharomyces cerevisiae*
Group of Prof. Dr. Enno Hartmann, Institute of Biology, University of Lübeck

School 2003 – 2012
General matriculation standard, Theodor-Mommsen school, Bad Oldesloe

Publications

Aga, E., Mukherjee, A., Rane, D., More, V., Patil, T., van Zandbergen, G., Solbach, W., Dandapat, J., Tackenberg, H., Ohms, M., et al. (2018). Type-1 interferons prolong the lifespan of neutrophils by interfering with members of the apoptotic cascade. Cytokine *112*, 21–26.

Ohms, M., Möller, S., and Laskay, T. (2020). An Attempt to Polarize Human Neutrophils Toward N1 and N2 Phenotypes in vitro. Front. Immunol. *11*, 532.